

**Investigation on Wearable Antennas
for
Body Area Network**

*Thesis submitted to Jawaharlal Nehru University
for the partial fulfilment of the requirements for the award of*

Doctor of Philosophy

By

Hari Singh

Under the Supervision of

Prof Binod Kumar Kanaujia



School of Computational and Integrative Sciences

Jawaharlal Nehru University

New Delhi, India

March-2022



जवाहरलाल नेहरू विश्वविद्यालय
Jawaharlal Nehru University
संगणकीय एवं समेकित विज्ञान संस्थान
School of Computational and Integrative Sciences
नई दिल्ली-110067, भारत / New Delhi-110067, INDIA

Tel.: +91-011-26704171, 26704082

CERTIFICATE

This is to certify that the research work embodied in the thesis entitled “**Investigation on Wearable Antennas for Body Area Network**” is the original work of the candidate for the partial fulfilment of the requirements for the award of the degree of **Doctor of Philosophy in Electronics and Communication** and has been carried out at School of Computational and Integrative Sciences, Jawaharlal Nehru University, New Delhi, India.

This work has not been submitted so far, in part or full, for the award of any degree or diploma from any University.

Hans
7/4/22

Hari Singh
(Candidate)
School of Computational and Integrative Sciences
Jawaharlal Nehru University
New Delhi, India

Binod Kumar Kanaujia
07/04/22
Prof. Binod Kumar Kanaujia
(Supervisor)
School of Computational and Integrative Sciences
Jawaharlal Nehru University
New Delhi, India.

Ashwani Kumar
07/04/2022
Dr Ashwani Kumar
(Co-Supervisor)
School of Engineering
Jawaharlal Nehru University
New Delhi, India

Mukesh Jain
21.04.2022
Prof. Mukesh Jain
(Dean)
School of Computational and Integrative Sciences
Jawaharlal Nehru University
New Delhi, India.

Dedicated to Almighty and My Family

ACKNOWLEDGEMENT

First and foremost, praises and thanks to the *ALMIGHTY*, for showering his choicest blessings and for being my inner strength and guide throughout my research work. I pray that the growth I have achieved would be used in his service.

One of the joys of completion is to look over the journey past and remember all those who have inspired, encouraged and supported me along this long but fulfilling road. My research thesis would not have been materialized if there had not been the contribution of the following individuals. I take this opportunity to acknowledge the assistance and support of the many people who contributed to the completion of this work.

I would like to express my sincere gratitude and profound reverences to my supervisor *Prof Binod Kumar Kanaujia*, for his continuous support, guidance and wholehearted supervision throughout the progress of this research work. I am deeply grateful to him for acquainting me with the world of advanced research. He has been a great mentor with his enthusiasm, determination and patience. He has been instrumental in providing me with timely support in difficult times. Without his inspiration and encouragement, this work would have never been completed. He shared with me not only his expertise but also his exceptional professionalism. Throughout my life, I will be benefitted from the knowledge and experience I acquired working with him.

I wish to extend my deep gratitude to my co-supervisor *Dr Ashwani Kumar*, School of Engineering, Jawaharlal Nehru University, for his consistent guidance and support throughout my academic life. He is the torchbearer who created interest in me for this field during my post-graduation. His conscientious academic spirit and open-minded personality inspire me both in academic study and daily life.

I am truly indebted to *Prof Shandar Ahmad* and *Prof Kedar Singh*, my research advisory committee (RAC) members, for their constant support and guidance at various stages of my research. They have always encouraged my research efforts and provided me with insight and directions right up to the end. I sincerely thank them for their valuable time and assistance.

My heartfelt gratitude is also extended to **Prof Andrew M. Lynn**, Former Dean, School of Computational and Integrative Sciences (SCIS), Jawaharlal Nehru University, for his kind help and support during the initial phase of my research. He always supported and guided me starting from my enrolment to the completion of the Course Work. I sincerely thank him for his invaluable support and encouragement.

I would like to sincerely thank the eminent faculty members of the School of Computational and Integrative Sciences (SCIS), Jawaharlal Nehru University, **Prof Indira Ghosh (Emeritus)**, **Dr Gajendra Pratap Singh**, **Dr Rita Sharma** and **Dr Sapna Ratan Shah** for the knowledge and support I received from all of them during my Course Work. I find myself fortunate enough to be associated with such renowned and distinguished persons from different fields. I express my sincere gratitude to all of them for being available for me always, despite their busy schedules.

I would like to give a heartfelt thanks to **Dr Kunal Srivastava**, for his thorough support and help. He was the one who not only inspired me to begin my research exploration but also guided and supported me during my entire journey. I sincerely thank him for giving his valuable time and assistance and being so supportive, understanding and generous in sharing his knowledge of Antenna Technology. I will always be grateful to him for his much-appreciated efforts in the review and correction of my research papers throughout my research work.

My heartfelt thanks are also extended to **Dr Sachin Kumar**, SRM Institute of Science and Technology, Chennai, for his kind support and guidance throughout my research work. He not only posed very thought-provoking questions about my work but also provided me with constructive feedback. I appreciate his willingness to review and correct my research papers and make this thesis possible. For this, I cannot thank him enough. I am forever grateful.

I would like to acknowledge and appreciate the contribution of **Dr Ravi Arya**, National Institute of Technology, Delhi, **Dr Maifuz Ali**, International Institute of Information Technology, Naya Raipur and **Mr Prashant Chaudhary**, Department of Electronic Science, University of Delhi, South Campus, for their key roles in the group discussions. They always pointed out critical points in our discussions and encouraged me to solve the problems.

I also wish to express my sincere appreciation and thanks to **Dr Satya Kesh Dubey**, Senior Scientist and **Mr Asheesh Kumar** from the Council of Scientific and Industrial Research-National Physical Laboratory, New Delhi, India, for helping me in doing characterization of textile materials. My exploration of fully-textile antennas would not have begun without their support.

I would like to extend my heartfelt thanks to my fellow lab mate **Mr Vikrant Kain**, for his thorough support and help. I also thank my fellow lab mates, learned colleagues and friends associated with Prof Binod Kumar Kanaujia for their support and encouragement.

Thanks are also extended to the School of Computational and Integrative Sciences, Jawaharlal Nehru University and its staff members for providing me with the research laboratory to carry out my research work. My heartfelt thanks are also extended to **Mr Ashish Bharti**, for the co-operation and administrative support provided by him throughout my research work.

I am also indebted to **Dr P. Hemlatha Reddy** and **Prof C Sheela Reddy**, the former and current principals of Sri Venkateswara College, University of Delhi for allowing me to pursue my research work along with teaching. I am deeply grateful for their thorough encouragement and support.

I will be simply failing to express myself if I do not mention the names of my senior colleagues **Dr Neeru Kumar** and **Dr Nutan Joshi** from Sri Venkateswara College, University of Delhi. They both were always there to inspire and encourage me to begin my research exploration. My heartfelt thanks are also due to **Dr Sunita Jain**, for her motherly care and support. She has always been there to encourage and motivate me to achieve this goal. I express my sincere thanks to **Dr J Lalita** who has always given her best to shape my academic and interpersonal skills ever since my post-graduation. I extend my sincere thanks and heartfelt gratitude to all of them.

I would also like to sincerely thank the eminent faculty members of the Sri Venkateswara Collge, University of Delhi, **Dr Mukul Sharma**, **Dr Chandra Mohan Singh Rawat** and **Prof Sanjay Kumar**. They were always concerned about my research work and kept motivating and encouraging me from time to time.

I am also thankful to my colleague **Dr Swati Sharma** for the honest opinion and advice she gave at the beginning of my research work. I also thank my other co-workers

Ms Shubhra Gupta and *Dr Rakhi Narang* for their supportive association. My sincere thanks are also extended to the technical staff of Department of Electronics, Sri Venkateswara College, University of Delhi, *Ms K Sri Lakshmi*, *Mr G Krishna Murthy*, *Mr P Narasimha Rao*, *Mr Reji Joseph* and *Ms Jayamma*, for their concern and wishes throughout my research work. I would also like to thank my all-old and present *students* for their faith, respect and love.

My heartfelt thanks and gratitude are also due to my invaluable mentor *Mr Ved Prakash Sharma*, for his constant support and encouragement for the past more than two decades. He has always inspired and guided me in all personal and professional endeavours. He has always been keener than me to see me as a Doctor of Philosophy.

A special note of thanks goes to my *family members*. I am short of words to express how grateful I am to my parents. They have always shown unconditional faith and trust in me. My special thanks to my lovely sister, *Hem Lata*, younger brother, *Vijender Kumar*, and his wife, *Sangeeta Solanki*, for all the care and support I received from all of them. I am equally grateful to my parents-in-law for their concern, consistent encouragement and moral support throughout my research work. My thanks are also due to my brother-in-law, *Rahul Verma*, for all the technical support he provided me for completing this research work.

My heartfelt thanks and love goes to my two years old niece *Mohana*. She has been the apple of my eyes and endowed me with endless power and spirit to accomplish my goals. She acted as my bundle of joy and happiness ever since her birth. She has been a true stress buster even in the lockdowns imposed by authorities due to the prevailing Covid19 pandemic. I humbly pray to Almighty to always shower his choicest blessings over her.

Finally, as a special remark, I would like to express my heartfelt and warmest appreciation to my tender and considerate wife, *Dr Neha Verma*. She has been the true pillar of my success who always stood by me in all difficulties. She has been an incredible support during this period and she believed in me unconditionally. Without her support and sacrifices, this work would not have been possible. I would like to thank her for being with me patiently throughout this period with love and understanding.

I feel truly indebted to all those, whose names remain unmentioned but who have never retraced back from helping whenever the need arose.

Hari Singh

New Delhi, India

April 2022

LIST OF PUBLICATIONS

1. **H. Singh**, K. Srivastava, S. Kumar, and B. K. Kanaujia, “A Planar Dual-Band Antenna for ISM/Wearable Applications,” *Wirel. Pers. Commun.*, vol. 118, no. 1, pp. 631–646, 2021, doi: 10.1007/s11277-020-08036-0.
2. **H. Singh**, B. K. Kanaujia, A. Kumar, K. Srivastava, and S. Kumar, “Dual-resonance ultra-miniaturised textile antenna for ISM/wearable applications,” *Int. J. Electron.*, pp. 1–21, 2021, doi: 10.1080/00207217.2021.2001870.
3. **H. Singh**, B. K. Kanaujia, S. Kumar, and K. Srivastava, “A Compact Wideband Flexible Antenna for Wireless Medical Telemetry Services,” *Wirel. Pers. Commun.*, no. 0123456789, pp. 1–19, 2021, doi: 10.1007/s11277-021-09246-w.
4. **H. Singh**, B. K. Kanaujia, A. Kumar, K. Srivastava, and S. Kumar, “Wideband textile multiple-input-multiple-output antenna for industrial, scientific and medical (ISM)/wearable applications,” *Int. J. RF Microw. Comput. Eng.*, vol. 30, no. 12, pp. 1–14, 2020, doi: 10.1002/mmce.22451.
5. **H. Singh**, B. K. Kanaujia, A. Kumar, K. Srivastava, and S. Kumar, “Design and development of a Dual-Band Dual-Polarization Dual-Sense Textile MIMO Antenna for WBAN/WLAN/ISM/Wearable Applications,” *IEEE Internet of Things Journal* (*Communicated*)

CONTENTS

Acknowledgement	vii-xi
List of publications	xiii
Contents	xv-xix
List of Figures	xxi-xxix
List of Tables	xxxi-xxxii
List of Abbreviation	xxxiii-xxxv
Abstract	xxxvii-xxxix
Chapter 1- Introduction	3
1.1 What is an Antenna?	3
1.2 Types of Antennas	3
1.2.1. Wire Antennas	3
1.2.2. Aperture Antennas	4
1.2.3. Microstrip Antennas	4
1.2.4. Array Antennas	4
1.2.5. Reflector Antennas	4
1.2.6. Lens Antennas	4
1.3 Overview of Microstrip Patch Antenna (MPA)	4
1.4 Feeding Techniques of Microstrip Patch Antenna (MPA)	7
1.4.1. Microstrip Line Feed	7
1.4.2. Co-Axial Feed	8
1.4.3. Proximity Coupling Feed	8
1.4.4. Aperture Coupling Feed	9
1.4.5. Coplanar Waveguide (CPW) Feed	10
1.5 Properties of Microstrip Patch Antenna (MPA)	10
1.5.1. Voltage Standing Wave Ratio (VSWR)	10
1.5.2. Radiation Pattern	11
1.5.3. Gain	11
1.5.4. Polarization	11
1.6 Advantages of Microstrip Patch Antenna (MPA)	12

1.7 Disadvantages of Microstrip Patch Antenna (MPA)	13
1.8 Applications of Microstrip Patch Antenna (MPA)	13
1.9 Multiple-Input-Multiple-Output (MIMO) Antenna	14
1.10 Advantages of MIMO	14
1.11 Disadvantages of MIMO	15
1.12 Wireless Body Area Network (WBAN)	15
1.13 Non-Textile and Textile Wearable Antennas for WBAN	17
1.14 Advantages of Fully-Textile Antenna	17
1.15 Disadvantages of Fully-Textile Antenna	17
1.16 Challenges of Designing Wearable Antennas	17
1.16.1 Bending	18
1.16.2 Specific Absorption Rate (SAR)	18
1.16.3 Integration and Placement	18
1.16.4 Water Absorption	18
1.17 Applications of Wearable Antennas	19
1.18 Objective of Thesis	19
1.19 Methodology	20
1.19.1. Designing of the Antenna	20
1.19.2. Simulation of the Antenna	21
1.19.3. Fabrication of the Antenna	21
1.19.4. Measurement of the Antenna	22
1.20 Organization of Thesis	22
Chapter 2- Literature Review	27
2.1 Introduction	27
2.2 Non-Textile Antennas for Wearable Applications	27
2.3 Textile Antennas for Wearable Applications	34
2.4 Circularly Polarized Textile Antennas for Wearable Applications	44
2.5 Textile Multiple-Input-Multiple-Output Antennas for Wearable Applications	49
Chapter 3-A Planar Dual-Band Antenna for ISM/Wearable Applications	61
3.1 Introduction	61

3.2 Antenna Topology	63
3.3 Parametric Analyses	67
3.4 Antenna Performances in Free Space	69
3.4.1 Reflection Coefficients	69
3.4.2 Radiation Pattern and Gain	70
3.4.3 Surface Current Distribution	70
3.5 Antenna Performances on Human Body	71
3.5.1 Bending Analysis	71
3.5.2 Specific Absorption Ratio (SAR)	74
3.6 Conclusions	75
Chapter 4-A Compact Wideband Flexible Antenna for Wireless Medical Telemetry Services	79
4.1 Introduction	79
4.2 Antenna Topology	81
4.3 Parametric Analysis	85
4.4 Antenna Performances in Free Space	89
4.4.1 Radiation Patterns and Gain	90
4.4.2 Surface Current Distribution	91
4.5 Antenna Performances on Human Body	91
4.5.1 Bending of the Antenna	91
4.5.2 Specific Absorption Ratio (SAR)	92
4.6 Conclusions	93
Chapter 5-Dual-Resonance Ultra-Miniaturized Textile Antenna for ISM/Wearable Applications	97
5.1 Introduction	97
5.2 Antenna Topology	99
5.2.1 Preparation and Characterization of Non-Conductive and Conductive Materials	99
5.2.2 Step-Wise Designing of the Proposed Antenna	107
5.3 Antenna Performances in Free Space	108

5.3.1 Reflection Coefficients (S_{11}) and Gain	108
5.3.2 Radiation Patterns	109
5.3.3 Surface Current Distribution	110
5.3.4 Crumpling Analysis	111
5.4 Antenna Performances on Human Body	112
5.4.1 Reflection Coefficients, Gain, Radiation Efficiency and Front-To-Back Ratio for various Tissue Models	112
5.4.2 Bending Analysis	114
5.4.3 Radiation Pattern	116
5.4.4 SAR Analysis	116
5.5 Conclusions	120
Chapter 6-Wideband Textile Multiple-Input-Multiple-Output Antenna for Industrial, Scientific and Medical (ISM)/Wearable Applications	123
6.1 Introduction	123
6.2 Antenna Topology	125
6.3 Antenna Performances in Free Space	129
6.3.1 Return Loss, Isolation, and Gain	129
6.3.2 Isolation Study	130
6.3.3 Diversity Performance	131
6.3.4 Surface Current Distribution	133
6.3.5 Radiation Pattern	133
6.4 Antenna Performances on Human Body	136
6.4.1 Return Loss, Isolation, Gain, and Radiation Efficiency	137
6.4.2 Diversity Performance	139
6.4.3 Radiation Pattern	139
6.4.4 Bending Analysis	141
6.4.5 SAR Analysis	142
6.5 Conclusions	143
Chapter 7- Fully-Textile Dual-Band Dual-Sense MIMO Antenna for WBAN/WLAN/ISM/Wearable IoT Applications	147

7.1 Introduction	147
7.2 Antenna Topology	150
7.2.1 Antenna Design	150
7.2.2 Antenna Evolution	152
7.2.3 Polarization Diversity	155
7.2.4 Circuit Model	156
7.3 Antenna Performances in Free Space	158
7.3.1 Return Loss, Isolation, Axial Ratio, and Gain	158
7.3.2 Diversity Performance	159
7.3.3. Surface Current Distribution	162
7.3.4 Radiation Pattern	162
7.4 Antenna Performances on Human Body	163
7.4.1 Return Loss, Isolation, Axial Ratio, Gain, and Radiation Efficiency	164
7.4.2 Diversity Performance	167
7.4.3 Radiation Pattern	167
7.4.4 Bending Analysis	169
7.4.5 Specific Absorption Rate (SAR)	170
7.5 Conclusions	172
Chapter 8- Conclusion and Future Scope	175
8.1 Conclusion	175
8.2 Impact of Proposed Work	178
8.3 Limitations of Proposed Work	178
8.4 Future Scope	178
References	181
Publications	203

LIST OF FIGURES

Chapter 1	Introduction	3
1.1	Geometry of Microstrip Patch Antenna (MPA)	6
1.2	Various geometries of the microstrip patch (a) Square, (b) Rectangular, (c) Triangular, (d) Circular, (e) Dipole, (f) Elliptical, (g) Circular-ring, (h) Circular-ring-sector and (i) Other (E-shaped)	6
1.3	Feeding Method: Microstrip Line Feed	7
1.4	Feeding Method: Co-axial Feed	8
1.5	Feeding Method: Proximity Coupling Feed	9
1.6	Feeding Method: Aperture Coupling Feed	9
1.7	Feeding Method: Co-planar Feed	10
1.8	Classification of polarization	12
1.9	A 3×3 MIMO Antennas Configuration	14
1.10	Illustration of Wireless Body Area Network (WBAN)	16
1.11	The methodology adopted in the current work	21
Chapter 2	Literature Review	27
2.1	Designed and Fabricated Prototypes of the antenna presented [29] (a) Antenna Configuration and (b) Fabricated Prototype	28
2.2	Photograph of antenna prototype presented in [30]	28
2.3	Photograph of the antenna prototype presented in [31] (a) Top View, (b) Bottom View, (c) Feeding Network PCB, and (d) Zoomed in connection	29
2.4	Photograph of the antenna presented in [32] (a) Antenna Configuration and (b) Fabricated Prototype under Bending	29
2.5	Fabricated Prototype of the antenna presented in [33]	30
2.6	Photograph of the fabricated prototype presented in [34] (a) Flat Condition and (b) Bent Condition	31
2.7	Photographs of the antenna presented in [35] (a) Designed Antenna (b) Fabricated Antennas for Wireless Power Transfer	31

2.8 Designed and Fabricated Prototypes presented in [36] (a) Designed Antenna, (b) Fabricated Antenna, and (c) Fabricated Antenna with Metallic Casing	32
2.9 Photographs of the antenna presented in [37] (a) Designed Antenna and (b) Fabricated Antenna	33
2.10 Antenna Configuration presented in [38]	34
2.11 Antenna Configuration presented in [39]	35
2.12 Antenna Configuration presented in [40]	35
2.13 Antenna Configuration presented in [41]	36
2.14 Antenna Configuration presented in [43]	36
2.15 Antenna Prototype (Fabricated) of the antenna presented in [44]	37
2.16 Antenna Prototypes presented in [45] (a) Disc Monopole CPW Antenna and (b) Annular Slot Circular Antenna	37
2.17 Antenna Configuration presented in [46]	38
2.18 Photographs of the antenna presented in [47] (a) Designed Antenna and (b) Fabricated Antenna	38
2.19 Designed and Fabricated Prototype of the antenna presented in [48]	39
2.20 Photographs of the antenna presented in [49] (a) Designed Antenna and (b) Fabricated Prototype	39
2.21 Photographs of the antenna presented in [50] (a) Designed Antenna, (b) Top View of Fabricated Antenna, and (c) Bottom View of Fabricated Antenna	40
2.22 Photographs of the antenna presented in [51] Fabricated Prototypes using different conductive parts: (a) pure copper antenna, (b) e-textile in the patch and pure copper in-ground, and (c) fully electro textile antenna	41
2.23 Antenna Prototypes presented in [52] (a) Designed Configuration and (b) Fabricated Antenna	41
2.24 Antenna Prototype presented in [53] (a) Designed Configuration and (b) Fabricated Prototype	42
2.25 Fabricated Prototype of the antenna presented in [54]	44
2.26 Fabricated Prototype of the antenna presented in [55]	45
2.27 Fabricated Prototype of the antenna presented in [56]	45
2.28 Fabricated Prototype of the antenna presented in [57]	46

2.29 Photograph of the antenna presented in [58]: (a) Front View and (b) Back View	46
2.30 Antenna Configuration presented in [59]	47
2.31 Photographs of the antenna presented in [60] (a) Antenna Design and (b) Fabricated Prototype	47
2.32 Designed and Fabricated Prototypes of the antenna presented in [61]: (a) Antenna Configuration and (b) Fabricated Prototype	48
2.33 Photographs of the antenna presented in [62] (a) Antenna Design and (b) Fabricated Antenna	48
2.34 Photographs of the antenna presented in [63] (a) Designed Antenna and (b) Fabricated Prototype	49
2.35 Antenna Prototypes presented in [64] (a) Antenna Configuration and (b) Fabricated Prototype	50
2.36 Antenna Prototypes presented in [65] (a) Antenna Configuration and (b) Fabricated Prototype	51
2.37 Antenna Configuration presented in [66] (a) Top View and (b) Back View	51
2.38 Antenna Configuration presented in [67]	52
2.39 Antenna Prototypes presented in [68] (a) Antenna Configuration and (b) Fabricated Prototype	52
2.40 Antenna Prototypes presented in [69] (a) Antenna Configuration and (b) Fabricated Prototype	53
2.41 Antenna Prototypes presented in [70] (a) Antenna Configuration and (b) Fabricated Prototype	53
2.42 Antenna Prototypes presented in [71] (a) Antenna Configuration and (b) Fabricated Prototype	54
2.43 Antenna Prototypes presented in [72] (a) Antenna Configuration and (b) Fabricated Prototype	55
2.44 Antenna Configuration presented in [73] (a) Top View and (b) Bottom View	55
2.45 Antenna Configuration presented in [74] (a) Top View and (b) Bottom View	56
2.46 Photographs of the antenna presented in [75] (a) Designed Antenna and (b) Fabricated Prototype	56

Chapter 3 A Planar Dual-Band Antenna for ISM/Wearable Applications 61

3.1 Antenna layout (a) top view (b) bottom view (c) top view of the fabricated prototype (d) bottom view of the fabricated prototype	64
3.2 Design steps of the proposed antenna (a) step 1 (b) step 2 (c) step 3 (d) step 4 (e) step 5.	65
3.3 Reflection coefficients $ S_{11} $ of the design steps (a) 1 to 3 (b) 4 to 5.	66
3.4 Reflection coefficients $ S_{11} $ due to variation in parameter f	67
3.5 Reflection coefficients $ S_{11} $ due to variation in parameter g	68
3.6 Reflection coefficients $ S_{11} $ due to variation in parameter l	68
3.7 Reflection coefficients $ S_{11} $ due to variation in parameter m	69
3.8 Simulated and measured reflection coefficients $ S_{11} $	69
3.9 Simulated and measured radiation patterns (a) 918 MHz (b) 2450 MHz	70
3.10 Surface current distribution of the proposed antenna (a) 918 MHz (b) 2450 MHz	71
3.11 Bending analysis of the antenna along (a) x-axis (b) y-axis (c) y+45° axis (d) y-45° axis	72
3.12 Reflection coefficients $ S_{11} $ due to bending along (a) x-axis (b) y-axis (c) y+45° axis (d) y-45° axis	74
3.13 Simulated average SAR of the proposed antenna for 1 g of tissue (a) 918 MHz (b) 2450 MHz	74

Chapter 4 A Compact Wideband Flexible Antenna for Wireless Medical Telemetry Services 79

4.1 Proposed antenna (a) schematic (b) fabricated prototype	83
4.2 Stepwise designing of the proposed antenna (a) step 1 (b) step 2 (c) step 3 (d) step 4 (e) step 5 (f) step 6 (g) step 7 (h) step 8 (i) step 9 (j) step 10	84
4.3 Stepwise reflection coefficients (a) steps 1-5 (b) steps 6-10	85
4.4 Reflection coefficients due to variation in the position of the feed line	86
4.5 Reflection coefficients due to variation in parameter ‘m’	86
4.6 Reflection coefficients due to variation in parameter ‘n’	87
4.7 Reflection coefficients due to variation in parameter ‘p’	87
4.8 Reflection coefficients due to variation in parameter ‘q’	88

4.9 Reflection coefficients due to variation in parameter ‘r’	88
4.10 Reflection coefficients due to variation in parameter ‘s’	89
4.11 Simulated and measured reflection coefficients of the proposed antenna	89
4.12 Simulated and measured radiation patterns (a) 1397.5 MHz (b) 1429.5 MHz	90
4.13 Simulated and measured gain of the proposed antenna	90
4.14 Surface current distribution of the proposed antenna (a) 1397.5 MHz (b) 1429.5 MHz	91
4.15 Bending direction of the antenna along the x-axis	91
4.16 Reflection coefficients due to bending along the x-axis	92
4.17 Simulated average SAR of the proposed antenna for 1 g of tissue (a) 1397.5 MHz (b) 1429.5 MHz	92
Chapter 5 Dual-Resonance Ultra-Miniaturized Textile Antenna for ISM/Wearable Applications	97
5.1 Textile materials: (a) Cordura 500D Nylon, (b) Polyester, (c) Cordura General, (d) Denim	100
5.2 Textile materials: (a) Lycra, (b) Felt	100
5.3 Preparation of textile fabric samples (a) size of the sample, (b) preparation of samples	101
5.4 Measurement setup: (a) sample holder (dielectric material test fixture), (b) samples	101
5.5 Variation of dielectric constant and frequency for different textile materials: (a) Cordura 500D Nylon, (b) Polyester, (c) Cordura General, (d) Denim	103
5.6 Variation of dielectric constant and frequency for different textile materials: (a) Lycra, (b) Felt	104
5.7 Proposed textile antenna: (a) front view (b) back view	106
5.8 Step-wise evolution of the textile antenna: (a) ANT. 1, (b) ANT. 2, (c) ANT. 3.	107
5.9 Simulated reflection coefficients for different antenna configurations	108
5.10 Prototype of the proposed textile antenna: (a) front view, (b) back view, (c) reflection coefficients measurement	109
5.11 Simulated and measured reflection coefficients and gain of the antenna (ANT. 3)	109

5.12 Radiation patterns of the antenna (red: measured, black: simulated): (a) E-plane at 2.45 GHz, (b) H-plane at 2.45 GHz, (c) E-plane at 5.8 GHz, (d) H-plane at 5.8 GHz	110
5.13 Simulated surface current distributions at: (a) 2.45 GHz, (b) 5.8 GHz	111
5.14 Crumpling effect on the antenna	111
5.15 Tissue models: (a) small cubic phantom-X, (b) small cubic phantom-Y, (c) cylindrical bent-X, (d) cylindrical bent-Y	112
5.16 Simulated reflection coefficients for different tissue models	113
5.17 Simulated results of the textile antenna for different tissue models: (a) gain, (b) efficiency	114
5.18 Front-to-back ratio of the antenna	114
5.19 Bending analysis of the proposed textile antenna: (a) bent-X, (b) bent-Y	115
5.20 Radiation patterns of the antenna for different tissue models: (a) E-plane at 2.45 GHz, (b) H-plane at 2.45 GHz, (c) E-plane at 5.8 GHz, (d) H-plane at 5.8 GHz	116
5.21 SAR distribution patterns for arm model (simulated power=10 mW): (a) 2.45 GHz (1 g), (b) 5.0 GHz (1 g), (c) 5.8 GHz (1 g)	117
5.22 SAR distribution patterns for arm model (simulated power=10 mW): (a) 2.45 GHz (10 g), (b) 5.0 GHz (10 g), (c) 5.8 GHz (10 g)	117
5.23 Simulated results for maximum SAR	118

Chapter 6 Wideband Textile Multiple-Input-Multiple-Output Antenna for Industrial, Scientific and Medical (ISM)/Wearable Applications 123

6.1 Configuration of the textile MIMO antenna (a) top view (b) bottom view	126
6.2 Prototype of the textile MIMO antenna (a) top view (b) bottom view	126
6.3 Step-wise designing of the two-element MIMO antenna (a) step-1 (b) step-2 (c) step-3 (d) step-4 (e) step-5 (f) step-6 (g) step-7	127
6.4 Simulated S11 of the design steps of the two-element MIMO antenna	128
6.5 Simulated S21 of the design steps of the two-element MIMO antenna	128
6.6 Simulated and measured S-parameters and gain of the two-element MIMO antenna	129
6.7 Top view of the two-element MIMO with meander-line structure	130
6.8 Simulated S-parameters of the two-element MIMO with meander-line structure	131

6.9 ECC and DG of the two-element MIMO antenna	132
6.10 ME of the two-element MIMO antenna	132
6.11 Surface current distribution of the MIMO antenna at (a) 2.45 GHz (b) 5.8 GHz	133
6.12 Simulated and measured radiation patterns of the two-element textile MIMO antenna (at $\varphi=0^\circ$) (a) 2.45 GHz/port-1 (b) 2.45 GHz/port-2 (c) 5.8 GHz/port-1 (d) 5.8 GHz/port-2	134
6.13 Simulated and measured radiation patterns of the two-element textile MIMO antenna when both port-1 and -2 are excited simultaneously (at $\varphi=0^\circ$) (a) 2.45 GHz (b) 5.8 GHz	135
6.14 3-D radiation patterns of the two-element textile MIMO antenna (a) 2.45 GHz/port-1 (b) 2.45 GHz/port-2 (c) 5.8 GHz/port-1 (d) 5.8 GHz/port-2	135
6.15 3-D radiation patterns of the two-element textile MIMO antenna when both port-1 and -2 are excited simultaneously (a) 2.45 GHz (b) 5.8 GHz	136
6.16 Human tissue models (a) cubic phantom/x-direction (b) cubic phantom/y-direction (c) cylindrical phantom/x-direction (d) cylindrical phantom/y-direction	136
6.17 Simulated S-parameters of the textile MIMO antenna for different tissue models (a) S11 (b) S21	138
6.18 Simulated results of the textile MIMO antenna for different tissue models (a) gain (b) efficiency	139
6.19 Simulated radiation patterns of the two-element textile MIMO antenna (at $\varphi=0^\circ$) (a) 2.45 GHz/port-1 (b) 2.45 GHz/port-2 (c) 5.8 GHz/port-1 (d) 5.8 GHz/port-2	140
6.20 Simulated radiation patterns of the two-element textile MIMO antenna when port-1 and -2 are excited simultaneously (at $\varphi=0^\circ$) (a) 2.45 GHz (b) 5.8 GHz	141
6.21 Bending analysis of the proposed textile MIMO antenna for various tissue models (a) S11 (b) S21	142
6.22 Simulated results for maximum SAR	142
Chapter 7 Fully-Textile Dual-Band Dual-Sense MIMO Antenna for WBAN/WLAN/ISM/Wearable IoT Applications	147
7.1 Illustration of textile antenna for IoT	148

7.2 Proposed fully-textile dual-band MIMO antenna: (a) top view, (b) bottom view	151
7.3 Prototype of the fully-textile MIMO antenna: (a) top view, (b) bottom view	151
7.4 Step-wise development of the fully-textile two-element MIMO antenna: (a) ANT~1, (b) ANT~2, (c) ANT~3, (d) ANT~4, (e) ANT~5, (f) ANT~6	153
7.5 Simulated S_{11} of the design steps	154
7.6 Simulated S_{21} of the design steps	154
7.7 Simulated axial ratio of the design steps	155
7.8 Surface current distribution at 5.8 GHz when port#1 and port#2 are excited	156
7.9 (a) Equivalent circuit of the MIMO antenna, (b) $ S_{11} $ and $ S_{12} $ comparison of the EM and circuit models	157
7.10 Simulated and experimental results of the proposed antenna: (a) S-parameters (S_{11} and S_{22}), (b) gain and axial ratio	159
7.11 ECC and DG of the proposed antenna	160
7.12 ME of the fully-textile two-element MIMO antenna	161
7.13 TARC of the fully-textile two-element MIMO antenna	161
7.14 Surface current distribution of the fully-textile MIMO antenna: (a) 2.45 GHz, (b) 5.8 GHz	162
7.15 Radiation patterns of the proposed antenna: (a) 2.45 GHz/Port#1, (b) 2.45 GHz/Port#2, (c) 5.8 GHz/Port#1, (d) 5.8 GHz/Port#2	163
7.16 Radiation patterns of the proposed antenna when port#1 and port#2 are excited simultaneously: (a) 2.45 GHz, (b) 5.8 GHz	163
7.17 Human tissue models/phantoms: (a) cubic phantom, (b) cylindrical phantom/x-direction, (c) cylindrical phantom/y-direction	164
7.18 Simulated S-parameters of the proposed antenna for different phantoms: (a) S_{11} , (b) S_{21}	165
7.19 Axial ratio (simulated) of the proposed antenna for various phantoms	166
7.20 Simulated results of the proposed antenna for different phantoms: (a) gain, (b) radiation efficiency	167
7.21 3-D radiation patterns of the proposed antenna: (a) cubic model, (b) bent x-model, (c) bent y-model	169

7.22 Bending analysis of the proposed fully-textile MIMO antenna for various phantoms: (a) S_{11} , (b) S_{21} , (c) axial ratio	170
7.23 Simulated results for maximum SAR	171

LIST OF TABLES

Chapter 1	Introduction	3
Table 1.1	Frequency Bands of Operation for WBAN	16
Chapter 2	Literature Review	27
Table 2.1	Non-Textile Antennas for Wearable Applications	33
Table 2.2	Textile Antennas for Wearable Applications	43
Table 2.3	Circularly Polarized Textile Antennas for Wearable Applications	49
Table 2.4	Textile Multiple-Input-Multiple-Output Antennas for Wearable Applications	57
Chapter 3	A Planar Dual-Band Antenna for ISM/Wearable Applications	61
Table 3.1	Comparison of the proposed antenna with other antennas	63
Table 3.2	Dimensions of the proposed antenna	64
Table 3.3	Simulated and Measured Gain	70
Chapter 4	A Compact Wideband Flexible Antenna for Wireless Medical Telemetry Services	79
Table 4.1	Comparison of the proposed antenna with other antennas	81
Table 4.2	Dimensions of the proposed antenna	83
Chapter 5	Dual-Resonance Ultra-Miniaturized Textile Antenna for ISM/Wearable Applications	97
Table 5.1	Properties of the textile materials at 2.45 GHz	105
Table 5.2	Dimensions of the proposed textile antenna	107
Table 5.3	Performance summary of different antenna configurations	108
Table 5.4	Maximum allowable input power	118
Table 5.5	Performance comparison of the proposed textile antenna with other reported works	119

Chapter 6	Wideband Textile Multiple-Input-Multiple-Output Antenna for Industrial, Scientific and Medical (ISM)/Wearable Applications	123
Table 6.1	Parameters of the two-element MIMO antenna	126
Table 6.2	Dimensions of the various layers of tissue models	137
Table 6.3	Comparison of the proposed work with other MIMO antennas	143
Chapter 7	Fully-Textile Dual-Band Dual-Sense MIMO Antenna for WBAN/WLAN/ISM/Wearable IoT Applications	147
Table 7.1	Dimensions of the two-element textile MIMO antenna	151
Table 7.2	Dimensions of the tissue models	164
Table 7.3	Comparison of the proposed work with other reported MIMO antennas	171
Chapter 8	Conclusion and Future Scope	175
Table 8.1.	Summary of proposed antennas	177

LIST OF ABBREVIATIONS

Ag	Argentum (Silver)
BAN	Body Area Network
BCC	Body Centric Communication
BER	Bit Error Rate
BSN	Body Sensor Network
CCo	Carbon-Coated Cobalt
CPW	Coplanar Waveguide
CPW	Circularly Polarization
CST	Computer Simulation Technology
CT	Computed tomography
Cu	Copper
DAK	Dielectric Assessment Kit
DG	Diversity Gain
ECC	Envelope Correlation Coefficient
EM	Electromagnetic
FCC	Federal Communications Commission
FlexIFA	Flexible Inverted-F Antenna
GHz	Giga Hertz
GPS	Global Positioning System
HMSIW	Half-Mode Substrate Integrated Waveguide
ICNIRP	International Commission on Non-Ionizing Radiation Protection
IEEE	Institute of Electrical and Electronics Engineers
IoT	Internet of Things
ISM	Industrial, Scientific and Medical
ITU	International Telecommunication Union
LHCP	Left-Handed Circular Polarization
LP	Linear Polarization

LTE	Long-Term Evolution
LV	Louis Vuitton
MASB	Meteorological Aids Service Band
MBAN	Medical Body Area Network
ME	Multiplexing Efficiency
MEG	Mean Effective Gain
MHz	Mega Hertz
MICS	Medical Implant Communication System
MIMO	Multiple-Input-Multiple-Output
mmW	Millimeter-Wave
MPA	Microstrip Patch Antenna
MRI	Magnetic Resonance Imaging
Ni	Nickel
NL	Neutralization Line
PANI	Polyaniline
PCB	Printed Circuit Board
PCS	Personal Communication Services
PET	Polyethene Terephthalate
QMSIW	Quarter-Mode Substrate Integrated Waveguide
QoS	Quality of Service
RF	Radio Frequency
RFID	Radio Frequency Identification
RHCP	Right-Handed Circular Polarization
SAR	Specific Absorption Ratio
SEM	Scanning Electron Microscopy
SISO	Single-Input-Single-Output
SIW	Substrate Integrated Waveguide
SMA	Sub-Miniature Version A
SMP	Sub-Miniature Push-on
SNR	Signal-to-Noise Ratio
SRR	Split-Ring Resonators

TARC	Total Active Reflection Coefficient
TDR	Time-Domain Reflectometry
TM	Transverse Magnetic
UMTS	Universal Mobile Telecommunication System
UWB	Ultra Wide Band
VNA	Vector Network Analyzer
VSWR	Voltage Standing Wave Ratio
WBAN	Wireless Body Area Network
WiMAX	Worldwide Interoperability For Microwave Access
WMTS	Wireless Medical Telemetry System
WPAN	Wireless Personal Area Network

**Investigation on Wearable Antennas
for
Body Area Network**

By

Hari Singh

School of Computational and Integrative Sciences

Jawaharlal Nehru University

New Delhi, India

March-2022

*“We want that education by which character is formed, strength of mind is increased,
the intellect is expanded, and by which one can stand on one’s own feet”*

–Swami Vivekananda

ABSTRACT

The requirement for wearable technology has increased enormously in the recent past. Some of the key areas that have really accelerated this growth are the demand for miniaturized & portable wireless devices, the advent of high-speed & low-power wireless networks and the ever-evolving energy-harvesting techniques. Nowadays, wearable technology finds numerous applications in the areas of positioning, navigation, military, prevention of diseases, maintenance of health, remote patient management, fashion, entertainment, infotainment, etc. The choice of antenna plays a key role in most of these applications. This has led to the evolution of compact, lightweight, planar, conformal and efficient wearable antennas. These wearable antennas are made to work wirelessly in a body area scenario for body area network applications (BANs).

Wearable antenna design and development are of particular importance in this context. This is in line with the current thesis, which comprises five main objectives. Firstly, the dissertation presents a planar, dual-band antenna for ISM band applications. This antenna is made up of a non-textile flexible substrate with a ground plane, a rectangular patch and a 50Ω microstrip feedline. The antenna is loaded with a number

of slots for obtaining dual resonance in the spectra of 902-928 MHz and 2400-2480 MHz. The bending and specific absorption rate (SAR) analysis done for the antenna show that the presented antenna can be employed for wearable applications.

Secondly, the thesis focuses on the design and development of a planar small size coplanar waveguide (CPW)-fed wideband antenna for “*wireless-medical-telemetry-service (WMTS) bands.*” This antenna is also designed on a non-textile flexible substrate. The designed antenna operates at centre frequencies of 1397.5 MHz and 1429.5 MHz covering “*1395-1400 MHz*” and “*1427-1432 MHz*” frequency bands. The antenna has a 620 MHz bandwidth that is greater than the bandwidth of conventional narrow and wearable antennas. The concept of a meander line is used for increasing the bandwidth of the presented antenna. The demonstration of SAR and bending analysis show that the presented antenna can be designed on flexible substrates and show its candidature for the wearable applications.

Thirdly, an ultra-miniaturized, dual-band fully-textile antenna is presented in the thesis. All the layers of the antenna i.e. the ground plane, the substrate layer and the radiating patch are designed using textile fabrics. It also considered various textile fabrics for the characterization to investigate the different possibilities for designing fully textile antennas. Such antennas are a good candidate for body area networks (BAN) as they can be easily integrated into clothing. The proposed antenna uses Felt and Shieldit™ Super conductive material as non-conducting and conducting textile materials. The dual-resonant antenna covers “*2.45 GHz and 5.80 GHz ISM (industrial, scientific and medical) bands*” with bandwidths of 14.2% and 27.5% respectively. The proposed antenna's on-body performance demonstrates that it can be used for wearable applications in all practical situations.

Fourthly, a compact, wideband, two-element, fully-textile “*multiple-input-multiple-output (MIMO)*” antenna is presented for ISM and WLAN band wearable applications. The ground plane and radiating patch of the proposed MIMO antenna are prepared using Shieldit™ Super conductive material on a non-conducting Felt substrate. The antenna covers a wide impedance band of 2.00–6.23 GHz with a maximum mutual coupling of $(S_{21, \max}) -29.26$ dB over the entire resonating band. The antenna uses three rectangular rings and a T-shaped stub for achieving desired isolation between the radiating elements. The realised gain of the proposed antenna is greater

than 2.88 dBi., an envelope-correlation-coefficient (ECC) of less than 0.1, and a diversity-gain (DG) of 9.95 dB. The reasonable on- and off-body performances endorse that ability of the proposed antenna to work efficiently for wearable applications.

Lastly, a compact, dual-resonance, dual-sense, two-element, fully-textile “multiple-input-multiple-output (MIMO)” antenna is included in the thesis. This MIMO antenna is developed using Felt and Shieldit™ Super textile fabrics as non-conducting and conducting materials respectively. It covers 2.18-3.29 GHz and 3.92-6.90 GHz frequency bands with circular polarization (CP) in the 4.92-5.94 GHz band. It provides isolation of more than 15 dB over both resonating bands. The MIMO antenna uses a rectangular-, two triangular- and a T-shaped stubs for reducing the mutual interaction between the radiating elements of the antenna. The “realised gain” of this antenna is > 2.00 dBi, an “envelope correlation coefficient (ECC)” of < 0.12, a “diversity gain (DG)” of ~9.90 dB, and a “multiplexing efficiency (ME)” between ± 2.0 over the resonating bands. The proposed antenna is a good candidate for WBAN/WLAN/ISM/Wearable IoT Applications.

“It still fascinates me to think that here in this room you have radio signals from stations all over the world going through, and we can stick up an antenna and receive them.”

James Alfred Van Allen

1

INTRODUCTION

Over the past few decades, there has been enormous advancement in the field of wireless technology. Although, the term was first introduced in the 19th century but it has seen many developments in the recent past. It has a wide range of applications such as locating, tracking, enhancing security, connecting devices, making calls, accessing the internet, etc. The antennas primarily govern the performance of wireless systems. Thus, the development of lightweight, economical and efficient antennas become almost essential.

1.1 WHAT IS AN AERIAL/ANTENNA?

“A metallic structure that receives and/or transmits electromagnetic or radio waves is known as an aerial/antenna [1].” It is an interface between the electric current flowing through the metal conductors and electromagnetic waves propagating through space. In transmitting mode, the antenna receives the electric current at its terminals from a radio transmitter and radiates the energy as electromagnetic or radio waves. In receiving mode, the antenna intercepts some power of an electromagnetic or radio wave and produces an electric current at its terminals. They come in a wide range of sizes and designs, from little ones that can be seen on rooftops to massive ones capable of collecting signals from satellites millions of miles away. [1]–[3].

1.2 TYPES OF ANTENNAS

In radio systems, various types of antennas are used for different applications. These antennas can be classified in various ways such as operating principle, shape, etc. [1].

1.2.1. Wire Antennas

The wire antennas are available in many shapes like straight-wire/dipole, loop and helical. Loop antennas can take any shape such as square, rectangle, ellipse, or any

other configuration. They can be seen on buildings, automobiles, aircraft, ships, and spacecraft.

1.2.2. Aperture Antennas

The aperture antennas are the most commonly used antennas for microwave applications with several different geometrical configurations available. They can take the form of a horn or a waveguide having rectangular, square, circular, elliptical and other apertures. They are practically used for aircraft & missile, spacecraft and mobile applications as they could be easily mounted on their surfaces.

1.2.3. Microstrip Antennas

A radiating patch is placed over a grounded substrate in microstrip antennas. The radiating patch can be configured in a variety of ways. Rectangular and circular radiating patches, on the other hand, are the most commonly employed due to their simplicity of analysis and fabrication.

1.2.4. Array Antennas

To create the required radiation pattern, a number of radiating components are electrically and geometrically arranged to form array antennas. The array can be arranged such that the arrangement gives maximum, minimum, or desired radiation in a particular direction.

1.2.5. Reflector Antennas

Reflector antennas are used to send and receive radio signals that must traverse millions of miles. Parabolic reflector antennas having a diameter as large as 305 m have been built.

1.2.6. Lens Antennas

The lens antennas are classified in terms of their shapes or types of materials used for their constructions. These antennas are used to transform divergent energy into plane waves. This can be achieved by selecting an appropriate material for the lenses and properly shaping the geometry of the antenna configurations.

1.3 OVERVIEW OF MICROSTRIP PATCH ANTENNA (MPA)

Microstrip patch antennas are most popular in both industry and academia due to their small size, lightweight, low cost, good performance, ease of fabrication and installation. These antennas are conformable to planar as well as non-planar surfaces.

They can be easily manufactured using low-cost printed circuit technology. They show robustness when mounted on any rigid surface. They can be used in high-performance satellite, missile, aircraft and spacecraft applications.

There are some operational disadvantages of microstrip patch antenna such as very narrow bandwidth, low power, low efficiency, high quality-factor, poor polarization, poor scanning performance, etc. However, there are many methods, which can be used to overcome these shortcomings. The antenna's efficiency can be improved by raising the substrate's height [4]. However, the increase in the height introduces undesirable surface waves, which worsens the radiation and polarization characteristics [5], [6]. These undesired surface waves can be lowered by using the concept of cavities [7]. Methods like stacking, probe-feeding, creation of slots & notches and impedance matching can be used for enhancing the bandwidth of these antennas [8].

As with most technological advancements, it is not easy to categorically state who was the originator of the microstrip antenna. The concept of a microstrip patch antenna can be tracked back to the year 1953 (G. A. Deschamps). In the year 1955, H. Gutton and G. Baissinot (French Patent No. 703 113) also filed a patent. However, the fabrication of a microstrip antenna was not possible at that time due to the absence of printing technology and desired substrate materials. It gained popularity in the 1970s. The first microstrip antenna was realized by Robert E. Munson in 1974 [9]. All these developments initiated a rigorous research on the advancement of microstrip patch antenna (MPA) design and development.

A microstrip patch antenna (MPA) consists of a radiating patch, a substrate and a ground plane. The substrate is made up of a non-conducting dielectric material while the radiating patch and the ground plane are made up of a conducting material. The substrate is sandwiched in between the radiating patch and the ground plane as depicted in Fig. 1.1. A lot many dielectric materials having dielectric constants (ϵ_r) in between 2.2 and 12 can be used as substrates. The radiating patch and ground plane can be made using any metallic material such as copper, silver and gold. The dimensions of the ground plane and radiating patch can be calculated for the desired resonant frequency. The thickness of the substrate should be in the range of $0.003\lambda_0 \leq h \leq 0.05\lambda_0$, where λ_0 is the wavelength of the free space [1], [10], [11].

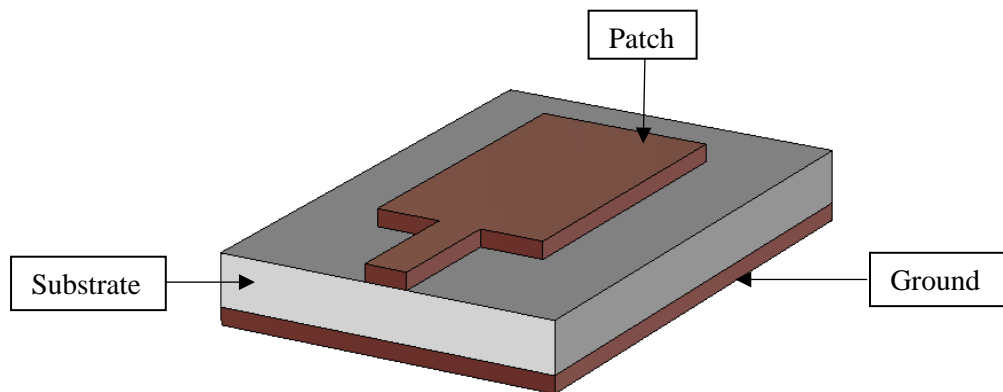


Fig. 1.1 Geometry of “Microstrip Patch Antenna (MPA)”

Often, the microstrip patch antenna is also called as a patch antenna. The conducting radiating patch and the feedline are usually photoetched on a non-conducting dielectric substrate material. The shape and size of the radiating patch may take any configuration such as square, rectangular, triangular, circular, dipole, elliptical, circular ring, circular ring-sector, or any other as shown in Fig. 1.2.

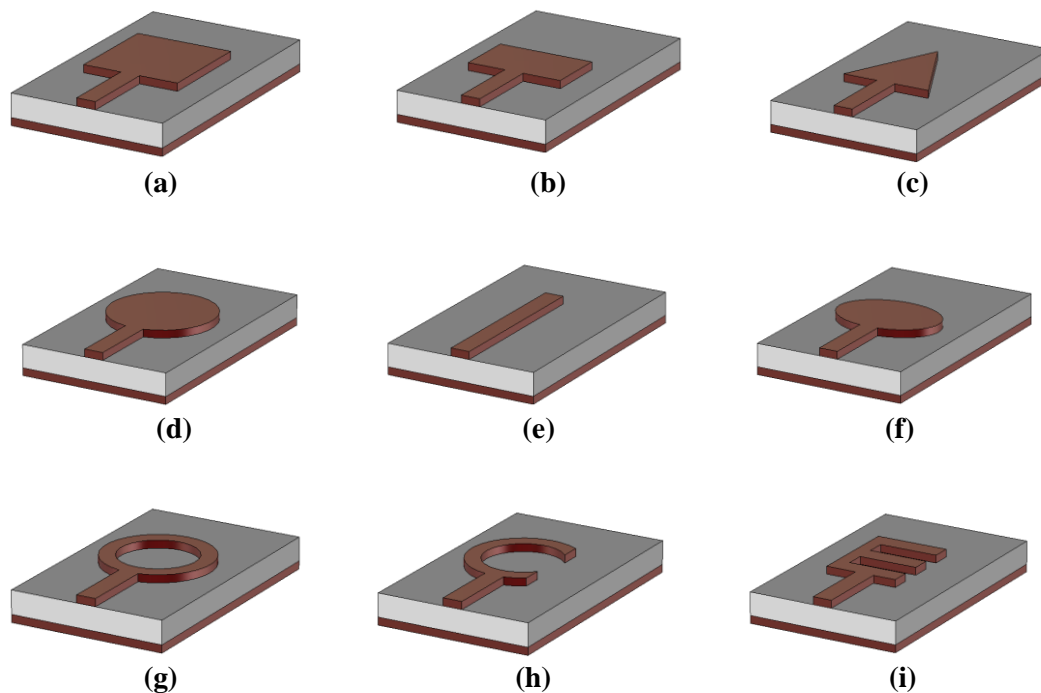


Fig. 1.2 Various geometries of the microstrip patch: “(a) Square, (b) Rectangular, (c) Triangular, (d) Circular, (e) Dipole, (f) Elliptical, (g) Circular-ring, (h) Circular-ring-sector and (i) Other (E-shaped)[1]”

1.4 FEEDING TECHNIQUES OF MICROSTRIP-PATCH-ANTENNA (MPA)

In the designing and development of a microstrip patch antenna, the ground plane and the radiating patch must be joined to excite the antenna. There are various approaches to excite the antenna and are commonly known as feeding techniques. These feeding techniques play a vital role in deciding the working of the antennas. The most popular feeding practises are microstrip line feed, co-axial feed, proximity coupling feed, aperture-coupling feed and coplanar waveguide feed [1], [10], [12], [13]. Every method has its own merits and demerits. Several factors are considered in choosing a suitable feeding technique over others for designing a particular type of antenna. One of the important factors is how effectively and efficiently, the antenna is transferring the input energy to the radiating element. A good impedance matching between the feed and radiating element is required for the efficient working of the microstrip patch antenna. This technique is much easy to model as the dimension and location of the feedline can be optimized in achieving the desired impedance matching.

1.4.1. Microstrip Line Feed

As shown in Fig. 1.3, a conducting strip is constructed on top side of the substrate, together with the patch. The width of the feedline is usually much smaller in comparison with the width of the patch. Through this microstrip-line, RF energy is directly delivered to the radiating patch. However, the increase in the substrate thickness upsurges the surface waves & spurious feed radiation. The resonance bandwidth of this design is practically limited to 2-5%. This technique has been used in [14], [15] because of its ease of modelling and fabrication.

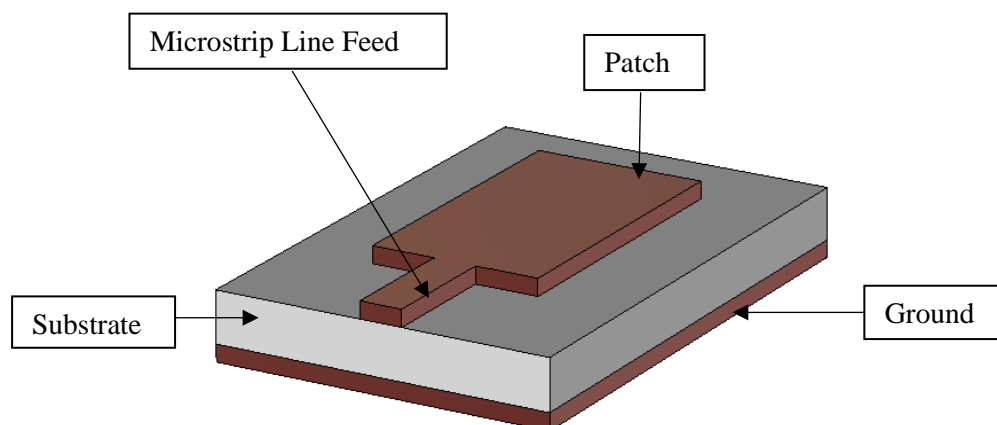


Fig. 1.3. Feeding Method: Microstrip Line Feed

1.4.2. Co-axial Feed

In this technique, the inner (core) and outer (cladding) conductors of the co-axial cable are connected with the radiating patch and the ground plane respectively as depicted in Fig. 1.4. The coaxial feed is simple to manufacture and match, although it does necessitate a substrate slot. It has narrow bandwidth but low spurious radiation. However, it is difficult to employ this feed for the thicker substrates ($h > 0.02\lambda_0$). This technique has been used in [16]–[18] because of its various advantages over microstrip line feed.

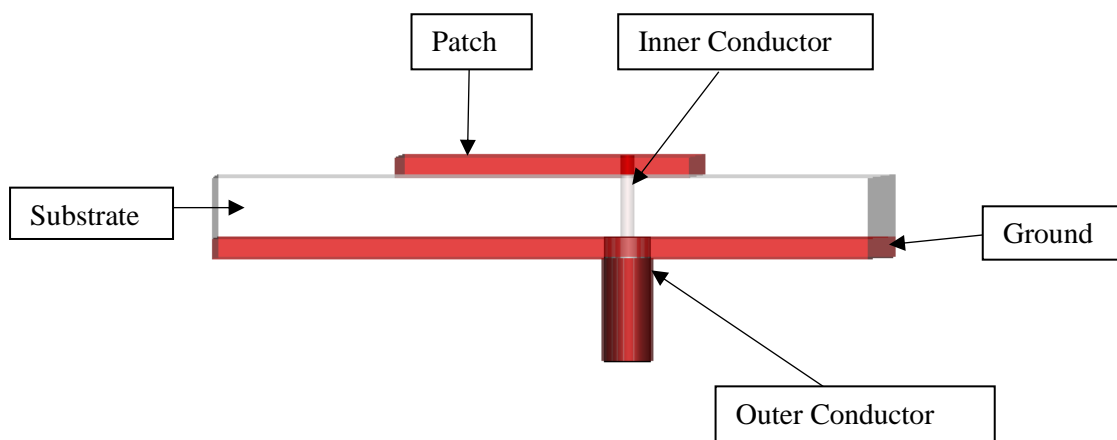


Fig. 1.4. Feeding Method: Co-axial Feed

1.4.3. Proximity Coupling Feed

In this technique, two layers of substrate are used as depicted in Fig.1.5. On the bottom layer substrate, the exciting feed line is printed, while the radiating patch is printed on the upper layer substrate. This technique is well-recognized for its low spurious radiations and wide bandwidth. It provides the maximum bandwidth (as good as 13%) because of the overall increased substrate thickness and coupling between the feedline and the radiating patch. This technique is somewhat easy to model but slightly difficult to fabricate. The alignment of two layers of the substrates is tedious and increases the size of the designed antenna with regard to the thickness. The length of the tuning stub and the patch's 'width-to-line-ratio' can be modified to control the antenna's response [19]. This technique has been used in [20], [21] because of its advantages over the aforementioned techniques.

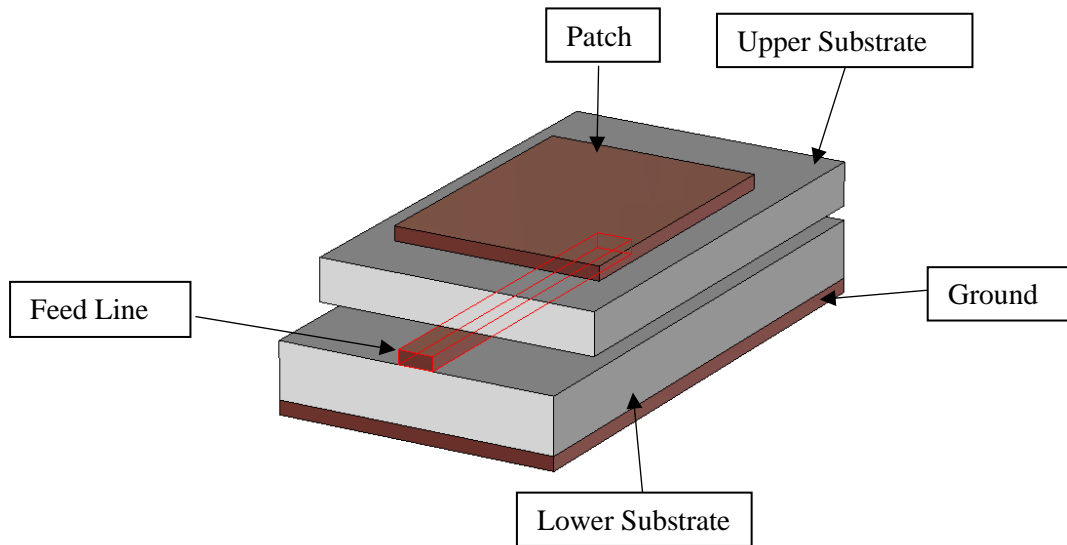


Fig. 1.5. Feeding Method: Proximity Coupling Feed

1.4.4. Aperture Coupling Feed

This technique uses two substrates parted by a ground-plane as shown in Fig. 1.6. Here, the microstrip feedline is placed underneath the lower substrate. The radiating patch of the antenna allowed to couple with the feedline through a slot created on the ground plane parting the two substrates. Typically, the dielectric constant of the lower-side substrate is higher than that of the upper-side substrate while the

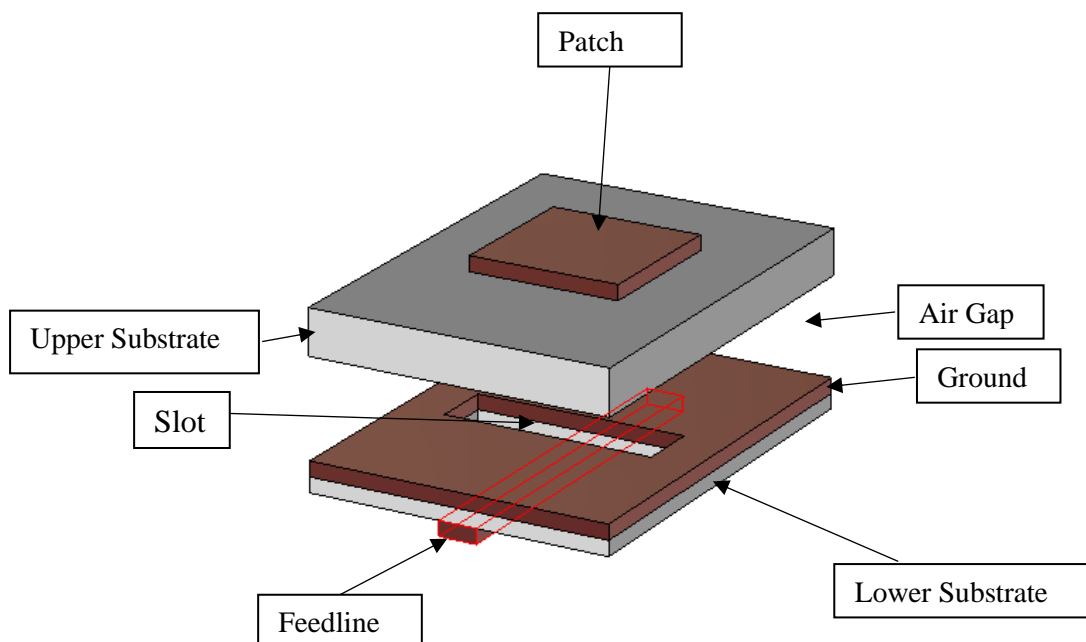


Fig. 1.6. Feeding Method: Aperture Coupling Feed

1.4.5. Coplanar Waveguide (CPW) Feed

In this technique, a single-sided ground and a feeding strip attached to the patch are used. As seen in Fig. 1.7, a small gap separates the feeding strip from the ground plane. On the same side of the dielectric substrate, the entire design, including the radiating patch, ground plane, and feeding strip, is constructed. The key highlights of this technique are its straightforward engineering, minimal efforts required because of monoplane structure, small size, low scattering, low spurious radiation and more extensive data transfer capacity. This technique has been used widely because of its various advantages over other techniques [22], [23].

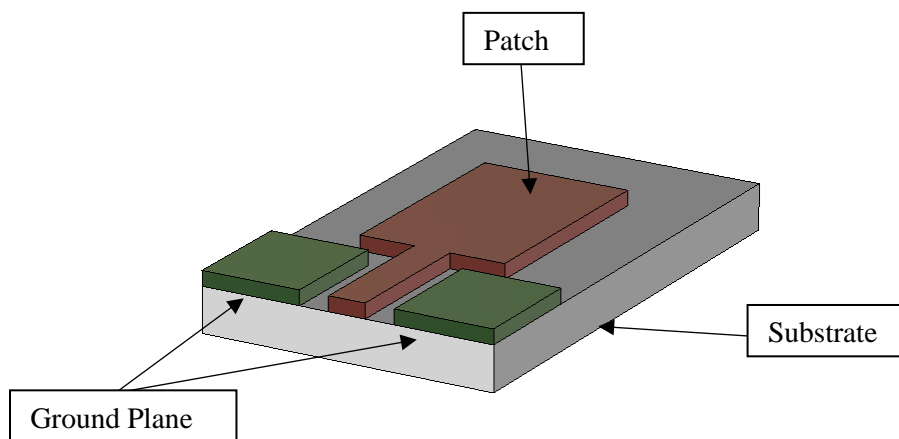


Fig. 1.7. Feeding Method: Co-planar Feed

1.5 PROPERTIES OF MICROSTRIP PATCH ANTENNA (MPA)

The properties of “*Microstrip Patch Antenna (MPA)*” can be best described using several parameters. The definitions of a few important parameters are as follows:

1.5.1. Voltage-Standing-Wave-Ratio (VSWR)

The efficiency of a system to transfer radio frequency power from a power source to a load is known as “*Voltage-Standing-Wave-Ratio (VSWR)*.” This requires a perfect matching between the impedances of source, transmission line, all connectors and load. Ideally, 100% input energy can be transmitted. In real-time systems, some of the energy is reflected back because of imperfect matching.

Mathematically, it is expressed as the ratio of highest and lowest voltage on the transmission line.

$$VSWR = \frac{|V_{max}|}{|V_{min}|} \quad (1.1)$$

It can also be defined as

$$VSWR = \frac{(1 + \Gamma)}{(1 - \Gamma)} \quad (1.2)$$

where Γ =Reflection Coefficient

1.5.2. Radiation Pattern

“The mathematical (or graphical) depiction of an antenna's radiation properties as a function of spatial coordinates is known as the radiation pattern [1].”

The radiation properties include field strength, radiation intensity, flux density and polarization. Mostly, the radiation pattern is plotted for the far-field region i.e., for $R \gg 2D^2/\lambda$, where D represents the largest dimension. The radiation pattern consists of a various lobes such a major lobe, minor lobe(s), side lobe(s) and back lobe(s). The major or main lobe is the radiation lobe that contains the direction of main beam ($\theta=0^\circ$). The radiation in the undesired direction is represented by the minor lobe. The radiation lobes which are adjacent to the main lobe, normally the largest of the minor lobes, are called side lobes.

1.5.3. Gain

“An antenna's gain is defined as the ratio of the radiation intensity in one direction to the radiation intensity that would be gained if the antenna's power was radiated isotopically [1].”

1.5.4. Polarization

An antenna's polarisation is defined as the direction in which a radio wave's electric-field-vector oscillates. As illustrated in Fig. 1.8, antenna polarization can be characterised as linear, elliptical, or circular. The point of reference can be realized by standing behind the radiating antenna and looking in the direction it is aimed. In cases of horizontal and vertical polarizations, the electric field vector oscillates sideways and up and down in horizontal and vertical planes respectively. The polarization plays a pivotal role in the selection and installation of the antenna.

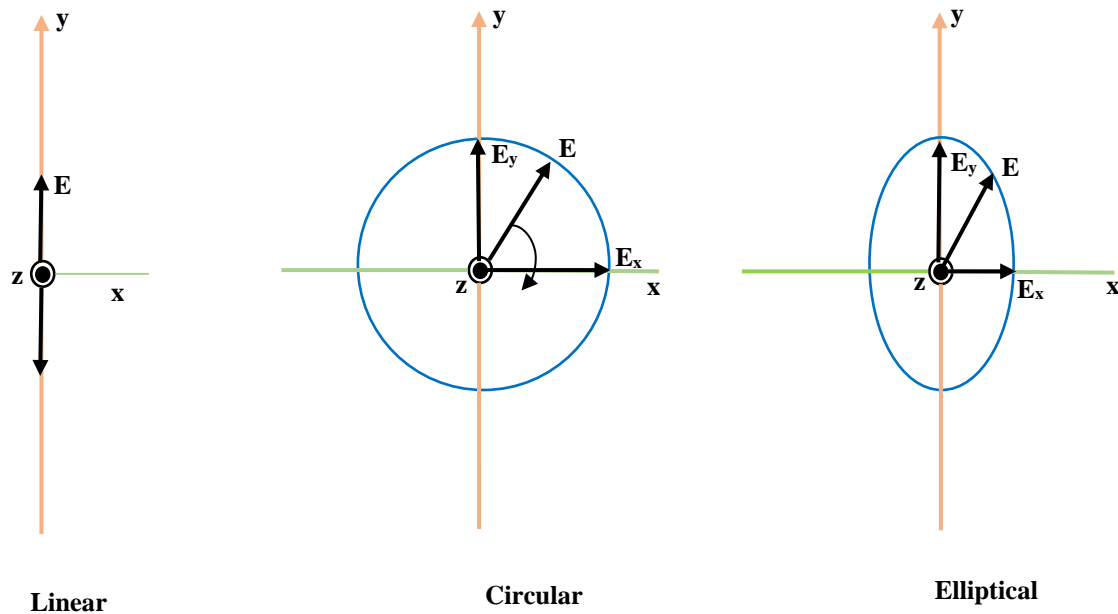


Fig. 1.8. Classification of Polarization

Circularly Polarized (CP) antennas are widely preferred over Linearly Polarized (LP) antennas as they do not require the transmitting and receiving antennas to have a similar orientation. The transmitted CP wave can be received in the horizontal or vertical or any other plane in between. While the LP wave can radiate only in one plane which is undesirable for most wireless applications. Furthermore, the CP wave suffers less reflection and absorption as the transmission is in every plane.

1.6 ADVANTAGES OF MICROSTRIP PATCH ANTENNA (MPA)

A few important advantages of the microstrip patch antennas over standard antennas are as follows:

- Planar, low profile and conformal design.
- Lightweight and less bulky.
- Low manufacturing cost.
- Supports all kinds of polarizations namely linear, elliptical and circular.
- Easy integration with microwave integrated circuits (MICs)
- Capability to handle multi-band and wide-band activities.
- Easy fabrication on hard and flexible substrates.

1.7 DISADVANTAGES OF MICROSTRIP PATCH ANTENNA (MPA)

Some of the disadvantages of the microstrip patch antennas over conventional antennas are as follows:

- Narrow bandwidth due to high Q-factor.
- Low efficiency and gain.
- Undesired radiation coming from feeds and junctions.
- Difficulty in achieving polarization purity.
- Low power handling capability.

1.8 APPLICATIONS OF MICROSTRIP PATCH ANTENNA (MPA)

Some of the key areas in which microstrip patch antennas have found applications are as follows [24], [25]:

- Mobile and Satellite Communication
- Radio Frequency Identification (RFID)
- Global Positioning System (GPS)
- Direct Broadcast Services
- Satellite Navigation Receivers
- Worldwide Interoperability For Microwave Access (WiMax)
- Rectifiers and Radars
- Radio Altimeters
- Feed Elements in Complex Antenna
- Command and Control Systems
- Environmental Instrumentation
- Remote Sensing
- Telemedicine
- Intruder Alarms
- Biomedical Radiators
- Feed Element in Complex Antennas
- Integrated Antennas
- Wireless Body Area Network (WBAN)

1.9 MULTIPLE-INPUT-MULTIPLE-OUTPUT (MIMO) Antenna

In 1948, Shanon highlighted the limits of single-input-single-output (SISO) systems. As wireless traffic has been increasing dramatically over the years, both wireline and wireless communication have seen many developments. The idea of multiple-input-multiple-output (MIMO) was given by D.A. George, A.R. Kaye and W. van Etten in the 1970s. The approach was first proposed in 1992 and a corresponding patent [26] was issued in 1994.

MIMO can be considered as a group of antenna arrays. Formally, it employs multiple transmitting and receiving antennas for increasing the data transmission rate. It does so by increasing the reliability of the system using spatial multiplexing. It escalates the channel capacity without increasing the bandwidth requirement. In MIMO systems, very high isolation is required between radiating antennas. A basic 3×3 MIMO antenna configuration is shown in Fig. 1.9.

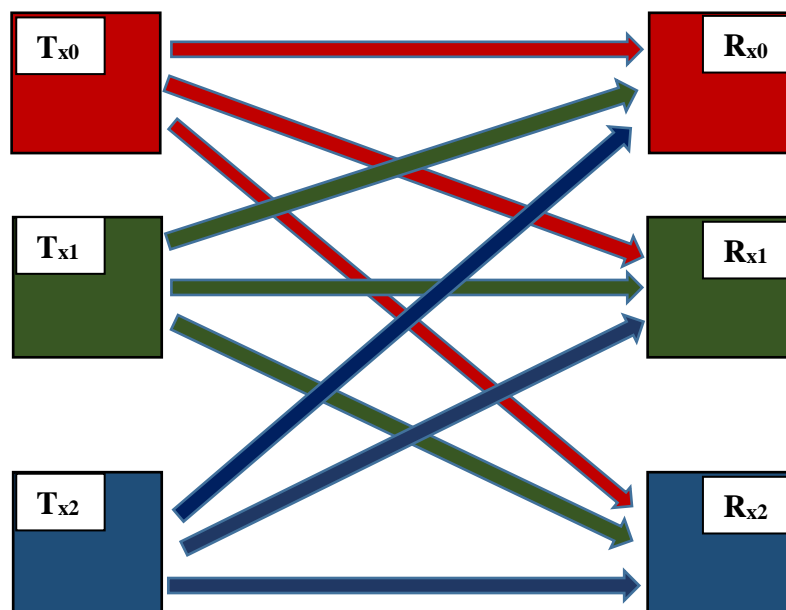


Fig. 1.9. A 3×3 MIMO Antenna Configuration

1.10 ADVANTAGES OF MIMO Systems

Some of the advantages of the MIMO systems are as follows:

- Capacity
- High Data Transfer Rate
- Low Bit Error Rate (BER)

- Spectral Efficiency
- Signal-to-Noise Ratio (SNR)
- Throughput
- Reliability
- High Quality of Service (QoS)

1.11 DISADVANTAGES OF MIMO

Some of the disadvantages of the MIMO systems are as follows:

- Hardware Complexity
- Advanced Software Requirement
- Requirement of Multiple Antennas
- Increased Power Requirement
- Higher Cost

1.12 WIRELESS BODY AREA NETWORK (WBAN)

A “*wireless-body-area-network*” is also referred to as a “*body-area-network (BAN)*” or a “*wireless personal area network (WPAN)*”, or a “*medical body area network (MBAN)*” or a “*body sensor network (BSN)*”, is a network of wearable devices. These devices are implantable in humans, or surface mounted on the human body or can be integrated into clothing and accessories such as belts, bags, jewellery, etc. Typically, wearable devices are spread over the whole human body and connected through a wireless communication channel. Every device has its specific requirements and dedicated mission. Apart from measuring the vital signs of a person, these devices can also be used for detecting emotions such as happiness, distress, fear, anxiety, etc. The schematic for the WBAN is illustrated in Fig. 1.10.

The IEEE standardization group (IEEE 802.15) was instituted to standardize on-, off-, or in-body communication applications for wearable applications. Various bands have been allocated and used for WBAN as shown in Table 1.1. Navigation, positioning, remote health monitoring/care, biofeedback, assisted living, and other innovative applications are available through the WBAN. Due to numerous promising applications, both non-textile and textile antennas have found their importance in

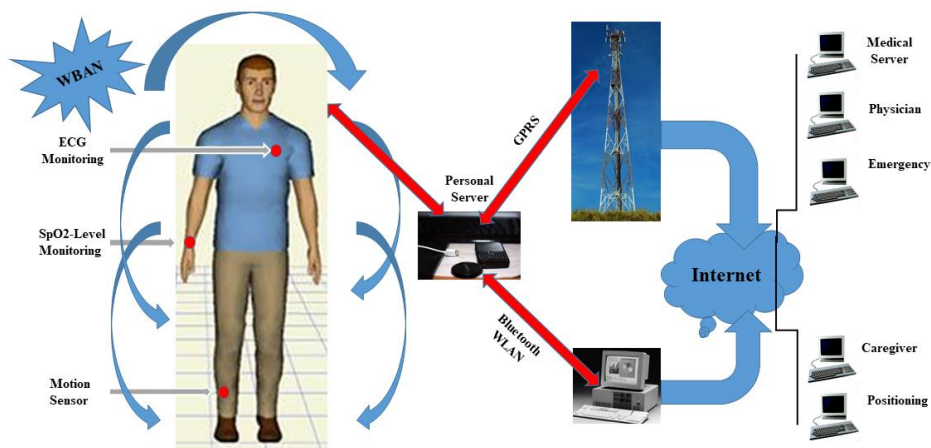


Fig. 1.10. Illustration of “Wireless Body Area Network (WBAN)”

wearable technology. One of the crucial requirements of these antennas is that they should be invisible and non-invasive for the user.

Table 1.1. Frequency Bands of Operation for WBAN

Band	Frequency (MHz/GHz)	Applications
MASB (Meteorological Aids Service Band)	401-406 MHz	Implantable
MICS (Medical Implant Communication System)	402-405 MHz	Implantable
	420-429 MHz	Wearable
	420-449 MHz	Wearable
WMTS (Wireless Medical Telemetry System)	608-614 MHz	Wearable
	1.395-1.400 GHz	Implantable
	1.427-1.432 GHz	
WiMAX (World-Wide Interoperability for Microwave Access)	3.5 GHz	Wireless Body Area Network
ISM (Industrial, Scientific and Medical Band)	433.1-434.8 MHz	Wearable
	902-928 MHz	Wearable
	2.40-2.50 GHz	Wearable
	5.725-5.875 GHz	Wearable
UWB (Ultra Wide Band)	3.10-10.6 GHz	Wearable

1.13 NON-TEXTILE AND TEXTILE WEARABLE ANTENNAS FOR WBAN

Both non-textile and textile antennas can be used as wearable devices for the wireless-body-area-networks (WBANs). The non-textile antennas can be surface-mounted on huma-body and accessories like Glasses, Belts, Bags, Shoes and Jewellery. Whereas the textile antenna can be directly integrated into clothing. For non-textile wearable antennas, both flexible and non-flexible dielectric materials can be used as substrates but conformal antennas cannot be made using non-flexible substrate materials. For a textile antenna, only the clothing materials can be used as dielectric substrates. The flexible substrates such as polyethene terephthalate (PET) and polyimide allow bending. In contrast, the textile materials exhibit a property called drapability i.e. the antennas made up of textile materials can be bent in arbitrary directions.

1.14 ADVANTAGES OF FULLY TEXTILE ANTENNA

- Flexibility
- Light-weight
- Low Dielectric Constant (ϵ_r)
- Low Tangent Loss ($\tan \delta$)
- Seamless integration in clothes without any discomfort to the user and any wearability issues.

1.15 DISADVANTAGES OF FULLY TEXTILE ANTENNA

- Need of proper characterization of Textile Fabrics
- Narrow Range of Dielectric Constant (ϵ_r)
- Porosity and Anisotropy
- Dielectric Constant may change due to constant exchange of water with surroundings

1.16 CHALLENGES OF DESIGNING WEARABLE ANTENNAS

There are various challenges associated with the designing and fabrication of wearable antennas. Some important challenges are as follows:

1.16.1 Bending

In wearable technology, conventional flat antennas cannot be used. As a result, the antenna's performance must be evaluated under various bending and crumpling circumstances. All antenna parameters such as s-parameters (return loss and isolation), axial ratio, gain, radiation efficiency, SAR, etc. need to be checked under bending conditions in various directions.

1.16.2 Specific Absorption Rate (SAR)

The “*specific-absorption-rate (SAR)*” is the rate at which the human body absorbs radio frequency radiation. It's the amount of energy absorbed per unit mass of human tissue. It is measured in Watts/Kg.

Human tissue is typically regarded as a lossy material. An antenna positioned near a person's body demonstrates alterations in the frequency of operation, low antenna gain and distortions in the radiation patterns. These issues can be reduced/overcome by having an antenna with low fringing fields and low SAR values.

1.16.3 Integration and Placement

The integration of wearable antennas is challenging, as they should be invisible to the wearer/user. The antenna should have robust performances under the situations like sweating, washing and ironing. For such applications, the size of the antenna does not seem to be an issue. In contrast, the antenna embedded in accessories like glasses, buttons, jewellery, etc. has to be compact in size.

The placement of a wearable antenna is also an issue. An antenna placed around the chest/back can severely affect the vital organs like the heart and lungs. It also increases the risk of breast cancer. The placement of the antenna near the waist area could be prone to digestive, excretive and reproductive systems. The lower leg, wrist and arm are considered as best and more comfortable places for the placement of antennas. However, the wearable antenna having limited SAR values can be placed anywhere.

1.16.4 Water Absorption

The fully textile antennas are made up of textile fabrics that are porous in nature. These textile fabrics can easily absorb moisture and water from sweat or an open environment. This can lead to a shift in the frequency of resonance and impedance bandwidth of the antenna.

1.17 APPLICATIONS OF WEARABLE ANTENNAS

- Positioning and Navigation
- Military and Defence
- Health and Security
- Sports and Fitness
- Fashion and Entertainment
- Wearable Accessories such as Garments, Buttons, Bags, Belts, Shoes and Jewellery
- Care for Child and Elderly

1.18 OBJECTIVE OF THESIS

In the recent years, wearable antennas have been gaining much popularity and attention because of their alluring features such as low profile, lightweight, flexibility, conformal structure, low cost and portability. These antennas can be used for wireless communication and sensing. The flexibility of these antennas is critical since they are attached to numerous regions of the human body. As a result, they must be implemented on flexible substrate materials, which makes them conformal. The main objectives of the presented thesis are

- Design and development of a planar dual-band antenna for “*ISM/wearable applications.*”
- Design and development of a compact wideband flexible antenna for “*wireless medical telemetry services (WMTS).*”
- Design and development of a dual-resonance ultra-miniaturized textile antenna for “*ISM/wearable applications.*”
- Design and development of a wideband *textile “multiple-input-multiple-output (MIMO) antenna”* for “*industrial, scientific and medical (ISM)/wearable applications.*”
- Design and development of a Fully-Textile Dual-Band Dual-Sense MIMO Antenna for “*WBAN/WLAN/ISM/Wearable IoT Applications.*”

In objective I, a flexible dual resonant antenna is developed for the lower (902-928 MHz) and middle (2400-2480 MHz) ISM frequency bands. In objective II, a flexible wideband antenna covering 1395-1400 MHz and 1427-1432 MHz bands is developed for the WMTS applications. In objective III, an all textile dual-band antenna is developed for 2.45/5.8 GHz ISM/Wearable applications. In objective IV, an all textile wideband MIMO antenna covering a 2.00–6.23 GHz frequency band is developed for ISM/wearable applications. In objective V, an all textile dual-band dual-sense MIMO antenna covering 2.18-3.29 GHz and 3.92-6.90 GHz frequency bands is developed WBAN/WLAN/ISM/wearable IoT applications.

The simulations were carried out with the help of the “*CST Microwave Studio software*®.” The fabrication and testing of all the presented antennas have also been carried out.

1.19 METHODOLOGY

The design and development of the proposed wearable antennas were achieved by a multi-step approach as discussed below:

- Designing of the Antenna
- Simulation of the Antenna
- Fabrication of the Antenna
- Measurement of the Antenna

The schematic for the methodology adopted in the current work is shown in Fig. 1.11.

1.19.1. Designing of the Antenna

This is the first and foremost step in the development of a wearable patch antenna at desired frequency band(s). The shape and dimensions of the basic microstrip patch antenna are calculated using the well-established formula available in the textbooks and published literature. A reliable feeding technique is adopted to achieve the desired results. A parametric analysis is done to get the optimized dimension of the designed antenna.

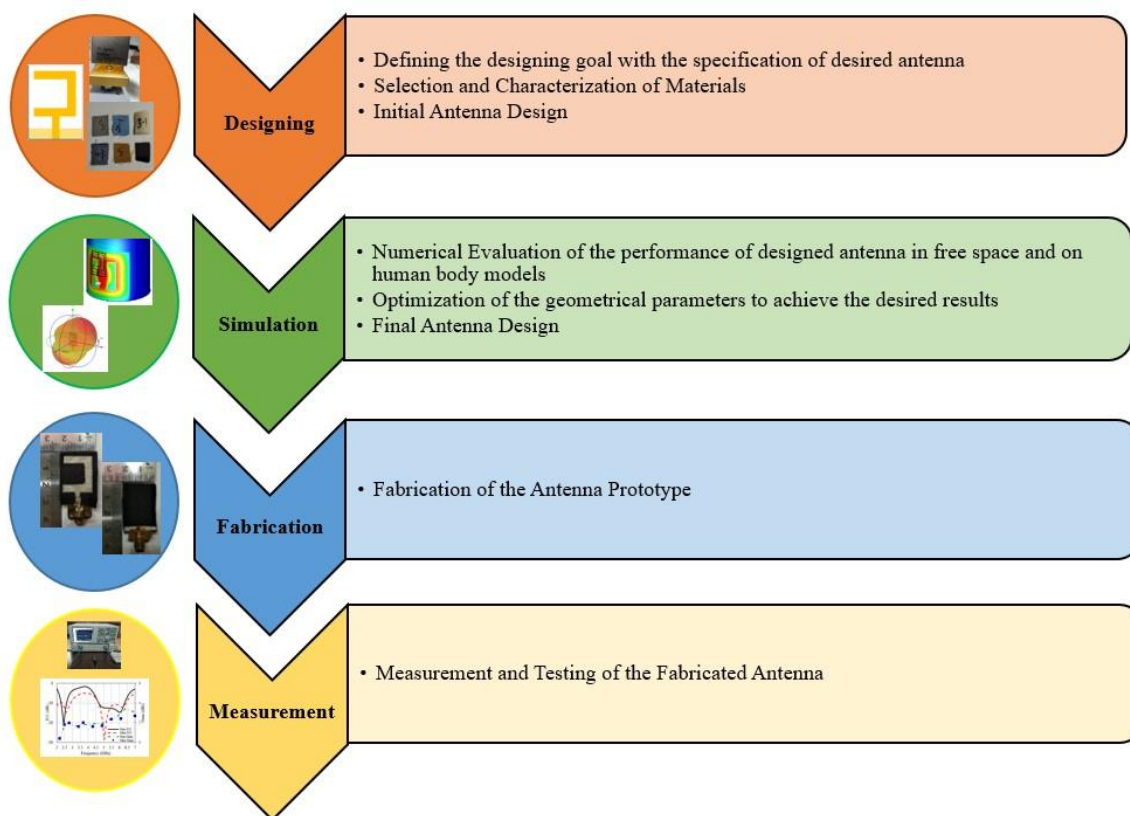


Fig. 1.11. The methodology adopted in the current work

1.19.2. Simulation of the Antenna

The CST Microwave Studio software[®] is used for the simulation of the presented work. It is a high-performing EM analysis software, which is used for modelling, optimizing and analysing electromagnetic systems.

Initially, the basic microstrip-patch-antenna (MPA) is designed for the desired band of operations. The properties of the designed antenna such as return loss, isolation, axial ratio, bandwidth, surface current density, gain and radiation characteristics are analyzed. The parameters of the antenna are optimized to achieve the desired results of the antenna. For MIMO antennas, various properties such as ECC, MEG, DG and TARC are evaluated. In the case of wearable antennas, the bending/crumpling analysis and evaluation of SAR are also performed for the designed antenna.

1.19.3. Fabrication of the Antenna

Different approaches are followed for fabricating the non-textile and textile antennas. For the fabrication of non-textile antennas, the .dxf file is exported to the automated control proto-etch machine. Subsequently, the routing and milling processes

are performed by the software installed in the automated machine and finally, the fabrication process begins. For the fabrication of a textile antenna, the substrate material was characterized using a radio frequency impedance/material analyzer (Agilent E4991A). The radiating patch, substrate, and ground-plane of the desired antennas were all created using manual cutting procedures. Then, the different layers of the antenna are joined using a dry iron. Lastly, an SMA connector is soldered to the fabricated antenna in both cases before proceeding with the testing and measurement of the fabricated prototype.

1.19.4. Measurement of the Antenna

The experimental results were acquired with the help of an Agilent Technologies “*vector network analyzer (VNA)*” N5230A (frequency range: 10 MHz to 40 GHz). Initially, the calibration of VNA was done using mechanical equipment comprising of a short, an open and a broadband load. After this, the frequency range of operation was set before performing the analysis. Other characteristics of the designed antennas, such as axial ratio, gain, radiation pattern and efficiency were measured with the help of an Anechoic chamber. There was a small difference between the experimental and simulated findings.

1.20 ORGANIZATION OF THESIS

The presented thesis is organized as follows:

In Chapter 1, firstly, a brief introduction about antenna and their types are described. After that, an overview of the microstrip patch antenna, their feeding techniques, advantages, disadvantages and applications are discussed. Secondly, an introduction to MIMO along with its advantages and disadvantages is presented. Thirdly, a brief description of Wireless Body Area Network (WBAN) and its frequency bands of operation is given. Following this, the idea of non-textile and textile antennas for WBAN is discussed. Afterwards, the advantages and disadvantages of fully textile antennas are presented. Lastly, the challenges of designing wearable antennas and their applications are discussed. In addition, the objective of the current thesis and the methodology adopted is presented.

In Chapter 2, the importance of the literature review is discussed. It presents the published work on non-textile and textile antennas for wearable applications. After this,

a brief review of circularly polarized textile wearable antennas is presented. Lastly, a review of textile MIMO antennas for wearable applications is done. It also details the various strategies employed by the researchers to reduce mutual interaction amongst MIMO system radiating antenna parts. It identifies the limitations of existing research work and briefly explains the need for the current research.

In Chapter 3, a planar dual-band antenna for “*ISM/wearable applications*” is presented. This antenna resonates over “*902-928 MHz*” and “*2400-2480 MHz*” frequency bands to cover the lower and middle ISM bands. The low resonating frequency band reduces the health hazards that may arise due to the exposure of RF waves. The concept of slotting has been used to achieve dual resonance. The antenna has a gain of 2.51 and 3.89 dBi for “*902-928 MHz*” and “*2400-2480 MHz*” frequency bands respectively. The antenna operates in permissible standard limits of SAR and can be used as a flexible antenna for wearable applications.

In Chapter 4, a compact wideband flexible antenna for “*wireless medical telemetry services (WMTS)*” is presented for wearable applications. This antenna resonates over “*1395-1400 MHz*” and “*1427-1432 MHz*” WMTS bands. This is a low-profile compact planar coplanar waveguide (CPW) fed antenna which can be easily integrated. To cover the low frequency range, the antenna uses a meander-lined method to increase the conducting path. In comparison to other wearable antennas, the antenna has a large impedance bandwidth. The bending and SAR analysis are performed to show that antenna can be used for wearable applications.

In Chapter 5, a dual-resonance ultra-miniaturized textile antenna is presented for “*ISM/wearable applications.*” A microstrip line-fed C-shaped monopole and a partial ground plane have been used in this antenna. The antenna covers “*2.45 GHz*” and “*5.8 GHz*” ISM bands. This is a fully-textile antenna having a dimension of 20 mm×30 mm×1 mm. The antenna has bandwidths of 14.2% and 27.5% for ‘lower’ and ‘upper’ resonating bands respectively. In addition, the characterization of various textile fabrics is done to explore the possibilities of developing textile antennas. The designed antenna is simple, compact, simple-to-construct and can be efficiently used for wearable/textile applications. The antenna shows consistent on-body performance under bending conditions. The SAR analysis is also performed to find the maximum allowable input powers.

In Chapter 6, a wideband textile multiple-input-multiple-output antenna is presented for “*industrial, scientific and medical (ISM)/wearable applications.*” The fully textile MIMO antenna covers a wide impedance band of “*2.00-6.23 GHz*” with a very low radiation correlation between the radiating elements. The antenna uses a T-shaped stub and three rectangular rings for reducing the mutual-coupling (achieving low correlation) between the radiating antenna elements. The MIMO antenna has a size of $76 \times 37 \text{ mm}^2$ low envelope correlation coefficients, high diversity gain and a realized gain of more than 2.88 dBi over the entire resonating band. The antenna has a compact size, stable radiation patterns and reasonable on-body performance within the acceptable limits of SAR.

In Chapter 7, a fully-textile dual-band dual-sense MIMO antenna is presented for “*WBAN/WLAN/ISM/Wearable IoT Application.*” The fully textile MIMO antenna resonates in “*2.18-3.29 GHz*” and “*3.92-6.90 GHz*” bands and provides circular polarization in the 4.92-5.94 GHz band. The antenna has an area of $43 \text{ mm} \times 92 \text{ mm}$, isolation of more than 15 dB between the radiating elements, low ECC (envelope correlation coefficient), high DG (diversity gain) and a realized gain of greater than 2.00 dBi over both resonating bands. The antenna uses a T-shaped stub, two triangular-shaped stubs and a rectangular-shaped stub loaded on the backside of the antenna to achieve the isolation between the radiating elements. The antenna can be easily integrated into clothes and provides reasonably stable performance for both on-body and off-body conditions. The SAR analysis performed for cubic and cylindrical phantoms (mimicking human chest/back and arm) shows that the proposed antenna can work efficiently. Hence, the antenna is a good candidate for a

In Chapter 8, the brief conclusion of this research is presented. It is concluded that both non-textile and textile antennas can be used for wearable applications in wireless body area networks (WBAN). It also sum up the outcomes and limitations of the presented research along with the possible future scope for further study.

“It is the great beauty of our science that advancement in it, whether in a degree great or small, instead of exhausting the subject of research, opens the doors to further and more abundant knowledge, overflowing with beauty and utility.”

Michael Faraday

2

LITERATURE REVIEW

The search and evaluation of the available state-of-the-art in the given domain is called Literature Review. In a true sense, it is an overview of the previously published work in a specific field of interest. It records the available literature concerning the given subject. It plays a vital role in any kind of research as it critically analyzes the gathered information to identify the gaps in the existing literature. It enables the researcher to have an in-depth knowledge of the subject to understand the limitations of the available theory and formulate areas for further research.

2.1 INTRODUCTION

In recent years, there has been a rapid growth in the area of wearable applications mainly due to wearable antennas. Wearable Antennas refer to the systems associated with the human body. Such antennas should be compact, robust, lightweight, highly flexible, and efficient and should not affect the human body [27], [28].

In this chapter, the development and analysis of non-textile and textile antennas are presented with an emphasis on novelty, compactness, linear and circular polarized antennas for wearable applications. In addition, the textile MIMO antennas are included in the succeeded sections.

2.2 NON-TEXTILE ANTENNAS FOR WEARABLE APPLICATIONS

In [29], a miniaturized wide-band antenna is presented for wearable applications. It utilizes a coplanar waveguide (CPW) feed on a Rogers RO 3210 substrate. It is fed through a sub-miniature push-on (SMP) connector instead of a traditional SMA connector. The use of an SMP connector assists in the overall size reduction of the antenna as it is modelled along with the antenna. The designed antenna occupies a volume of $7.90 \text{ mm} \times 16.38 \text{ mm} \times 1.25 \text{ mm}$. It covers the frequency range of 4900-11000 MHz. The presented antenna can be used in the upper half of the ultra-wide band.

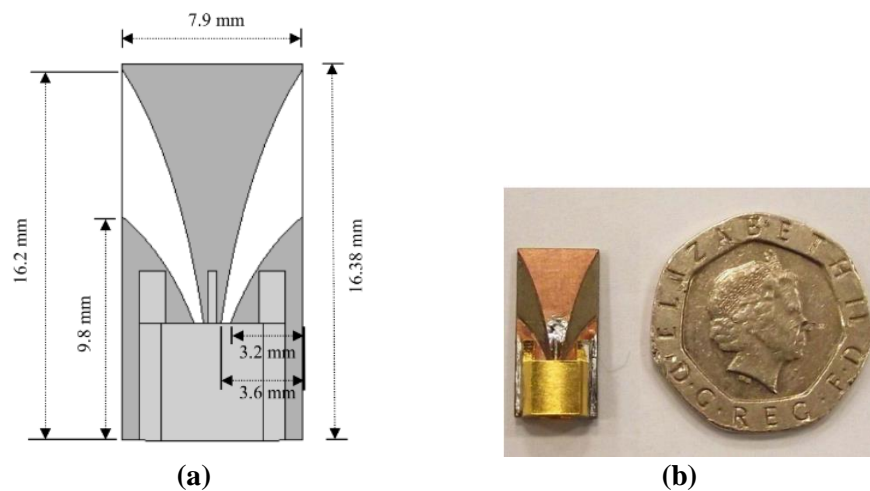


Fig. 2.1. Designed and Fabricated Prototypes of the antenna presented in [29]: (a) Antenna Configuration and (b) Fabricated Prototype

In [30], a novel, planar, via-free antenna (like an adhesive bandage) is presented for on-body “*wireless-medical-telemetry-service (WMTS)*” applications. The antenna has a basic construction that allows it to be easily implanted into human tissue. It can be used as a standalone antenna with coaxial feeding, or it can be combined with a single-chip WMTS sensor. The designed antenna occupies a volume of $78.0 \text{ mm} \times 20.0 \text{ mm} \times 0.8 \text{ mm}$. It covers the frequencies of 1427-1432 MHz. The presented antenna can be used in wireless body area networks (WBAN).

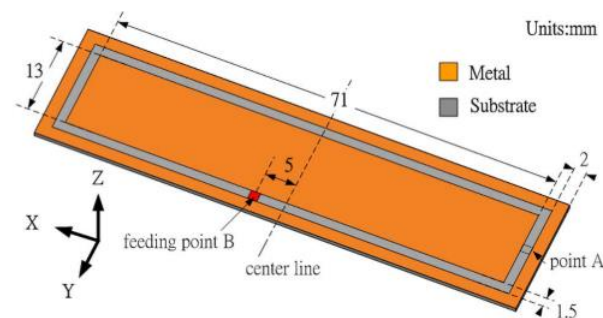


Fig. 2.2. Photograph of antenna prototype presented in [30]

In [31], a smallest aperture coupling feeding network is presented for wearable applications. It is utilised in wearable systems to reduce the area of the rigid “*Printed Circuit Board (PCB)*” carrying the circuitry and feeding the textile antenna. It utilizes the periodic fingers loading the coupling aperture and a T-shape structure is printed at the microstrip feed line's terminus. It can be easily integrated with any sensor chip. It

has no vertical conducting parts, which aids to robustness when the antenna deforms. The designed antenna occupies a volume of $100.0 \text{ mm} \times 100.0 \text{ mm} \times 3.0 \text{ mm}$. It covers the frequencies of 2330-2490 MHz.

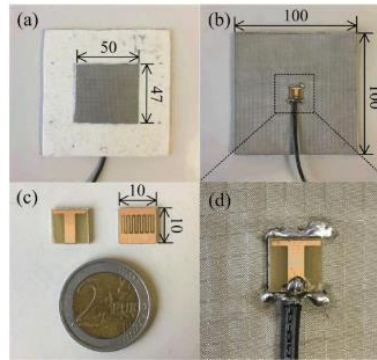


Fig. 2.3. Photograph of the antenna prototype presented in [31]: (a) Top View, (b) Bottom View, (c) Feeding Network PCB, and (d) Zoomed in connection

In [32], a dual-resonant bendable-antenna is presented for on-body applications. It is excited using a coplanar-wave-guide (CPW) configuration. A flexible substrate Rogers Ultralam 3850 is used as a substrate for exhibiting high flexibility. It utilizes a monopole antenna with two narrow slots used for achieving the resonance at 2450 MHz. In addition to this; two inverted L-shaped slots are introduced to create resonance at 5800 MHz. The arrow shape helps in getting the impedance matching at both the resonant frequencies. The designed antenna occupies a size of $35.0 \text{ mm} \times 20.0 \text{ mm} \times 0.1 \text{ mm}$. It covers the frequencies of 2385-2495 MHz and 5500-6100 MHz.

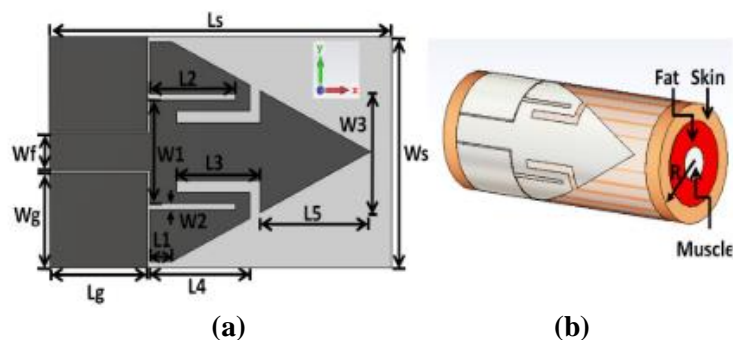


Fig. 2.4. Photograph of the antenna presented in [32](a) Antenna Configuration and (b) Fabricated Prototype under Bending

In [33], a dual-band flexible antenna is presented for on-body applications. It utilizes a Kapton (Polyimide) substrate covered with a flexible magnetodielectric nanocomposite polymer. The novel nanocomposite is made using carbon-coated cobalt (CCo) covered with polyaniline (PANI). The morphology of the conjugated polymer PANI is studied using scanning electron microscopy (SEM). The designed antenna occupies a volume of $35.0 \times 20.0 \times 0.1 \text{ mm}^3$. It covers the frequencies of 1800–2450 MHz (PCS and WLAN) and 5150–5825 MHz (wireless networks). Even in complicated bending circumstances, the presented antenna proves to be a strong candidate for wearable applications.



Fig. 2.5. Fabricated Prototype of the antenna presented in [33]

In [34], a paper substrate-based flexible antenna is presented for 2.45 GHz ISM band applications. It utilizes a bendable photo-paper and adhesive copper-strips as substrate and radiating antenna elements respectively. The performance functioning of the antenna is analyzed for flat and bent conditions. Additionally, the functioning of the antenna for human tissues is investigated. The designed antenna occupies a volume of $40.0 \times 35.0 \times 0.6 \text{ mm}^3$. It operates in the frequency range of 2330-2530 MHz. The antenna can be used for an intra-body telemedicine system.

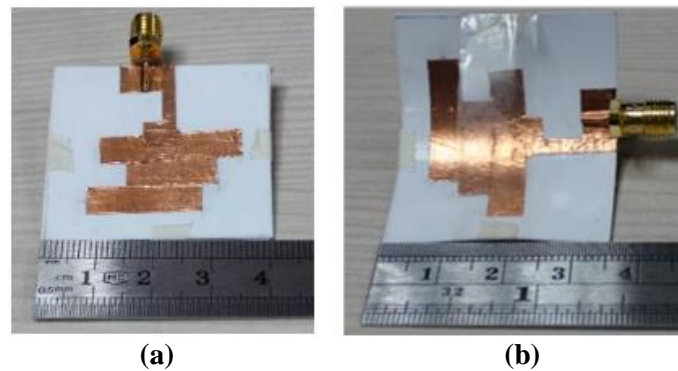


Fig. 2.6. Photograph of the fabricated prototype presented in [34]: (a) Flat Condition and (b) Bent Condition

In [35], a planar, dual-band printed antenna is proposed for wearable applications. The receiving and transmitting antennas are printed on Kapton polyimide and FR-4 substrate respectively. The flexible Kapton material is physically robust, very durable, mechanically strong and distortion resistant to the harsh environment. The antennas are based on split-ring resonators (SRRs). The dimensions of the antenna can be optimized and hence the resonating frequencies of the antennas can be modified. The designed antenna occupies an area of $15.0 \text{ mm} \times 14.0 \text{ mm}$. It operates at two frequency bands of 2500 MHz and 4500 MHz.

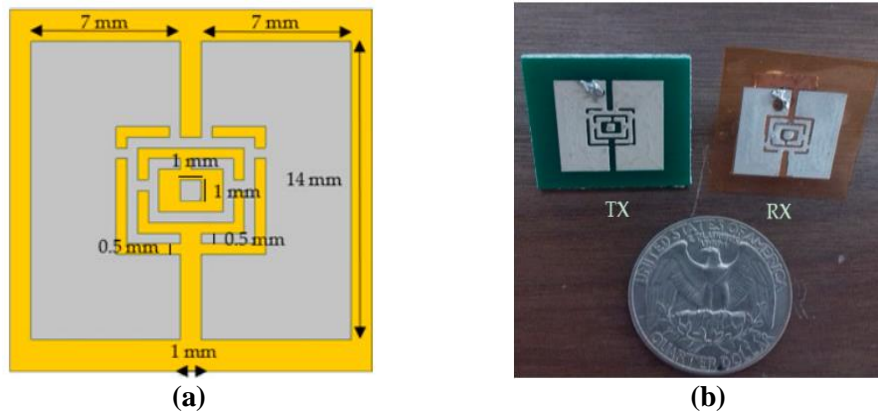


Fig. 2.7. Photographs of the antenna presented in [35]: (a) Designed Antenna (b) Fabricated Antennas for Wireless Power Transfer

In [36], a microstrip-patch-antenna (MPA) with a metallic casing is presented for wearable applications. The metallic casing is used to reduce the specific absorption ratio (SAR) so that it can provide safe communication in all situations. The designed

antenna measures $57.0 \times 20.3 \times 1.56 \text{ mm}^3$ in size. It operates at 900 MHz GSM and 2400 MHz ISM bands. A study on the effects of electromagnetic waves on the human head with earrings of different sizes is performed to see the most destructive effects on the human body. It produces 0.52 W/Kg and 0.25 W/Kg SARs at 900 MHz and 2400 MHz respectively. It can be employed in most of telecommunication applications.

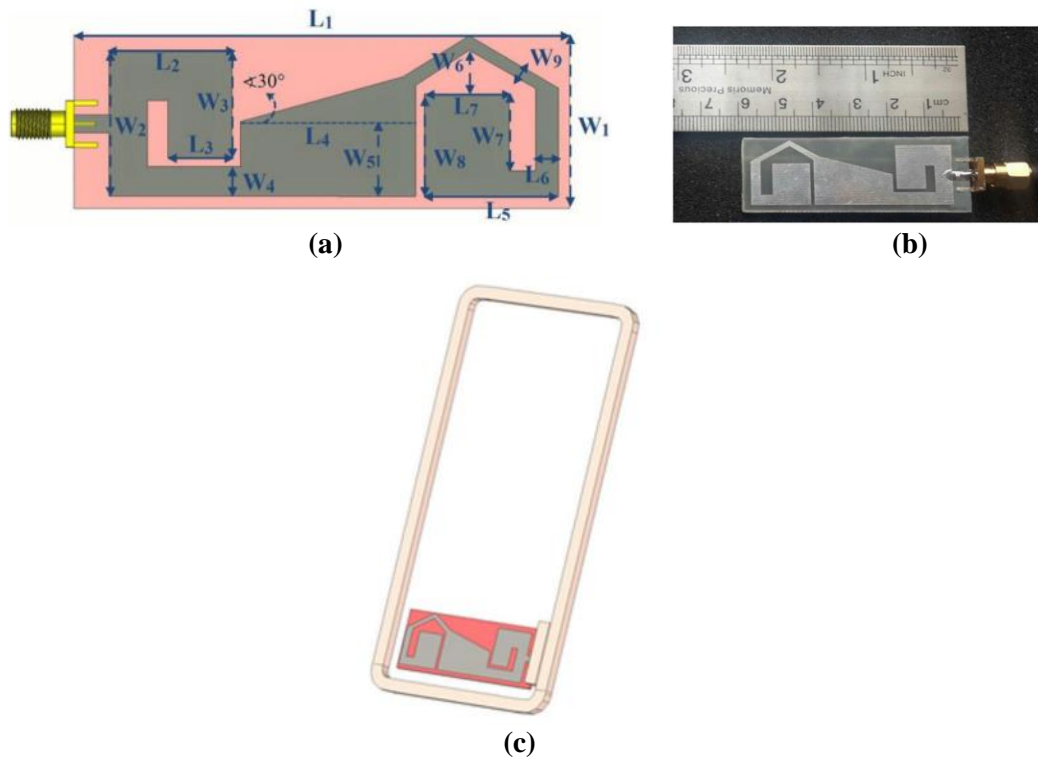


Fig. 2.8. Designed and Fabricated Prototypes presented in [36]: (a) Designed Antenna, (b) Fabricated Antenna, and (c) Fabricated Antenna with Metallic Casing

In [37], a low-profile wideband antenna is proposed for wearable applications. It is designed on a semi-flexible material of Duroid RT 5880. It utilizes a conventional rectangular patch modified using rectangular slots with a partial ground plane. The bandwidth of the antenna is enhanced using a hook-shaped stub with the ground plane. The antenna shows reasonably good performance in the bending scenario. It also meets the standard limits of SAR for an input power of less than 265 mW. The designed antenna occupies a size of $17.0 \text{ mm} \times 25.0 \text{ mm} \times 0.787 \text{ mm}$. It covers the frequency range of 1620-3000 MHz.

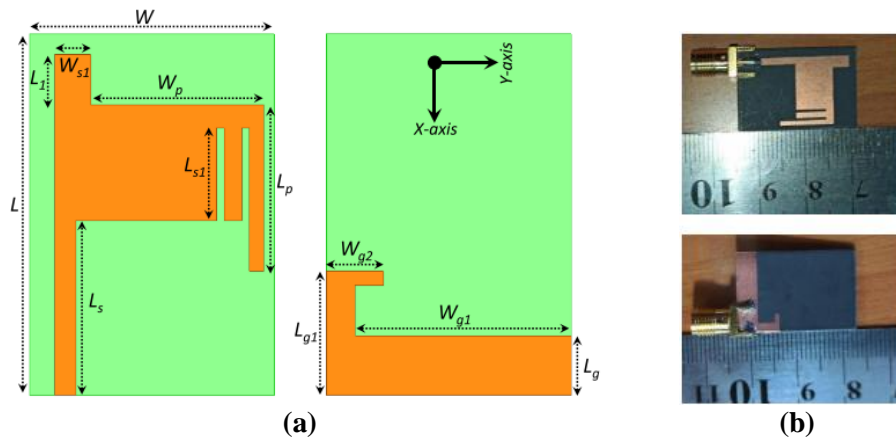


Fig. 2.9. Photographs of the antenna presented in [37]: (a) Designed Antenna and (b) Fabricated Antenna

Table 2.1. Non-Textile Antennas for Wearable Applications

Ref. Year	Antenna size (mm×mm×mm)	Impedance Band (MHz)	Impedance Bandwidth (MHz)	Gain (dBi)	Dielectric Material (ϵ_r)	Resonance Bands Covered	Application Band(s)
[29] 2013	7.90×16.38×1.25	4900-11000	6100	4.8	Rogers RO 3210 (10.2)	Wideband	UWB (Top Half)
[30] 2014	78.0×20.0×0.8	1427-1432	4.3	4.19	Duroid RT 5880 (2.2)	Single	WMTS
[31] 2017	100.0×100.0×3.0	2330-2490	160	5.6	FR-4 (4.3)	Single	ISM
[32] 2018	35.0×20.0×0.1	2385-2495, 5500-6100	110, 600	1.13, 3.17	Rogers Ultralam 3850 (2.9)	Dual	ISM
[33] 2018	58.0×40.0×0.130	1800-2450, 5150-5825	650, 675	1.05, 3.12	Kapton (Polyimide) (3.5)	Dual	WLAN
[34] 2018	40.0×35.0×0.6	2330-2530	200	2.00	Photo Paper ()	Single	ISM
[35] 2019	15.0×14.0×0.17 15.0×14.0×1.56	2500, 4500	---	5.34, 4.49	Kapton Polyimide (3.14) FR4 (3.66)	Dual	ISM
[36] 2019	57.0×20.3×1.56	900, 2400		1.25,	FR-4 (4.3)	Dual	GSM, ISM
[37] 2020	17.0×25.0×0.787	1620-3000	1380	2.50	Duroid RT 5880 (2.2)	Single	WMTS

From Table 2.1, it is observed that various single and dual-band non-textile antennas have been proposed for wearable applications. However, dual-band antennas designed for ISM bands have targeted higher frequency bands only. Thus, there is a need of designing a dual-band non-textile antenna for covering both lower and upper ISM bands. In addition, the antennas designed for WMTS bands do not cover all frequency bands. The WMTS bands are specially dedicated to remote health monitoring

as it is an interference-free spectrum that prevents the overcrowded popular ISM bands. Hence, there is a need to design a wideband flexible antenna that can cover two or three frequency bands for WMTS applications.

2.3 TEXTILE ANTENNAS FOR WEARABLE APPLICATIONS

In [38], a flexible inverted-F shaped antenna (FlexIFA) is presented for wearable applications. It introduces the concept of smart clothing in Bluetooth and UMTS (Universal Mobile Telecommunication System) for unobtrusive wearable applications. As far as the authors know, it is the foremost thin and flexible antenna designed for commercial smart clothing. Here, a FlexIFA is studied for single as well as dual-band operations. The antenna is designed to be placed on the sleeve of clothing. The length of the longer and upper arms can control the lower and upper resonant frequencies, respectively. The designed antenna occupies a volume of $42.0 \text{ mm} \times 50.0 \text{ mm} \times 20.236 \text{ mm}$. It covers frequencies of 2.20-2.50 GHz.

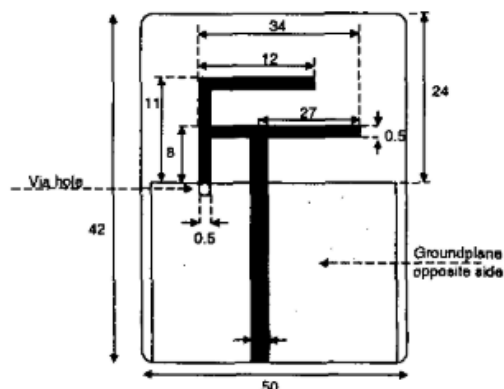


Fig. 2.10. Antenna Configuration presented in [38]

In [39], A unique textile WLAN antenna is demonstrated for on-body applications such as sporting and a paramedic uniforms. The substrate is made of fleece, and the radiating elements (patch and ground) are made of knitted copper. The “*cavity perturbation method*” is utilised to determine the fleece's dielectric measurement. The designed antenna occupies a volume of $76.0 \text{ mm} \times 71.0 \text{ mm} \times 3.0 \text{ mm}$. It covers frequencies of 2.20-2.53 GHz. The presented textile antenna is versatile and it can be easily made operational at any desired frequency with the well-known available methods for patch antenna designing.

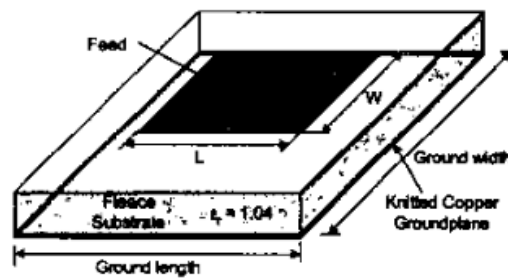


Fig. 2.11. Antenna Configuration presented in [39]

In [40], a study on the characterization of various textile fabrics is done with special attention on GPS antennas for wearable applications. It considers five different textile materials namely Fleece, Upholstery, Vellux, Felt and Cordura®. It utilizes a square patch with cut-off corners to achieve right-handed circular polarization (RHCP). It concludes that all the considered textile materials are appropriately suitable for CP antennas. However, the flexibility of the textile material can cause difficulties in maintaining the antenna's electrical performance characteristics. It is shown that the Cordura® turns out to be the best material in terms of maintaining its mechanical dimensions. In addition, it is highly resistant to water that makes it a smart-cloth.

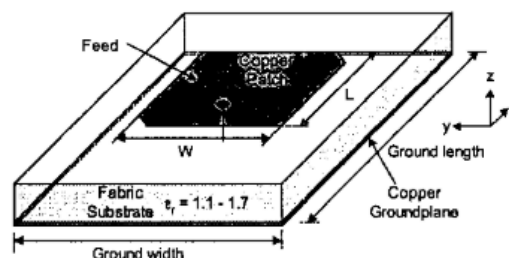


Fig. 2.12. Antenna Configuration presented in [40]

In [41], a textile antenna is presented for wearable applications with the main focus on studying the antenna performance in close proximity to a person's body. The paper addresses various issues such as input-match performance, radiation characteristics, power absorbed by the human body and values of specific absorption ratio (SAR) for 1 g tissue at “2.45 GHz ISM band” under the influence of the human body. It uses two different models for studying the performance of the antenna. It makes use of a Torso model made from CT and MRI pictures of a genuine human body with cell size of 4.0 mm × 4.0 mm × 4.0 mm. Another simplified three-layer arm model

containing skin, muscle and bone with a cell size of $1.00 \text{ mm} \times 1.00 \text{ mm} \times 1.00 \text{ mm}$ is also used. The electrical parameter of each of the tissue around 2.4 GHz is obtained from the data published in [42]. The designed antenna occupies a volume of $72.0 \text{ mm} \times 66.0 \text{ mm} \times 8.0 \text{ mm}$. It covers the frequencies of 2.20-2.70 GHz.

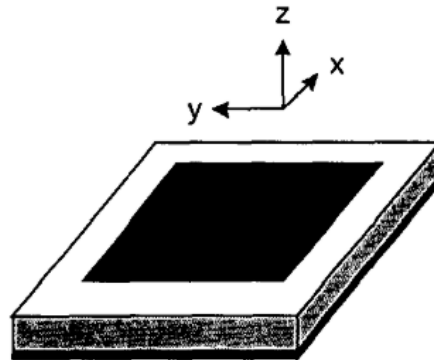


Fig. 2.13. Antenna Configuration presented in [41]

In [43], a dual-band textile antenna is presented for wearable applications. It uses a U-shaped slot structure mounted on a fleece fabric utilized as a dielectric. The conducting elements are made up of adhesive copper strips. The designed antenna occupies a volume of $110.0 \text{ mm} \times 130.0 \text{ mm} \times 3.5 \text{ mm}$. It covers the frequency spectra of 188-1.94 GHz and 2.42-2.48 GHz.

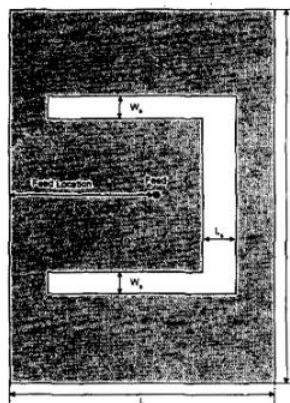


Fig. 2.14. Antenna Configuration presented in [43]

In [44], wearable applications will benefit from a dual-band E-shaped patch textile antenna. The antenna covers 2.2 GHz and 3.0 GHz frequency bands. The lower and upper frequencies of resonance are determined by the length of the antenna's outer and inner arms respectively. The designed antenna occupies a volume of $150.0 \text{ mm} \times$

180.0 mm × 4.0 mm. It covers the frequency spectra of 2.15-2.25 GHz and 2.945-3.055 GHz.

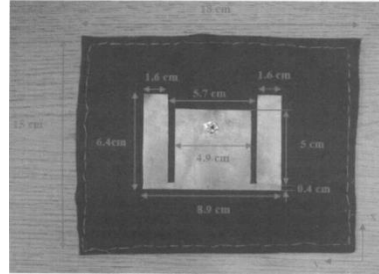


Fig. 2.15. Antenna Prototype (Fabricated) of the antenna presented in [44]

In [45], a new “*ultra-wide-band (UWB)*” textile antenna is presented for the “*wireless body area network (WBAN)*.” The antenna uses Nora, a high conductive metalized Nylon fabric, as a conductive material. The surface resistivity of its three metalized layers (Ni/Cu/Ag) is 0.03/square, which provides extreme flexibility and protection against corrosion. A substrate material of 0.5 mm acrylic fabric is employed. As adhesive sheets can be evenly applied as a thin layer on conducting material by ironing, it is used to unite conductive and non-conductive elements of the antenna. Here, two different textile antenna designs are given. Firstly, it proposes a ultra-wide-band disc-monopole antenna excited by a coplanar line. Secondly, a UWB annular slot antenna that is fed by a small microstrip-line is presented. The designed antennas show the possibility of transmitting very short UWB pulses using textile antennas.

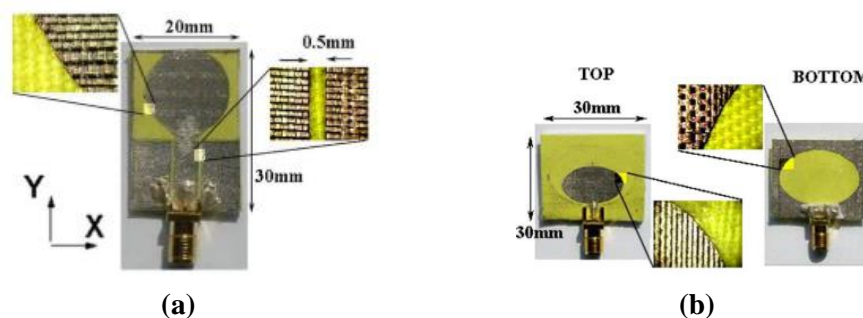


Fig. 2.16. Antenna Prototypes presented in [45]: (a) Disc Monopole CPW Antenna and (b) Annular Slot Circular Antenna

In [46], the development of four different rectangular patch textile antennas are

presented for the 2.45 GHz WLAN band. It employs four different textile materials namely Wash Cotton, Curtain Cotton, Polyester and Polycot for the development of antennas. Copper is used for the conductors, the radiating patch, and the ground plane. It determines the impedance and radiation characteristics experimentally in flat positions of the antennas. It also examines the antennas' performance under bending situations to ensure that they are compatible with wearable applications. The results show that these antennas are suitable for on-body wireless communications.

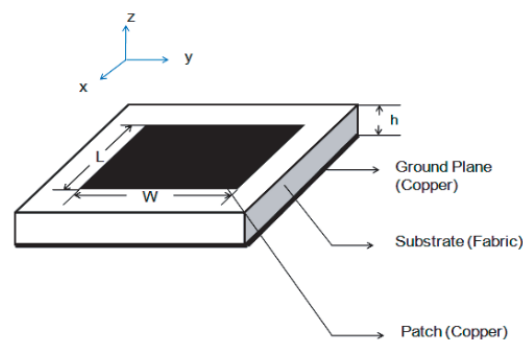


Fig. 2.17. Antenna Configuration presented in [46]

In [47], a novel dual-band textile antenna is presented for wearable applications. It utilizes a half-mode SIW cavity and brass eyelets for the realization of the antenna. The concept of shorting vias and slots is used for miniaturization. The antenna radiations are directed away from the wearer. The designed antenna occupies a volume of $64.6 \text{ mm} \times 61.7 \text{ mm} \times 3.94 \text{ mm}$. It operates the frequency spectra of “2.4–2.48 GHz”

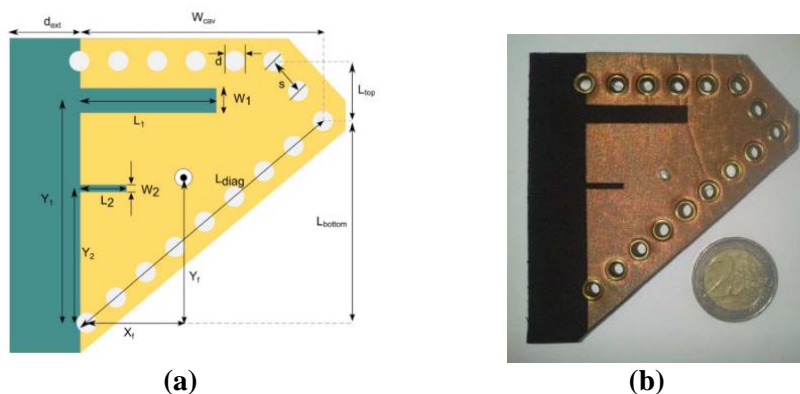


Fig. 2.18. Photographs of the antenna presented in [47]: (a) Designed Antenna and (b) Fabricated Antenna

and “5.72–5.87 GHz.” The antenna design is appropriate for wearable electronics that are worn on the body.

In [48], a miniaturized textile antenna is presented for wearable applications. It relies on quarter-mode substrate integrated waveguide (QWSIW) topology for achieving compact dimensions and high isolation from the body of the wearer. The designed antenna occupies a volume of $63.9 \text{ mm} \times 63.9 \text{ mm} \times 3.7 \text{ mm}$. It covers the frequency spectra of 2.4–2.5 GHz. The proposed antenna is excellently suitable for off-body communication in wearable systems and provides stable on-body performance.

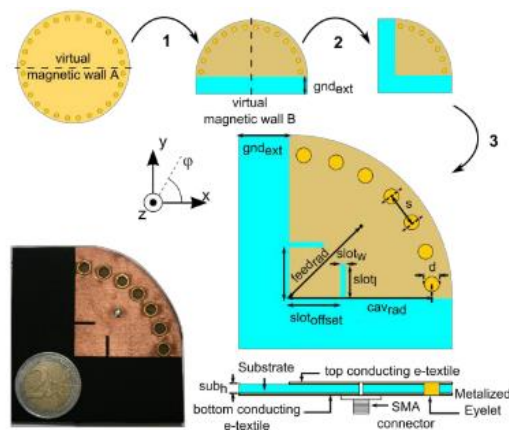


Fig. 2.19. Designed and Fabricated Prototype of the antenna presented in [48]

In [49], a Louis Vuitton (LV) Logo textile antenna is presented. It uses leather and conductive textile as a substrate and radiating antenna. The antenna has a realistic logo size that can be used for wireless anti-theft and wireless communication for

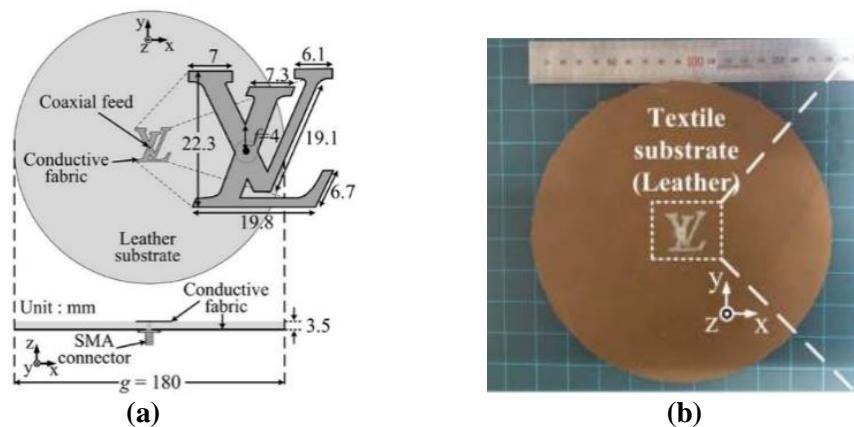


Fig. 2.20. Photographs of the antenna presented in [49]: (a) Designed Antenna and (b) Fabricated Prototype

fashionable wearables. The designed antenna occupies a volume of $180.0 \times 180.0 \times 3.5$ mm³. It covers the frequencies of 2.31–2.54 GHz and 4.12–4.39 GHz.

In [50], a textile antenna with a cavity-backed SIW is presented for off-body wearable applications in a 2.45 GHz ISM radio band. It uses metamaterial-inspired slots for the reduction of antenna size. The designed antenna occupies a volume of 74.5 mm \times 48.0 mm \times 3.0 mm. It covers the frequencies of 2.40–2.50 GHz.

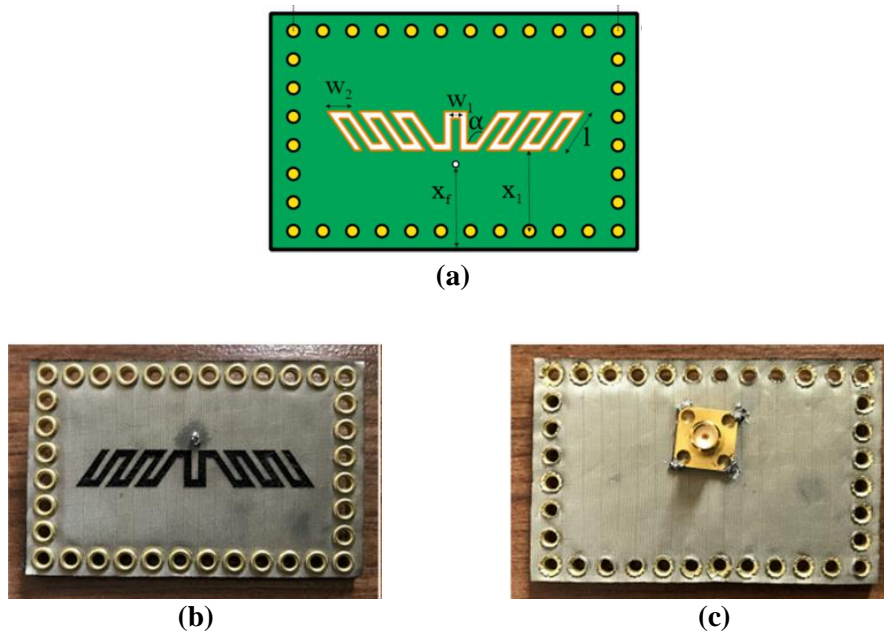


Fig. 2.21. Photographs of the antenna presented in [50]: (a) Designed Antenna, (b) Front View of Fabricated Antenna, and (c) Back View of Fabricated Antenna

In [51], a fully flexible textile antenna is presented for a 5.80 GHz ISM band for wearable applications. It uses conventional copper and woven electro-textile material as conducting parts to explore the wearability of the antenna in real-time. The dielectric properties of the non-conducting textile material are measured using two different methods namely: microstrip ring resonator method and Dielectric Assessment Kit (DAK) Equipment. The designed antenna occupies a volume of 40.0 mm \times 40.0 mm \times 0.6 mm. It covers the frequencies of 5.40-6.00 GHz.

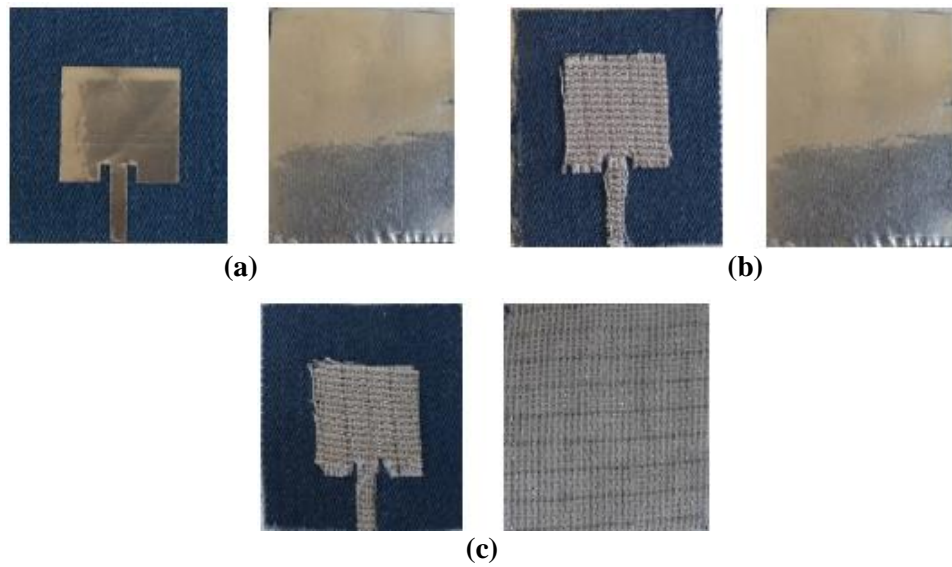


Fig. 2.22. Photographs of the antenna presented in [51], Fabricated Prototypes using different conductive parts: (a) pure copper antenna, (b) e-textile in the patch and pure copper in-ground, and (c) fully electro textile antenna

In [52], a low-profile light-weight and miniaturized textile antenna is presented for 2.40 GHz ISM band applications. It uses appropriate loading of rectangular slots with strip lines to form an inverted E-shaped radiator. The equivalent circuit of each slot and strip line is used to form the overall equivalent circuit of the presented antenna. The designed antenna occupies a volume of 20.0 mm × 30.0 mm × 0.7 mm. It covers frequencies of 2.20-2.53 GHz. The presented antenna can be incorporated into wearable systems and is a good candidate for ISM band applications due to its small size, low fabrication cost and acceptable radiation performance.

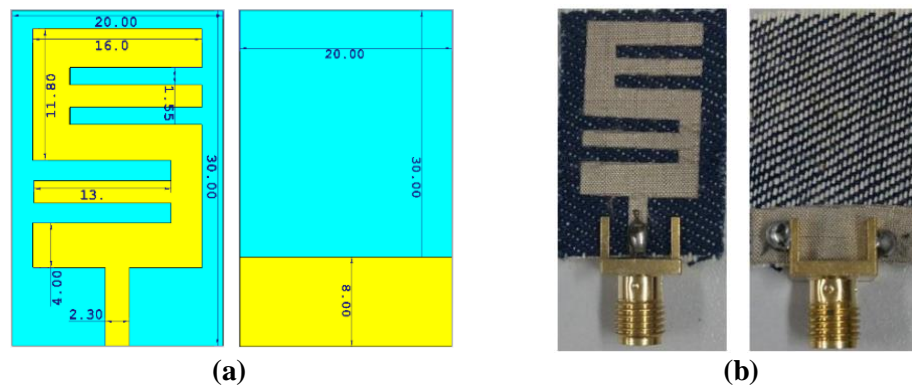


Fig. 2.23. Antenna Prototypes presented in [52]: (a) Designed Configuration and (b) Fabricated Antenna

In [53], a planar inverted-F textile antenna is presented for WLAN wearable applications. The structure is formed by using wool felt as substrate, nylon fabric as conductive element and hollow copper rivets. A pair of shorting pins and etched slots are used for achieving additional wide bandwidth. The antenna provides dual resonances of $TM_{0,1/2}$ and $TM_{0,3/2}$ modes. The designed antenna occupies a volume of $35.0 \text{ mm} \times 45.0 \text{ mm} \times 2.0 \text{ mm}$. It covers frequencies of 2.20-2.53 GHz.

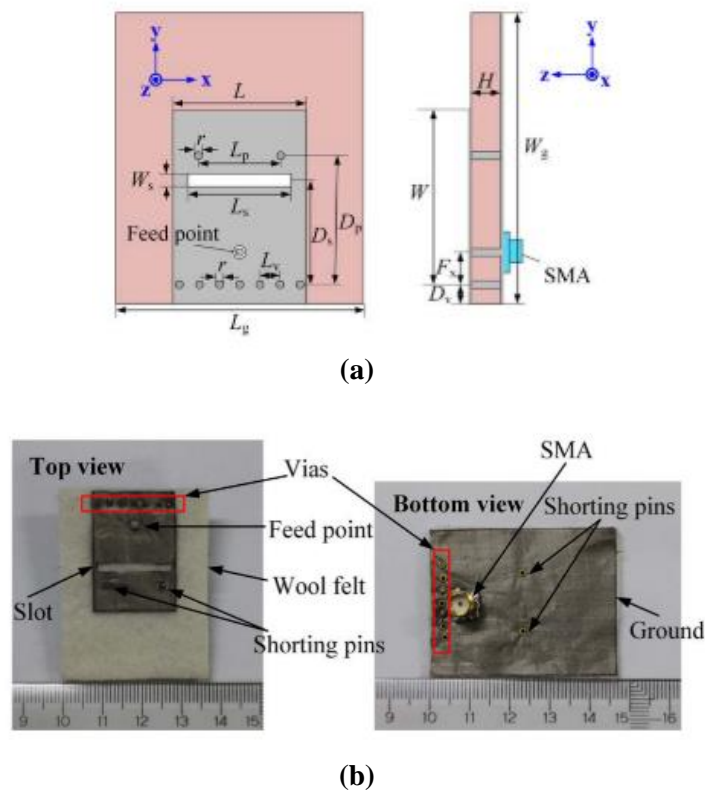


Fig. 2.24. Antenna Prototype presented in [53]: (a) Designed Configuration and (b) Fabricated Prototype

From Table 2.2, it is observed that the textile antennas designed for wearable applications are very large. The antenna presented in [52] is small-sized but it covers only one frequency band. Hence, there is a need of designing a dual-band miniaturized antenna for wearable applications.

Table 2.2. Textile Antennas for Wearable Applications

Ref. Year	Antenna Size (mm×mm×mm)	Impedance Band (GHz)	Impedance Bandwidth (MHz)	Gain (dBi)	Dielectric Material (ϵ_r)	Conductive Material	SAR (W/Kg) (For 500 mW)	Application Band
[38] 2002	42.0×50.0×0.236	2.2-2.5	300	2.2	Flexible (3.29)	---	---	UMTS
[39] 2003	76.0×71.0×3.0	2.4125-2.4875	75	6.82	Fleece (1.04)	Knitted Copper	---	WLAN/Bluetooth
[40] 2003	130.0×130.0×4.0, 130.0×130.0×1.1, 130.0×130.0×5.0, 130.0×130.0×4.0, 130.0×130.0×0.5	---	---	---	Fleece, Upholstery, Vellux, Felt, Cordura® (1.1-1.7)	Copper Tape	---	GPS
[41] 2004	72.0×66.0×8.0	2.2-2.7	500	---	Fleece (1.1)	Knitted Copper	0.00027 (1 g), 0.00215 (1g)	ISM
[43] 2004	110.0×130.0×3.5	1.88-1.94, 2.42-2.48	60, 60	9.26, 7.99	Fleece (1.1)	Copper Tape	--	GSM 1900 WLAN
[44] 2005	150.0×180.0×4.0	2.15-2.25, 2.945-3.055	100, 110	---	Felt (1.1)	Copper Tape	0.0006 (1 g), 0.00025 (1 g)	---
[45] 2006	30.0×20.0×0.5 30.0×30.0×0.5	3.10-10.6	7500	---	Acrylic Fabric (2.6 ±0.1)	Nora (Conductive Metallized Nylon Fabric)	---	UWB
[46] 2010	120.0×120.0×3.00 120.0×120.0×3.00 120.0×120.0×2.85 120.0×120.0×3.00	2.385-2.494, 2.386-2.493, 2.396-2.483, 2.376-2.483	108.97, 106.91, 87.31, 106.05	6.95, 7.04, 7.73, ---	Wash Cotton (1.51) Curtain Cotton (1.47) Polyester (1.44) Polycot (1.48)	Copper	---	WLAN
[47] 2014	64.6×61.7×3.94	2.4-2.48, 5.72-5.87	80, 150	4.2, 5.5	Foam (1.495)	Pure Copper Taffeta	0.5500 (1 g), 0.9000 (1 g)	ISM
[48] 2015	63.9×63.9×3.7	2.4-2.5	100	4.4	Foam (1.495)	Pure Copper Taffeta	0.4500 (1 g)	ISM
[49] 2015	180.0×180.0×3.5	2.31-2.54, 4.12-4.39	230, 270	0.29, 3.05	Leather (2.5)	Zell	---	ISM
[50] 2017	74.5×48.0×3.0	2.4-2.5	100	5.35	Wool Felt (1.4)	Sheildit Super	0.3800 (10 g)	ISM
[51] 2018	40.0×40.0×0.6	5.4-6.0	600	2.45	Jeans (1.78)	Copper Tape, Electrotexile	---	ISM
[52] 2018	20.0×30.0×0.7	2.2-2.53	330	2.05	Denim (1.7)	SheildIt	---	ISM
[53] 2019	35.0×45.0×2.0	5.15-5.825	675	5.90	Wool Felt (1.2)	Nylon	0.9307 (1 g), 0.4016 (10 g)	WLAN

2.4 CIRCULARLY POLARIZED TEXTILE ANTENNAS FOR WEARABLE APPLICATIONS

In [54], a novel circularly polarized (CP) textile antenna is presented. As reported, it is the first CP textile antenna. It shows that sophisticated antenna design methods are applicable to flexible textile antennas. It utilizes a single inset feeding for exciting the antenna. The concept of truncated corners along with a slit in the patch is used for achieving circular polarization. The measurement of S_{11} of the antenna was found to be complicated because of the 75Ω impedance of the feedline and flexible textile substrate. A special PCB board having two connectors, an in-house designed PCB connector on one side and an SMA connector on the other side, is deployed for the measurement. The time-domain reflectometry (TDR) method was used to extract the S_{11} to overcome the discontinuities that arise from different impedances. The designed antenna occupies a volume of $110.0\text{ mm} \times 60.0\text{ mm} \times 6.0\text{ mm}$. It covers the frequencies of 2.10-2.76 GHz.

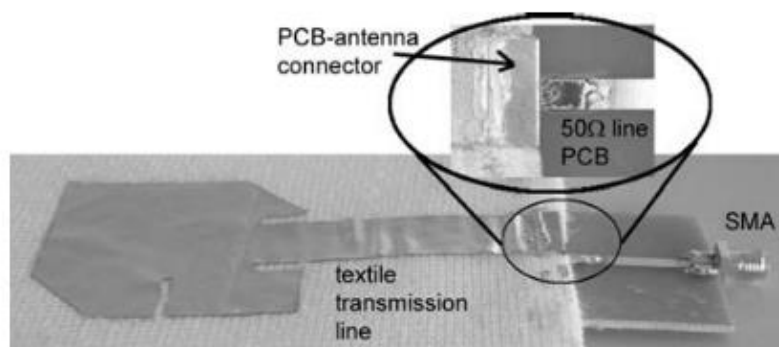


Fig. 2.25. Fabricated Prototype of the antenna presented in [54]

In [55], The foremost textile planar antenna is shown, which is made of flexible protective foam and is appropriate for firefighters' uniforms.. It uses a 3.94 mm flexible protective foam as a substrate. Shieldit Super and FlecTron are employed as conducting materials for radiating patch and ground plane respectively. It utilizes a rectangular patch with truncated corners to achieve circular polarization in the resonating band. The designed antenna occupies a volume of $66.0\text{ mm} \times 62.0\text{ mm} \times 3.94\text{ mm}$. It operates in the “2.4000-2.4835 GHz ISM band.”

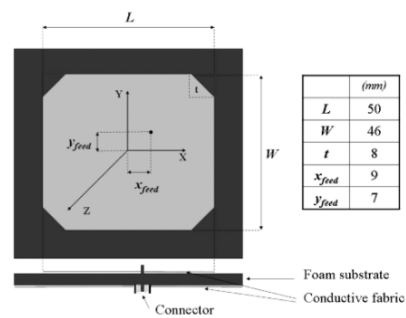


Fig. 2.26. Fabricated Prototype of the antenna presented in [55]

In [56], a circularly polarized textile antenna is presented for Iridium Satellite System. It achieves circular polarization by using a diagonally fed square-shaped patch antenna with a slot in the center. It primarily focuses on the analysis of radiation characteristics and antenna bending effects. The antenna is designed to take up a volume of $110.0 \text{ mm} \times 110.0 \text{ mm} \times 3.0 \text{ mm}$.

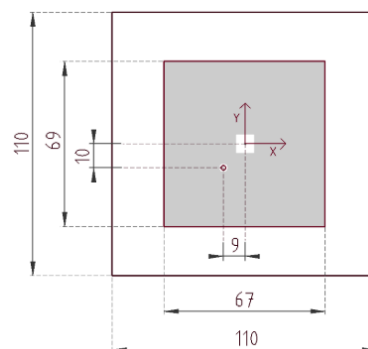


Fig. 2.27. Fabricated Prototype of the antenna presented in [56]

In [57], the possibility of creating a dual-band, flexible, and durable textile antenna for wearable applications is presented. It uses Cordura and Ballistic textile fabrics as substrates. Silver and copper-plated nylon fabric are used for the radiating patch and the ground plane, respectively. The textile layers are joined by sewing to avoid the losses caused by liquid adhesives and keep the structure bendable. The antenna maintains a right-hand-circular-polarization over 53 MHz operating band even under bending circumstances. The antenna's diversity performance is also investigated using the coverage area and isolation between two antennas. The suggested antenna measures $115.0 \text{ mm} \times 115.0 \text{ mm} \times 3.00 \text{ mm}$ in size. It operates in “1575 MHz GPS” and “1621.35–1626.50 MHz Iridium Satellite System bands.”

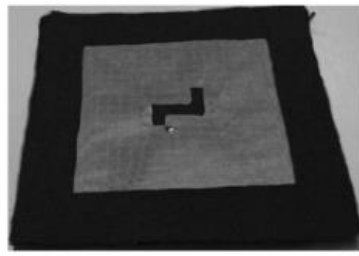


Fig. 2.28. Fabricated Prototype of the antenna presented in [57]

In [58], bending effect on the functioning of a CP textile antenna for wearable applications are investigated.. It uses a rectangular slot created along the diagonal axes for achieving circular polarization and partial and slotted ground for bandwidth enhancement. The bending effects are analyzed in xz and yz planes by placing the antenna on two cylindrical-shaped plastic bottles of different radii. The antenna's overall performance improves when it is bent in the direction of operating-resonant length. The designed antenna occupies a volume of $90.0 \text{ mm} \times 90.0 \text{ mm} \times 1.0 \text{ mm}$. It operates in the 2.42-2.58 GHz frequency band.

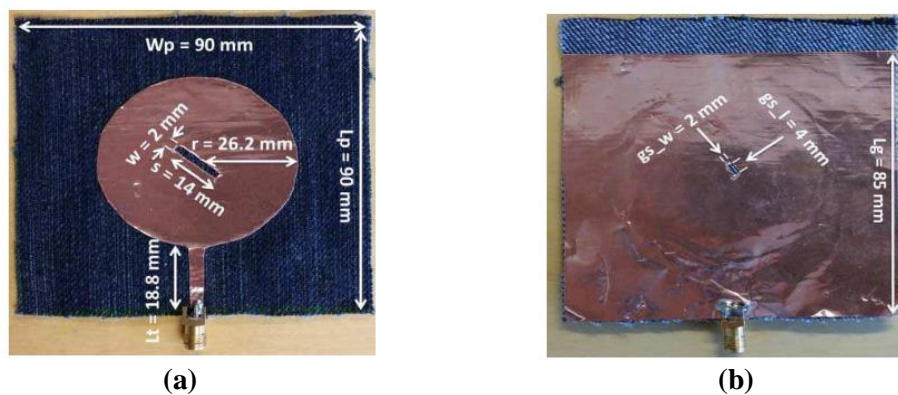


Fig. 2.29. Photograph of the antenna presented in [58]: (a) Front View and (b) Back View

In [59], for the 2.45 GHz band, a circularly polarized cloth antenna is presented.. To achieve CP, the antenna uses a complete ground plane and a square-shaped radiating element with an inverted z-shaped asymmetrical slot in the patch's center. A phase difference of 90 degrees is utilized to stimulate two perpendicular components of the electric field by incorporating a z-shaped slit. The antenna has a bandwidth of about 6.7 percent impedance and an axial ratio bandwidth of 80 MHz. The designed antenna measures $70.0 \text{ mm} \times 70.0 \text{ mm} \times 1.0 \text{ mm}$ in size. It covers frequencies of 2.42-2.59 GHz.

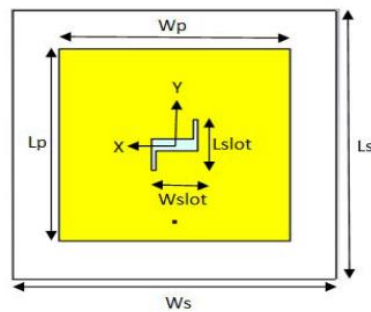


Fig. 2.30. Antenna Configuration presented in [59]

In [60], a dual-band CP textile antenna is presented for wearable applications. It consists of a complete ground plane and a slotted split-ring patch. The antenna provides dual-band coverage for 4G LTE and ISM bands. The designed antenna measures $70.0 \times 70.0 \times 3.0 \text{ mm}^3$ in size. It covers the frequencies of 1.76-1.83 GHz and 2.36-2.76 GHz.

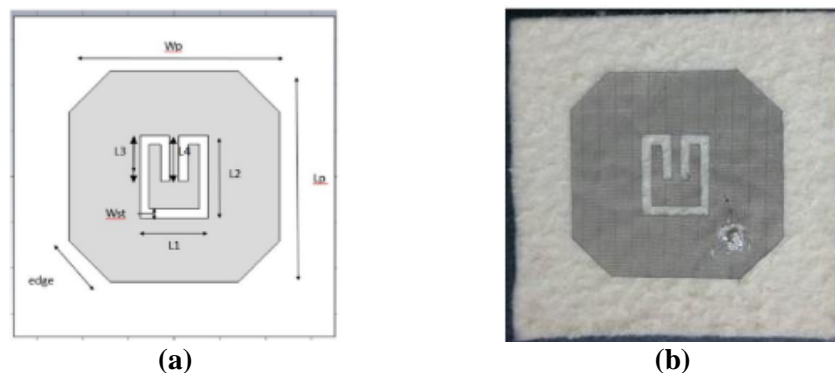


Fig. 2.31. Photographs of the antenna presented in [60]: (a) Antenna Design and (b) Fabricated Prototype

In [61], for wearable applications operating in the ISM bands, a dual-resonant dual-polarized textile antenna is presented.. The antenna is made up of a circular patch having eight slots. It uses TM_{11} mode for the first operating band used for off-body mode and TM_{02} mode for the second operating band used for on-body mode. The antenna has broadside and vertically polarized monopole-like radiation patterns in the first and second bands respectively. The designed antenna occupies a volume of $100.0 \times 100.0 \times 2.0 \text{ mm}^3$. It covers the frequencies of 2.398– 2.517 GHz and 5.697– 5.915

GHz. The antenna is suitable for a wireless body area network (WBAN) because of its on-body robustness.

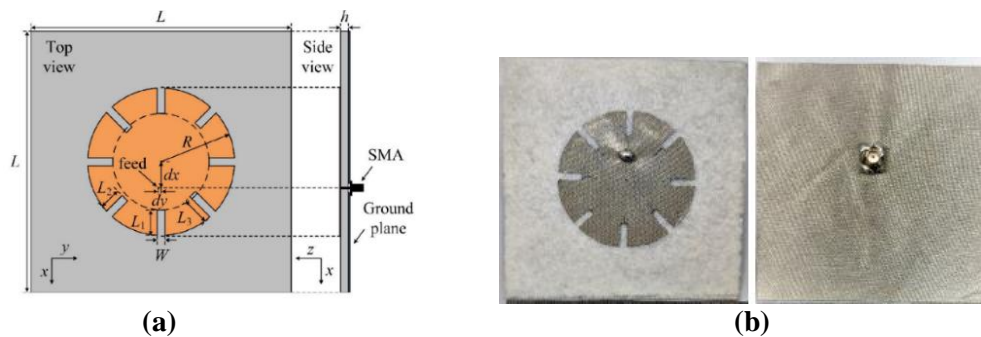


Fig. 2.32. Designed and Fabricated Prototypes of the antenna presented in [61]: (a) Antenna Configuration and (b) Fabricated Prototype

In [62], a circularly polarized triple-band antenna is presented for WLAN, C and X/Ku bands for wearable applications. It consists of a radiating patch and a defected ground plane. The parametric study of the antenna is given to validate its proper functioning. The dielectric constant (ϵ_r) of the substrate material is determined using both resonant and non-resonant approaches. The designed antenna occupies a volume of $25.0 \times 25.0 \times 1.0 \text{ mm}^3$. It covers the frequencies of 3.4-4.3 GHz, 4.7-8.4 GHz and 10.3-14.1GHz. The presented antenna has good gain and radiation performances with acceptable SAR values.

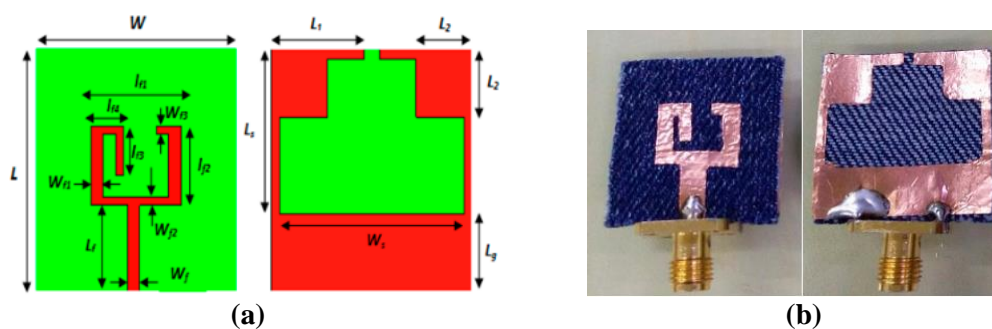


Fig. 2.33. Photographs of the antenna presented in [62]: (a) Antenna Design and (b) Fabricated Antenna

Table 2.3. Circularly Polarized Textile Antennas for Wearable Applications

Ref. Year	Antenna Size (mm×mm×mm)	Dielectric Material (ϵ_r)	Conductive Material	Gain (dBi)	Impedance Band (GHz)	Impedance Bandwidth (MHz)	Axial Ratio Band (GHz)	Axial Ratio BW (MHz)	Application Band
[54] 2004	110.0×60.0×6.0	Polyamide Spacer Fabric (1.15)	Nickel-Plated Woven Textile	---	2.1-2.76	660	2.29-2.36	70	ISM
[55] 2009	66.0×62.0×3.94	Flexible Protective Foam (1.52)	ShieldIt Super, FlecTron	6.99	2.32-2.55	230	2.36-2.54	180	ISM
[56] 2010	110.0×110.0×3.0	Cordura (1.88, 1.91, 1.67)	Woven Conductive Textile	---	1.605-1.670	65	1.600-1.620	20	Iridium satellite system
[57] 2011	115.0×115.0×3.0	Cordura (1.88, 1.91, 1.67) Ballistic 1.46, 1.46, (1.38)	Silver & Copper Plated Nylon	7.50	1.575, 1.62135–1.62650	80	1.575, 1.6250	28	Iridium, GPS
[58] 2015	90.0×90.0×1.0	Jeans (1.68)	Copper Tape	2.25	2.42-2.58	160	2.420-2.455	35	ISM
[59] 2017	70.0×70.0×1.0	Fleece (1.3)	Copper Tape	---	2.42-2.59	170	2.42-2.50	80	ISM
[60] 2018	70.0×70.0×3.0	Felt (1.44)	ShieldIt Super	---, 3.2	1.76-1.83, 2.36-2.76	70, 400	1.78-1.82, 2.415-2.485	40, 70	4G LTE, ISM
[61] 2020	100.0×100.0×2.0	Felt (1.2)	Nickel & Copper Coated Polyester Fibre	5.93, 6.02	2.398–2.517, 5.697–5.915	119, 218	2.448–2.472, ---	24	ISM
[62] 2020	25.0×25.0×1.0	Jeans (1.7)	Copper Tape	5.2, 4.18, 4.62	3.4-4.3, 4.7-8.4, 10.3-14.1	900, 3700, 3800	4.7–5.2, 5.9–6.2, 11.8–13.1	500, 300, 1300	---

2.5 TEXTILE MULTIPLE-INPUT-MULTIPLE-OUTPUT ANTENNAS FOR WEARABLE APPLICATIONS

In [63], for wearable applications, a dual-polarized cloth MIMO antenna is presented.. It consists of a square patch with two inputs to ensure the radiation or

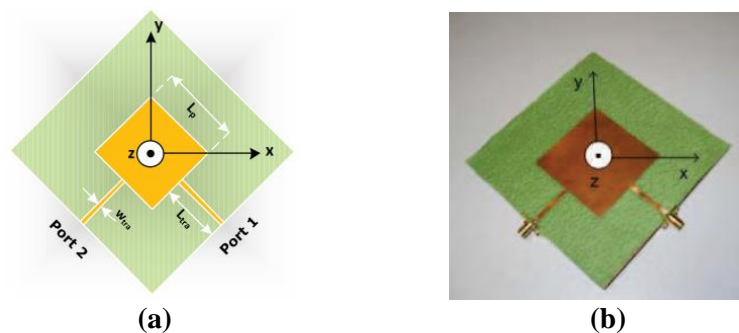


Fig. 2.34. Photographs of the antenna presented in [63]: (a) Designed Antenna and (b) Fabricated Prototype

detection of two orthogonally polarized waves. The antenna works for the 2.45 GHz ISM band. The designed antenna measures 110.0 mm x 110.0 mm x 1.05 mm in size. It operates in the 2.40-2.50 GHz frequency band.

In [64], a novel foldable thin four-elements electro-textile antenna array is presented for MIMO mobile router applications. A single rectangular conductor is used to form two antennas with two ports for space minimization. A slit is formed between the radiating elements for lowering the mutual coupling among the radiating elements. In addition, a decoupling slit is introduced in the ground plane for achieving the same purpose for MIMO applications. The antenna offers an isolation of greater than 15 dB in 1.6 to 3.1 GHz frequency range. The designed antenna measures 168.0 mm x 96.0 mm x 1.2 mm in size. It covers the frequency range of 1.40-5.00 GHz.

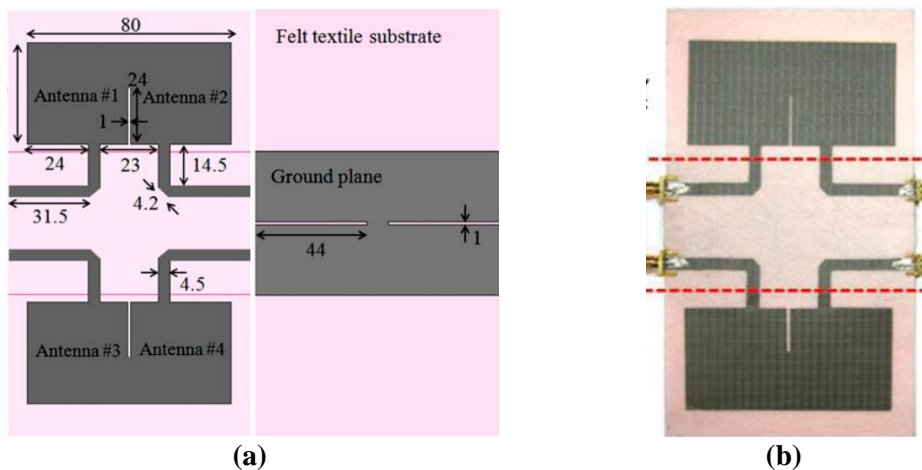


Fig. 2.35. Antenna Prototypes presented in [64]: (a) Antenna Configuration and (b) Fabricated Prototype

In [65], a dual-resonant textile MIMO antenna based on SIW is presented for wearable applications. To accomplish ISM and WLAN bands, it alters the modes of resonance by using a through in the SIW cavity. The suggested antenna's two elements are assembled in six distinct configurations to evaluate “*mutual-coupling*” and “*envelope-correlation-coefficient*” performance in order to confirm its suitability for MIMO applications. The designed antenna occupies a volume of 92.3 mm × 101.9 mm × 3.0 mm. It operates in “2.367-2.530 GHz” and “5.147-5.863 GHz” frequency bands.

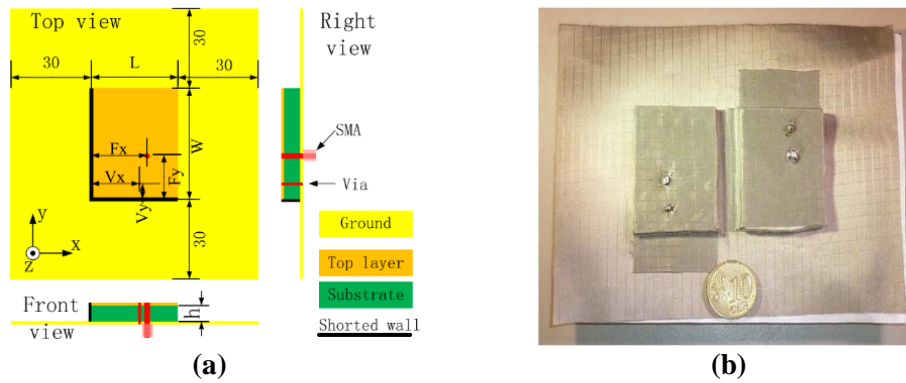


Fig. 2.36. Antenna Prototypes presented in [65]: (a) Antenna Configuration and (b) Fabricated Prototype

In [66], a novel dual-resonant quad-mode SIW Textile MIMO antenna is presented for body-worn applications. The antenna uses copper vias of diameter 2.8 mm for making electric walls for designing SIW resonators. It reduces coupling between antenna parts by using a single slot in the ground plane. The designed antenna occupies a volume of 122.0 mm × 115.0 mm × 4.1 mm. It operates in the 2.36–2.52 GHz and 4.9–6.2 GHz frequency ranges.

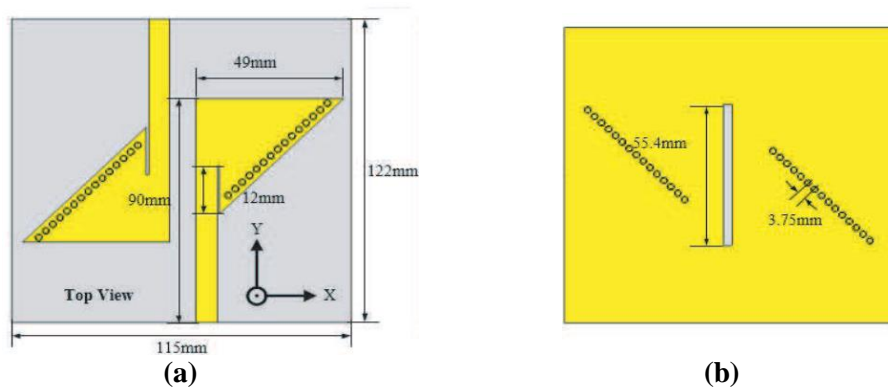


Fig. 2.37. Antenna Configuration presented in [66]: (a) Top View and (b) Back View

In [67], a textile MIMO Yagi-Uda antenna at Millimeter-Wave-Band (mmW) is presented for on-body communications. The antenna uses ten directors for achieving high directivity. Then antenna is designed to be used as a textile sensor on the human body for collecting various physiological parameters for wireless health monitoring. The designed antenna measures 26.0 mm x 9.0 mm in size. It operated in 57.0–64.0 GHz frequency band.

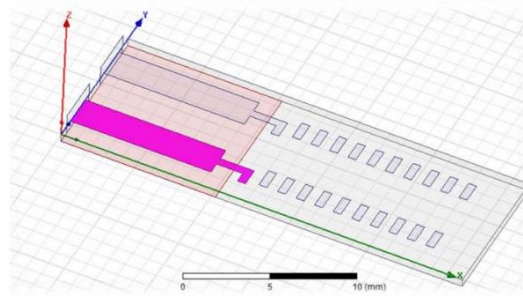


Fig. 2.38. Antenna Configuration presented in [67]

In [68], a small-size single-layer MIMO antenna made up of textile material is presented for body-worn applications. It utilizes a small ground plane capacitively loaded using two conducting strips along the two edges that are orthogonal as a radiator. It uses the theory of characteristic mode for antenna design and analysis. Each of the antenna elements has a dipole-like radiation pattern. The antenna elements have an isolation of greater than 12 dB with pattern and polarization diversities. The proposed antenna measures $38.1 \times 38.1 \times 2.0 \text{ mm}^3$ in size. It operates in the 2.40–2.485 GHz frequency band.

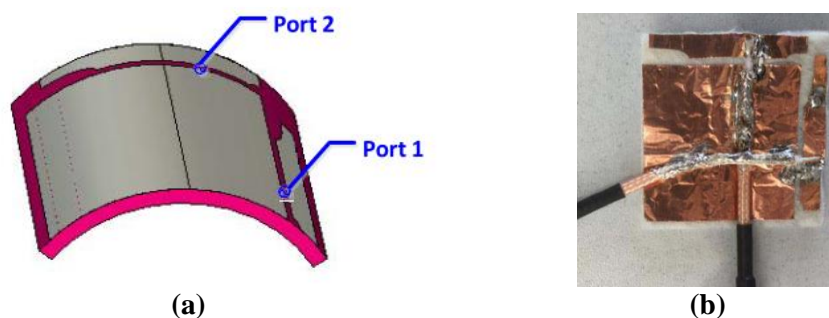


Fig. 2.39. Antenna Prototypes presented in [68]: (a) Antenna Configuration and (b) Fabricated Prototype

In [69], a compact wideband textile MIMO antenna is presented for body-worn applications. Several designs are used for investigating the decoupling between the antenna elements. Finally, a “*microstrip neutralization line (MNL)*” is used for achieving the port isolation of greater than 32 dB. The designed antenna occupies a volume of $30.0 \times 50.0 \times 1.5 \text{ mm}^3$. It covers the frequency range of 3.14–9.73 GHz and fulfils the bandwidth requirements of WiMAX, WLAN, C-band downlink-uplink, downlink defence and ITU bands.

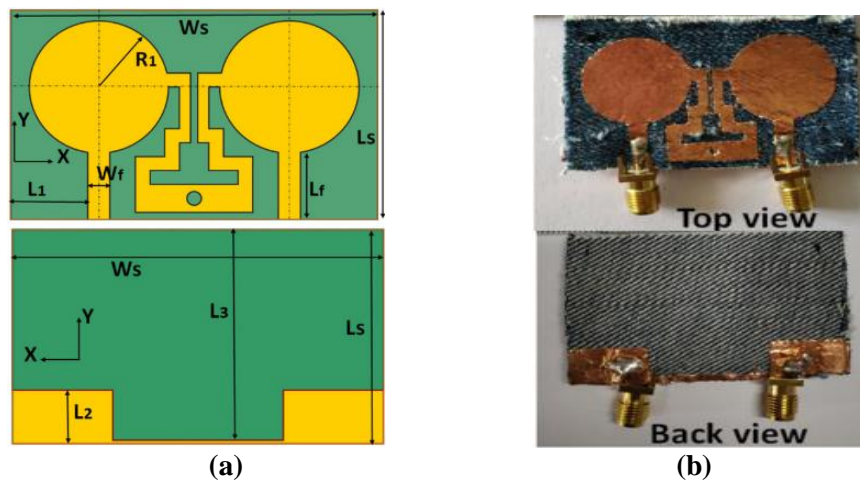


Fig. 2.40. Antenna Prototypes presented in [69]: (a) Antenna Configuration and (b) Fabricated Prototype

In [70], for body-worn applications, a compact wideband textile MIMO antenna with good isolation is given.. It utilized two “I” shaped stubs connected in series and employed on the ground plane for reducing the mutual coupling between the antenna elements. At 2.40 GHz and 5.92 GHz, it has lowest and highest port isolations of 22.0 dB and 53.0 dB, respectively. The antenna measures 40.0 mm x 70.0 mm x 1.0 mm in size. It covers the frequency range of 1.83-8.00 GHz and can be used for WiMAX, WLAN and C-band downlink-uplink applications.

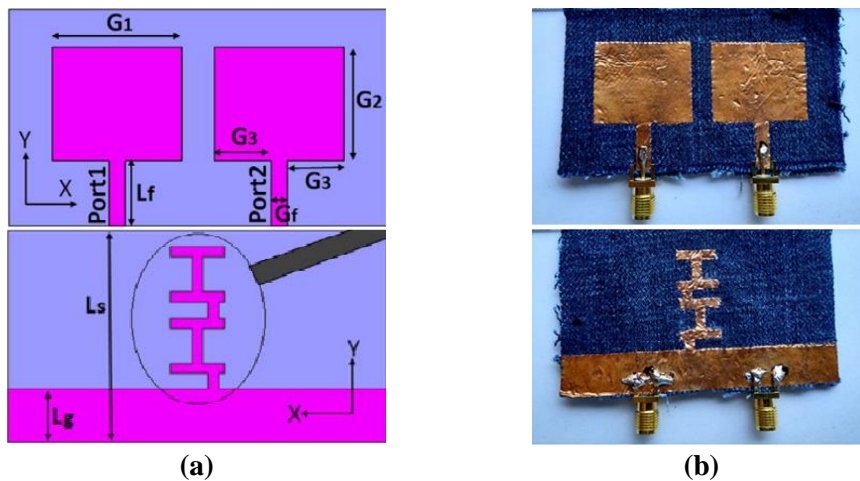


Fig. 2.41. Antenna Prototypes presented in [70]: (a) Antenna Configuration and (b) Fabricated Prototype

In [71], a two-element “*ultra-wide-band (UWB)*” textile MIMO antenna is presented for wearable applications. It achieves low mutual coupling over the whole frequency range by placing an '8' shaped stub in the centre of the partial ground plane. The designed antenna measures $35.0 \times 55.0 \times 1.5 \text{ mm}^3$ in size. It can be utilised for UWB applications and has an operating range of 2.74-12.33 GHz frequency band.

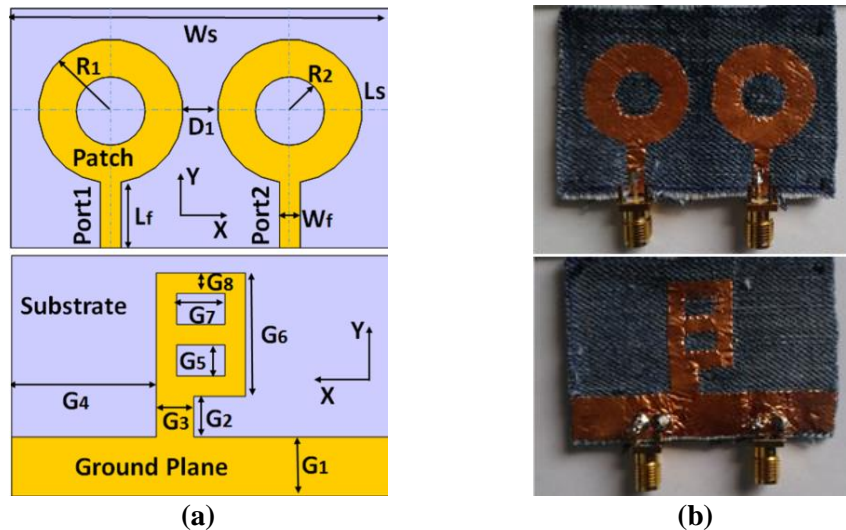


Fig. 2.42. Antenna Prototypes presented in [71]: (a) Antenna Configuration and (b) Fabricated Prototype

In [72], two and four elements dual-polarized dual-wideband textile MIMO antenna is proposed for WLAN and WiMAX applications. The antenna's diversity performance (ECC, MEG, DG and TARC) is improved by using meandered-line arrangements on both planes. The two-element MIMO antenna provides linear polarisation at all necessary frequencies, whereas the four-element MIMO antenna gives CP at 2.40 GHz and LP at 5.20 and 5.80 GHz. The designed antenna measures $110.0 \times 97.0 \times 1.4 \text{ mm}^3$ in size. It covers the frequency ranges of 1.50-3.80 GHz and 4.10-6.10 GHz.

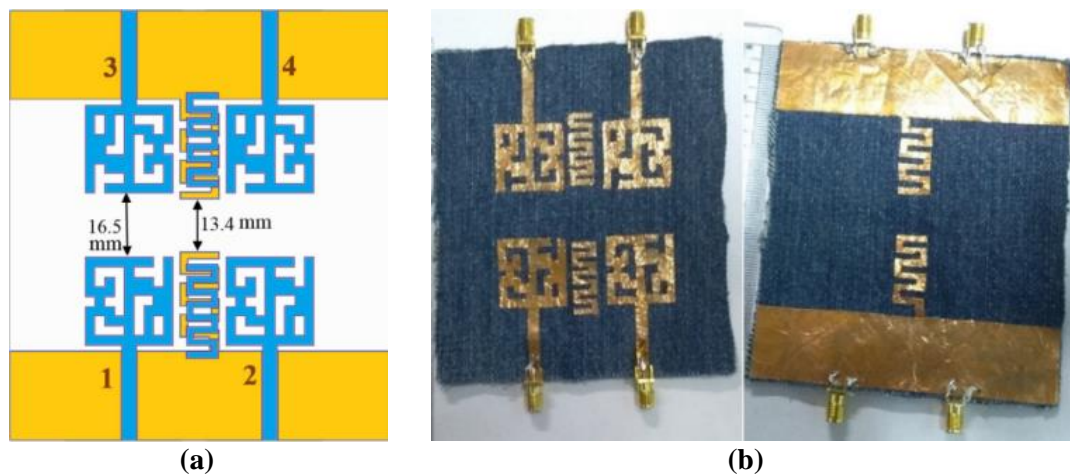


Fig. 2.43. Antenna Prototypes presented in [72]: (a) Antenna Configuration and (b) Fabricated Prototype

In [73], a compact low mutual coupling textile MIMO is presented for 2.4 GHz ISM band applications for “*wireless-body-area-network (WBAN)*.” It uses an inverted S-shaped radiator as an antenna element. The isolation between the radiating elements is achieved by inserting slots in the ground plane. The designed antenna measures 40.0 mm x 86.0 mm x 1.6 mm in size. It covers the frequency ranges of 2.42-2.47 GHz.

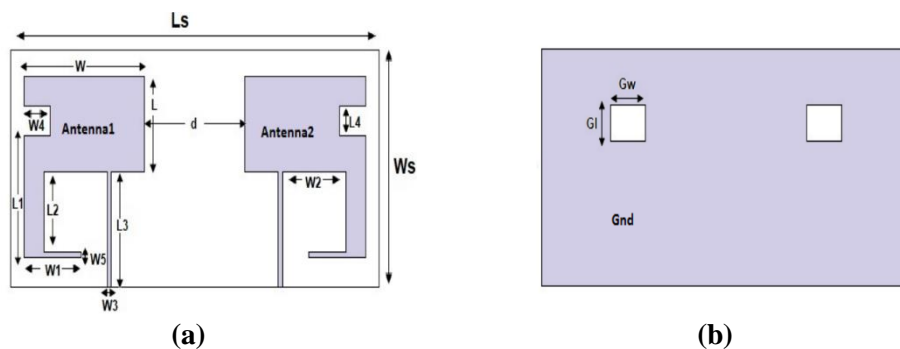


Fig. 2.44. Antenna Configuration presented in [73]: (a) Front View and (b) Back View

In [74], a two half-ring-typed textile MIMO antenna is proposed for wearable applications. With the use of a defective ground structure, it provides greater than 15.5 dB isolation over the full operational frequency range. The designed antenna occupies a volume of $100.0 \times 60.0 \times 1.0 \text{ mm}^3$. It covers the frequency spectra of 6.95-16.46 GHz and fulfils the bandwidth requirements of ITU band, full X-band and Ku-band downlink-uplink application bands.

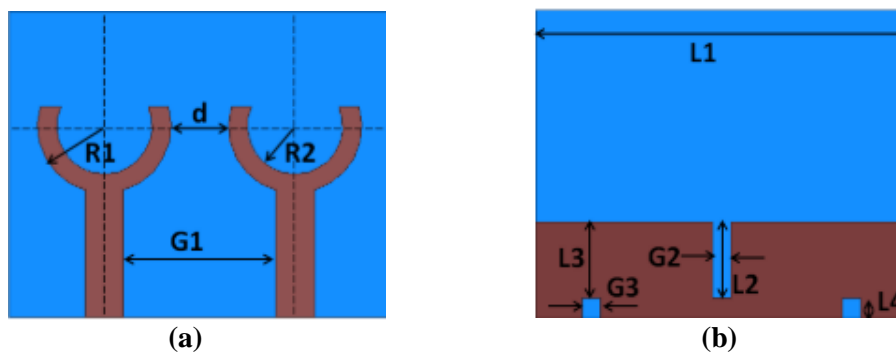


Fig. 2.45. Antenna Configuration presented in [74]: (a) Front View and (b) Back View

In [75], a two-element textile MIMO antenna is presented for wearable applications. It utilizes a unique split ring resonator meta-inspired decoupling structure to reduce the correlation between the antenna elements. It offers an isolation of lower -18 dB, -38 dB and -34 dB at 2.40 GHz, 5.20 GHz and 5.80 GHz respectively. The designed antenna occupies a volume of $16.0 \times 20.0 \times 1.0 \text{ mm}^3$. It is designed to cover the frequency spectra of Bluetooth (2.45 GHz), WiMAX (3.50 GHz), IEEE 802.11a and b/g/n WLAN applications. It covers the frequency ranges of 1.34-3.92 GHz and 4.34-6.34 GHz.

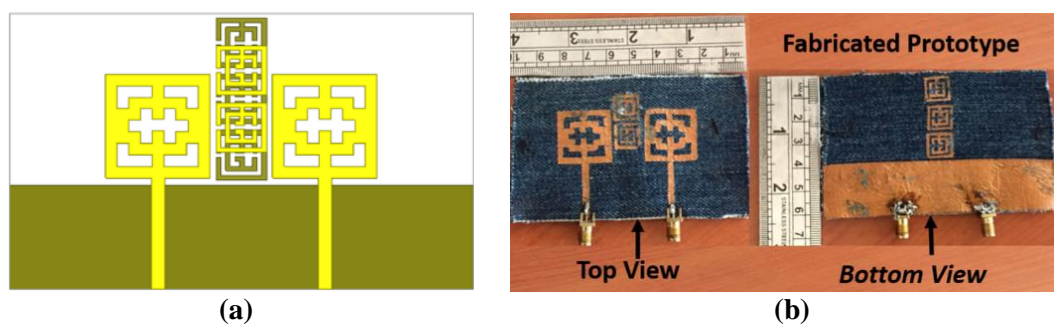


Fig. 2.46. Photographs of the antenna presented in [75]: (a) Designed Antenna and (b) Fabricated Prototype

Table 2.3 presents various circularly polarized textile antennas while Table 2.4 presents the textile MIMO antennas for wearable applications. Most of the textile MIMO antennas presented in existing literature have very low resonance bandwidth except very few. Thus, there is a need for more textile MIMO antennas having novel compact designs and wide resonance bandwidth. In addition, the dual-band textile

MIMO antennas presented in the literature exhibits linear polarization for both resonating bands except [72]. Hence, the dual-band dual-polarized or dual-band circularly polarized textile MIMO antennas are needed.

Table 2.4. Textile Multiple-Input-Multiple-Output Antennas for Wearable Applications

Ref. Year	Area (mm×mm)	No. of Elements	Substrate (ϵ_r)	Gap between Elements (mm)	Impedance Band/ Bandwidth (GHz)	Axial Ratio Band (GHz)/ Bandwidth (MHz)	Polarization	Application
[63] 2012	110.0×110.0	2	Fleece (1.05)	---	2.40-2.50/ 0.10	---	Linear	Wearable
[64] 2015	168.0×96.0	4	Felt (1.14)	---	1.40-5.00/ 3.60	---	Linear	Wearable
[65] 2015	92.3×101.9	2	Felt (1.30)	10	2.367-2.530/ 0.163, 5.147-5.863/ 0.716	---	Linear	Wearable
[66] 2017	122.0×115.0	2	Nylon-Taffet	13	2.40-2.50/ 0.100, 4.9-6.3/ 1.400	---	Linear	Wearable
[67] 2018	26.0×9.0	2	---	2.5	57.0-64.0/ 7.00	---	Linear	Wearable
[68] 2018	38.1×38.1	2	Felt (1.20)	10	2.40-2.485/ 0.085	---	Linear	Wearable
[69] 2019	30.0×50.0	2	Jeans (1.6)	7	3.14-9.73/ 6.59	---	Linear	Wearable
[70] 2019	40.0×70.0	2	Jeans (1.6)	7	1.83-8.00/ 6.17	---	Linear	Wearable
[71] 2019	35.0×55.0	2	Jeans (1.6)		2.74-12.33/ 9.59	---	Linear	Wearable
[72] 2020	110.0×97.0	4	Jeans (1.77)	10	1.50-3.80/ 2.30, 4.10-6.10/ 2.00	2.20-2.48/ 80, ---	Circular, Linear	Wearable
[73] 2020	40.0×86.0	2	Jeans (1.6)	23	2.42-2.47/ 0.05	---	Linear	Wearable
[74] 2020	16.0×20.0	2	Jeans (1.6)	3	6.95-16.46/ 9.51	---	Linear	Wearable
[75] 2020	100.0×60.0	2	Jeans (1.6)	13.5	1.34-3.92/ 2.58, 4.34-6.34/ 2.00	---	Linear	Wearable

“I happen to have discovered a direct relation between magnetism and light, also electricity and light, and the field it opens is so large and I think rich.”

Michael Faraday

3

A PLANAR DUAL-BAND ANTENNA FOR ISM/WEARABLE APPLICATIONS

In this chapter, the designing, modelling, analysis, fabrication and measurement of a planar, dual-band antenna for ISM band applications is proposed. The antenna comprises of a ground plane, a rectangular patch, and a microstrip feed line of 50Ω . The antenna patch is loaded with several slots to obtain dual resonances in the range of 902-928 MHz and 2400-2480 MHz, covering the lower and higher ISM band frequencies, respectively. The proposed antenna design is validated using simulated and measured results. The specific absorption rate results show that the proposed antenna operates within the approved standard limits and can be used as a flexible antenna.

3.1 INTRODUCTION

Due to the increasing demand for wearable electronics systems, the wireless body area networks (BANs) and biotelemetry devices have gained considerable attention, recently. With the rapid growth of wearable technology in health monitoring, telecommunication, search/rescue operation, and various other civil and military applications, the designing of wearable antennas has garnered significant attention from researchers and engineers [76]. The IEEE 802.15 standards group was formed to specify on-body, off-body, and in-body communication applications in support of body communication systems. Body-centric communication (BCC) has firmly established itself within the realm of “*personal area networks (PANs)*” and “*body area networks (BANs)*” [77].” Recent advances in wireless technology led to the advent of BANs, which is an active research area as it has great potential for improvement in the above-mentioned applications, particularly in the healthcare sector [78]. Numerous heterogeneous biological sensors are placed on various regions of the body or implanted beneath the skin in wireless BANs. Several communication nodes are situated near the

human body in BCC, and a wearable antenna is a critical component of BAN communication [79]. Various wearable antennas have been designed for wireless local area networks (WLANs) [80], [81], industrial, scientific and medical bands (ISM) [33], [82] and personal communication services (PCSs) [33], [81] applications. Wearable antennas require shielding when the antenna is in close proximity to the human body. A complete ground can be used to serve this purpose so that the wearable antennas can communicate efficiently without harming the human body exposed to the radio frequency (RF) energy, as characterized by the specific absorption ratio (SAR) [83]. The wearable technology not only unfolds the structural designs but also opens the field of material science to explore high-quality flexible dielectric and conducting materials for the RF/microwave range. This has led to many low loss flexible materials to be used as substrate and conducting strata, such as Ninja Flex [84], Cordura and Ballistics [57], Piezo-resistive Polymer [85], Polyimide [86] Zelt, Flectron, Pure Copper Polyester Taffeta, ShieldIt [87], etc.

Recently, several antennas have been designed to cover the ISM bands (433.95 MHz, 867 MHz, 915 MHz, 2380 MHz, 2450 MHz, and 5800 MHz). However, most of them are single-band antennas [31], [79], [88]–[90]. A few of them, which are dual-band have targeted higher frequency bands [18], [35], [49], [65], [91]. The proposed antenna covers lower frequency bands, to minimize the health hazards associated with radio wave exposure, and covers ISM band applications. The designed antenna resonates at two frequencies centred around 918 MHz and 2450 MHz. The fractional bandwidths of the two bands are 2.39 % and 3.26 %, respectively. A comparison of the presented built-in prototype with other reported works is given in Table 3.1.

This chapter is organized as follows: Section 3.2 gives an insight into the designing and analysis of the proposed antenna using CST microwave studio [92]. The overall size, patch length, and effective loading of the patch using slots to excite dual-band resonance are explained in this section. Section 3.3 provides a parametric analysis of the proposed antenna. In Section 3.4, simulated and measured reflection coefficients and radiation characteristics are provided. The simulated current density is also provided in the same section. The antenna's on-body performance, such as bending analysis and SAR, are provided in Section 3.5.

Table 3.1. Comparison of the Proposed Antenna with other Antennas

Ref.	Size (mm ³)	Bands Covered	Frequency of Application Band(s) (MHz)	BW (MHz)	Application Band(s)	Gain (dBi)	Application Area
[79]	80×80×2.15	Single	2450	100	ISM	4.1	Wearable
[88]	13×13×1.27	Single	915	160	ISM	32	Implantable
[31]	100×100×3	Single	2450	160	ISM	5.6	Wearable
[90]	54.8×47.4×2	Single	2450	90	ISM	7.1	Wearable
[48]	77.8×77.8×3.7	Single	2450	107	ISM	4.2	Wearable
[93]	44×44×3.94	Single	2450	83.5	ISM	6.49	Wearable
[17]	57×50×1.97	Single	2450	100	ISM	4.17	Wearable
[33]	58×40×0.075	Dual	1800–2450, 5150–5825	650, 675	WLAN	1.05, 3.12	Wearable
[91]	100×100×3	Dual	2450, 5000	490, 1710	ISM, WLAN	4.7, 3	Wearable
[65]	101.9×92.3×3	Dual	2450, 5500	163, 157	ISM, WLAN	3.2, 5.8	Wearable
[94]	100×80×5	Dual	2450, 5000	277, 850	ISM, HiperLAN	5.31, 9.34	Wearable
Prop	50×70×0.8	Dual	902–928, 2400–2500	23, 80	ISM	2.51, 3.89	Wearable

3.2 ANTENNA TOPOLOGY

The top and bottom layouts of the presented antenna are shown in Figs. 3.1(a) and (b), respectively. The antenna is designed on FR-4 substrate of thickness (h) = 0.8 mm, loss tangent ($\tan \delta$) = 0.02 and dielectric constant (ϵ_r) = 4.4. FR-4 dielectric substrate is used due to its easy availability, however, the antenna can be designed on any flexible substrate having the same electrical properties. The top and bottom views of the fabricated antenna prototype are illustrated in Figs. 3.1(c) and (d), respectively. The antenna's overall size is 50 mm × 70 mm × 0.8 mm. The dimensions of the proposed antenna are stated in Table 3.2.

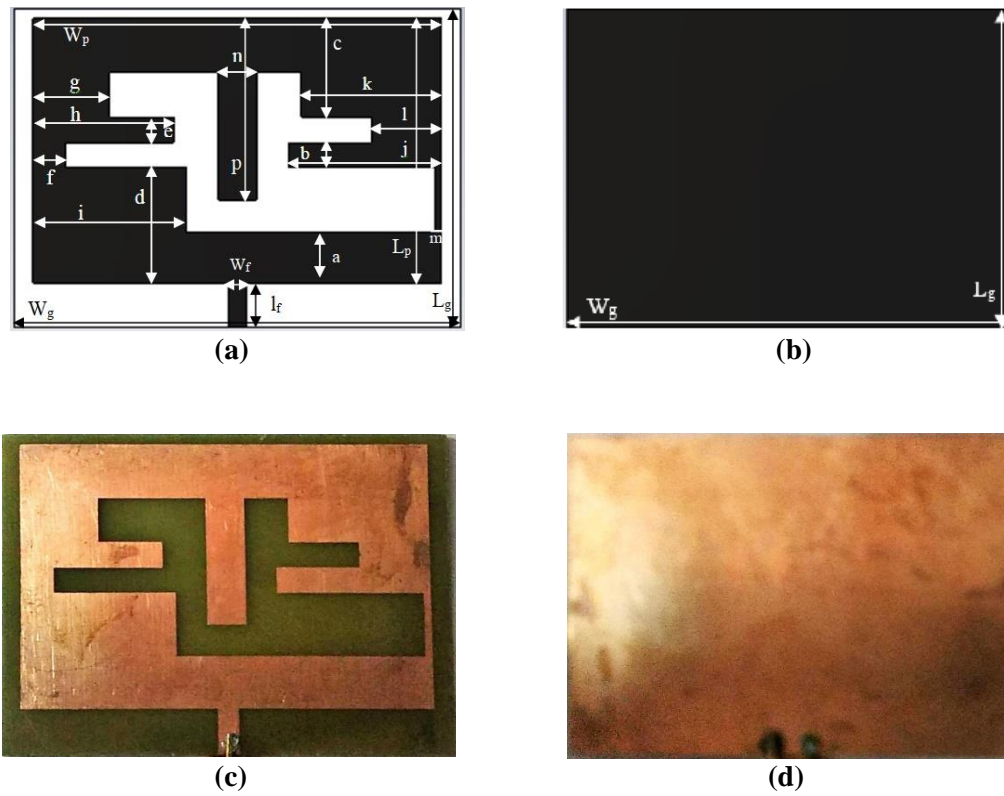


Fig. 3.1. Antenna layout: (a) top view (b) bottom view (c) top view of the fabricated prototype (d) bottom view of the fabricated prototype.

Table 3.2. Dimensions of the Proposed Antenna

Parameter	Value (mm)	Parameter	Value (mm)
L_p	41.4	f	5
W_p	64	g	12
L_G	50	h	22
W_G	70	i	24
a	8	j	24
b	4	k	22
c	15.4	l	11
d	18	m	1
e	4	n	6
l_f	7	p	26
W_f	1.5		

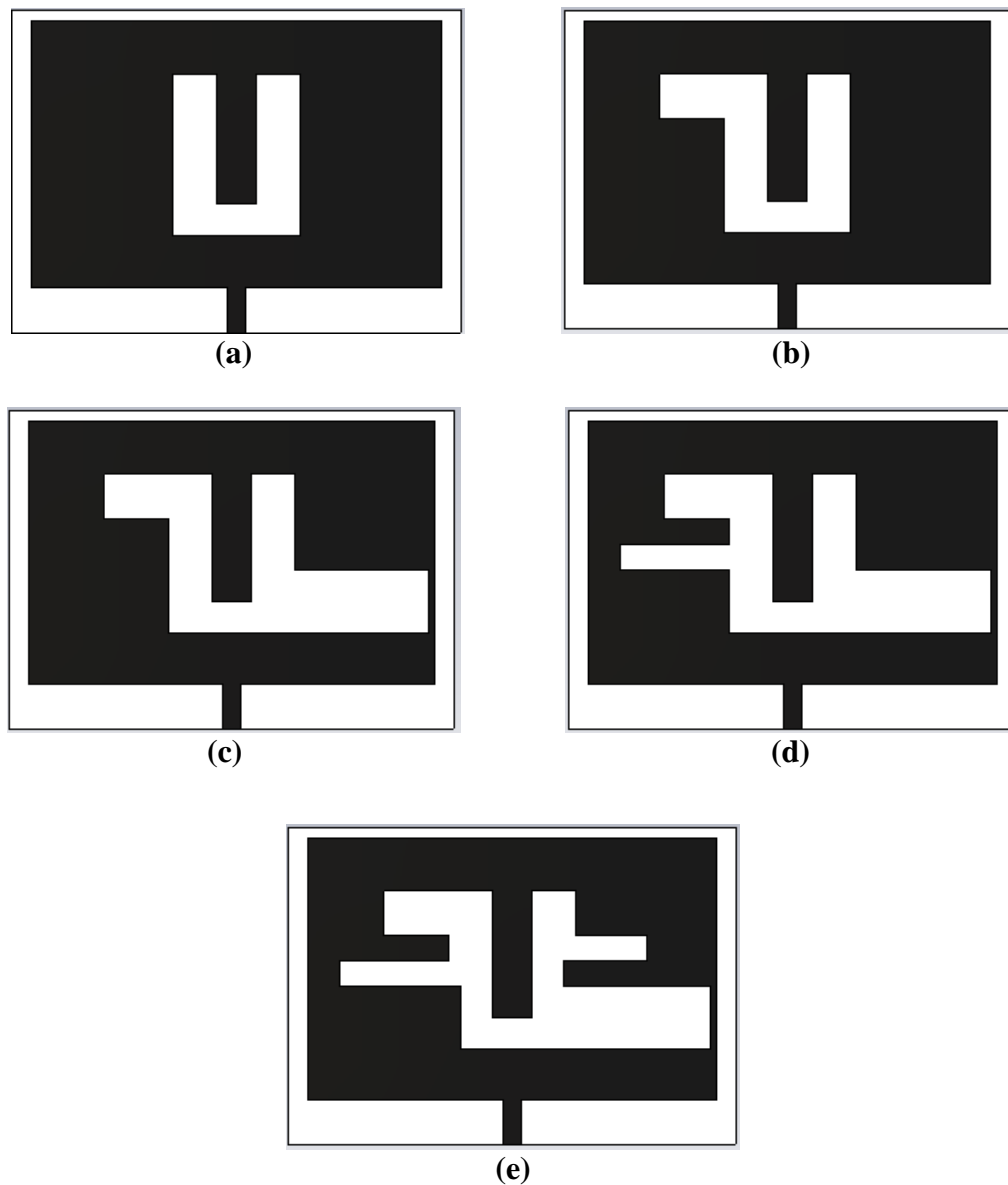
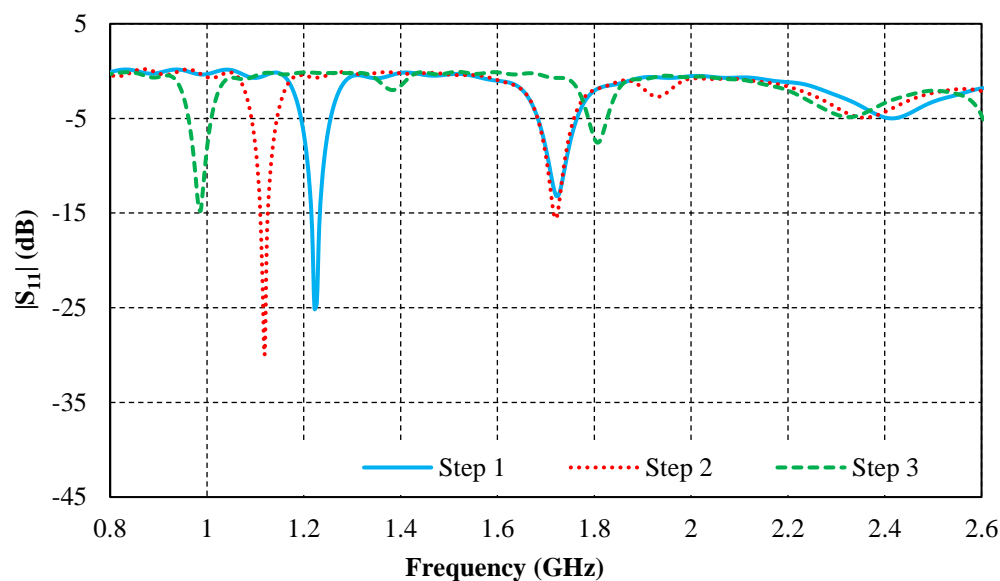


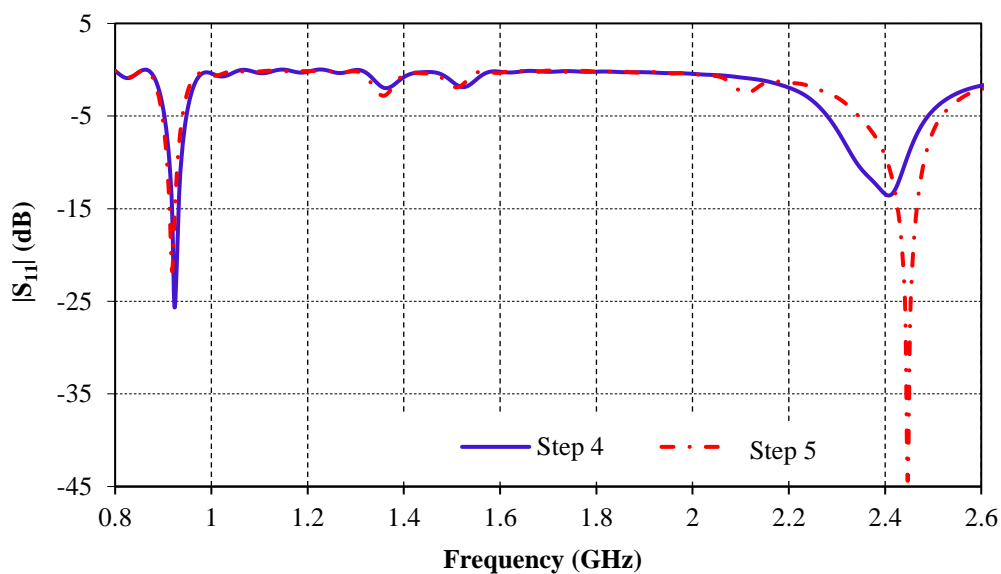
Fig. 3.2. Design steps of the proposed antenna: (a) step 1 (b) step 2 (c) step 3 (d) step 4 (e) step 5.

The evolution steps of the proposed antenna are shown in Fig. 3.2. The reflection coefficients of the design steps are shown in Figs. 3.3(a) and (b). In step 1, a U-shape slot is inserted in the centre of the rectangular patch as depicted in Fig. 3.2(a). Fig. 3.3(a) shows that the antenna resonates at 1222 MHz and 1721 MHz. In step 2, as depicted in Fig. 3.2(b), a stub is formed on the left side of the U-shape slot, which keeps the upper resonating frequency almost the same as of step 1, while a significant change is seen in the lower resonating frequency band (a shift of 103 MHz towards left). This

antenna resonates at 1119 MHz (with $|S_{11}|$ -29.88) and 1720 MHz (with $|S_{11}|$ -15.67 dB). Another stub was created in step 3 on the lower right side of the U-shape slot as shown in Fig. 3.2(c). This step shifts the lower band to 987 MHz while the upper band shift towards the right with a minor mismatching of impedance. The antenna resonates at 987 MHz and 1805 MHz. In step 4, another slot was introduced on the left side of the U-shape slot, shown in Fig. 3.2(d). Here, the lower band shifts towards the left while the upper band shifts towards the right with improved impedance matching.



(a)



(b)

Fig. 3.3. Reflection coefficients $|S_{11}|$ of the design steps: (a) 1 to 3 (b) 4 to 5.

This results in resonances at 923 MHz and 2408 MHz. The antenna is further modified in step 5 by introducing a small stub on the right side of the U-shape slot to obtain the desired frequency bands as depicted in Fig. 3.2(e). Finally, the parameters h and k (shown in Fig. 3.1(a)) are optimized to obtain the desired 918 MHz and 2450 MHz resonating bands as shown in Fig. 3.3(b).

3.3 PARAMETRIC ANALYSES

The response of the proposed antenna depends upon various design parameters. The parametric analyses of these parameters are performed for obtaining optimal dimensions. The reflection coefficient variations due to parameter f are shown in Fig. 3.4.

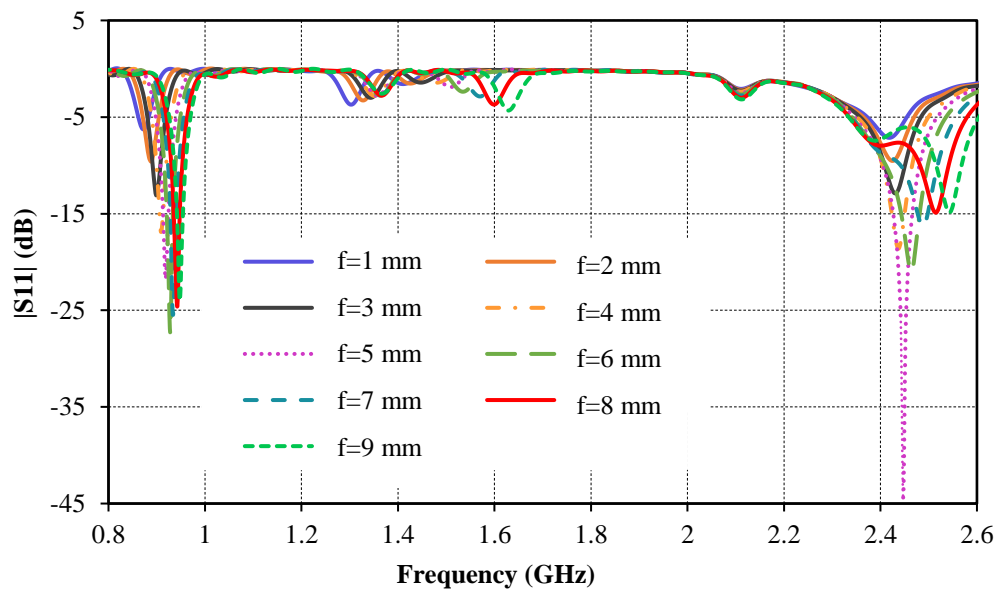


Fig. 3.4. Reflection coefficients $|S_{11}|$ due to variation in parameter f .

The lower resonating band shift towards the upper side with an increment in f . When f is greater than or equal to 7 mm, the upper resonance disappears. Fig. 3.5 depicts reflection coefficients due to variation in g . The lower band's resonance frequency falls as the value of g increases, but the top band has no resonance. The reflection coefficient variations due to the change in parameter l are shown in Fig. 3.6. The parameter l shifts both the resonating bands towards the lower frequency range.

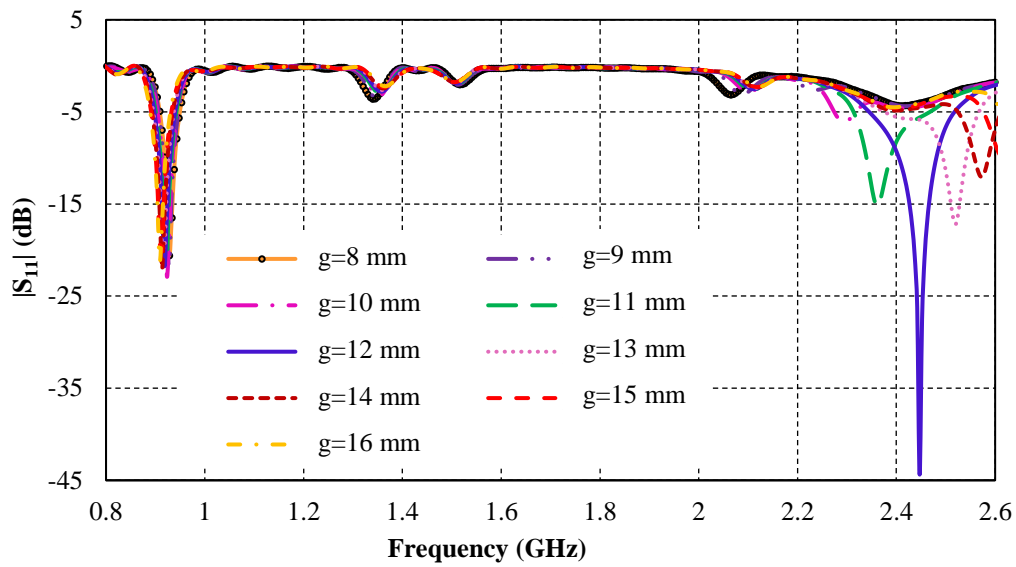


Fig. 3.5. Reflection coefficients $|S_{11}|$ due to variation in parameter g .

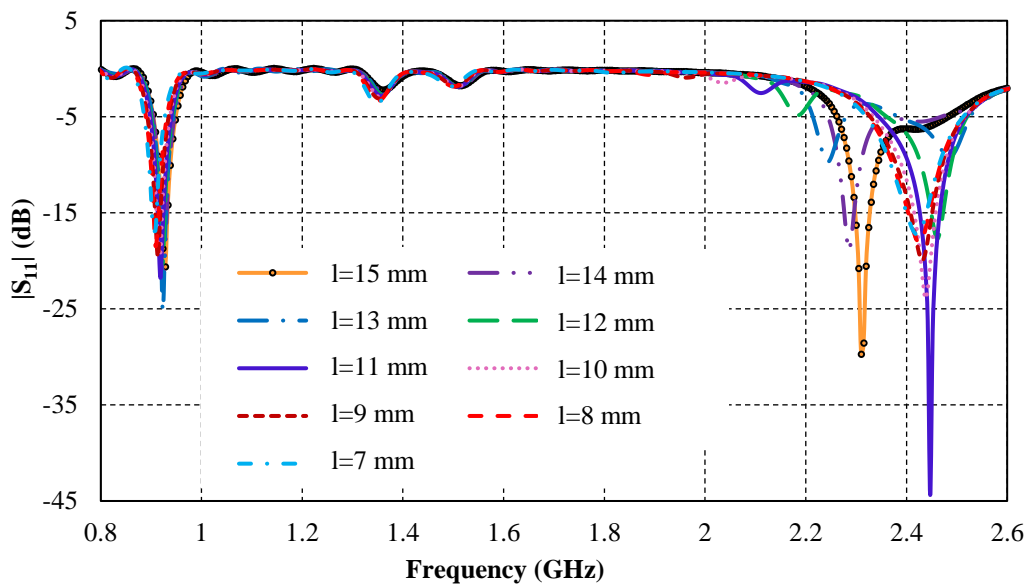


Fig. 3.6. Reflection coefficients $|S_{11}|$ due to variation in parameter l .

An increment in m shifts the frequencies of the upper resonating band as shown in Fig. 3.7. After 6 mm, the resonant frequencies of the upper band shift towards the lower side. The parameter m does not much affect the lower frequency band of the antenna.

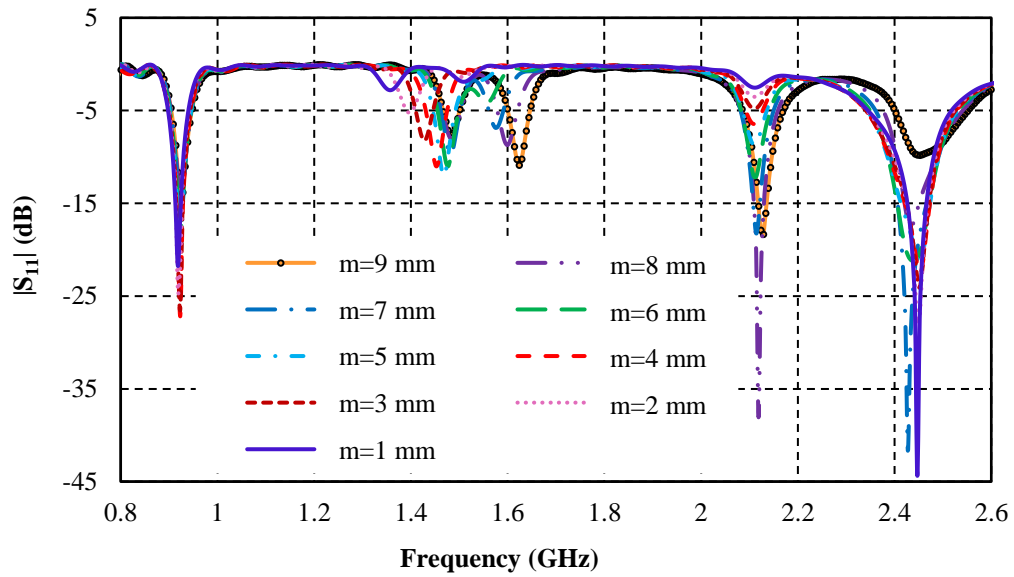


Fig. 3.7. Reflection coefficients $|S_{11}|$ due to variation in parameter m .

3.4 ANTENNA PERFORMANCES IN FREE SPACE

3.4.1 Reflection Coefficients

The simulated and measured reflection coefficients of the proposed antenna are shown in Fig. 3.8. The antenna was tested using the Agilent N5222A network analyzer. Both simulated and experimental results are in good agreement at both frequencies, which validates the dual-band operation of the presented antenna. The measured -10dB

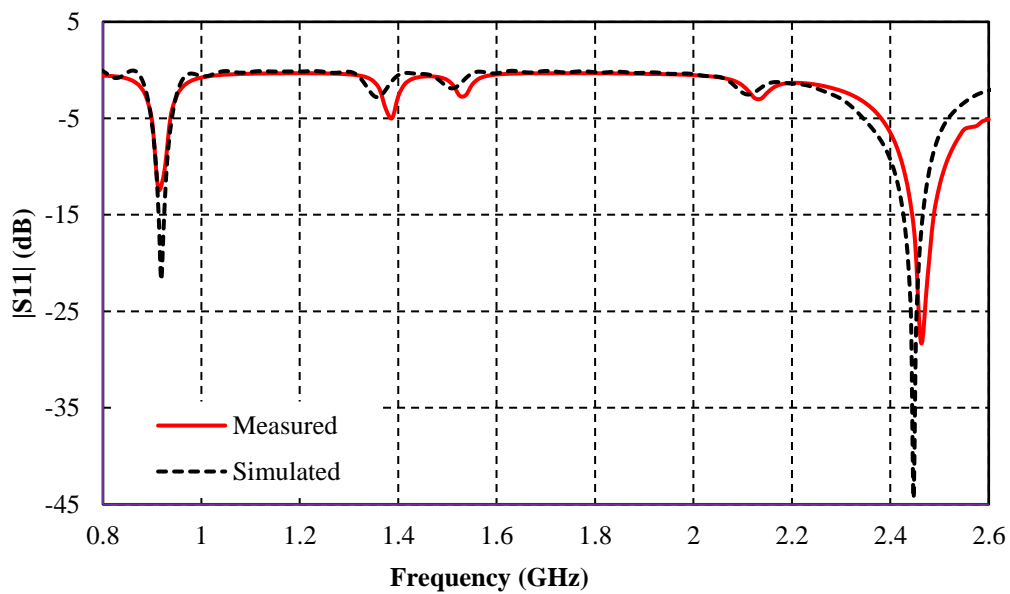


Fig. 3.8. Simulated and measured reflection coefficients $|S_{11}|$.

bandwidths are 907-929 MHz and 2400-2480 MHz in free space.

3.4.2 Radiation Pattern and Gain

Figs. 3.9(a) and (b) shows the radiation patterns of the antenna at 918 MHz and 2450 MHz in E-plane and H-plane. It can be observed that E-plane patterns are unidirectional while H-plane patterns are bidirectional. In Table 3.3, the proposed antenna's simulated and experimental gain values are presented.

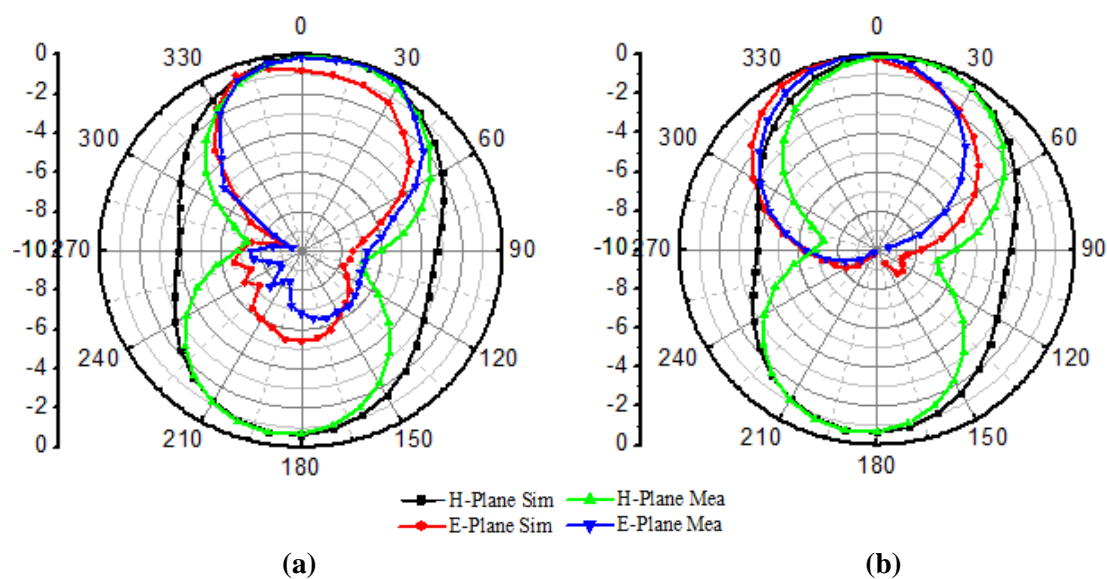


Fig. 3.9. Simulated and measured radiation patterns: (a) 918 MHz (b) 2450 MHz.

Table 3.3. Simulated and Measured Gain

Frequency (MHz)	Gain (dBi)	
	Simulated	Measured
918	2.51	2.23
2450	3.89	3.31

3.4.3 Surface Current Distribution

Figures 3.10(a) and (b) show the surface current distribution plots of the presented antenna at 918 MHz and 2450 MHz, respectively. It is observed that the current intensity is higher in the region of the slot than in other portions of the patch.

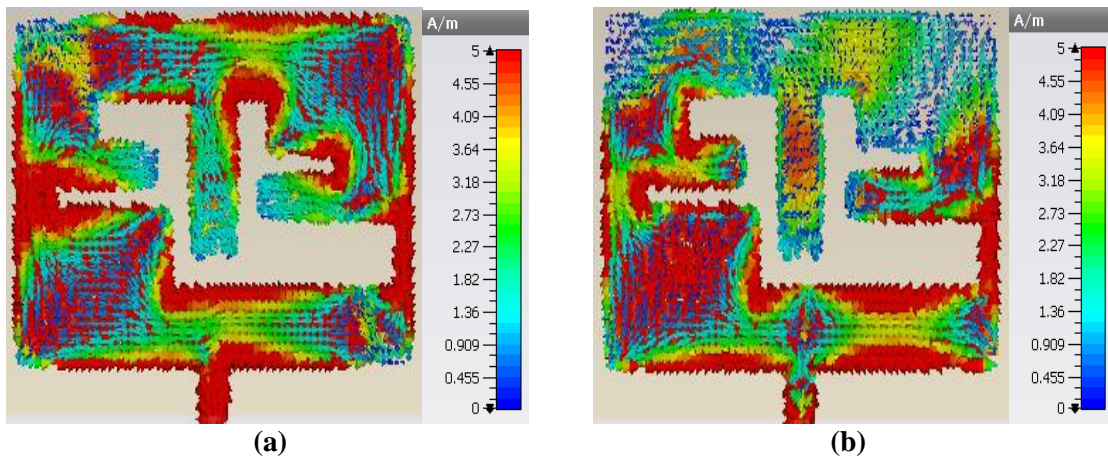
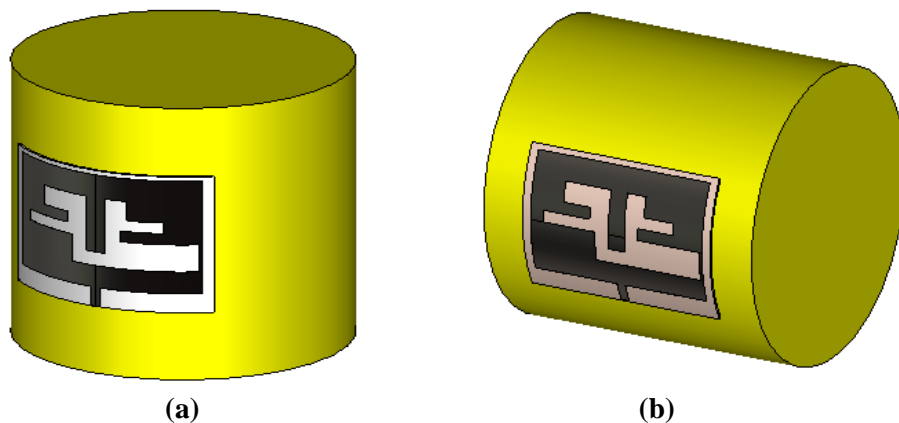


Fig. 3.10. Surface current distribution of the proposed antenna: (a) 918 MHz (b) 2450 MHz.

3.5 ANTENNA PERFORMANCES ON HUMAN BODY

3.5.1 Bending Analysis

To see how bending affects the performance of the proposed antenna, it was bent in four different directions: (a) parallel to the x -axis, (b) parallel to the y -axis, (c) along the axis of $y+45^\circ$, and (d) along the axis of $y-45^\circ$, as shown in Fig. 3.11. The bending radii were assumed as 50 mm and 75 mm to emulate the typical size of a human arm and shoulder, respectively.



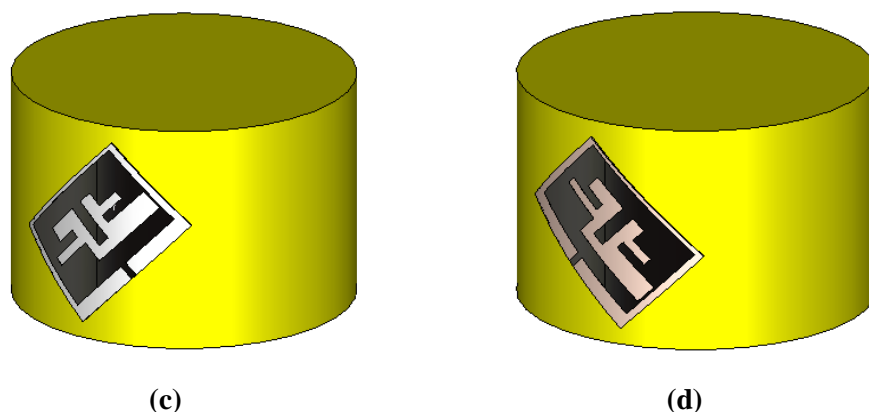
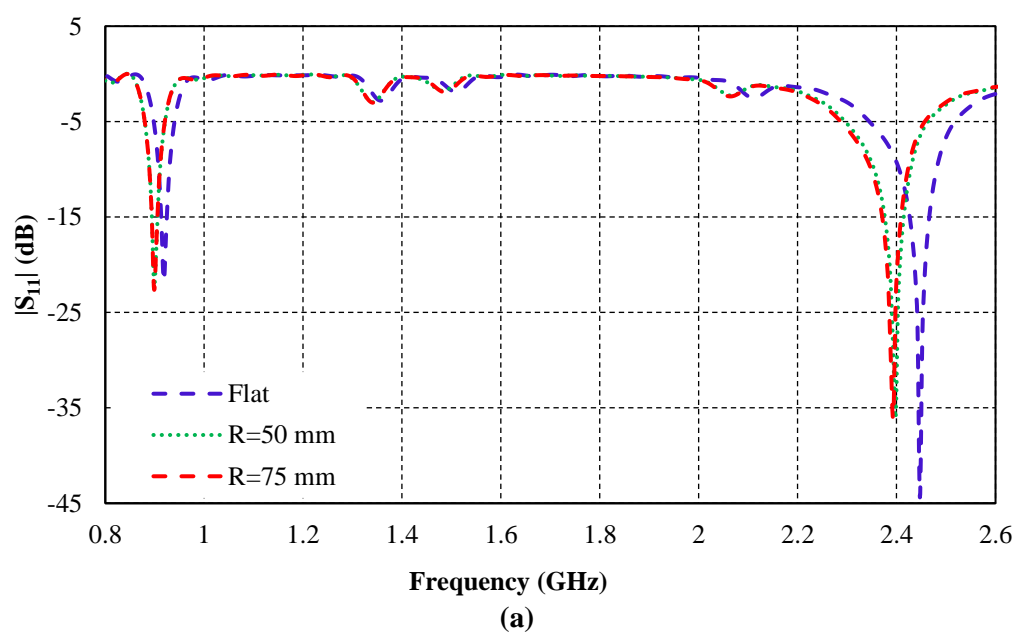


Fig. 3.11. Bending analysis of the antenna along: (a) x -axis (b) y -axis (c) $y+45^\circ$ axis (d) $y-45^\circ$ axis.

The simulated results for different bending directions are shown in Fig. 3.12. The variation in reflection coefficients due to bending parallel to the x -axis is shown in Fig. 3.12(a). It is found that there is no significant change in the resonance frequencies of the lower band while the resonance frequencies of the upper band shift towards the left. The bending performance of the antenna parallel to the y -axis is shown in Fig. 3.12(b). A slight change in the upper band is noted, the resonating frequency band shifts towards the left, while there is no considerable change in the lower resonance band.



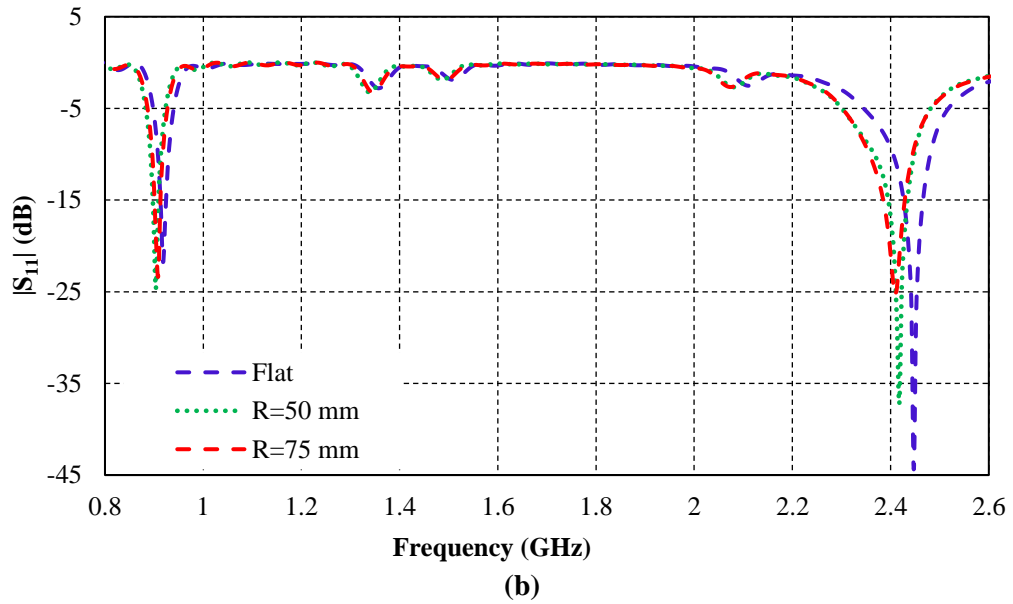
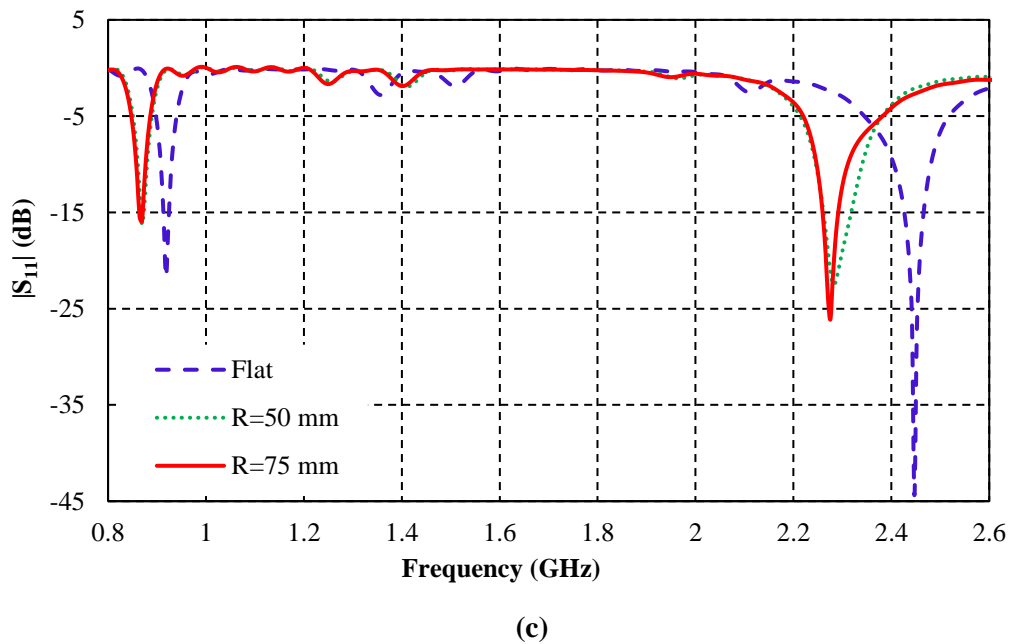
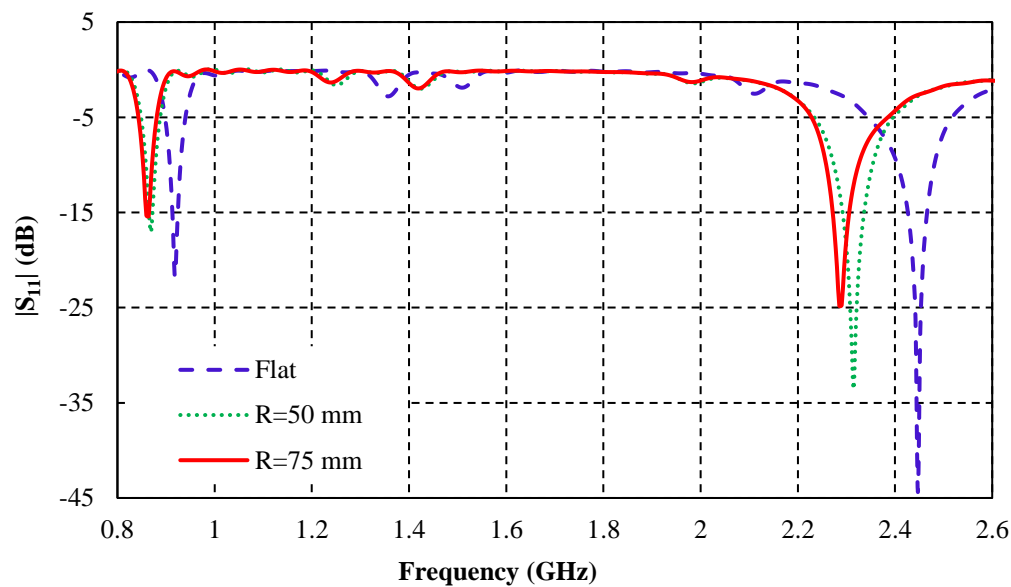


Fig. 3.12(c) shows the variation of reflection coefficients due to the bending of the antenna in the $y+45^\circ$ axis. A significant change in reflection coefficients is seen for both the upper and lower bands. The variation in reflection coefficients along the $y-45^\circ$ axis is shown in Fig. 3.12(d). Both, the lower and upper resonance frequencies represent a significant shift towards the lower side.





(d)

Fig. 3.12. Reflection coefficients $|S_{11}|$ due to bending along: (a) x-axis (b) y-axis (c) $y+45^\circ$ axis (d) $y-45^\circ$ axis.

3.5.2 Specific Absorption Ratio (SAR)

The simulated average SAR of the proposed antenna over 1 g of tissue model in CST (for a density of 2000 Kg/m^3) is presented in Fig. 3.13. The average value of SAR at 918 MHz is approximately 278 W/kg (for 1 g of tissue), when the input power is 1 W, whereas, the average SAR at 2450 MHz is found to be approximately 455 W/Kg .

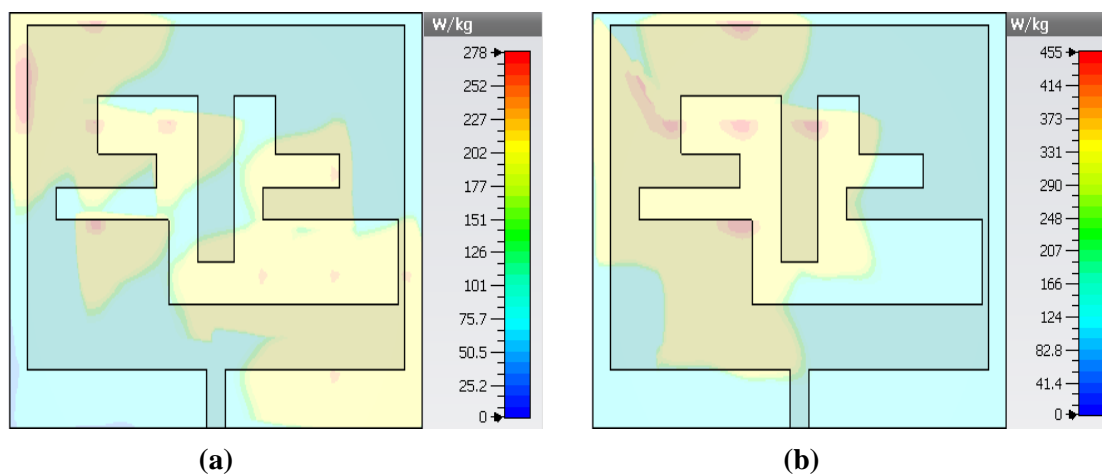


Fig. 3.13. Simulated average SAR of the proposed antenna for 1 g of tissue
(a) 918 MHz (b) 2450 MHz.

To comply with IEEE Std C95.1 (2005), the maximum input power is kept at 5.75 mW [95]. The simulation conducted at 2450 MHz allows a maximum power of 3.5 mW for safe usage. As a result of the findings, the proposed antenna appears to be a viable option for wearable wireless communication applications.

3.6 CONCLUSION

This chapter presents a new dual-band patch antenna covering 902-928 MHz and 2400-2500 MHz ISM band frequencies. The reflection coefficients, radiation patterns, surface current density, and gain of the proposed antenna have been investigated. The bending analyses of the proposed antenna are also studied at the two resonances. The SAR results show that the proposed antenna operates within the approved standard limits. The antenna occupies an area of 50 mm × 70 mm. The antenna may be a suitable choice for wearable applications.

“Your heart has a powerful little antenna and its pulses and vibrations can be felt throughout the universe.”

Suzy Kassem

4

A COMPACT WIDEBAND FLEXIBLE ANTENNA FOR WIRELESS MEDICAL TELEMETRY SERVICES

In the previous chapter, the design and development of a planar, dual-band antenna for ISM band applications were presented. In this chapter, the designing, modelling, analysis, fabrication and measurement of a planar small size coplanar waveguide (CPW)-fed wideband antenna is presented for wearable applications. The antenna operates for “1395-1400 MHz” and “1427-1432 MHz wireless medical telemetry service (WMTS) bands.” The centre frequencies of the two bands are 1397.5 MHz and 1429.5 MHz. The antenna occupies a volume of 48 mm × 52 mm × 0.8 mm. The proposed antenna design is validated when the simulated and measured reflection coefficients, radiation patterns, and gain are calculated and shown to be in good agreement. The simulation results for SAR and bending are also presented to demonstrate that the proposed antenna operates within the approved limits and can be fabricated on a flexible substrate.

4.1 INTRODUCTION

Wearable antennas are gaining popularity these days due to their attractive features, functionality and applications. Planar, conformal, flexible, lightweight, low cost and portable antennas are preferred for wireless communication and sensing applications. These antennas must be able to communicate with the human body in close proximity. All of these requirements make designing wearable antennas difficult, particularly in terms of size compactness, structural bending effects, interaction to the human body, complexity of manufacture, and precision [96]. The remote monitoring of patients, especially the elderly, requires a substantial effort in the field of wearable antennas [97]. The increasing demand for wearable devices has led to numerous advancements, including the miniaturization of antennas for both invasive and non-

invasive wearable applications [78]. The wearable applications include remote health monitoring, bio-feeding, telemedicine, etc.

Several bands have been used in the literature for wearable applications, such as the “*medical implant communication service (MICS) band (402-405 MHz), industrial, scientific and medical (ISM) bands (433.1-434.8 MHz, 902-928 MHz, 2400-2480 MHz) and wireless medical telemetry service (WMTS) bands (608-614 MHz, 1395-1400 MHz, 1427-1432 MHz) [98].*” The WMTS band is specially designed (by Federal Communications Commission) for remote health monitoring of patients [99]. This band can be used for both implantable and wearable medical devices [100]. It provides an interference-free spectrum, preventing overcrowding in the popular ISM band [30]. It has allocated three frequency bands, namely 608-614 MHz, 1395-1400 MHz and 1427-1432 MHz. These services are used to remotely monitor the patient’s vital signs and other physiological parameters such as pulse, respiration rates, pH, blood pressure, body temperature, pulse oximeter, EEG, ECG, etc.

Most of the antennas presented in the literature for WMTS were single band structures [30], [101]. The reported dual [32], [102], [103] and triple-band [104], [105] antennas covered only one WMTS band, whereas other resonances covered ISM [23], [102], [106] or MICS [103] bands. The proposed design is a small size planar coplanar waveguide (CPW)-fed wideband antenna. The CPW-fed antennas have a low profile and are easily integrated, allowing them to be easily placed inside a package. The proposed antenna also overcome the limitations of a narrow impedance bandwidth of wearable patch antennas [107]–[108]. The proposed antenna covers two WMTS bands (1395-1400 MHz and 1427-1432 MHz). The FR-4 substrate material is used for fabrication due to its low cost and easy availability in the market. The same antenna can also be designed using flexible substrates with similar electrical properties, such as polyimide. The proposed antenna is compared to other antennas in Table 4.1. The antenna is designed, analyzed and optimized using CST Microwave Studio® [92]. The proposed antenna covers two WMTS bands (1395-1400 MHz and 1427-1432 MHz) and can be used for biomedical telemetry services.

Table 4.1. Comparison of the Proposed Antenna with other Antennas

Ref.	Resonance Bands Covered	Antenna Size (mm×mm×mm)	Substrate (ϵ_r)	Frequency Band (MHz)	Application	BW (MHz)	Application Area
[7]	Single	78×20×0.8	Duroid RT 5880 (2.2)	1427-1432	WMTS	4.3	Wearable
[8]	Single	37×20×1.6	FR-4 (4.3)	608-614	WMTS	9.0	Implantable
[10]	Dual	35×20×0.1	Rogers Ultralam 3850 (2.9)	2385-2495, 5500-6100	ISM	110, 600	Wearable
[11]	Dual	23.6×19.4×2.4	RO 3210 (10.2)	402-405, 1427-1432,	MICS, WMTS	100, 120	Implantable
[13]	Triple	20×17×1.6	FR-4 (1.6)	402-405, 1427-1432, 2400-2480	MICS, WMTS, ISM	50, 18, 130	Implantable
[14]	Dual	12.6×8.5×2.4	FR-4 (4.4)	1427-1432, 2400-2480	WMTS, ISM	50, 210	Implantable
[79]	Single	80×80×2.15	Felt (1.17)	2400-2500	ISM	100	Wearable
[31]	Single	100×100×3	FR-4 (4.3)	2330-2490	ISM	160	Wearable
[90]	Single	80×84×2	Denim (1.6)	2409-2451	ISM	42	Wearable
Prop.	Dual	52×48×0.8	FR-4 (4.4)	1395-1400, 1427-1432	WMTS	620	Wearable

4.2 ANTENNA TOPOLOGY

The antenna is made of FR-4 with a thickness of 0.8 mm, a loss tangent of 0.02, and a dielectric constant of 4.4. The design of the proposed antenna and its fabricated prototype are shown in Figs. 4.1(a) and (b), respectively. All the dimensional parameters of the designed antenna are presented in Table 4.2. The overall size of the proposed antenna is 52 mm × 48 mm × 0.8 mm and occupies a total volume of 1.996 cm³.

The proposed antenna design steps are shown in Fig. 4.2. The stepwise

simulated reflection coefficients are presented in Fig. 4.3. In step 1, a CPW-fed patch antenna is designed as shown in Fig. 4.2(a). The antenna does not show resonance due to poor impedance matching, as illustrated in Fig. 4.3(a). In step 2, the antenna is modified by changing the size of the ground plane (Fig. 4.2(b)). The antenna resonates at 2000 MHz with a bandwidth of 88 MHz (1954-2042 MHz). In step 3, as shown in Fig. 4.2(c), a large slot is created in the radiating patch of the antenna. This increases the effective length of the patch, decreasing the resonating frequency to 1724 MHz. As illustrated in Fig. 4.3(a), this step not only shifts the resonating band to a lower frequency but also increases the bandwidth from 88 MHz to 274 MHz (1601-1875 MHz). In step 4, the effective length of the patch is further increased by using a meander line shape (Fig. 4.2(d)). This decreases the resonating frequency further with a minor drop in the bandwidth. The antenna resonates at 1678 MHz with a bandwidth of 236 MHz (1569-1805 MHz). The effective length of the patch is further increased by using a similar procedure to the previous step (Fig. 4.2(e)). The antenna resonates at 1534 MHz with a bandwidth of 148 MHz (1465-1613 MHz).

A further increment in the effective length of the radiating patch (shown in Fig. 4.2(f)) improves the impedance matching of the antenna. Here, the resonating frequencies are 1517 MHz and 2174 MHz with $|S_{11}|$ of -17.5 dB and -13.6 dB, respectively, as illustrated in Fig. 4.3(b). The bandwidth obtained in step 6 is 143 MHz (1448-1591 MHz) for a resonating frequency of 1517 MHz. In step 7, the effective length of the patch is further increased, as shown in Fig. 4.2(g). This step reduces the first resonating frequency slightly while making no difference to the second. The antenna is resonating at 1510 MHz with $|S_{11}|=-19.3$ dB and 2174 with $|S_{11}|=-14.9$ dB. Step 8 employs the same sinuous approach, resulting in an increment in the effective length of the patch (as shown in Fig. 4.2(h)). The antenna resonates at 1361 MHz with a bandwidth of 95 MHz (1315-1410 MHz). The second resonance bandwidth increases to 153 MHz (2047-2200 MHz) with $|S_{11}|=-26.9$ dB at 2130 MHz. In step 9, the position of the feed line is optimized to obtain the desired results. The final position of the feed line is shown in Fig. 4.2(i). This step affects the results obtained in the previous step and merges the two bands to obtain a wideband. In step 10, the effective length of the antenna is further increased by using a rotated E-shaped structure as shown in Fig. 4.2(j). This step plays a major role as it provides a wide bandwidth of 590 MHz (1335-

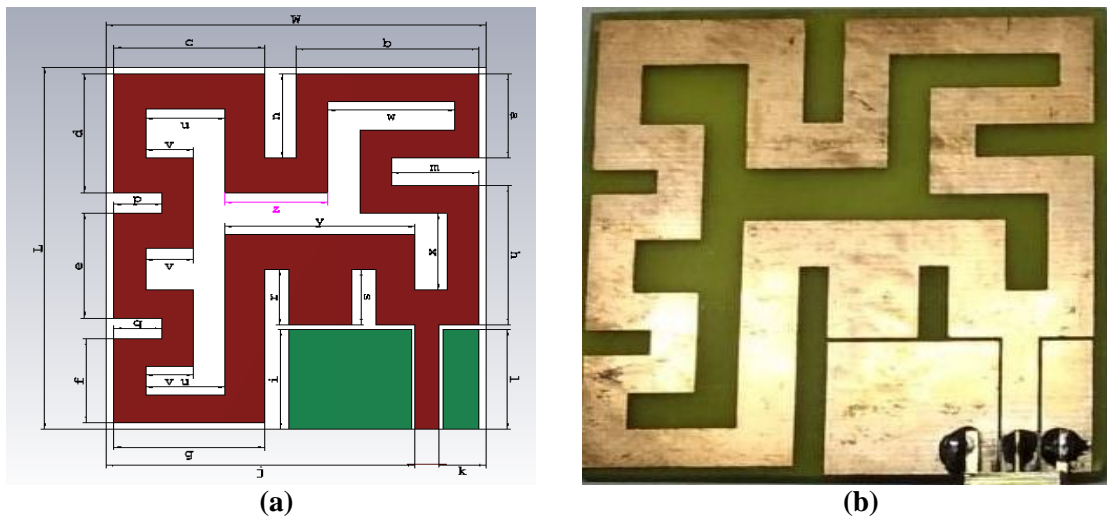


Fig. 4.1. Proposed antenna: (a) schematic (b) fabricated prototype.

Table 4.2. Dimensions of the Proposed Antenna

Parameter	Value (mm)	Parameter	Value (mm)
L	52	l	14
W	48	m	11
a	12	n	12
b	23	p	6
c	19	q	6
d	17	r	8
e	15	s	8
f	12	u	10
g	19	v	6
h	20	w	16
i	14	x	11
j	39	y	24
k	6	z	13

1925 MHz). This step considerably enhances the antenna's impedance matching. The antenna is seen resonating at 1457 MHz with $|S_{11}|=-24.2$ dB and 1760 MHz with $|S_{11}|=-21.4$ dB. The proposed antenna covers two WMTS bands (1395-1400 MHz and 1427-1432 MHz), which are commonly used for remote health monitoring.

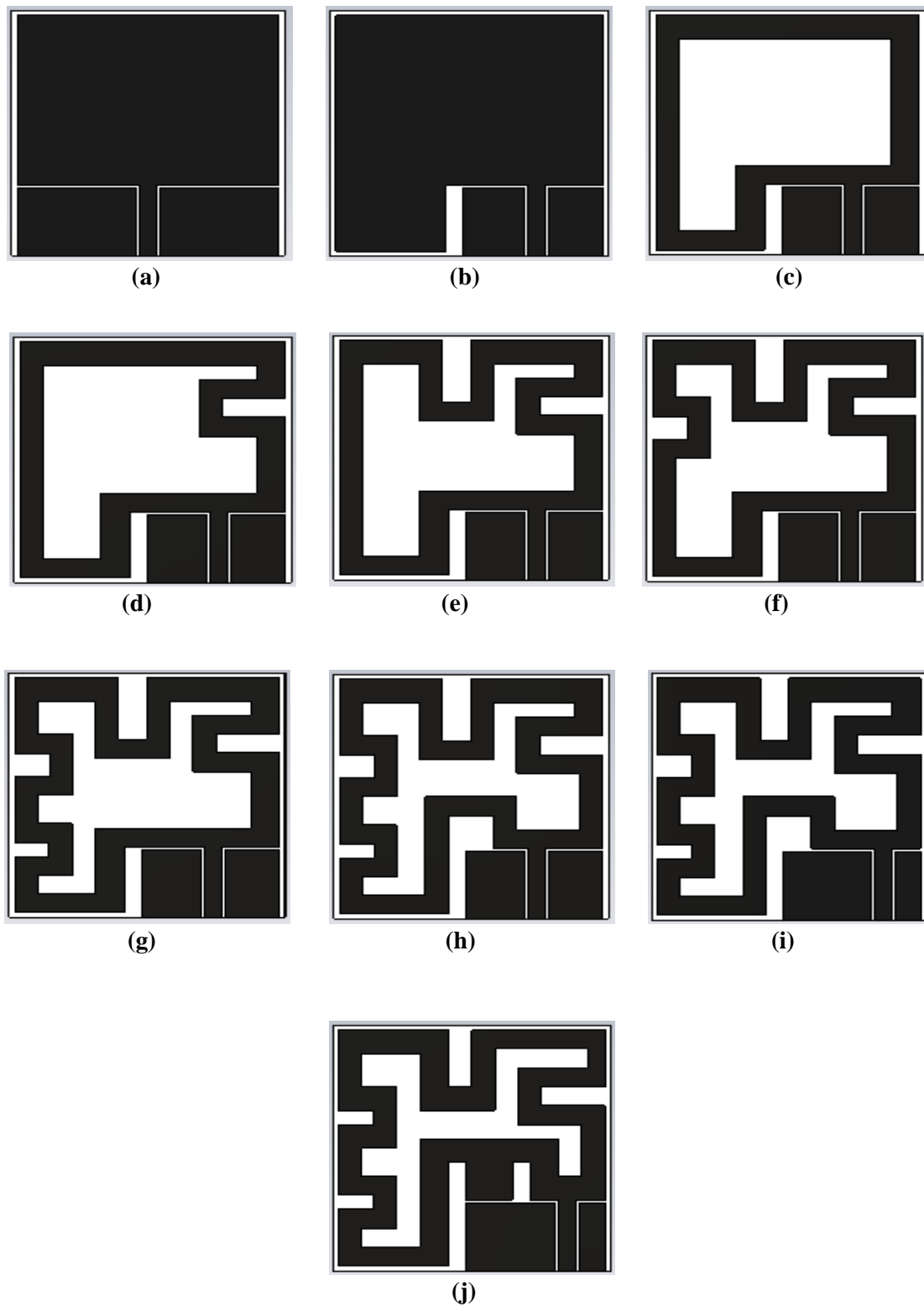
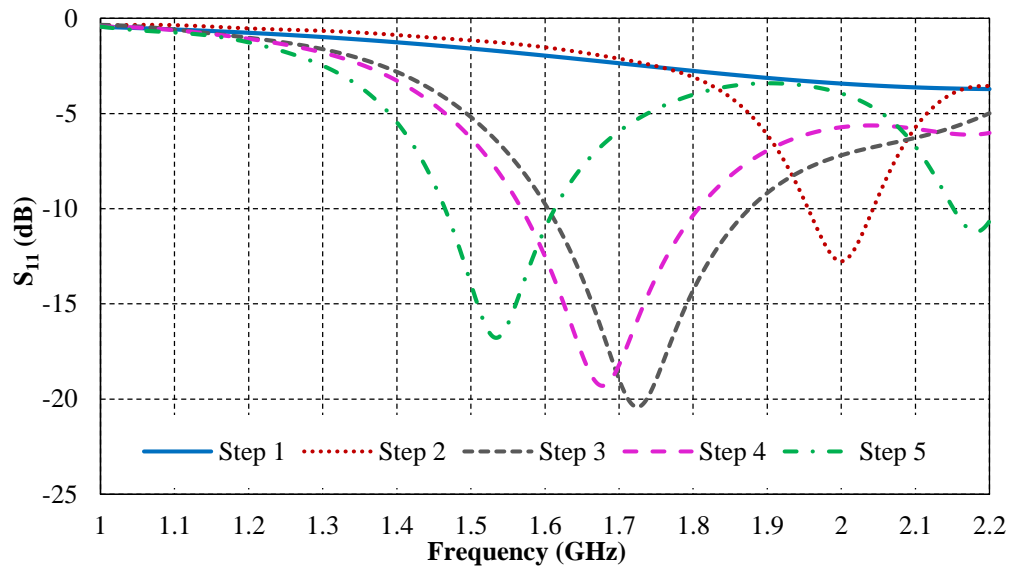
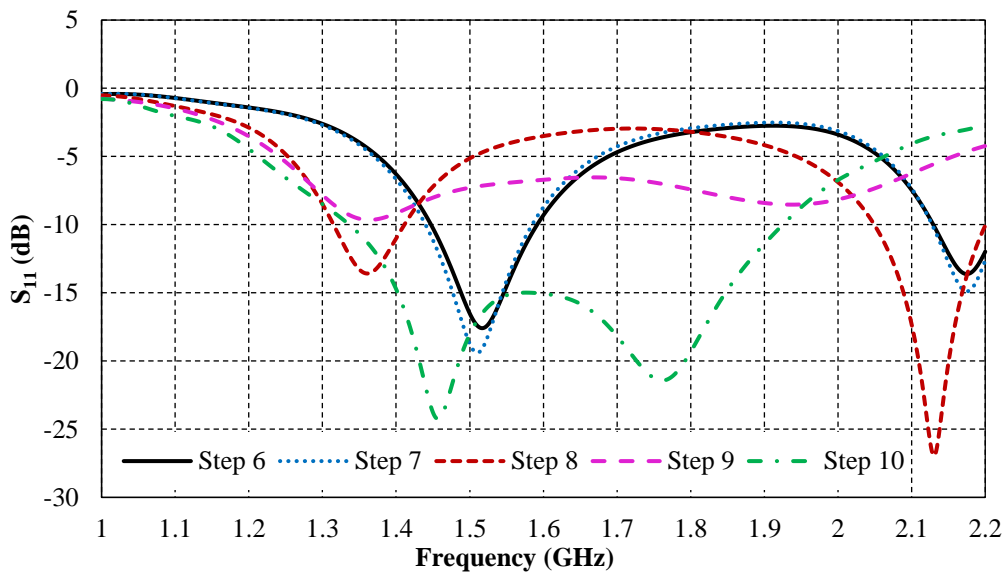


Fig. 4.2. Stepwise designing of the proposed antenna: (a) step-1 (b) step-2 (c) step-3 (d) step-4 (e) step-5 (f) step-6 (g) step-7 (h) step-8 (i) step-9 (j) step-10.



(a)



(b)

Fig. 4.3. Stepwise reflection coefficients (a) steps 1-5 (b) steps 6-10.

4.3 PARAMETRIC ANALYSIS

The response of the designed antenna varies with many parameters. The parametric analyses for a few of these parameters are as follows. The variations in reflection coefficients $|S_{11}|$ with the position of the feed line are shown in Fig. 4.4. By shifting the feed line to the left, the resonance frequency shifts in the opposite direction. While shifting the feed line to the right, keeps the resonance frequency within the desired limits with a minor shift to the left side.

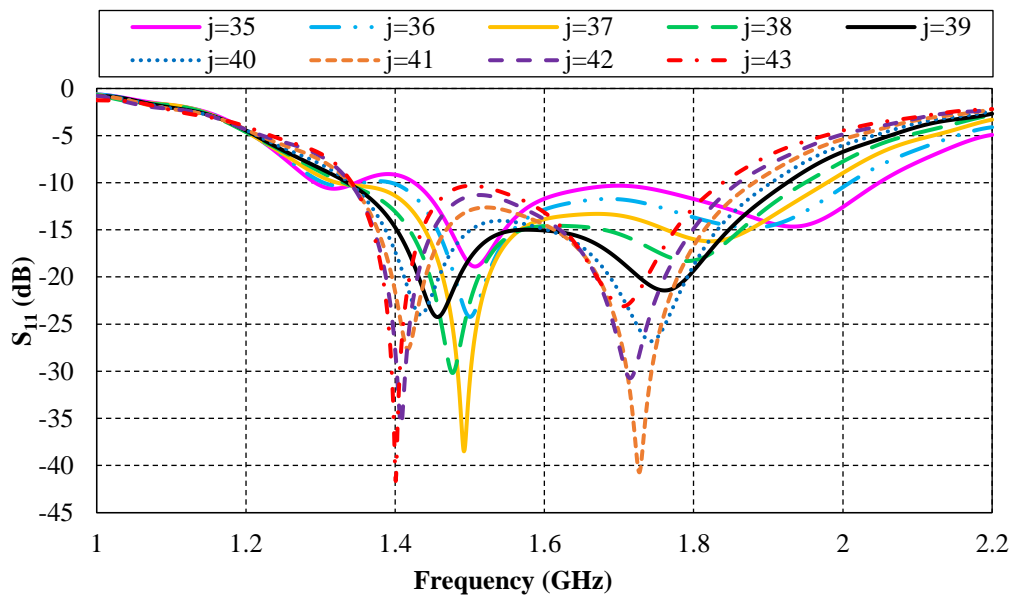


Fig. 4.4. Reflection coefficients due to variation in the position of the feed line.

The changes in reflection coefficients $|S_{11}|$ due to variation in parameter m are depicted in Fig. 4.5. When the parameter m is decreased, the overall response of the antenna resonance shifts to the upper side, whereas an increase in the parameter m causes a shift to the left. In both cases, the response of the antenna remains within the desired frequency limits.

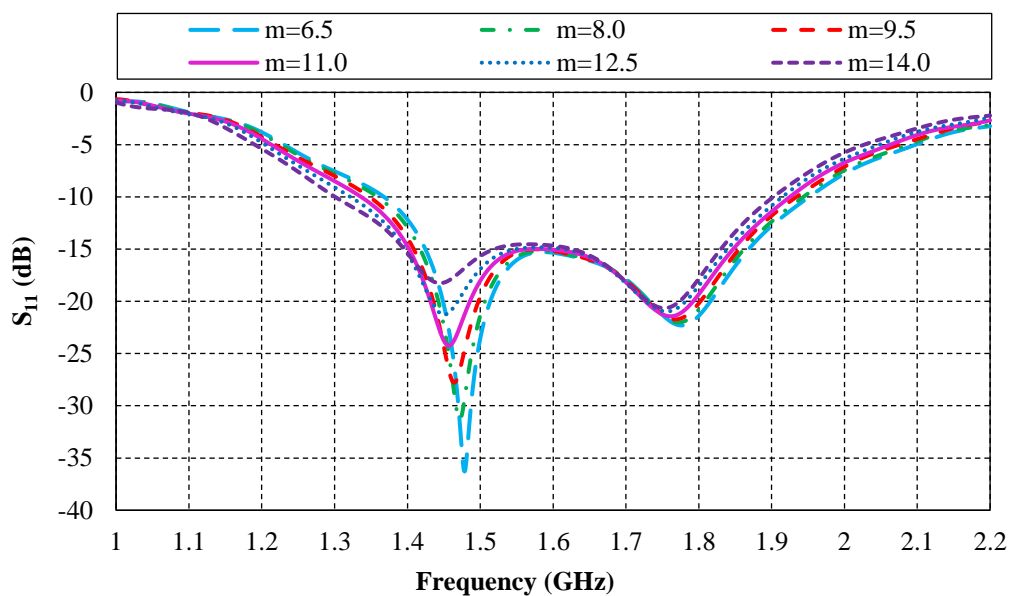


Fig. 4.5. Reflection coefficients due to variation in parameter ‘ m ’.

Fig. 4.6 depicts the changes in reflection coefficients $|S_{11}|$ due to variation in parameter n . When the value of n is decreased, the overall response of the antenna shifts to a lower frequency, whereas increasing the value of n results in a right shift. Variations in p have no effect on the antenna's performance in the desired frequency band, as shown in Fig. 4.7. An increase in the value of p shifts the response to a lower frequency band. As p decreases, the frequency band shifts to the upper frequency band.

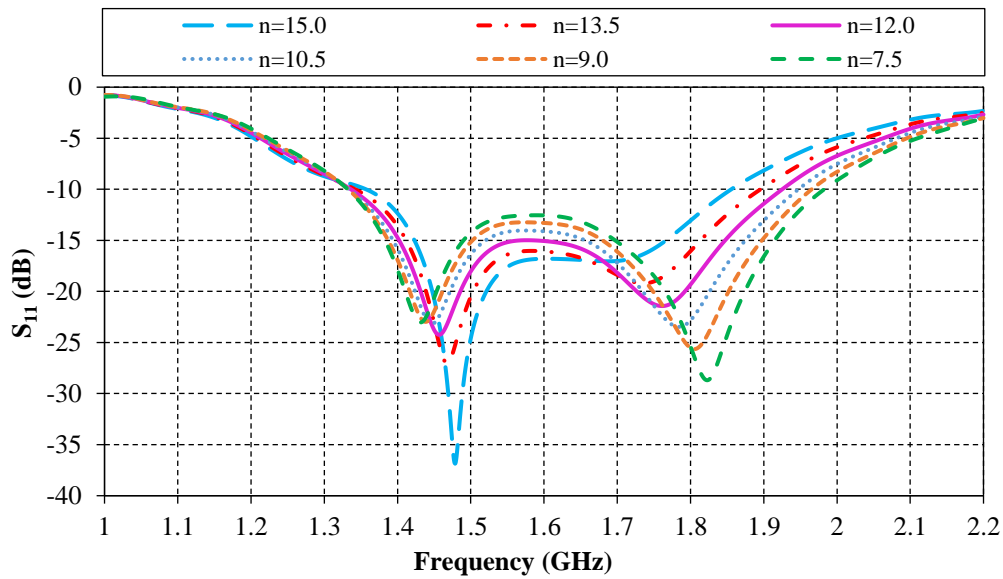


Fig. 4.6. Reflection coefficients due to variation in parameter 'n'.

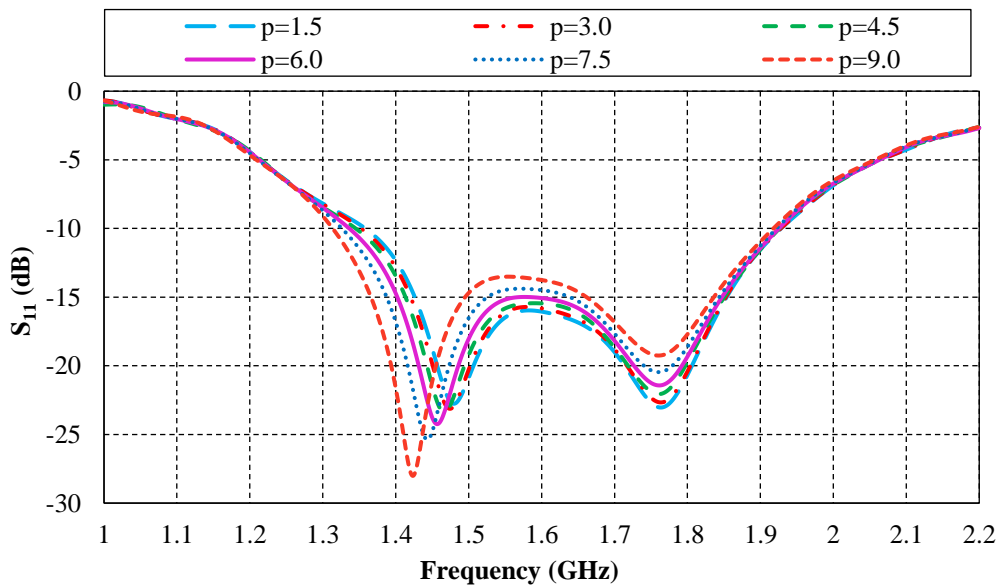


Fig. 4.7. Reflection coefficients due to variation in parameter 'p'.

Fig. 4.8 depicts the changes in reflection coefficients $|S_{11}|$ as q varies. The value of q has an inverse relationship with the antenna's overall response. When q increases, the response shifts to the left, while when q decreases, the response shifts to the right. Variations in r affect the $|S_{11}|$ for overall frequency response, as illustrated in Fig. 4.9. There is no change in the desired frequency bands when the value of r is increased or decreased.

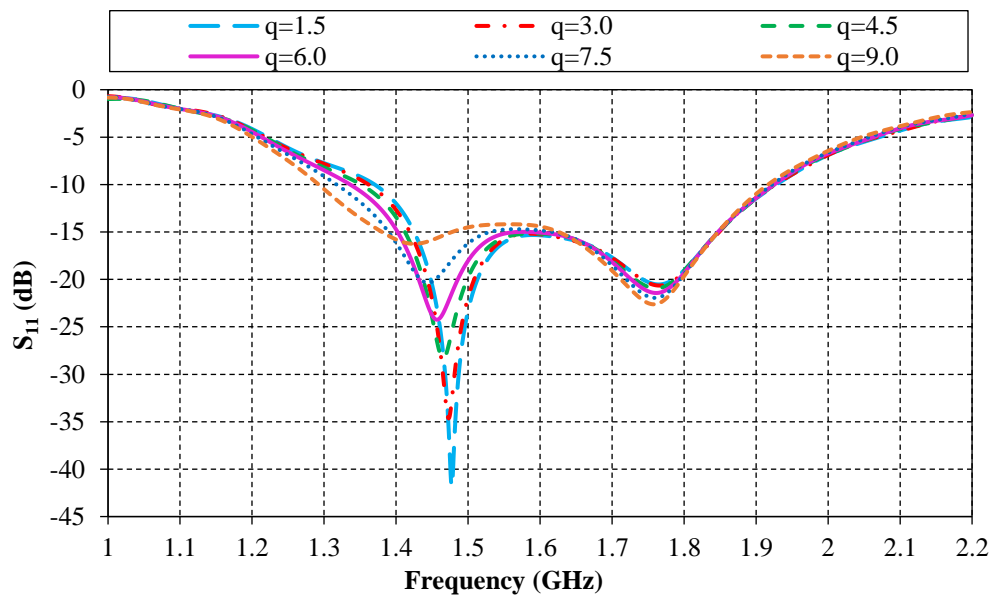


Fig. 4.8. Reflection coefficients due to variation in parameter ‘q’.

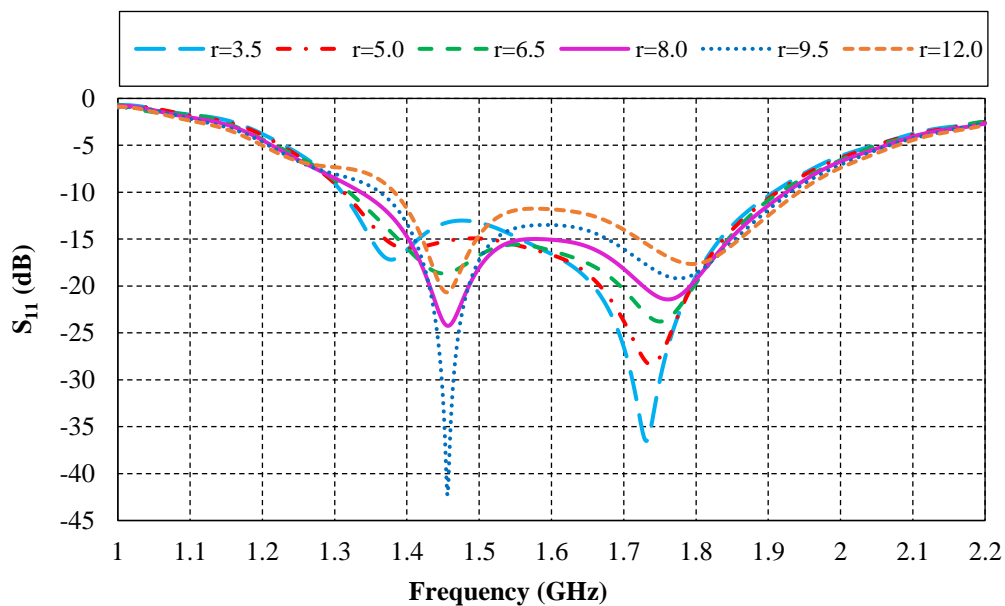


Fig. 4.9. Reflection coefficients due to variation in parameter ‘r’.

The reflection coefficients with variation in s are shown in Fig. 4.10. A change in the value of s keeps the response within the desired limits. The antenna loses its desired response if the values of s are further decreased.

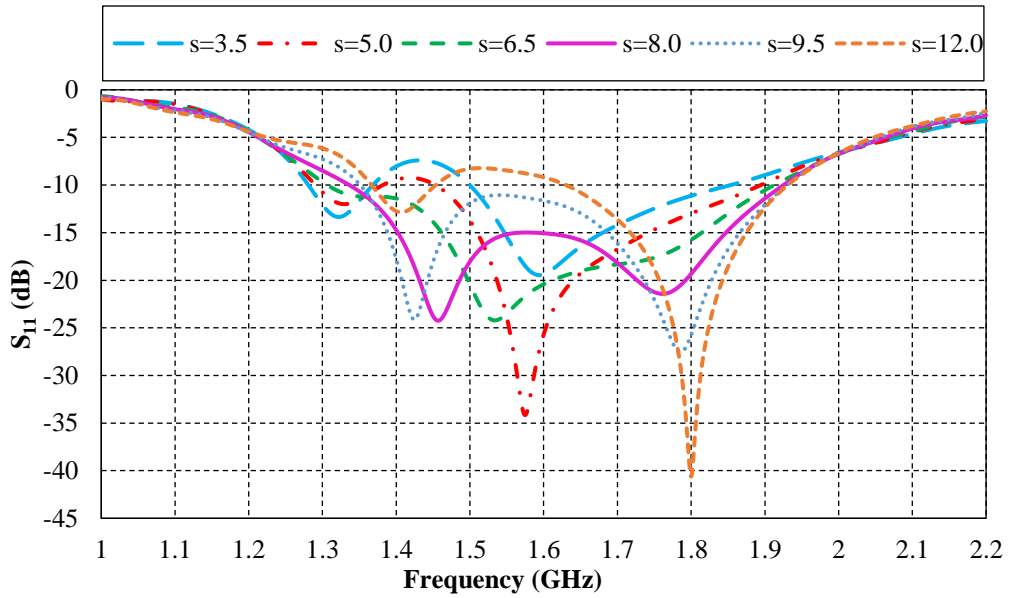


Fig. 4.10. Reflection coefficients due to variation in parameter 's'.

4.4 ANTENNA PERFORMANCES IN FREE SPACE

Figure 4.11 shows the proposed antenna's simulated and measured reflection coefficients. Agilent N5222A network analyzer was used for testing the

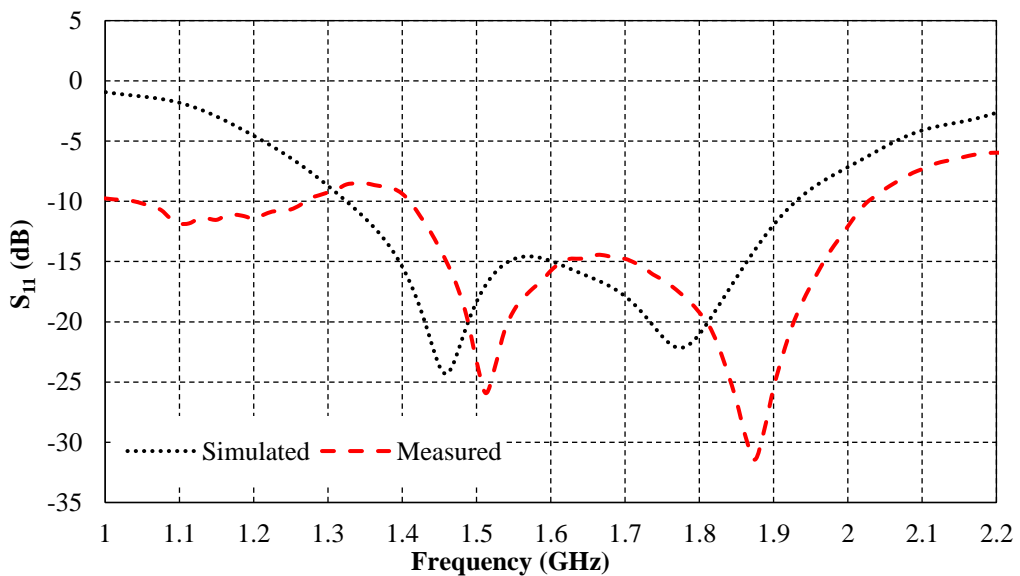


Fig. 4.11. Simulated and measured reflection coefficients of the proposed antenna.

fabricated prototype antenna. The simulated and measured results are found in good agreement for the entire resonance band, which confirms that the proposed antenna can be used for WMTS bands (1395-1400 MHz and 1427-1432 MHz) and other health monitoring applications.

4.4.1 Radiation Patterns and Gain

Figure 4.12 depicts the proposed antenna's simulated and measured radiation patterns. Figure 4.13 shows the proposed antenna's simulated and measured gain plots. At both frequency bands, the observed gain yields reasonable results.

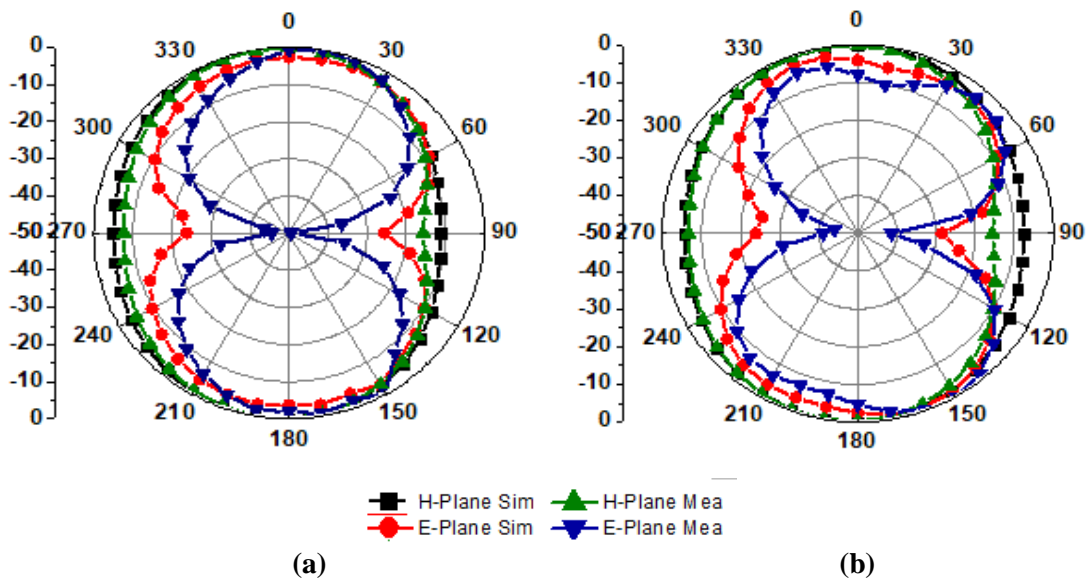


Fig. 4.12. Simulated and measured radiation patterns (a) 1397.5 MHz (b) 1429.5 MHz.

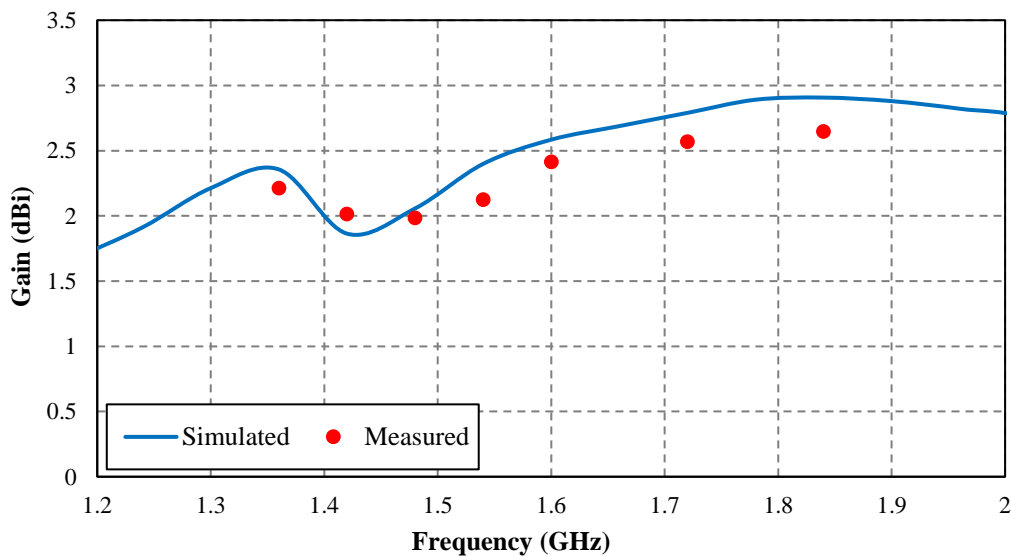


Fig. 4.13. Simulated and measured gain of the proposed antenna.

4.4.2 Surface Current Distribution

The surface current distributions of the designed antenna at resonant frequencies 1397.5 MHz and 1429.5 MHz are shown in Fig. 4.14. In both cases, the intensity of the current is observed to be higher around the meandered shape than the rest of the antenna. Hence, it is possible to conclude that the proposed antenna is resonating primarily because of its meandered shape.

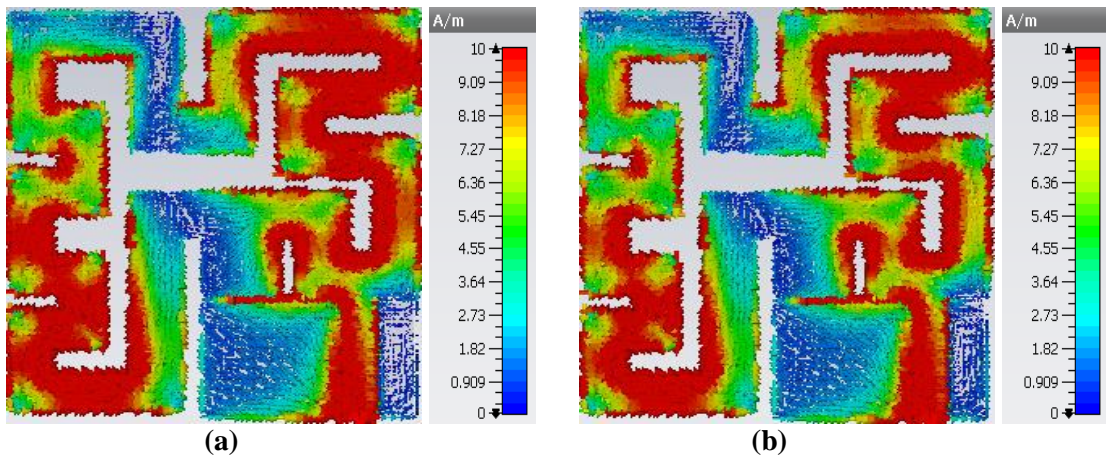


Fig. 4.14. Surface current distribution of the proposed antenna: (a) 1397.5 MHz (b) 1429.5 MHz.

4.5 ANTENNA PERFORMANCES ON HUMAN BODY

4.5.1 Bending of the Antenna

To test the effects of bending, the proposed antenna is bent parallel to the x -axis, as shown in Fig. 4.15. The bending radius is considered as 75 mm to imitate the typical size of the human shoulder. The bending radii are reduced to 70 mm, 65 mm and 60 mm, for which simulated results are shown in Fig. 4.16.

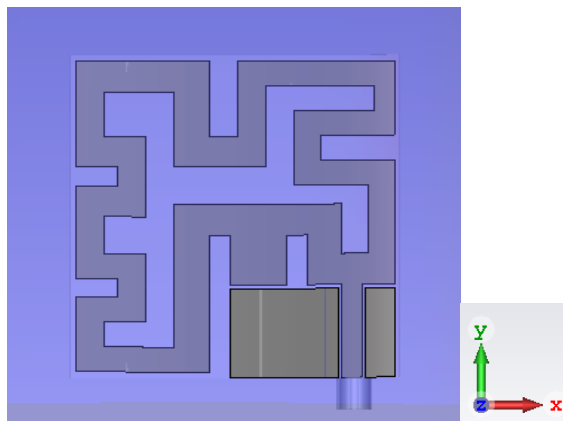


Fig. 4.15. Bending direction of the antenna along the x -axis.

In Fig. 4.16, it can be seen that there are not many variations in the reflection coefficients due to the bending of the antenna along the x -direction.

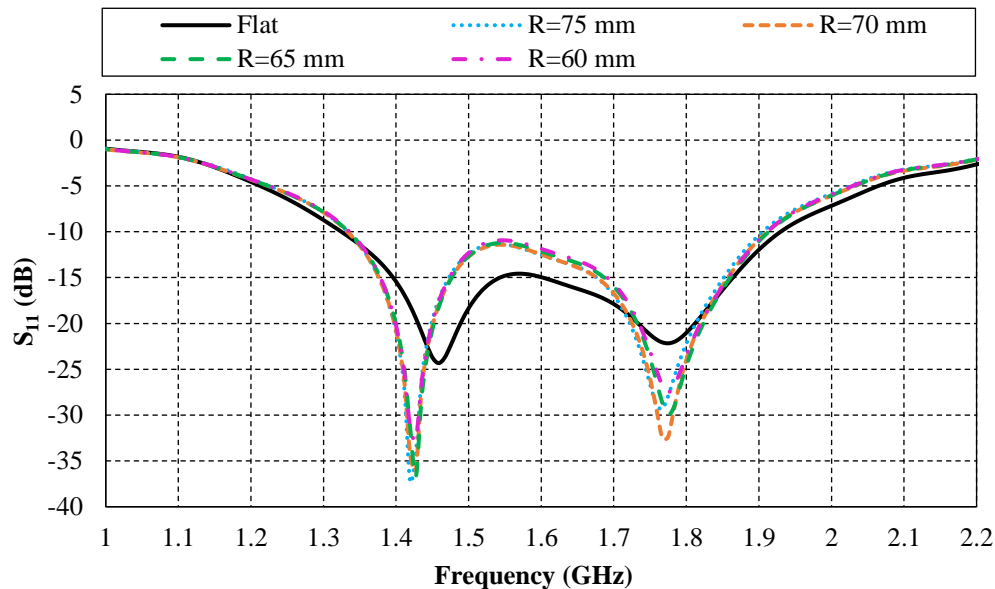


Fig. 4.16. Reflection coefficients due to bending along the x -axis.

4.5.2 Specific Absorption Ratio

The simulated average specific absorption ratio (SAR_{avg}) of the proposed antenna over 1 g of the tissue (for density = 2000 Kg/m³) is modelled in CST (as presented in Fig. 4.17). The maximal value of the simulated SAR_{avg} at 1397.5 MHz is approximately 30.1 W/kg (for 1 g of tissue) keeping input power as 0.5 W. On the other

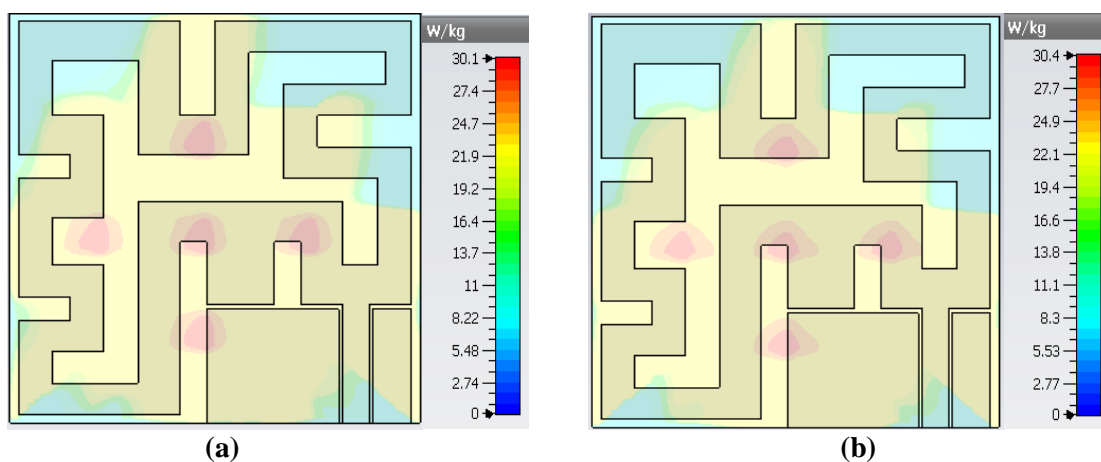


Fig. 4.17. Simulated average SAR of the proposed antenna for 1 g of tissue : (a) 1397.5 MHz (b) 1429.5 MHz.

hand, the SAR_{avg} at 1429.5 MHz is approximately 30.4 W/Kg for the same specifications. To comply with IEEE Std C95.1-2005, the maximum input power of 26.5 mW must be maintained for the 1395-1400 MHz band [109]. The simulation conducted at 1429.5 MHz permitted a maximum power of 26.4 mW for the 1427-1432 MHz band for safe usage. Hence, the results show that the proposed antenna can be printed on a flexible substrate and is a good solution for wearable applications.

4.6 CONCLUSION

This chapter presents the design and analysis of a wideband antenna covering the WMTS “1395-1400 MHz” and “1427-1432 MHz bands.” The meandering technique expands the total electrical path of the antenna to cover lower frequencies. The antenna occupies an area of 48 mm × 52 mm. This work also includes the effects of bending and sensitiveness of the antenna when it comes into close contact with the human body. This antenna is well suited for wearable applications.

“When wireless is perfectly applied the whole earth will be converted into a huge brain, which in fact it is, all things being particles of a real and rhythmic whole. We shall be able to communicate with one another instantly, irrespective of distance.”

Nikola Tesla

5

DUAL-RESONANCE ULTRA-MINIATURIZED TEXTILE ANTENNA FOR ISM/WEARABLE APPLICATIONS

In the previous chapter, the design and development of a compact wideband flexible antenna for wireless medical telemetry services were presented. In this chapter, an ultra-miniaturized textile antenna is designed and developed for “2.45/5.8 GHz industrial, scientific and medical (ISM) band” applications. The proposed microstrip line-fed dual-band antenna consists of non-conducting (Felt) and conducting (Sheildit Super) textile materials. The antenna is 20 mm x 30 mm x 1 mm in size, and its ($S_{11} \leq -10$) bandwidths in the lower and upper resonant bands are 14.2 % and 27.5 %, respectively. In addition, various fabrics are considered and characterized in order to investigate different possibilities for textile antennas. The proposed antenna configuration is simple, compact, simple to construct, and efficient for wearable/textile applications. The proposed textile antenna performance is studied for on-body situations using the three-layered human shoulder model and four-layered human arm model. The antenna offers consistent on-body performance even when subjected to deformations caused by bending.

5.1 INTRODUCTION

Over the past decade, wearable electronic systems have become well-known to everyone due to their diverse applications in medical care, health monitoring, telemedicine, patient tracking, and emergency rescue. Wearable devices such as a wristwatch, fitness band, smart ring, smart jewellery, scanner gloves, augmented reality glasses, and head-mounted displays have recently emerged as an essential component of the Internet of things (IoT) [52], [96], [110]–[112]. Wearable gadgets use embedded wireless modules, which typically include a battery, sensors, and an antenna, to communicate with external devices. An antenna is the most important module of

wearable devices as it determines the overall efficiency of the wireless link. Wearable and textile antennas have been widely used in wireless local area network (WLAN), radio frequency identification (RFID), and wireless body area network (WBAN) applications [53], [113].

Wearable antennas should be compact, flexible, lightweight, cost-effective, robust, and maintenance-free [77]. The implementation and stable performance of the wearable antenna is a major design challenge. Textile/wearable antennas are placed close to human-tissues under different bending conditions, as compared to conventional antennas, which are typically located in free space [53]. Therefore, the design procedure for the wearable flexible antenna is slightly different from that of traditional antennas. Electromagnetic coupling to the human body is the most important factor to consider, as it may affect the antenna's performance [114]. The human body must absorb the minimum amount of power (per unit mass) radiated by a wearable antenna used for health and safety applications, as measured by the specific absorption ratio (SAR). Textile materials have been widely accepted for wearable applications due to their lightweight, flexibility, low-profile, conformal, and unobtrusive properties [115], [116]. However, the fabrication tolerances for a textile antenna are relatively large when compared to those made using printed circuit board machining [114]. Also, the textile antenna's resistance to various structural changes, such as bending/crumpling, must be guaranteed. In the case of different fabrics, a proper characterization of textile materials is essential [96]. However, it is challenging to design a compact wearable antenna with consistent performance while maintaining a low-profile, simple design, desirable bandwidth, and easy integration capability with other circuits/devices.

The researchers have developed a variety of textile antennas that enable off-body communications, such as patch antennas in protective clothing of the firefighters, and logos, badges, etc., in ordinary garments [55], [117]. Wearable ultra-high frequency (UHF) RFID antennas were also developed and implemented on smart textiles for body-centric sensing and apnea detection applications [118]. With these ongoing advancements and developments, the authors of this paper proposed a compact, lightweight, low-profile textile antenna for ISM band frequencies. Several textile materials were considered and characterized in order to investigate all possibilities. The proposed textile patch antenna consists of a partial ground plane and a C-shaped

radiator fed by a microstrip line. The proposed antenna can also be used for “*WLAN (4.9 GHz, 5 GHz, and 5.9 GHz), IEEE 802.11n (Wi-Fi), wireless HDMI, ZigBee, and Bluetooth applications.*” The simulated and measured results show an acceptable agreement, indicating that the proposed textile antenna is a suitable candidate for ISM/wearable applications.

This chapter is organized as follows: Section 5.2 presents and discusses the fabrication process of the proposed wearable antenna. The performance of the antenna in free space is covered in Section 5.3. The performance of the antenna on the human body is discussed in Section 5.4, and the conclusion is provided in Section 5.5.

5.2 ANTENNA TOPOLOGY

5.2.1 Preparation and Characterization of Non-conductive and Conductive

Materials

Textile antenna design necessitates the use of both non-conductive and conductive materials. The non-conductive textile material serves as the substrate while the conductive textile material serves as the radiating element. Hence, understanding the electrical properties (such as relative dielectric constant, loss tangent, and thickness) of non-conductive textile materials, as well as the surface resistivity of conductive textile materials, becomes essential [87]. Several textile materials, namely Cordura 500D Nylon [119], Polyester, Cordura General, Denim, Lycra, and Felt, were considered for characterization (shown in Figs. 5.1(a)–(d) and 5.2(a)–(b)). All of these materials are easily available in the market.

A computer-operated CO₂ laser cutting machine [50], [117] or manual methods can be used to cut textile materials of the required size. A computer-based laser cutting method can achieve a resolution of 0.2 mm, whereas a manual cutting method can only achieve a resolution of 1 mm. A sample of size 60 mm × 60 mm is manually cut from each of the textile materials considered, as shown in Fig. 5.3 and the characterization of multi-layered samples prepared from different textile materials was performed.

Several techniques, including the transmission/reflection line method, resonant cavity technique, dielectric resonator, dielectric post resonator, whispering gallery mode resonator, open-ended coaxial probe method, dielectric probe, free space method,

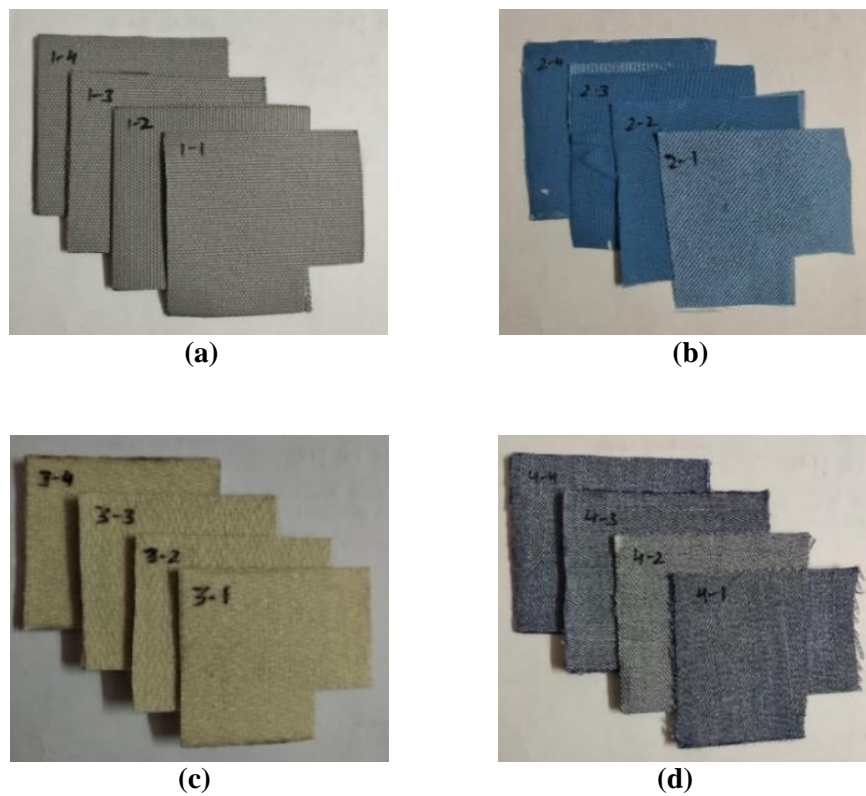


Fig. 5.1. Textile materials: (a) Cordura 500D Nylon, (b) Polyester, (c) Cordura General, (d) Denim.

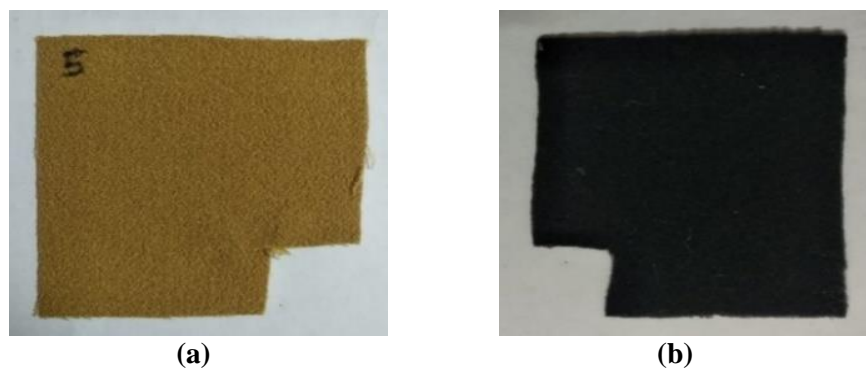


Fig. 5.2. Textile materials: (a) Lycra, (b) Felt.

and Nicholson–Ross–Weir (NRW) technique, have been suggested in the literature for measuring dielectric properties of materials [33], [120]–[123].

The above-mentioned textile samples were characterized using a radio frequency impedance/material analyzer (Agilent E4991A). It offers superior impedance measurement performance and a powerful built-in analysis function in the 1 MHz to 3

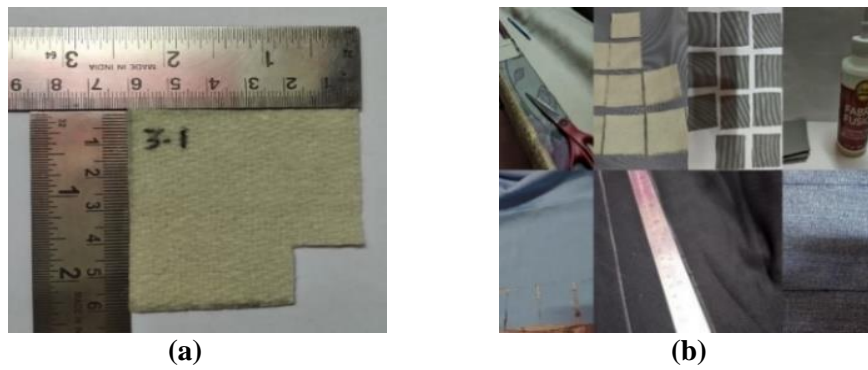


Fig. 5.3. Preparation of textile fabric samples: (a) Size of the sample, (b) Preparation of samples.

GHz frequency range with a resolution of 1 mHz. It uses the RF-IV technique for more accurate measurements across a wide impedance range. All prepared samples were cut into small pieces to fit into the dielectric material test fixture (Agilent 16453A) as shown in Figs. 5.4(a) and (b). The measurement data was plotted and analyzed as displayed in Figs. 5.5(a)–(d) and 5.6(a)–(b). The dielectric constant of the Cordura 500D Nylon sample ranges from 1.69 to 2.32 for different layers as shown in Fig. 5.4(a). It is noted that the dielectric constant of the four-layer sample is 3.24 at 1 MHz. The maximum and minimum dielectric constant values of Polyester were found to be 2.29 and 0.97, respectively.

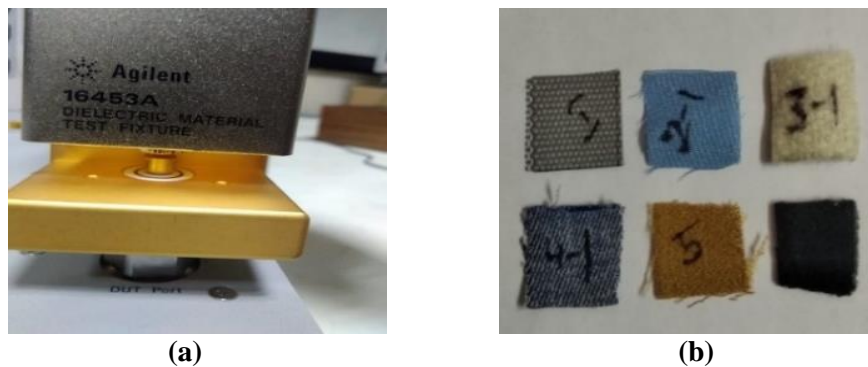
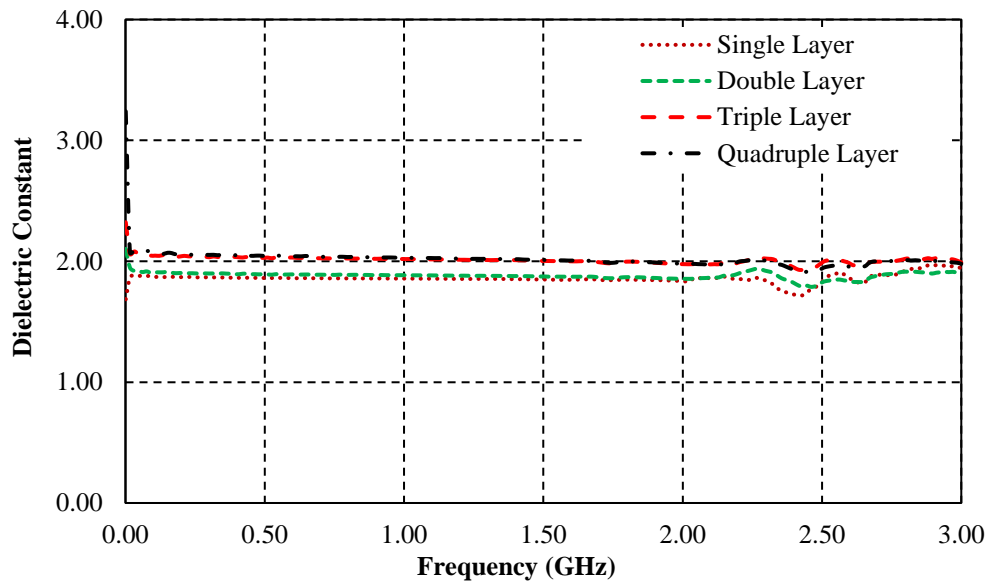
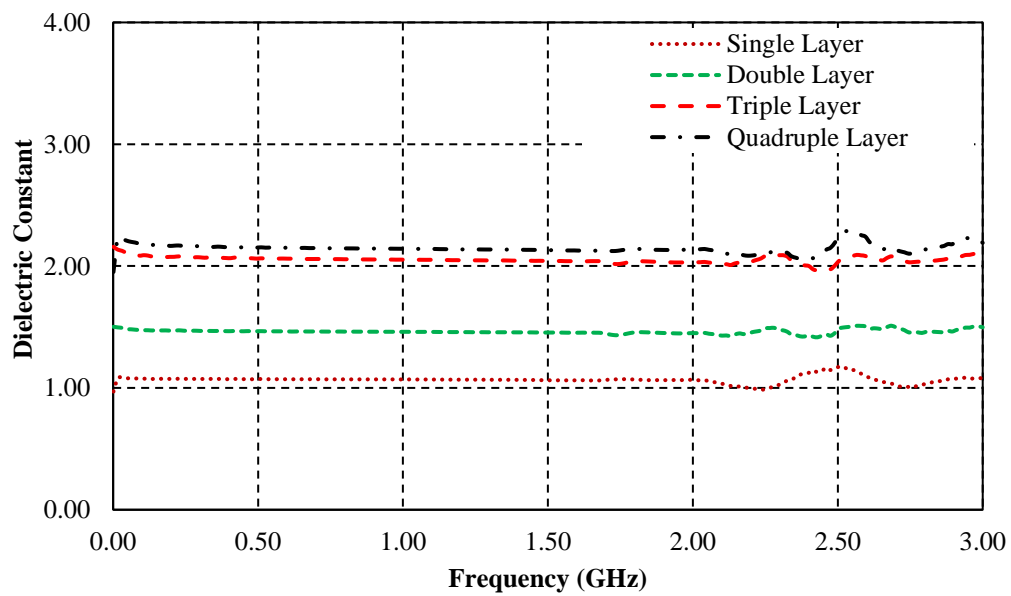


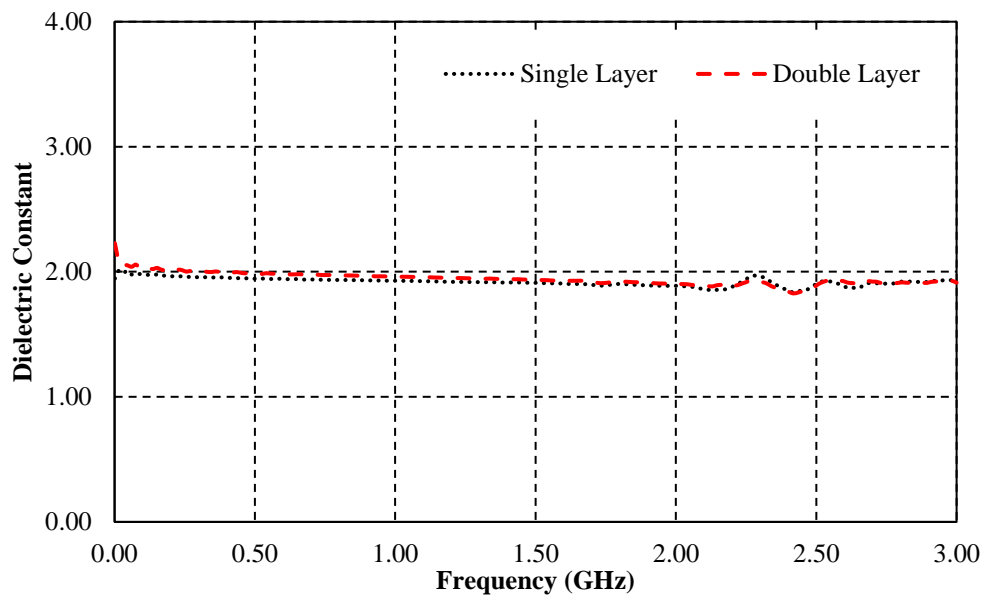
Fig. 5.4. Measurement setup: (a) sample holder (dielectric material test fixture), (b) samples.



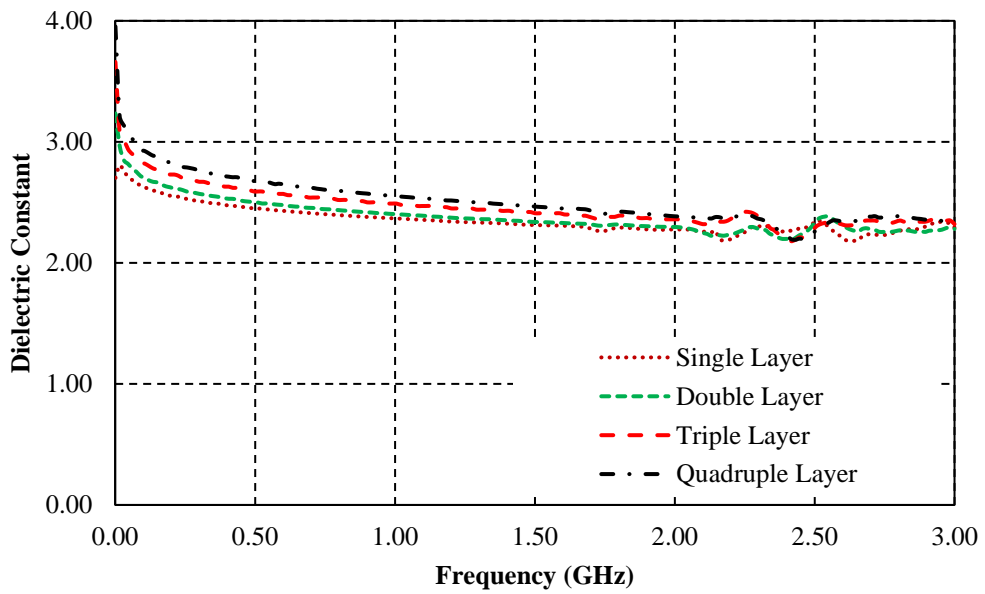
(a)



(b)

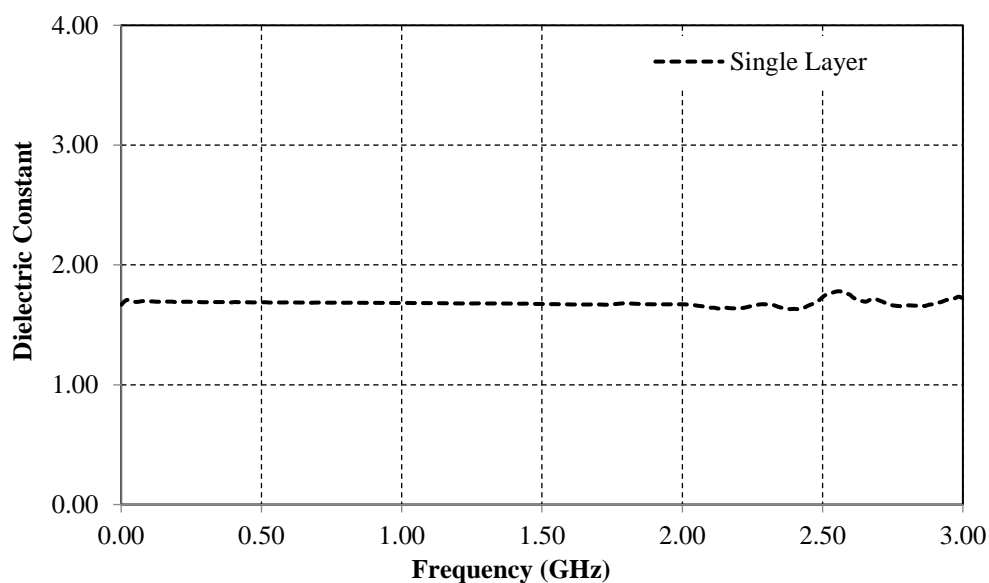


(c)

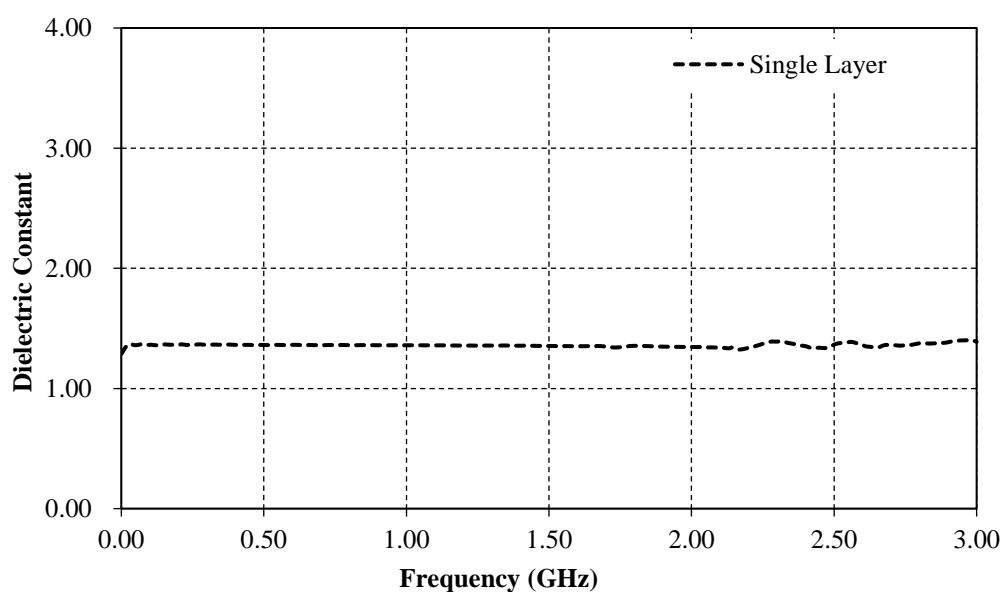


(d)

Fig. 5.5. Variation of dielectric constant and frequency for different textile materials: (a) Cordura 500D Nylon, (b) Polyester, (c) Cordura General, (d) Denim.



(a)



(b)

Fig. 5.6. Variation of dielectric constant and frequency for different textile materials: (a) Lycra, (b) Felt.

Polyester is a highly porous material that absorbs adhesive glue quickly. Therefore, it has a wide range of dielectric constants when compared to other non-conductive materials. The maximum dielectric constant of the textile fabric Denim was found to be 3.99, while the minimum dielectric constant was found to be 2.18. The maximum dielectric constant values for Lycra and Felt were found to be 1.78 and 1.4,

respectively. The minimum values of the dielectric constant were found as 1.63 and 1.29 for Lycra and Felt, respectively. Measurements of the triple and quadruple layer structures of the Cordura General were not possible due to the larger thickness of the samples. The thickness of the non-conductive textile samples was measured with a high precision Vernier Calliper. Table 5.1 shows the thickness, relative dielectric constant, and loss tangent of all samples (at 2.45 GHz). Moreover, a single-layer of non-conductive Felt material with a thickness of 1 mm, dielectric constant (ϵ_r) of 1.34, and loss tangent ($\tan \delta$) of 0.02 is used to fabricate the proposed antenna.

The physical dimensions of an antenna determine its electrical length, which directly affects its resonant frequency [124]. The physical dimensions of the patch must be maintained when implementing it to the substrate. Also, the attachment procedure

Table 5.1. Properties of the Textile Materials at 2.45 GHz

Material	Number of Layers	Thickness (mm)	Dielectric Constant	Loss Tangent
Cordura 500D Nylon	Single	0.5	1.75	0.0066
	Double	1.0	1.80	0.0066
	Triple	1.4	1.94	0.0098
	Quadruple	1.9	1.91	0.0098
Polyester	Single	0.1	1.14	0.0613
	Double	0.2	1.43	0.0320
	Triple	0.3	2.10	0.0530
	Quadruple	0.4	1.98	0.0124
Cordura	Single	1.0	1.85	0.0088
	Double	2.0	1.84	0.0124
	Triple	3.1	---	---
	Quadruple	4.2	---	---
Denim	Single	0.5	2.29	0.02
	Double	1.0	2.23	0.02
	Triple	1.5	2.21	0.04
	Quadruple	2.1	2.20	0.04
Lycra	Single	0.4	1.66	0.04
Felt	Single	1.0	1.34	0.02

should have no effect on electrical properties such as sheet resistance. Some of the methods proposed and used for combining/making the conductive patch and the non-conducting substrate are sewing, conductive embroidery, inkjet-printing, liquid textile adhesives, point-wise application of conductive adhesives, adhesive sheets, and thermally adhesive textile fabrics [87], [111], [125]–[127].

For the radiating patch and ground plane, a 0.17 mm thick Sheildit Super (UL 94V-0 Level Flame Retardant, RoHS Compliant) conductive material with a one-side resistivity of $<0.5 \Omega$ per square is used. It is a high-quality copper-/nickel-plated Polyester-based textile material suitable for microwave and radio frequency applications. The thermally adhesive nature of this material makes it suitable for antenna design because it can be attached to the substrate simply by using a dry iron [128].

The layout of the proposed textile antenna is displayed in Fig. 5.7. The antenna is designed using the CST Microwave Studio tool [129]. The top layer is a C-shaped geometry, and the bottom layer is a partial ground plane of size $20 \text{ mm} \times 3 \text{ mm}$. The partial ground plane plays a vital role in achieving broadband characteristics [130]. A 50 ohm microstrip feed line excites the patch, and the antenna is $20 \times 30 \times 1 \text{ mm}^3$ in size. The suggested textile antenna's dimensional specifications are provided in Table 5.2.

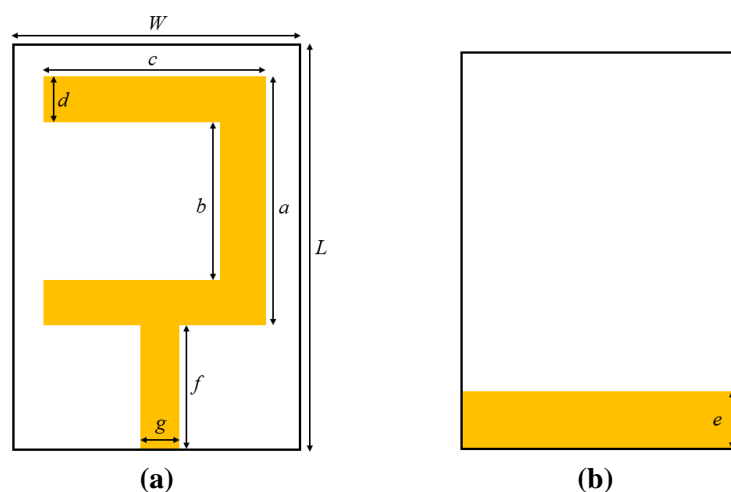


Fig. 5.7. Proposed textile antenna: (a) front view (b) back view.

Table 5.2. Dimensions of the Proposed Textile Antenna

Parameter	Value (mm)	Parameter	Value (mm)
L	30	d	4
W	20	e	3
a	20	f	8
b	12	g	2
c	16		

5.2.2 Step-wise Designing of the Proposed Antenna

This section describes the evolution of the proposed antenna. Fig. 5.8(a) shows an ordinary rectangular monopole antenna with a ground plane length of 3 mm. The simulated reflection coefficients (S_{11}) of the antenna design configurations are shown in Fig. 5.9. The ANT. 1 resonates at 2.93 GHz and 6.24 GHz. An antenna's effective current route length can be extended by adding slots/slits to the radiating patch. As a result, the resonant frequency shifts, providing the performance of a larger physical size antenna with broad bandwidth and a lower Q-value [52], [131]. As shown in Fig. 5.8(b), a small slot is introduced in ANT. 1 in the second step. The resonance frequencies of ANT. 2 decrease, and wide bands are obtained. The antenna resonates at 2.78 GHz and 5.34 GHz, with reflection coefficients of -17.7 dB and -22 dB, respectively. In the third step, the size of the slot introduced in the second step was increased to achieve the desired frequency as shown in Fig. 5.8(c). The final antenna (ANT. 3) covers the 2.45 GHz and 5.80 GHz (ISM) frequency bands as shown in Fig. 5.9.

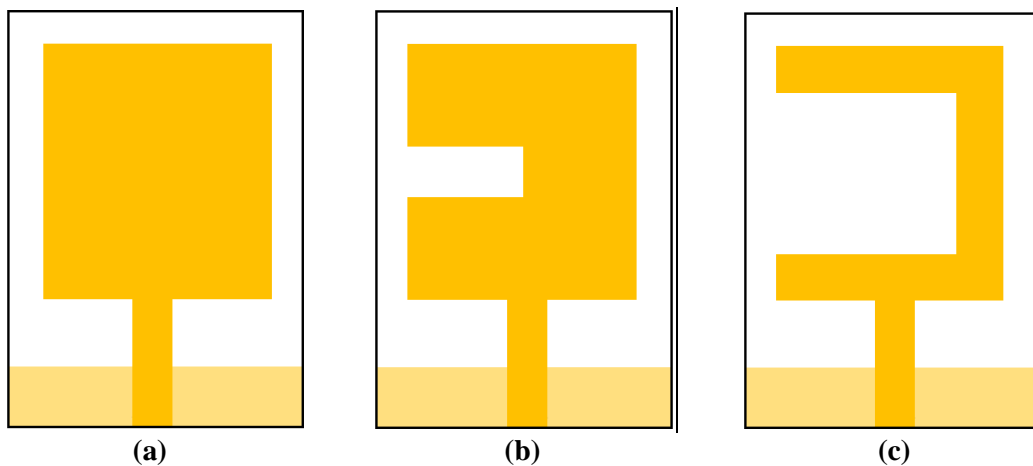


Fig. 5.8. Step-wise evolution of the textile antenna: (a) ANT. 1, (b) ANT. 2, (c) ANT. 3

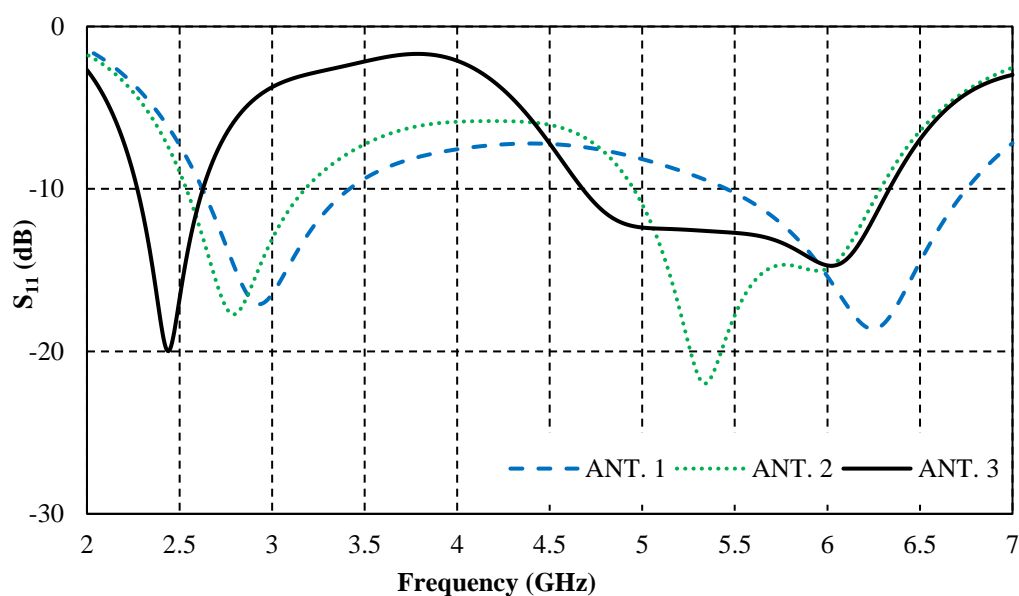


Fig. 5.9. Simulated reflection coefficients for different antenna configurations.

5.3 ANTENNA PERFORMANCES IN FREE SPACE

5.3.1 Reflection Coefficients (S_{11}) and Gain

The bandwidths of different antenna configurations are summarized in Table 5.3. The proposed textile ANT. 3 is fabricated and experimentally verified using a network analyzer (Agilent Technologies N5230A, 10 MHz to 40 GHz), as shown in Figs. 5.10(a), (b), and (c). The reflection coefficients of the antenna are measured and compared to the simulated results in Fig. 5.11. A reasonable agreement between the simulated and measured results is noticed. The fabricated prototype was found to have better impedance matching. The simulated and measured gain curves of the proposed antenna are shown in Fig. 5.11. The maximum gain values are found to be 1.63 dBi and 2.7 dBi at 2.45 GHz and 5.8 GHz, respectively.

Table 5.3. Performance Summary of Different Antenna Configurations

Ant. Conf.	Band I (GHz)	Bandwidth I (MHz)	Band II (GHz)	Bandwidth II (MHz)
ANT. 1	2.62-3.41	790	5.44-6.74	1300
ANT. 2	2.53-3.18	650	4.94-6.28	1340
ANT. 3	2.27-2.62	350	4.67-6.33	1660

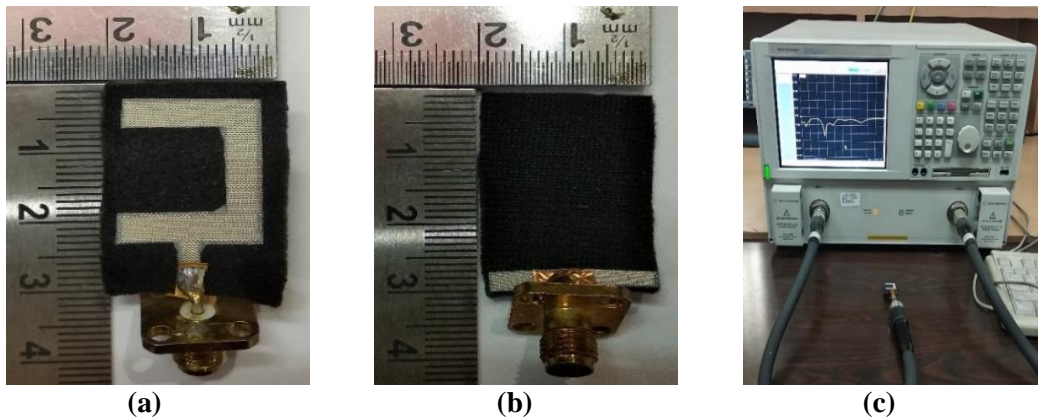


Fig. 5.10. *Prototype of the proposed textile antenna: (a) front view, (b) back view, (c) reflection coefficients measurement.*

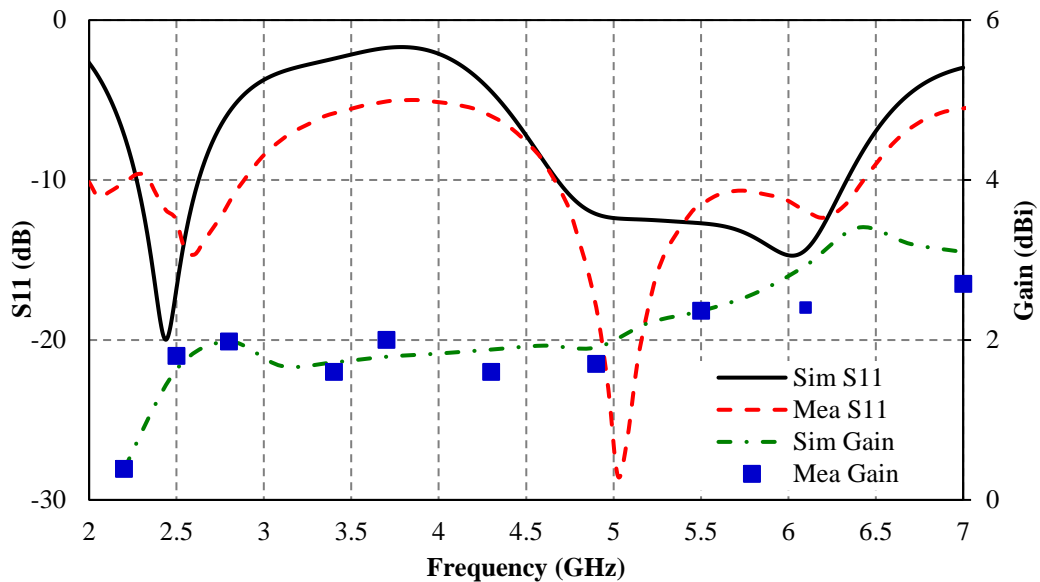


Fig. 5.11. *Simulated and measured reflection coefficients and gain of the antenna (ANT. 3).*

5.3.2 Radiation Patterns

When the antenna is in free space, Fig. 5.12 compares the computed and measured far-field radiation patterns of the proposed antenna at 2.45 GHz and 5.8 GHz. It is evident that a satisfactory agreement exists between simulated and measured patterns. Nearly bidirectional patterns are obtained for both the E-plane and the H-plane.

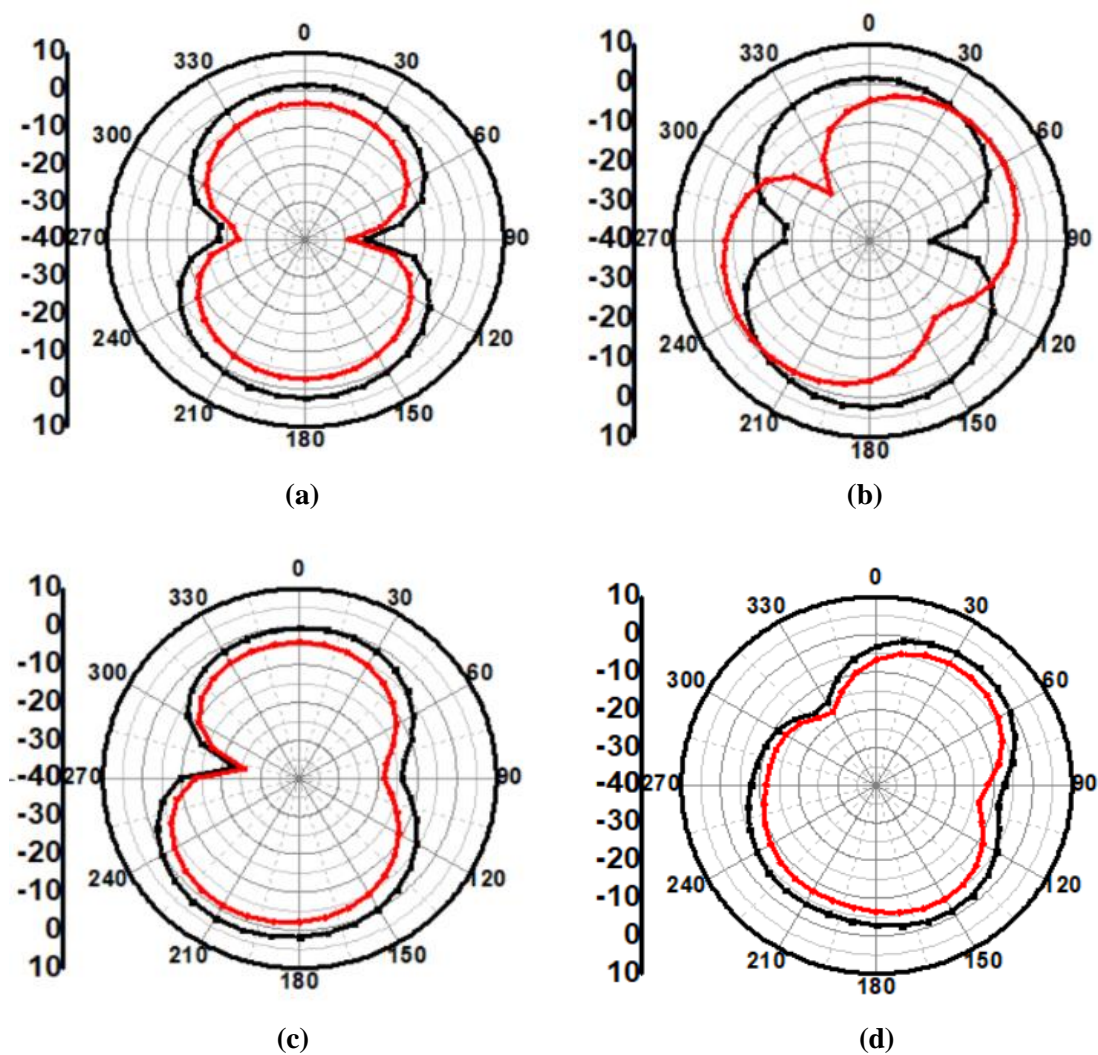


Fig. 5.12. Radiation patterns of the antenna (red: measured, black: simulated): (a) E-plane at 2.45 GHz, (b) H-plane at 2.45 GHz, (c) E-plane at 5.8 GHz, (d) H-plane at 5.8 GHz.

5.3.3 Surface Current Distribution

The simulated surface current distributions of the proposed antenna at 2.45 GHz and 5.8 GHz are shown in Figs. 5.13(a) and (b), respectively. In both cases, the maximum current density is concentrated close to the slot, indicating that the slot can control the resonant frequency of the proposed antenna.

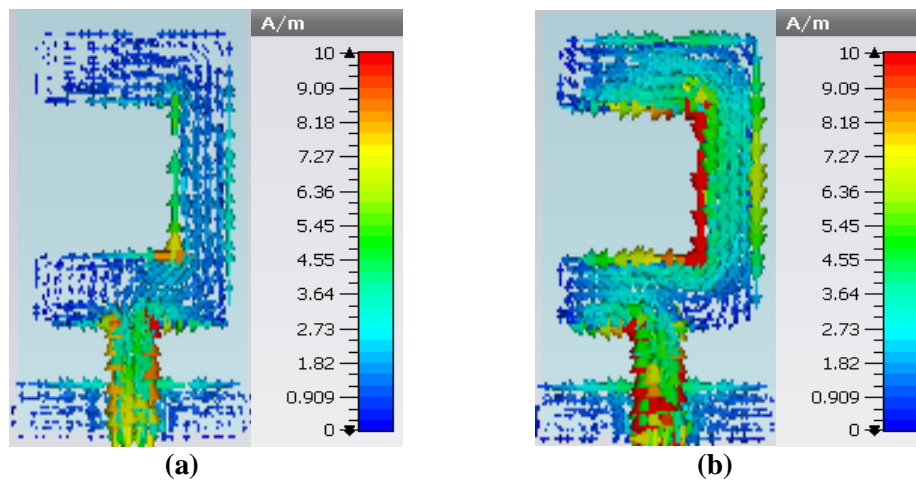


Fig. 5.13. Simulated surface current distributions at: (a) 2.45 GHz, (b) 5.8 GHz.

5.3.4 Crumpling Analysis

When integrated into clothing for off-body and on-body use, the textile antennas are likely to crumple. The resonance frequency and bandwidth of a textile antenna can be affected by crumpling. The off-body crumpling effects on the proposed textile antenna in different situations (flat, small, medium, and large) are shown in Fig. 5.14.

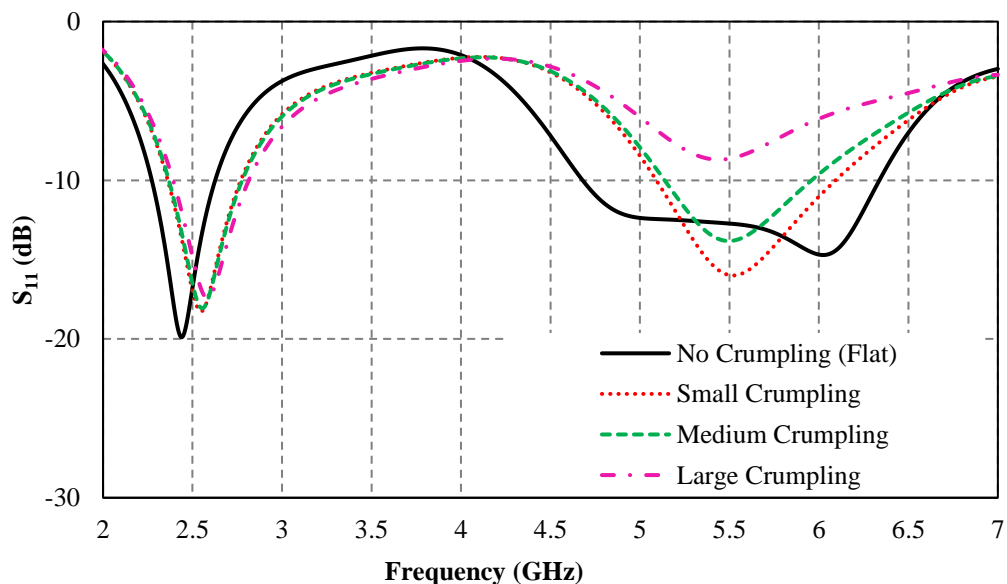


Fig. 5.14. Crumpling effect on the antenna.

5.4 ANTENNA PERFORMANCES ON HUMAN BODY

Furthermore, the proposed antenna is characterized for on-body situations. Two types of human tissue models (phantoms) are chosen to imitate the human shoulder and arm, as presented in Figs. 5.15(a), (b), (c), and (d). The human shoulder model is a three-layered structure comprised of a 3 mm thick layer of skin, a 7 mm thick layer of fat, and a 60 mm thick layer of muscle. The overall size of the phantom is 200 mm \times 100 mm \times 70 mm [82]. The human arm model is a four-layered structure comprised of a 2 mm thick layer of skin, 5 mm thick layer of fat, 20 mm thick layer of muscle, and the bone core (of radius 13 mm). The total length of the arm model is considered 350 mm [82]. The parameters defining the tissue models' attributes were gathered from CST's material library. To simulate the separation of layers of clothes from the human body, the antenna is placed 10 mm away from the skin, and it is kept in two mutually perpendicular orientations for both tissue models. For the human arm model, the antenna is bent parallel to the X- and Y-axes.

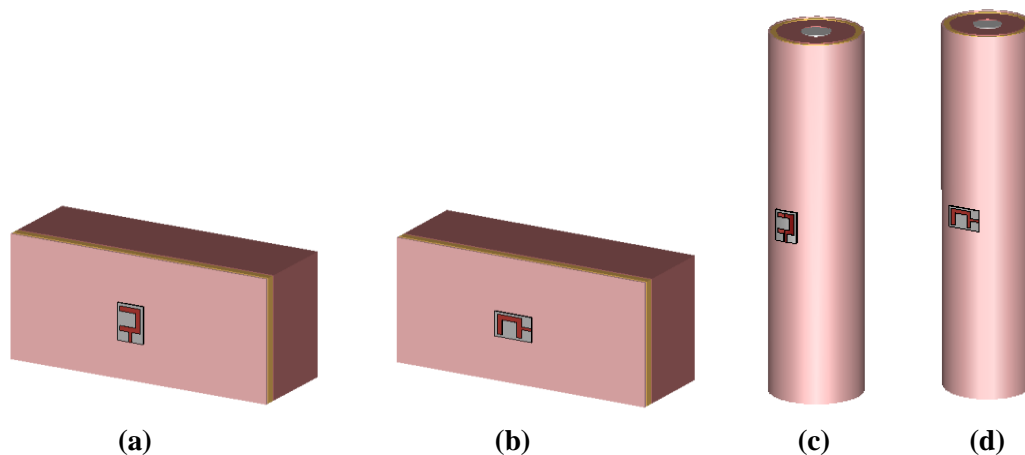


Fig. 5.15. Tissue models: (a) small cubic phantom-X, (b) small cubic phantom-Y, (c) cylindrical bent-X, (d) cylindrical bent-Y.

5.4.1 Reflection Coefficients, Gain, Radiation Efficiency and Front-to-Back Ratio for Various Tissue Models

The simulated reflection coefficients for human shoulder and arm tissue models (phantoms) are shown in Fig. 5.16. There is a significant difference between flat and bending conditions. The impedance matching is found to be within the desired range for both tissue models. Thus, the human shoulder and arm are ideal locations for the placement of the proposed antenna.

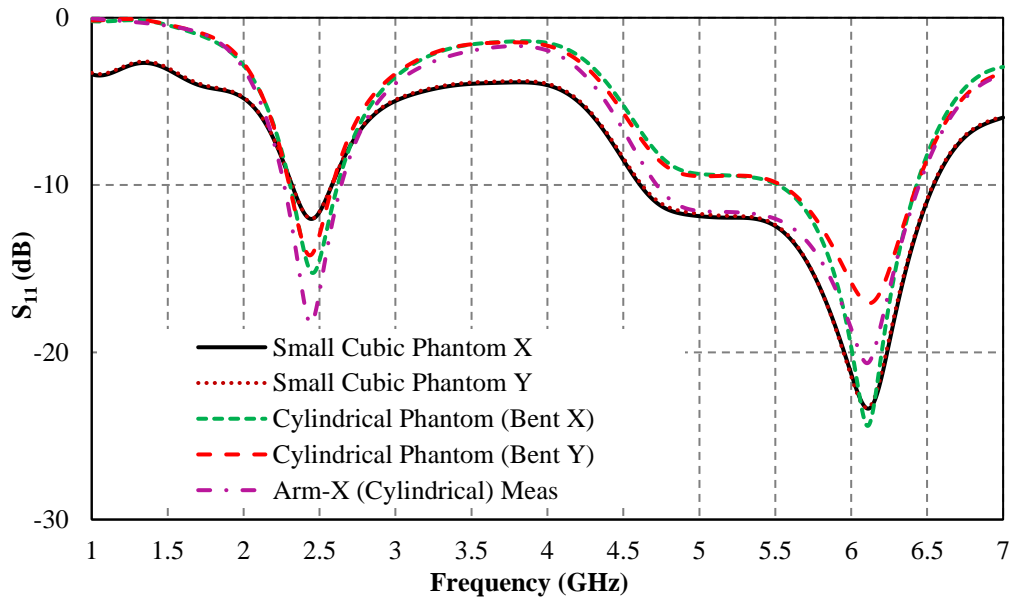
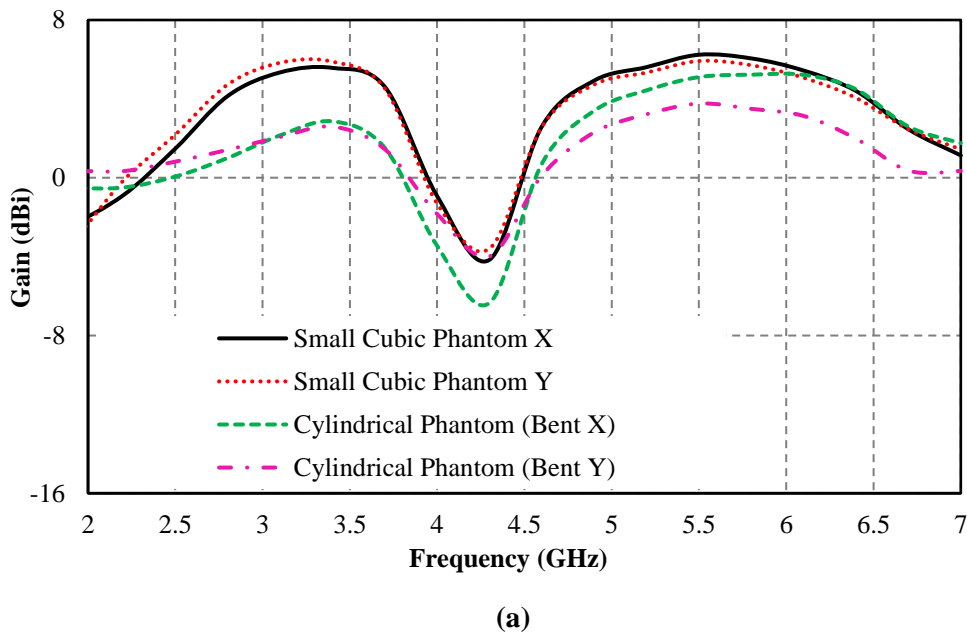


Fig. 5.16. Simulated reflection coefficients for different tissue models.

The gain and efficiency of the textile antenna are investigated for various phantoms as shown in Figs. 5.17(a) and (b), respectively. It is evident that the on-body simulated gains are found better in free space. The simulated radiation efficiency is greater at higher frequencies than at lower frequencies. The suggested antenna's front-to-back ratio (FBR) is depicted in Fig. 5.18.



(a)

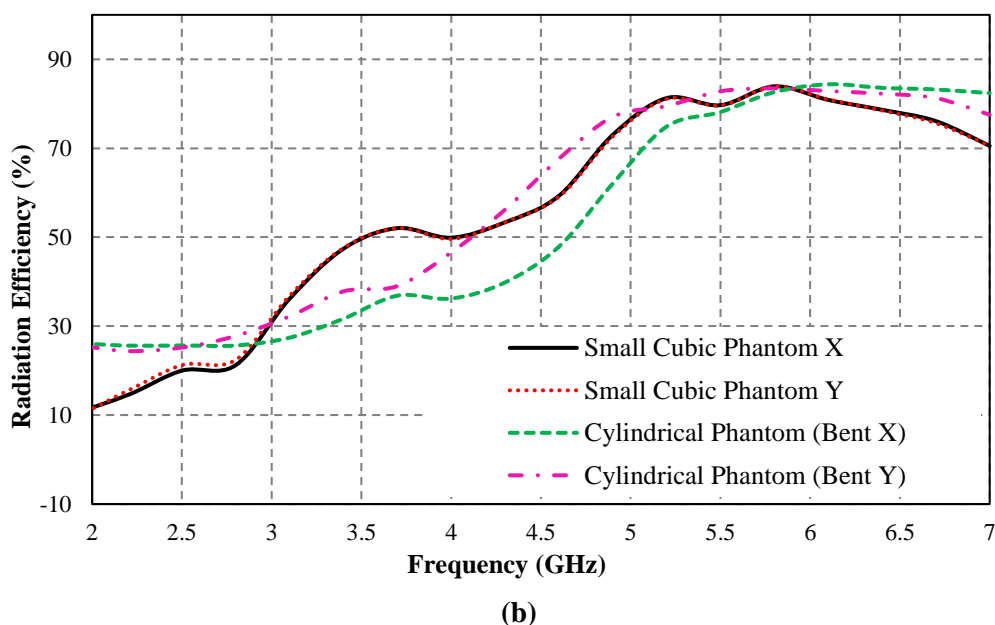


Fig. 5.17. Simulated results of the textile antenna for different tissue models: (a) gain, (b) efficiency.

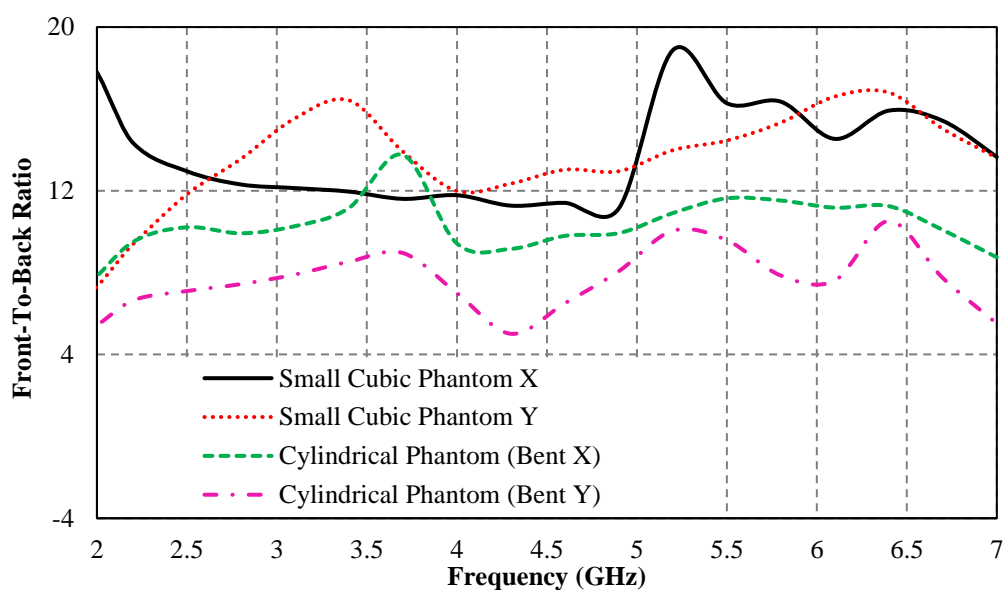
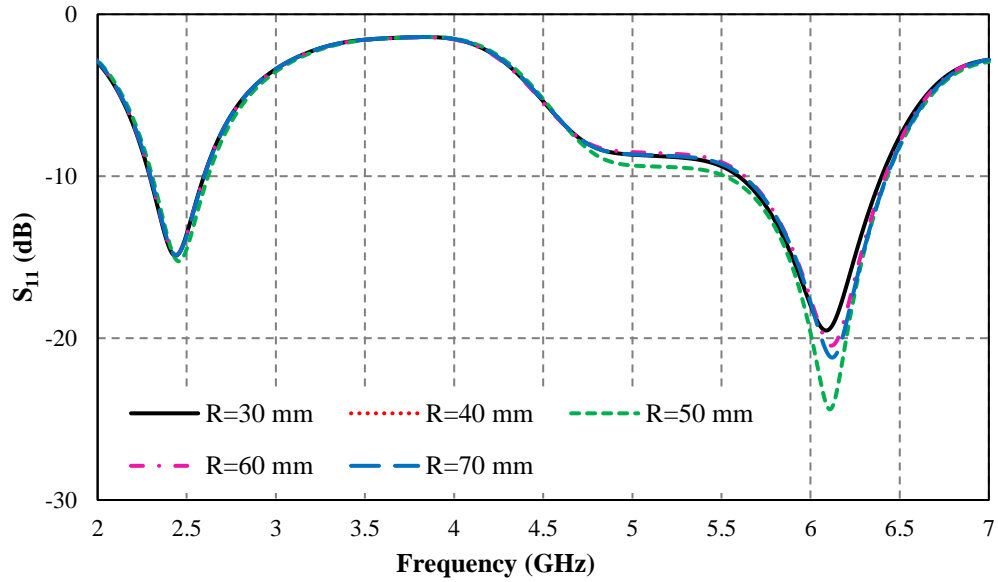


Fig. 5.18. Front-to-back ratio of the antenna.

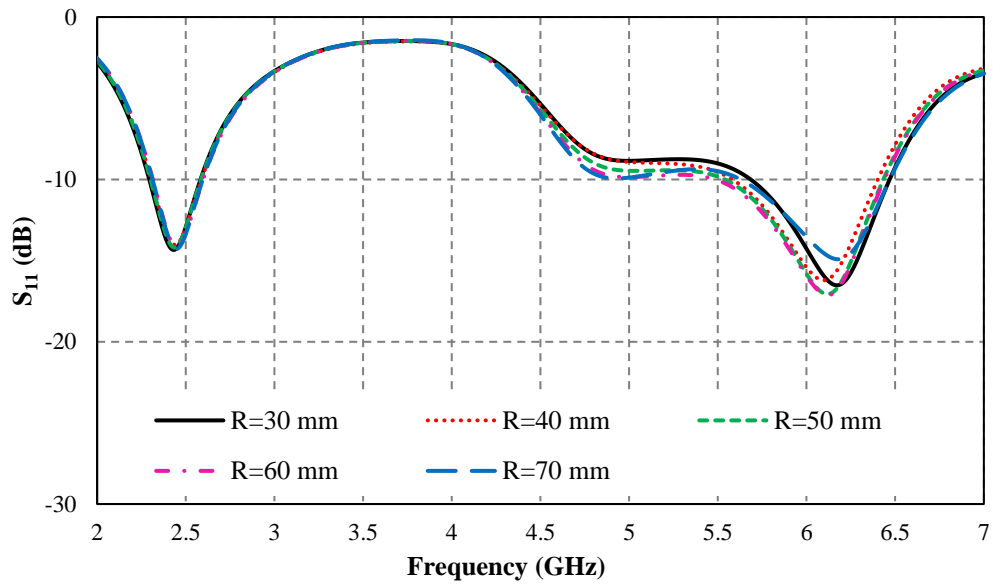
5.4.2 Bending Analysis

For the human arm tissue model, the bending analysis is performed at differing radii. The S-parameters of the textile antenna for different bending radii are shown in Figs. 5.19(a) and (b), respectively. The proposed textile antenna is kept 10 mm away from

the tissue model. A small change is noticed in the performance of the antenna. However, in all instances, the antenna is working within the required resonance bands.



(a)



(b)

Fig. 5.19. Bending analysis of the proposed textile antenna: (a) bent-X, (b) bent-Y.

5.4.3 Radiation Pattern

As illustrated in Fig. 5.20, the 2-D radiation patterns for several tissue models are explored at 2.45 GHz and 5.8 GHz. The radiation direction changes when the antenna is placed in Y-orientation.

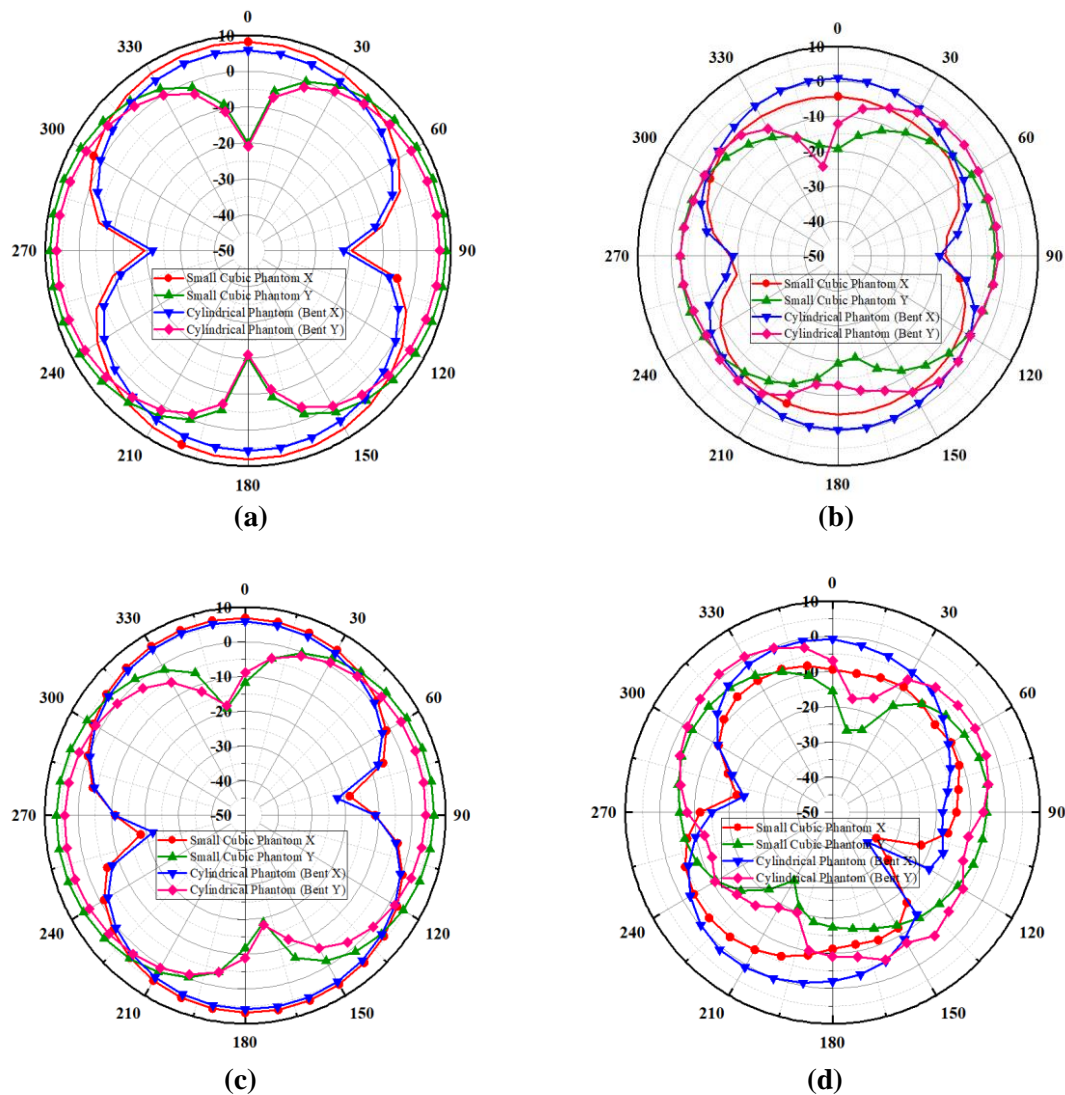


Fig. 5.20. Radiation patterns of the antenna for different tissue models: (a) E-plane at 2.45 GHz, (b) H-plane at 2.45 GHz, (c) E-plane at 5.8 GHz, (d) H-plane at 5.8 GHz.

5.4.4 SAR Analysis

Due to the close proximity of wearable antennas to the human body, it has always been necessary to calculate the amount of radiation penetrating the body. The SAR is calculated to determine the response of organic tissue to electromagnetic

radiations. It is measured in terms of “the amount of energy absorbed per unit of tissue mass.”

$$\text{SAR} = \frac{d}{dt} \cdot \frac{dW}{\rho dV} \text{ (W/Kg)} \quad (5.1)$$

“where W is the energy absorbed by the human tissue, ρ is the mass density, and V is the volume of the sample [50].”

In order to meet EMF exposure safety limits established by the “International Commission on Non-Ionizing Radiation Protection (ICNIRP)” and the “Federal Communications Commission (FCC)”, the maximum permissible values of input power must be evaluated. In this regard, several SAR calculations were performed for the proposed antenna, with different simulated powers such as 1mW, 10 mW, 0.1 W, and 1 W, over a simplified four-layered human arm model. The SAR distribution patterns for the arm model at various frequencies (for 1 g and 10 g) are depicted in Figs. 5.21 and 5.22, respectively.

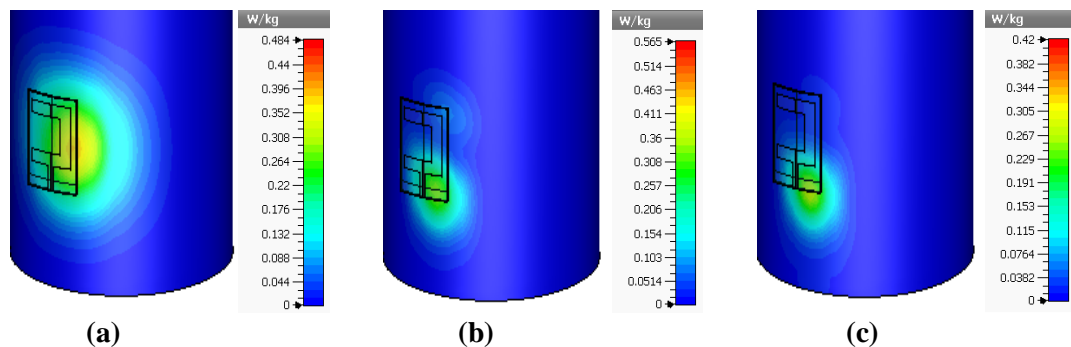


Fig. 5.21. SAR distribution patterns for arm model (simulated power=10 mW): (a) 2.45 GHz (1 g), (b) 5.0 GHz (1 g), (c) 5.8 GHz (1 g).

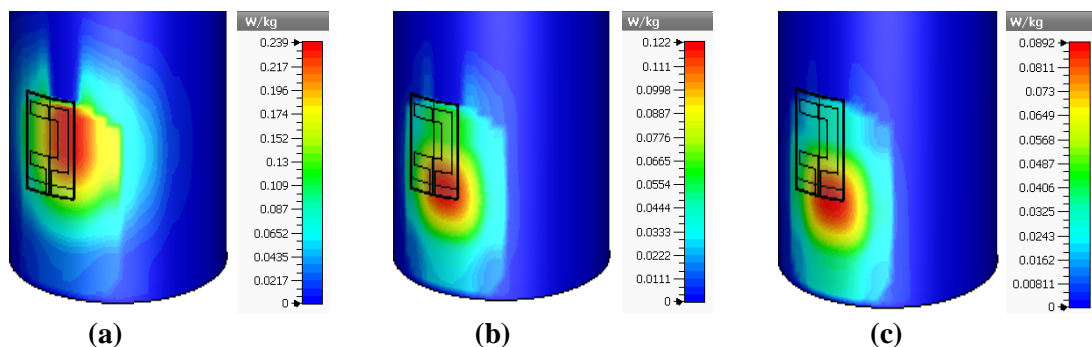


Fig. 5.22. SAR distribution patterns for arm model (simulated power=10 mW): (a) 2.45 GHz (10 g), (b) 5.0 GHz (10 g), (c) 5.8 GHz (10 g).

It can be seen that most of the back radiations are in the centre of the antenna for a lower frequency range. As the frequency increases, the back radiation starts shifting towards the lower side of the antenna. The simulated results obtained for maximum SAR are plotted in Fig. 5.23, and the maximum allowable input powers are listed in Table 5.4. It should be noted that the calculated SAR values for 1 g and 10 g have a linear relationship with the simulated power. It should also be noted that SAR values for 5.8 GHz and 5.9 GHz are almost the same. It is evident that natural situations such as water, snow, or body sweat have an effect on the performance of the textile antenna.

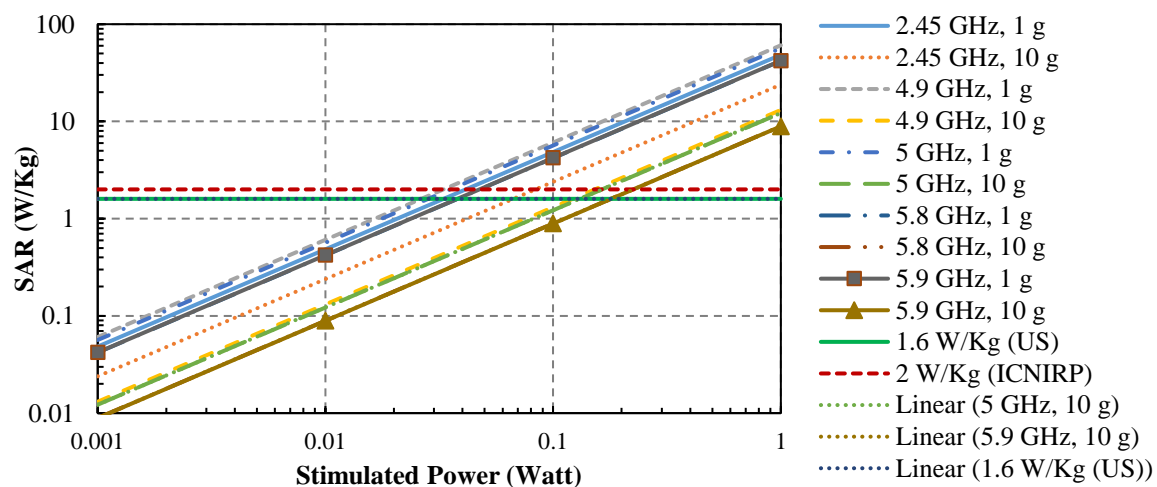


Fig. 5.23. Simulated results for maximum SAR.

Table 5.4. Maximum Allowable Input Power

Frequency	Average Mass (g)	Simulated Power				Maximum Allowable Input Power (mW)	
		1 mW	10 mW	0.1 mW	1 W	SAR=1.6 W/Kg	SAR=2 W/Kg
2.45	10	0.02391	0.2391	2.391	23.90	---	83.6
	1	0.04841	0.4841	4.841	48.41	33.05	---
4.9	10	0.01312	0.1312	1.312	13.12	---	152.4
	1	0.06066	0.6066	6.066	60.66	26.37	---
5.0	10	0.01222	0.122	1.22	12.2	---	163.9
	1	0.05654	0.5654	5.654	56.54	28.3	---
5.8	10	0.008924	0.08924	0.8924	8.924	---	224.1
	1	0.042	0.42	4.2	42.00	38.1	---
5.9	10	0.008902	0.08902	0.8902	8.902	---	224.6
	1	0.04212	0.4212	4.212	42.12	37.9	---

Table 5.5. Performance Comparison of the Proposed Textile Antenna with other Reported Works

Ref.	Antenna Size (mm×mm×mm)	Res. Freq. (GHz)	($S_{11} \leq -10$) Band (GHz)/ BW (MHz)	Gain (dBi)	Dielectric Material (ϵ_r)	Conductive Material	SAR (W/Kg) (For 500 mW)	App-lication Band
[52]	20×30×0.7/ 0.16 λ_0 ×0.24 λ_0 × 0.0057 λ_0	2.45	2.2–2.53/ 330	2.05	Denim (1.7)	ShieldIt	---	ISM
[53]	35×45×2/ 0.58 λ_0 ×0.75 λ_0 × 0.0333 λ_0	5	5.15–5.825/ 675	5.90	Wool Felt (1.2)	Nylon	0.9307 (1 g) 0.4016 (10 g)	WLAN
[114]	102×68×3.6/ 1.972 λ_0 ×1.31 λ_0 × 0.0696 λ_0	5.8	4.3–5.9/ 1600	6.12	Pellon (1.08)	Pure Copper Taffeta	0.1850 (1 g) 0.5900 (10 g)	ISM
[50]	74.5×48×3/ 0.60 λ_0 ×0.39 λ_0 × 0.0294 λ_0	2.45	2.4–2.5/ 100	5.35	Wool Felt (1.4)	Shieldit Super	0.3800 (10 g)	ISM
[51]	40×40×0.6/ 0.77 λ_0 ×0.77 λ_0 × 0.0116 λ_0	5.8	5.4–6/ 600	2.45	Jeans (1.78)	Copper Tape, Electrotextile	---	ISM
[48]	63.9×63.9×3.7/ 0.52 λ_0 ×0.52 λ_0 × 0.0302 λ_0	2.45	2.4–2.5/ 100	4.4	Foam (1.495)	Pure Copper Taffeta	0.4500 (1 g)	ISM
[49]	180×180×3.5/ 1.46 λ_0 ×1.46 λ_0 × 0.0285 λ_0	2.45, 4.5	2.31–2.54/ 230, 4.12–4.39/ 270	0.29, 3.05	Leather (2.5)	Zell	---	ISM
[47]	64.6×61.7×3.94/ 0.52 λ_0 ×0.52 λ_0 × 0.0322 λ_0	2.45, 5.8	2.4–2.48/ 80, 5.72–5.87/ 150	4.2, 5.5	Foam (1.495)	Pure Copper Taffeta	0.5500 (1 g), 0.9000 (1 g)	ISM
Prop.	20×30×1/ 0.16 λ_0 ×0.24 λ_0 × 0.0082 λ_0	2.45, 5.8	2.27–2.62/ 350, 4.67–6.33/ 1660	1.63, 2.7	Felt (1.34)	ShieldIt Super	21.000 (1 g) 4.4500 (10 g)	ISM

The performance comparison of the proposed textile antenna with other reported works is given in Table 5.5. The proposed antenna has a small size and dual-band performance, which is evident. The upper resonating band offers large bandwidth, therefore, it can be used for numerous applications. Because the proposed antenna is made of textile material, it may be easily integrated into garments.

5.5 CONCLUSION

This chapter presents design and analysis of an ultra-miniaturized textile antenna for 2.45 GHz and 5.8 GHz ISM band applications. The proposed textile patch antenna consists of a partial ground plane and a microstrip line-fed C-shaped monopole radiator. Several textile materials are considered and characterized to investigate various design possibilities. The proposed antenna is fabricated using Felt as the non-conducting dielectric material and Sheildit Super as the conducting material. The antenna performance is studied for on-body situations using the three-layered human shoulder model and four-layered human arm model. The proposed textile antenna, due to its small size, low fabrication cost, good impedance bandwidth, and acceptable on-body performance is a good candidate for ISM/wearable applications.

“Science is facts; just as houses are made of stone, so is science made of facts; but a pile of stones is not a house, and a collection of facts is not necessarily science.”

Jules Henri Poincaré

6

WIDEBAND TEXTILE MULTIPLE-INPUT-MULTIPLE-OUTPUT ANTENNA FOR INDUSTRIAL, SCIENTIFIC AND MEDICAL (ISM)/WEARABLE APPLICATIONS

In the previous chapter, the design and development of a dual-resonance ultra-miniaturized textile antenna for ISM/Wearable applications was presented. In this chapter, the designing, modelling, analysis, fabrication and measurement of a compact, wideband, two-element textile “*multiple-input-multiple-output (MIMO)*” antenna is presented for ISM/wearable applications. The proposed structure is composed of the Felt material substrate, and the ground plane and radiating patch are formed using Shieldit™ Super conductive material. The designed MIMO antenna offers a wide impedance matching bandwidth ($S_{11} \leq -10$ dB) of 2.00–6.23 GHz, a very low “*mutual coupling*” of $(S_{21, \max}) -29.26$ dB, low “*envelope correlation coefficient (ECC)*” < 0.01 , high “*diversity gain (DG)*” ~ 9.95 dB, and “*realized gain*” of more than 2.88 dBi, across the entire resonating band. The intended antenna geometry prototype has been fabricated and measures 76×37 mm². Because of its small size, all textile layers, ease of integration, resilience, and reasonable on-body performance, the proposed antenna could be a promising choice for wearable electrical devices.

6.1 INTRODUCTION

Recently, several studies have been done on wearable antenna design, as body-centric wireless communication systems are drawing substantial attention due to their broad applications in many areas [132], [133]. These wide ranges of applications include navigation, soldier communications, remote identification, security systems, wearable computer technology, entertainment, fashion, environmental/biophysical parameters, monitoring for rescue workers, and healthcare. The main component for all

the aforementioned applications is a wearable antenna that transfers the data wirelessly from on-body sensors to a centralized database/computing unit. The textile materials have been potential candidates for designing wearable antennas due to their comfort, robustness, and camouflaged integration with apparel. Moreover, the design and fabrication of a textile wearable antenna is a critical part of the performance of wearable links. These antennas need to radiate effectively and efficiently under different physical constraints such as stretching, crumpling, bending, and body movements [134]–[138].

With the rapid advancement of wireless communication technology, the high-performance modern communication systems with very high data rate and low cost are becoming imperative. The technological growth in wireless communication requires an increased data transfer rate, which can be achieved by increasing the bandwidth. Alternatively, this can also be achieved by a multi-antenna system with high isolation between the elements within the same bandwidth. One of the probable solution to increase the spectrum's efficiency is multiple-input-multiple-output (MIMO) technology, which is widely used presently. Since the signals emitted from the antenna are subject to interference and multipath fading while propagating in a real environment, the data transfer rate of the communication systems is constrained [139].

To enhance data transmission capacity and to reduce the multipath fading effects, the use of MIMO technology at terminals in the wireless communication systems has attracted many researchers both from academia and industry [140]. MIMO system increases the channel capacity, which accommodates a larger number of users to access various broadband services all together. The concept of MIMO has been adapted to the latest wireless systems such as “*wireless local area network (WLAN) standards [141], worldwide interoperability for microwave access (WiMAX) [142], long-term evolution (LTE) [143] and ultra-wideband (UWB) systems [144].*” Though MIMO techniques require complex structures, they are reliable and provide significant improvement in the “*transmission capacity, signal to noise ratio (SNR), and throughput*” of a system over the single antenna systems, without demanding an increased bandwidth and power [145]. When antennas are placed in the closed vicinity in MIMO configuration, the decoupling between the antenna elements is considered as another significant parameter. Various decoupling mechanisms have been used by authors in [146]–[148].

This chapter presents a wideband textile antenna with good physical parameters for the use of MIMO technology for ISM and WLAN applications. The off-body and on-body performances of the MIMO antenna are investigated. The presented MIMO antenna covers a frequency range from 2.00 to 6.23 GHz and exhibits low “*envelope correlation coefficient (ECC)*” < 0.01 and high “*diversity gain (DG)*” ~ 9.95 dB. In the analysis of the presented antenna, it is observed that maximum port isolation of 29.26 dB and stable radiation patterns at 2.45 GHz and 5.80 GHz are achieved, which renders this antenna as a good candidate for MIMO applications. The simulated and measured findings show a high level of agreement.

This chapter is organized as follows: Section-6.2 provides an insight into the design and fabrication of the MIMO antenna. The antenna performances in free space and on-body are discussed in sections 6.3 and 6.4, respectively. Section-6.5 gives a brief conclusion.

6.2 ANTENNA TOPOLOGY

The designed and fabricated configurations of the two-element MIMO antenna are shown in Figs. 6.1 and 6.2, respectively. The antenna is fabricated on 1 mm thick Felt material substrate, whose dielectric constant (ϵ_r) and loss tangent ($\tan \delta$) are 1.34 and 0.02, respectively. A radio frequency impedance/material analyzer (Agilent E4991A) was used for the characterization of textile materials. The metallic layers, ground plane, and radiating patch are formed using 0.17 mm thick Shieldit™ Super conductive material having sheet resistance of $< 0.07 \Omega$ per square. It is a polyester-based copper-/nickel-plated high-quality textile material. This material is thermally adhesive, which makes it convenient for antenna fabrication as it can easily be attached to the substrate, merely by dry ironing [128]. The antenna is simulated using “*CST Microwave Studio tool.*” The presented antenna structure is prepared through manual cutting tools. The detailed dimensions of the proposed MIMO antenna are given in Table 6.1. The antenna occupies an area of 37 mm \times 76 mm. The step-wise evolution of the two-element MIMO antenna is shown in Fig. 6.3.

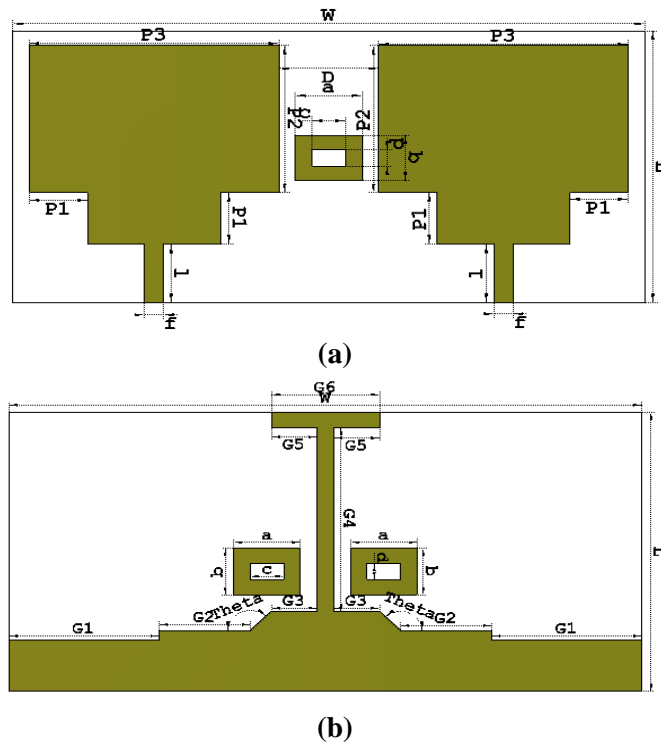


Fig. 6.1. Configuration of the textile MIMO antenna (a) top view (b) bottom view.

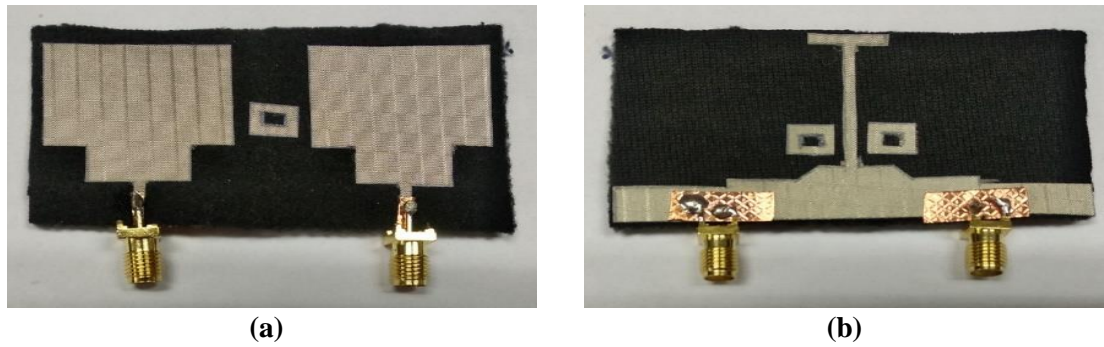


Fig. 6.2. Prototype of the textile MIMO antenna (a) top view (b) bottom view.

Table 6.1. Parameters of the Two-element MIMO Antenna

Parameter	Value (mm)	Parameter	Value (mm)
L	37	$P1$	7
W	76	$P2$	20
D	12	$P3$	30
f	2	$G1$	18
l	8	$G2$	11
a	8	$G3$	6
b	6	$G4$	24
c	4	$G5$	6
d	2	$G6$	13
Theta	135°		

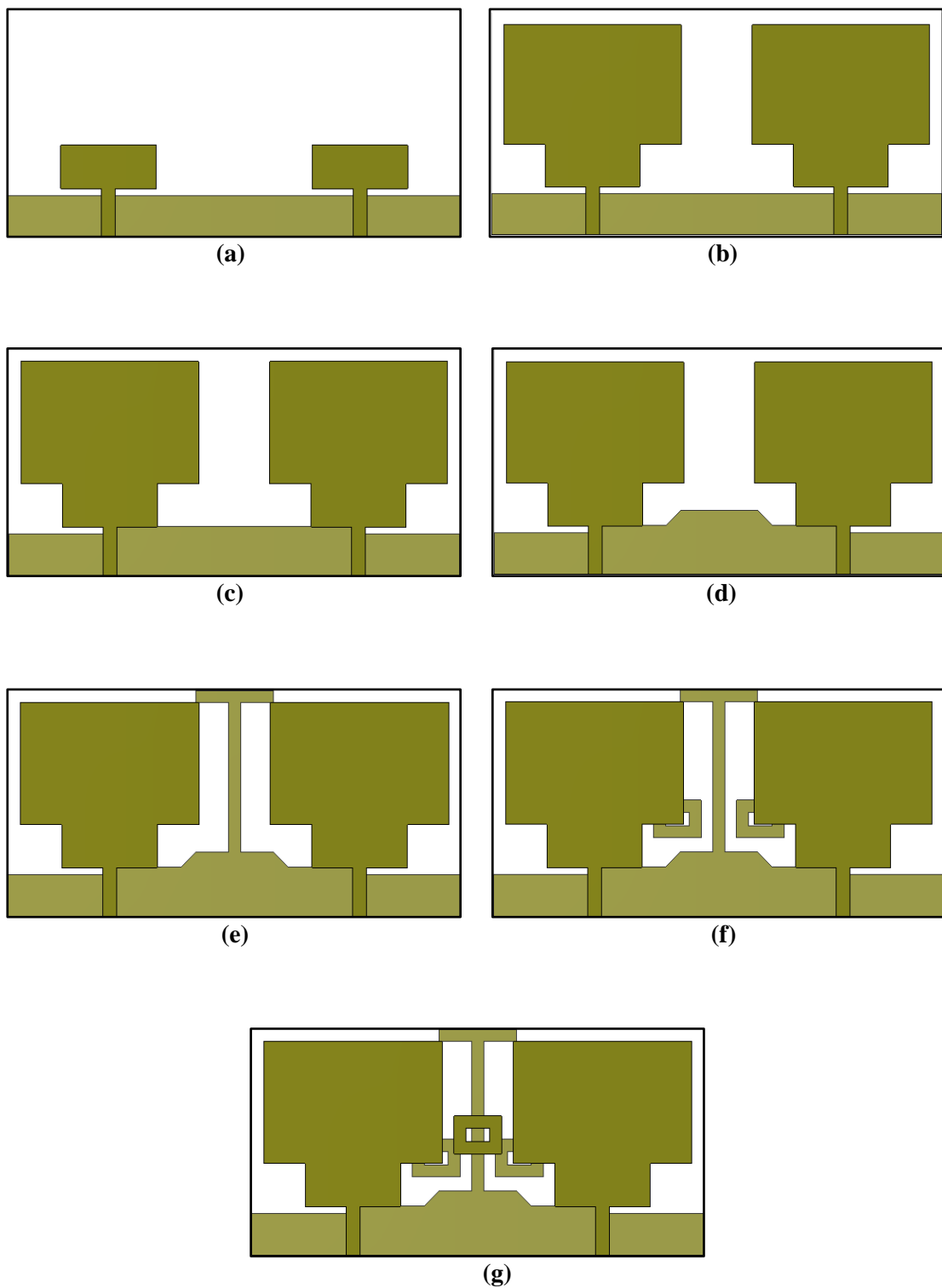


Fig. 6.3. Step-wise designing of the two-element MIMO antenna: (a) step-1 (b) step-2 (c) step-3 (d) step-4 (e) step-5 (f) step-6 (g) step-7.

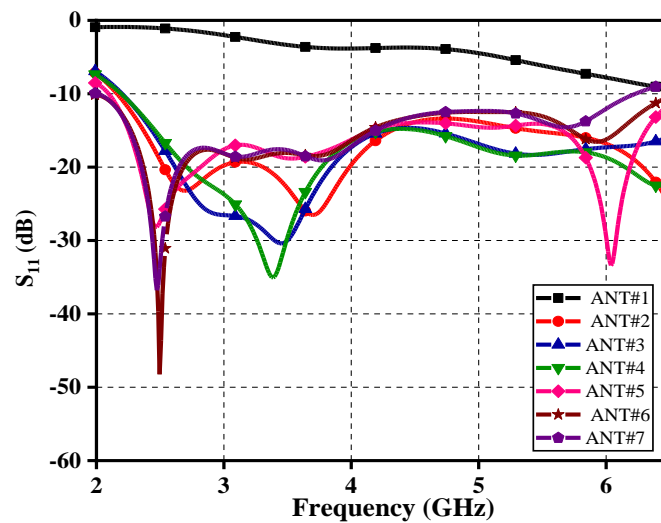


Fig. 6.4. Simulated S_{11} of the design steps of the two-element MIMO antenna.

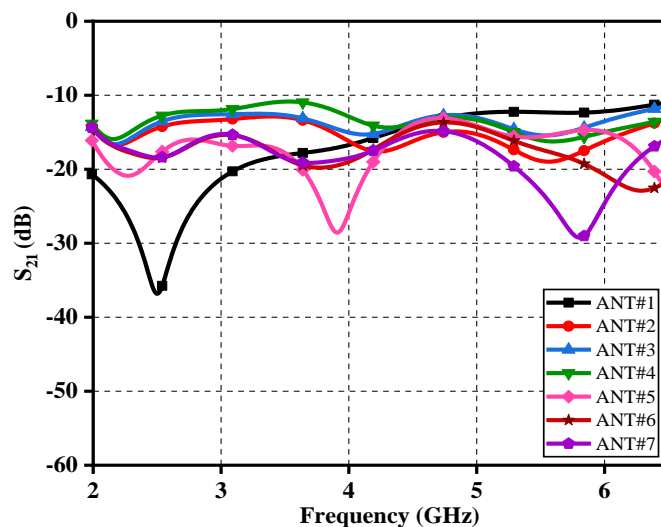


Fig. 6.5. Simulated S_{21} of the design steps of the two-element MIMO antenna.

The S-parameters of the evolution of the two-element MIMO antenna are shown in Figs. 6.4 and 6.5. In step-1, two rectangular-shaped elements are connected with the feed lines. The antenna (ANT#1) resonates at higher frequencies (8.3–14.6 GHz), and maintain isolation more than 15 dB up to the frequency of 4.32 GHz. In step-2, two rectangular patches are introduced in the ANT#1 to shift the resonating frequency towards the lower range. The antenna (ANT#2) has impedance matching band from 2.15 to 6.50 GHz, and isolation of more than 15 dB for a frequency range of 3.87–6.17 GHz. Hence, the ANT#2 provides proper impedance matching over a wide frequency band. Various other steps are taken to further improve the antenna performance. A

rectangular stub is added to the partial ground plane in step-3, which improves impedance matching of the ANT#3, but it does not affect the isolation between the radiating elements. A trapezium-shaped stub is added in step-4 (ANT#4) for further optimization. In step 5 (ANT#5), a T-shaped stub is introduced in the ground plane, which provides excellent isolation from 2.09 to 4.38 GHz, and an impedance matching for 2.09–6.50 GHz frequency range. In step-6 (ANT#6), two ring-shaped stubs are added in the ground plane of the MIMO antenna. This step not only provides excellent isolation for the entire frequency range (except 4.45–5.10 GHz) but also improves impedance matching around 2.50 GHz. In the last step, a ring-shaped stub (of the same size introduced in the previous step) is added between the radiating patches (ANT#7), which improves isolation over the entire operating frequency band. The proposed textile MIMO antenna covers a wide frequency range from 2.00 to 6.23 GHz that includes ISM and WLAN bands.

6.3 ANTENNA PERFORMANCES IN FREE SPACE

6.3.1 Return Loss, Isolation, and Gain

The proposed antenna structure was fabricated and tested using a vector network analyzer. The simulated and measured S-parameters of the proposed textile antenna are shown in Fig. 6.6. The frequency spans from 2.00 to 6.23 in both simulations and measurements.

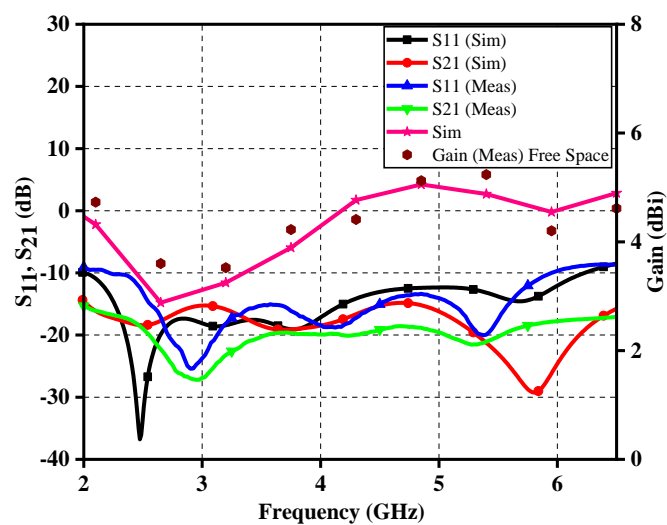


Fig. 6.6. Simulated and measured S-parameters and gain of the two-element MIMO antenna.

GHz, and it is observed that the simulated S_{21} parameters are -18.35 dB and -29.26 dB at 2.45 GHz and 5.8 GHz, respectively. Figure 6.6 depicts the proposed MIMO antenna's simulated and measured gains. In the designated band, the peak gains are 3 dBi and 4.33 dBi at 2.45 GHz and 5.8 GHz, respectively. The simulated and measured characteristics revealed a good agreement. Due to fabrication and measurement tolerances, there is a minor difference between the simulated and measured findings.

6.3.2 Isolation Study

In MIMO antenna, the radiating elements are placed closely to each other, but it affects the mutual coupling between them. In the proposed work, a T-shaped stub and three rectangular rings (loaded on the Felt substrate's top and bottom) are used for reducing interference between the antenna elements. The spacing between the radiators and position of the ring (present on the top of the substrate) are optimized in such a way that a compact geometry (with minimum mutual coupling) is achieved. The dimensions of the rectangular ring are optimized in such a manner that it does not much affect the S_{11}/S_{22} of the textile antenna while preserving a significant effect on the inter-element coupling.

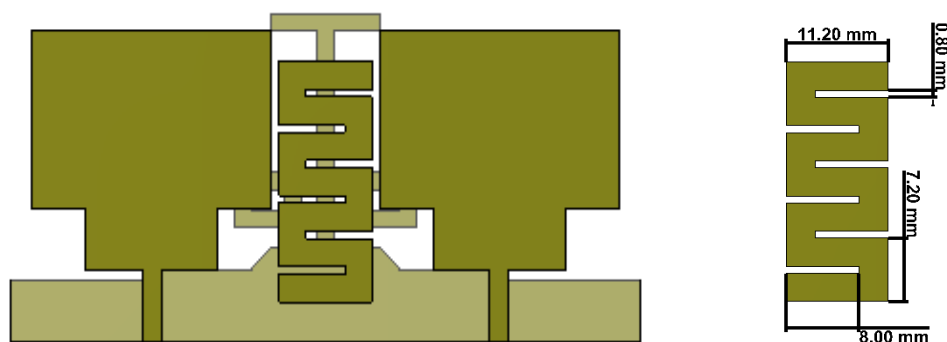


Fig. 6.7. Top view of the two-element MIMO with meander-line structure.

Here, another interesting technique is presented to enhance isolation between the antenna elements. In this approach, a meander line structure is introduced (on the top-side of the substrate) between the antenna elements as shown in Fig. 6.7. The backside of the antenna remains the same. It considerably increases the isolation of the

MIMO antenna. The simulated S_{21} parameters are -18.67 dB and -21.41 dB at 2.45 GHz and 5.8 GHz, respectively, as shown in Fig. 6.8.

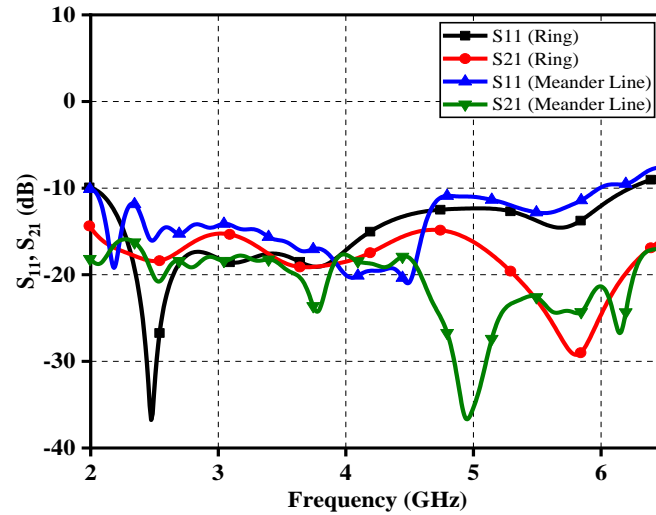


Fig. 6.8. Simulated S-parameters of the two-element MIMO with meander-line structure.

6.3.3 Diversity Performance

The diversity performance is a key parameter to judge the effectiveness of MIMO antennas. Thus, the investigation of the diversity and multiplexing performance becomes equally essential [16]. ECC can best assess diversity performance. The depth of ECC describes how good the communication channels are isolated/correlated with each other. In a MIMO antenna system, the ECC provides a measure of correlation in the radiation pattern produced by the n th element with the m th element. Due to the lossy nature of the planar printed antenna, the scattering parameters cannot be used appropriately for calculating ECC. Instead, the far-field radiation patterns are found more suitable for calculating ECC [149], and it is given by (5) in [150]. The ECC for the proposed MIMO antenna calculated using far-field radiation patterns is less than 0.1, as demonstrated in Fig. 6.9. Another essential parameter is DG, which is evaluated using (6) in [150]. Fig. 6.9 compares the ECC and DG of the textile MIMO antenna in free space and on-body. In section 6.4, the impacts of the human body on antenna performance are examined in detail. The suggested MIMO antenna has a high DG (>9.95) and an ECC of less than 0.01 in open space, as shown in Fig. 6.9.

Another fundamental parameter that increases the spectral efficiency of the

MIMO is called multiplexing efficiency (ME). It takes into account the correlation, efficiency imbalance, and total efficiency. The lesser the losses, the higher is ME. It can be evaluated using (20) in [151]. Fig. 6.10 compares the ME in free space and on-body. The ME of the proposed textile antenna (in free space) varies between -1.2 to +1.2 over the desired frequency range.

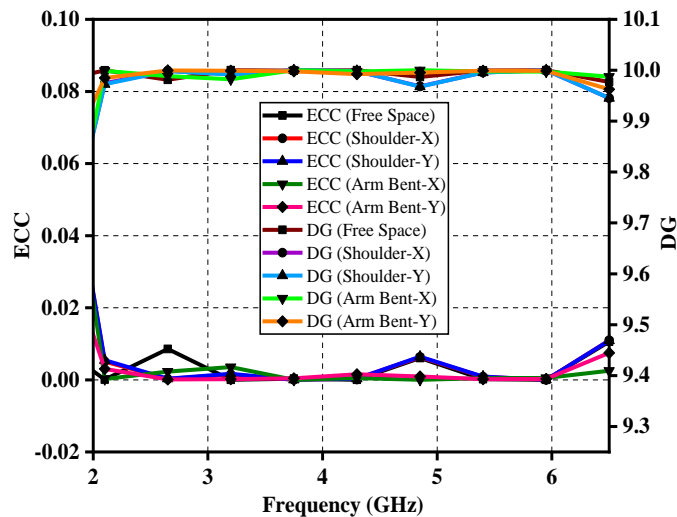


Fig. 6.9. ECC and DG of the two-element MIMO antenna.

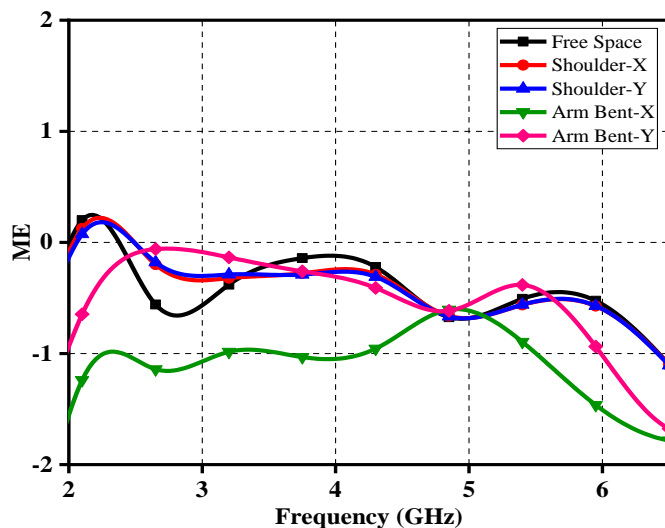


Fig. 6.10. ME of the two-element MIMO antenna.

6.3.4 Surface Current Distribution

To further understand the mutual coupling between the ports, the surface current distribution of the suggested two-element textile MIMO antenna is explored. Figs. 6.11(a) and (b) illustrates the surface current distributions of the MIMO antenna (with and without decoupling elements) at 2.45 GHz and 5.8 GHz, respectively. In the MIMO antenna design with decoupling devices, the amount of current flowing from one port to another is negligibly small. The antenna elements have relatively low mutual coupling because of the decoupling structures between them.

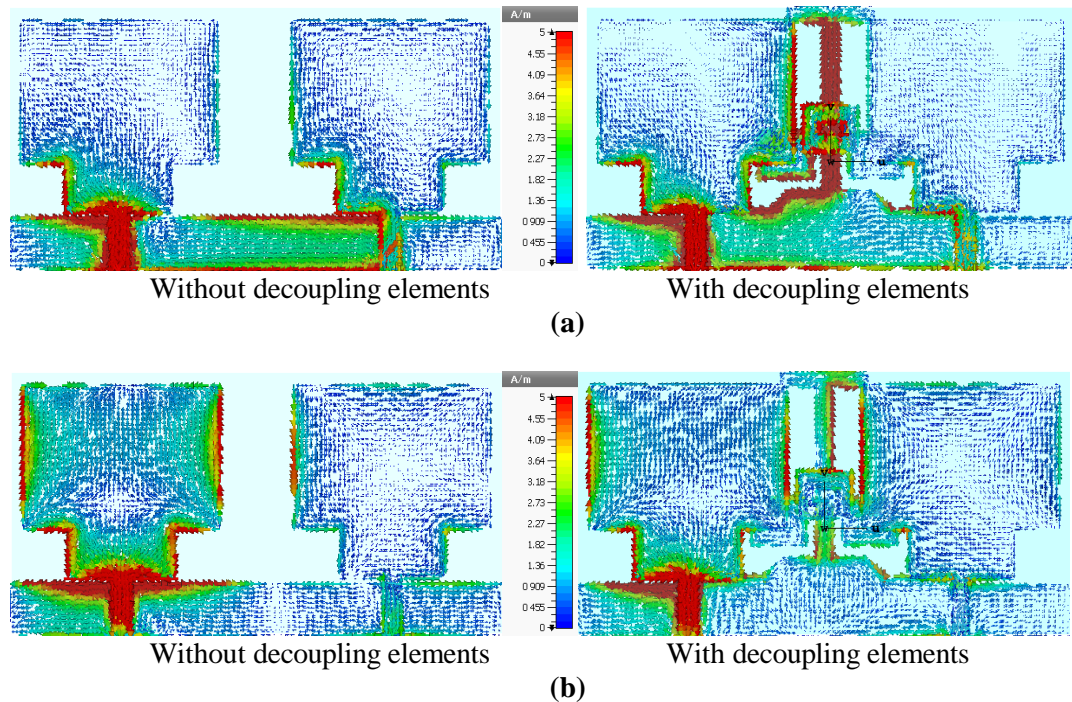
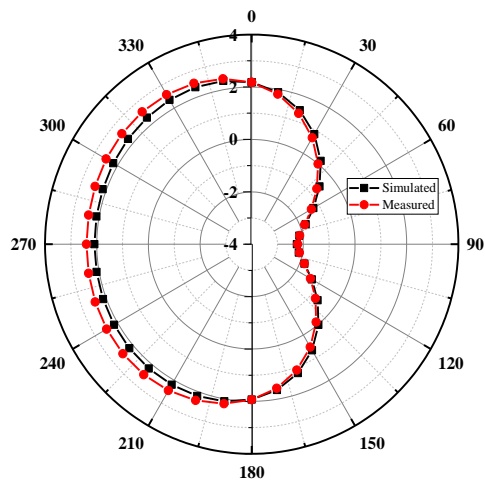


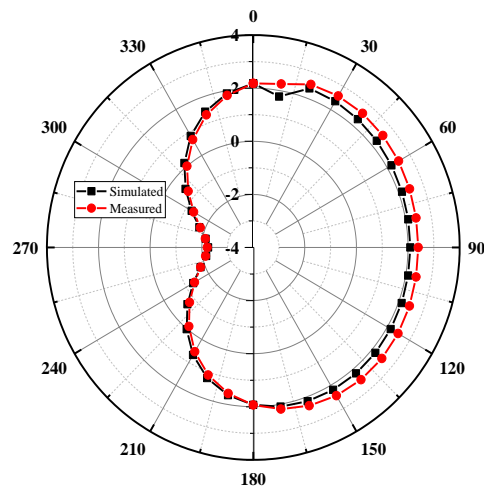
Fig. 6.11. Surface current distribution of the MIMO antenna at (a) 2.45 GHz (b) 5.8 GHz.

6.3.5 Radiation Pattern

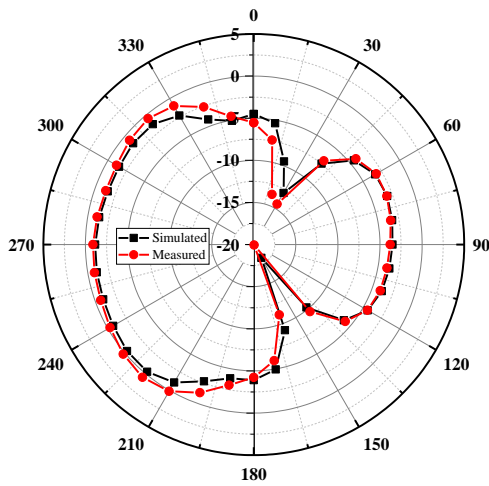
The simulated and measured 2-D far-field radiation patterns of the proposed MIMO antenna at 2.45 GHz and 5.8 GHz are shown in Figs. 6.12 and 6.13 when either port-1 or port-2 is excited and when both port-1 and -2 are excited simultaneously. The 3-D far-field radiation patterns of the proposed MIMO antenna are also investigated at 2.45 GHz and 5.8 GHz as shown in Figs. 6.14 and 6.15, when either port-1 or port-2 is excited and when both port-1 and -2 are excited simultaneously. It is evident that the proposed MIMO antenna offers a good pattern diversity and better isolation.



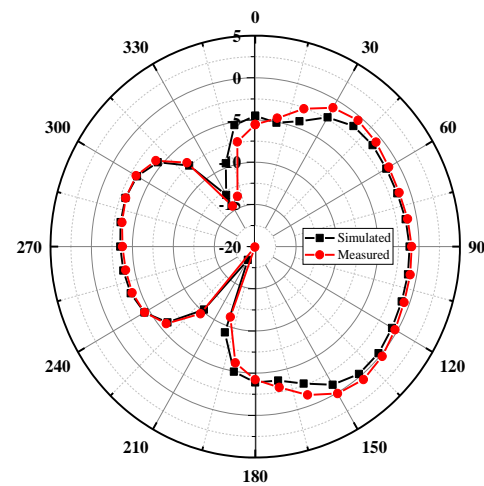
(a)



(b)



(c)



(d)

Fig. 6.12. Simulated and measured radiation patterns of the two-element textile MIMO antenna (at $\varphi=0^\circ$): (a) 2.45 GHz/port-1 (b) 2.45 GHz/port-2 (c) 5.8 GHz/port-1 (d) 5.8 GHz/port-2.

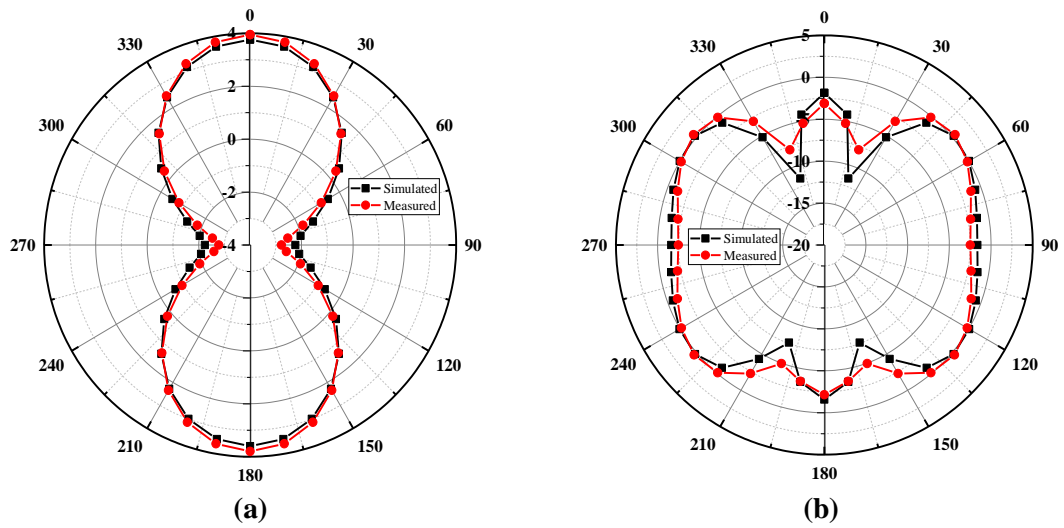


Fig. 6.13. Simulated and measured radiation patterns of the two-element textile MIMO antenna when both port-1 and -2 are excited simultaneously (at $\phi=0^\circ$) : (a) 2.45 GHz (b) 5.8 GHz.

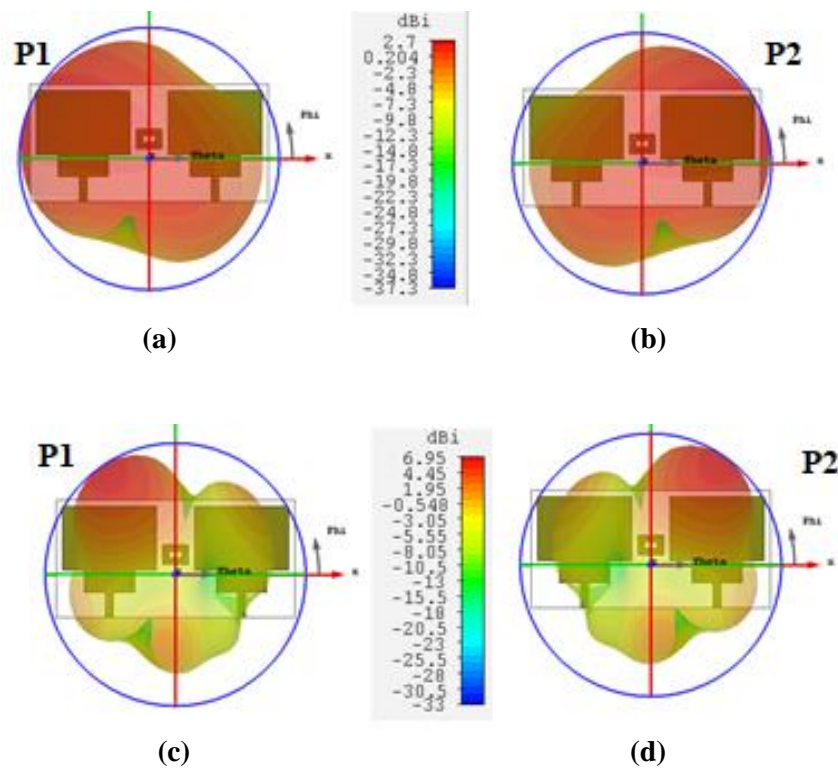


Fig. 6.14. 3-D radiation patterns of the two-element textile MIMO antenna (a) 2.45 GHz/port-1 (b) 2.45 GHz/port-2 (c) 5.8 GHz/port-1 (d) 5.8 GHz/port-2.

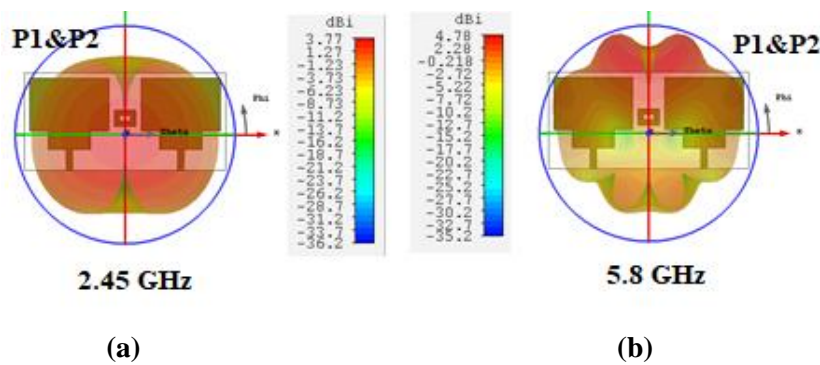


Fig. 6.15. 3-D radiation patterns of the two-element textile MIMO antenna when both port-1 and -2 are excited simultaneously (a) 2.45 GHz (b) 5.8 GHz.

6.4 ANTENNA PERFORMANCES ON HUMAN BODY

Furthermore, the proposed MIMO antenna is characterized for different on-body situations. Two types of phantoms (human tissue models) are chosen to imitate the human shoulder and arm as shown in Fig. 6.16. The human shoulder tissue model is a three-layered

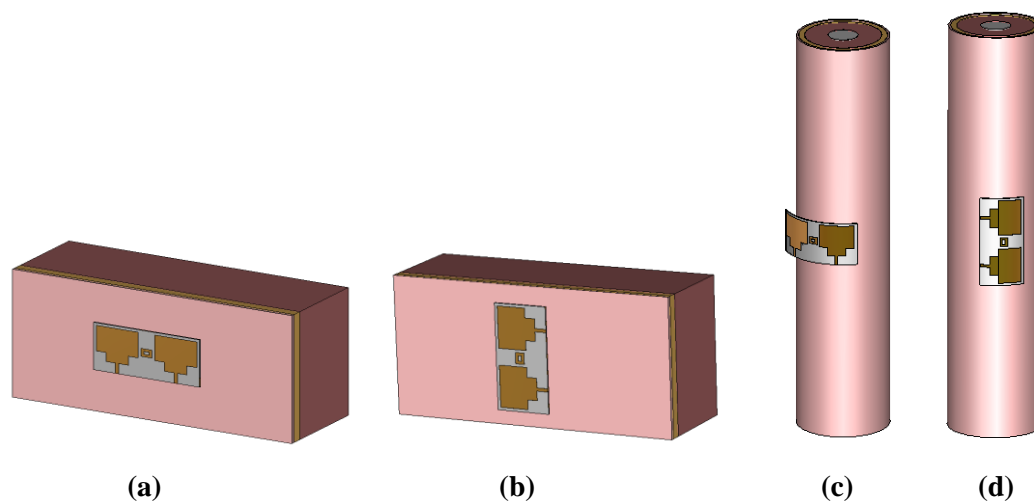


Fig. 6.16. Human tissue models: (a) cubic phantom/x-direction (b) cubic phantom/y-direction (c) cylindrical phantom/x-direction (d) cylindrical phantom/y-direction.

structure, while the human arm tissue model is a four-layered structure. The dimensions of the various layers of tissue models are given in Table 6.2. The size of the phantom for the shoulder model is taken as 200 mm × 100 mm × 70 mm. The length of the arm model is considered as 350 mm [152]. The model parameters defining the properties of tissues were taken from the material library of CST. To imitate the garment layers, the MIMO

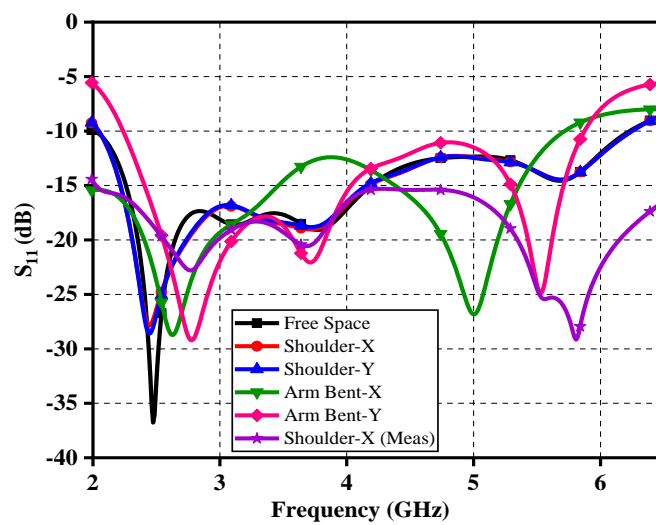
antenna was placed 10 mm away from the skin [18]. The performance is investigated in the x - and y -axis for both cubic and cylindrical tissue models. For the human arm model, the textile MIMO antenna was bent with a radius of 50 mm.

Table 6.2. Dimensions of the Various Layers of Tissue Models

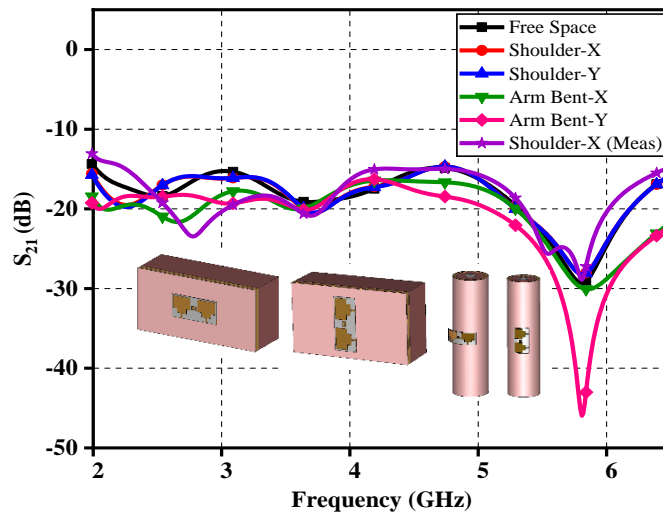
	Bone	Skin	Fat	Muscle
Shoulder Model	---	3 mm	7 mm	60 mm
Arm Model	13 mm	2 mm	5 mm	20 mm

6.4.1 Return Loss, Isolation, Gain, and Radiation Efficiency

The S-parameters (S_{11} and S_{21}) of the antenna in free space and on-body (along the x -axis and y -axis) are shown in Figs. 6.17(a) and (b), respectively. When the antenna is put on a small-cubic phantom, there is no significant difference. When the antenna is mounted on a cylindrical phantom, the impedance bandwidth changes slightly. The gain and efficiency of the antenna are investigated for various phantoms as shown in Figs. 6.18(a) and (b), respectively. It is evident that the gain of the antenna is varying between 3 to 5 dBi at 2.45 GHz and 4.8 to 6.6 dBi at 5.8 GHz for different tissue models. The on-body simulated gains are found to be better than free space [153]. The simulated efficiency is more than 90% for all the cases except arm bending along the x -direction. On the arm, the radiation efficiency reduces significantly due to a large bending and uneven placement of the antenna.



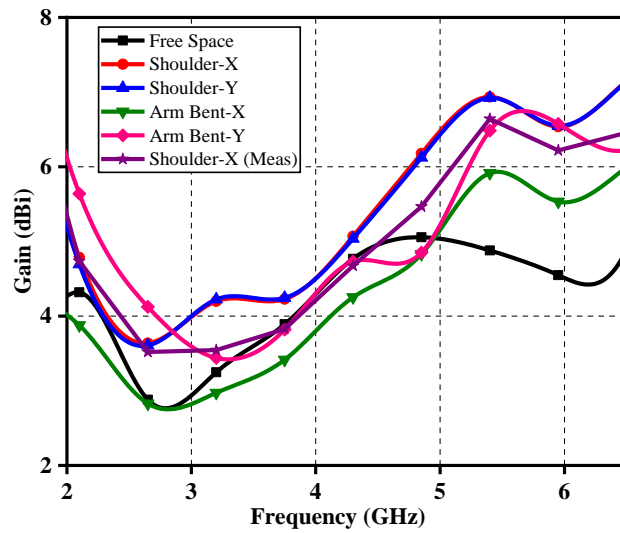
(a)



(b)

Fig. 6.17. Simulated S-parameters of the textile MIMO antenna for different tissue models

(a) S_{11} (b) S_{21} .



(a)

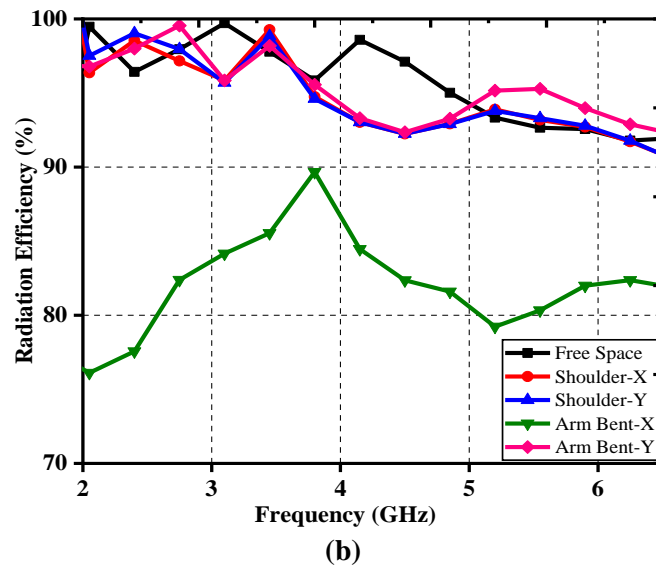


Fig. 6.18. Simulated results of the textile MIMO antenna for different tissue models: (a) gain (b) efficiency.

6.4.2 Diversity Performance

Furthermore, the suggested MIMO antenna's diversity performance is investigated for several tissue types. In Fig. 6.9, the ECC and DG of the textile MIMO antenna are shown on body situations. It is evident that the diversity performance of the antenna is within the desired range even under the influence of various tissue models. The ME of the antenna is also investigated and found between -3 and +3 for the entire frequency range in Fig. 6.10.

6.4.3 Radiation Pattern

The 2-D radiation patterns for various tissue models are investigated at 2.45 GHz and 5.8 GHz as shown in Figs. 6.19 and 6.20. As compared to the free space, there is an insignificant change in the radiation patterns for a cubic phantom. The changes in radiation patterns can be seen when the antenna is placed on a cylindrical phantom. In both cases, the pattern diversity is maintained, which provides good isolation between the antennas.

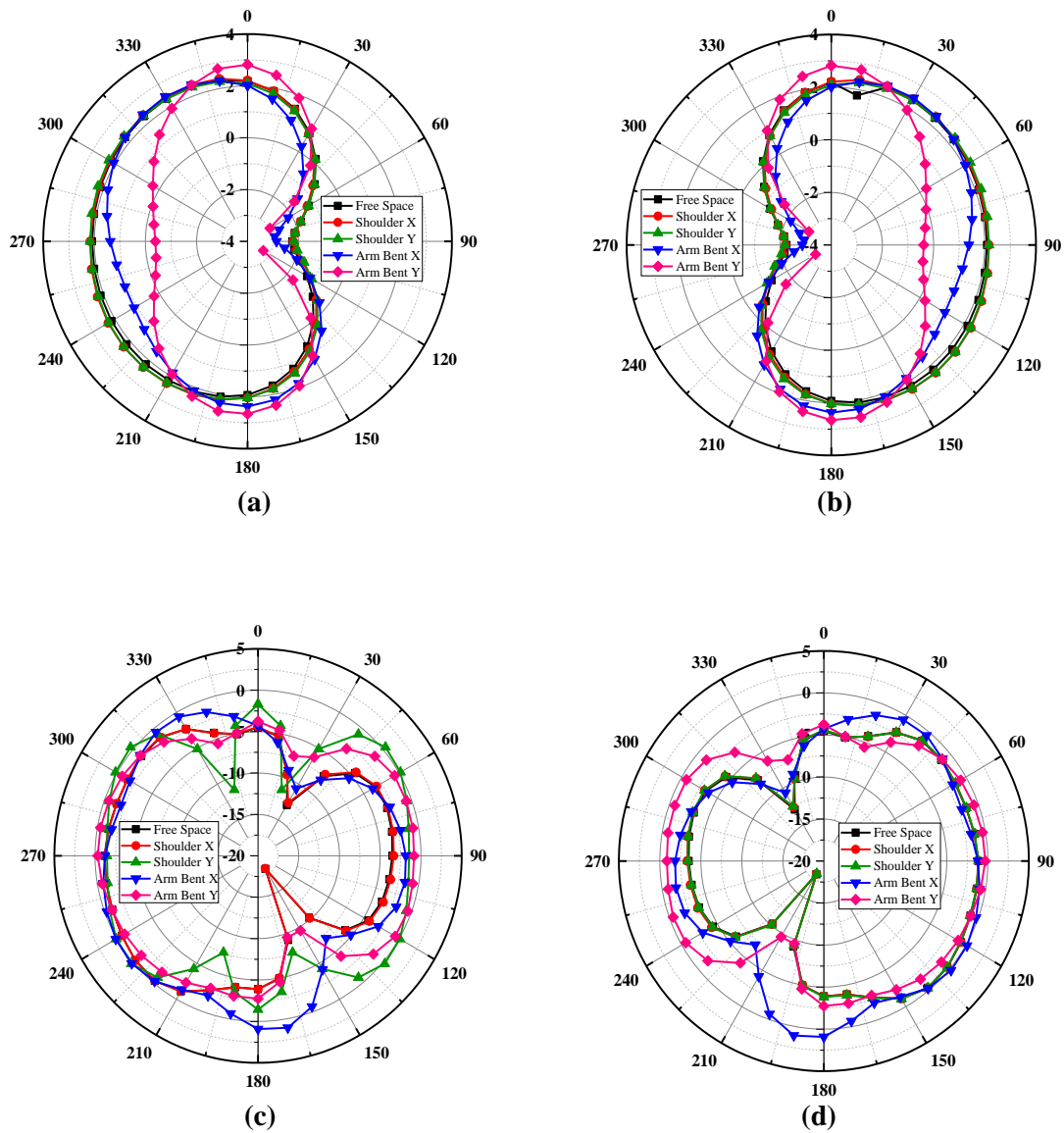


Fig. 6.19. Simulated radiation patterns of the two-element textile MIMO antenna (at $\phi=0^\circ$)
(a) 2.45 GHz/port-1 (b) 2.45 GHz/port-2 (c) 5.8 GHz/port-1 (d) 5.8 GHz/port-2.

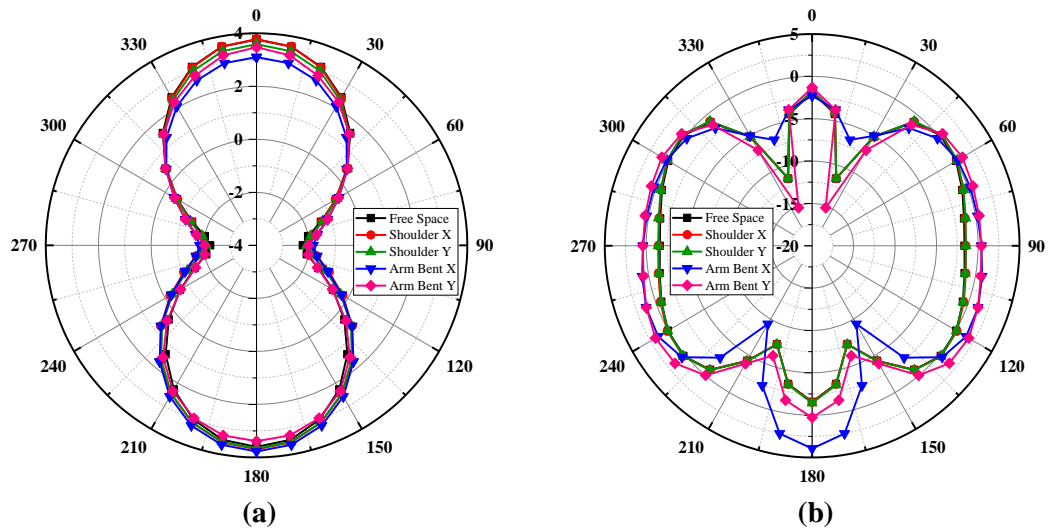
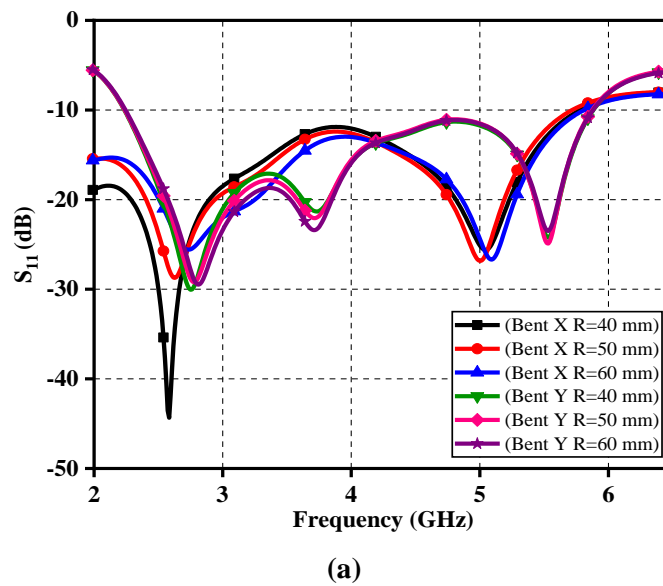
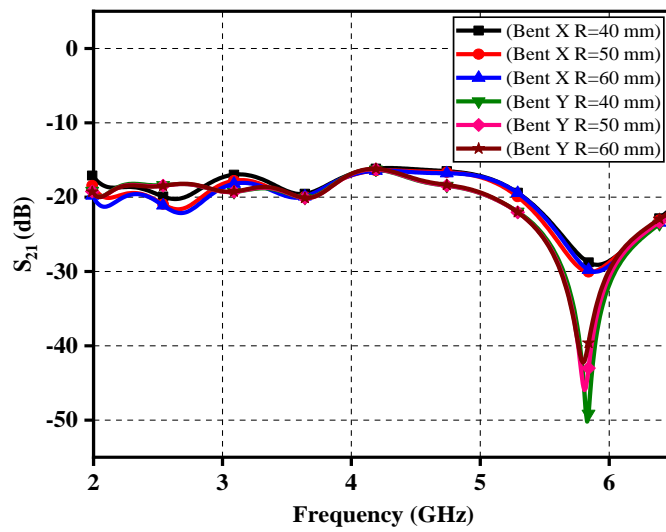


Fig. 6.20. Simulated radiation patterns of the two-element textile MIMO antenna when port-1 and -2 are excited simultaneously (at $\phi=0^\circ$) (a) 2.45 GHz (b) 5.8 GHz.

6.4.4 Bending Analysis

The bending analysis at differing radii for various tissue models is performed. The S-parameters (S_{11} and S_{21}) of the textile MIMO antenna for different bending radius are shown in Figs. 6.21(a) and (b), respectively. The center of the proposed MIMO antenna is kept 10 mm away from the tissue model in all the cases. A small change is noticed in the performance of the antenna. But, in all instances, the antenna is working within the required resonance band.





(b)

Fig. 6.21. Bending analysis of the proposed textile MIMO antenna for various tissue models (a) S_{11} (b) S_{21} .

6.4.5 SAR Analysis

Since the human body is in the closed vicinity of the wearable antenna, it is critically important to calculate the amount of electromagnetic radiation penetrating into the body. The SAR analysis of the proposed two-element MIMO antenna is performed numerically, using the CST, with the safety guidelines of the FCC. According to the FCC, the SAR value must be “less than 1.6 W/Kg for 1 g of human tissue.” The study was performed to find out SAR at 2.45 GHz and 5.8 GHz. The power level that can be used within an acceptable SAR range is shown in Fig. 6.22.

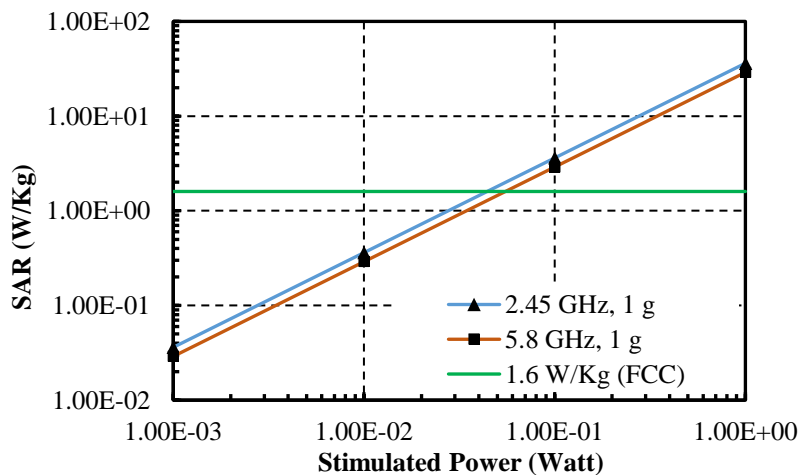


Fig. 6.22. Simulated results for maximum SAR.

A comparison of the proposed work with the recent wearable/textile-based MIMO antennas is illustrated in Table 6.3. Most of the wearable antennas presented in the literature were designed on the Jeans substrate, which exhibits poor performance at high frequencies. The proposed antenna, however, is designed with the high-performing Felt substrate of thickness of 1 mm. The proposed wideband textile MIMO antenna is easy to design and can be simply integrated with other RF circuitry (such as rectenna or transceiving components) due to its conformal, lightweight, low-profile, and simple geometry. For real-time applications, the performance of the antenna can be maintained by making use of protective coatings.

Table 6.3. Comparison of the Proposed Work with other MIMO Antennas

Ref.	Antenna Size	No. of Elements	Substrate (ϵ_r)	Gap between the Elements	Maximum Gain (dB)	Frequency Band (GHz)	Maximum Port Isolation (dB)
[137]	$0.31\lambda_0 \times 0.31\lambda_0$	2	Felt (1.20)	$0.082\lambda_0$	2.79	2.40–2.485	20.00
[72]	$0.49\lambda_0 \times 0.79\lambda_0$	2	Jeans (1.77)	$0.082\lambda_0$	4.00	1.5–3.8, 4.1–6.1	33.00
[69]	$0.245\lambda_0 \times 0.408\lambda_0$	2	Jeans (1.6)	$0.057\lambda_0$	2.70	3.2–8.5	32.00
[70]	$0.327\lambda_0 \times 0.572\lambda_0$	2	Jeans (1.6)	$0.049\lambda_0$	4.40	2.0–8.0	53.00
Prop.	$0.302\lambda_0 \times 0.621\lambda_0$	2	Felt (1.34)	$0.098\lambda_0$	4.33	2.00–6.23	29.26

6.5 CONCLUSION

The body of work described in this chapter was focused on the development of a textile-based, wideband antenna for MIMO systems. The antenna was fabricated using textile materials only, and its performance was studied in free space and on-body. A T-shaped stub and three rectangular rings (loaded on the top and bottom of the Felt substrate) were used for reducing interference between the antenna elements. The simulated and measured results are in agreement. The SAR analysis of the proposed textile antenna was also studied for tissue models (like shoulder and arm), and it works within the acceptable limits (1.6 W/Kg as specified by FCC) of SAR.

***“If you can’t figure out your purpose, figure out your passion. For
passion will lead you right into your purpose.”***

T.D. Jakes

7

FULLY-TEXTILE DUAL-BAND DUAL-SENSE MIMO ANTENNA FOR WBAN/WLAN/ISM/WEARABLE IOT APPLICATIONS

In the previous chapter, the design and development of a wideband textile “*multiple-input-multiple-output*” antenna for Industrial, Scientific and Medical (ISM)/Wearable applications was presented. In this chapter, the designing, modelling, analysis, fabrication and measurement of a compact fully-textile dual-band dual-sense two-element “*multiple-input-multiple-output (MIMO)*” wearable antenna is presented for “*WBAN/WLAN/ISM/IoT applications.*” The proposed antenna is constructed using the non-conducting textile material (Felt), and the ground plane and the radiating patches are designed with the conductive electro-textile material (Sheildit Superconductive). The fully-textile multiple-input-multiple-output (MIMO) wearable antenna provides an impedance-matching bandwidth ($S_{11} \leq -10$ dB) in 2.18-3.29 GHz and 3.92-6.90 GHz bands, circular polarization in the 4.92-5.94 GHz band, isolation greater than 15 dB, realized gain >2.00 dBi, diversity gain (DG) ~ 9.90 dB, envelope correlation coefficient (ECC) <0.12 and multiplexing efficiency between ± 2.0 over the resonating bands. The MIMO antenna occupies a volume of $43 \times 92 \times 1$ mm³. The proposed fully-textile MIMO antenna can be a suitable choice for all wearable electronics in body area networks (BANs) due to its compactness and reasonable performances in free space and on-body. The antenna can be integrated into garments because of its all-textile layers.

7.1 INTRODUCTION

Due to the rapid advancement of communication technology, wireless devices for body-centric communication are required [124], [154]. These devices should have a higher data rate in order to transmit high-quality audio and video messages. They can be used for remote identification, security system, soldier communication, navigation

fashion [17], [49], [155]–[157], entertainment, energy harvesting [158], biomedical telemetry [159], [160], spacesuit [161], healthcare [52], and Internet of things (IoT) applications [162], [163].

IoT technology wirelessly connects all devices or things, from household appliances to everyday consumer electronics. In IoT, the transfer of data does not necessitate any human or human-to-computer interaction. It has reformed several aspects of our daily lives. It is reshaping the means people receive medicare and providing patients and healthcare professionals with cutting-edge insights and analytics. IoT has covered a wide range of applications, including glucose monitoring, concussion protection, heart attack prevention, asthma monitoring, movement disorders, posture correction, medical adherence, and sleep monitoring, and many more [164], [165]. Wearable antennas play a pivotal role in the realization of “*wireless body area networks (WBANs)*” also known as “*body sensor networks (BSNs), or medical body area networks (MBANs)*” [166].” Various surveys predict that wearables will replace around 40% of smartphones in the coming years [167]. Textile antennas provide comfort and ease of integration as they can be designed as part of clothing and accessories. An illustration of a textile-based IoT antenna is shown in Fig. 7.1.

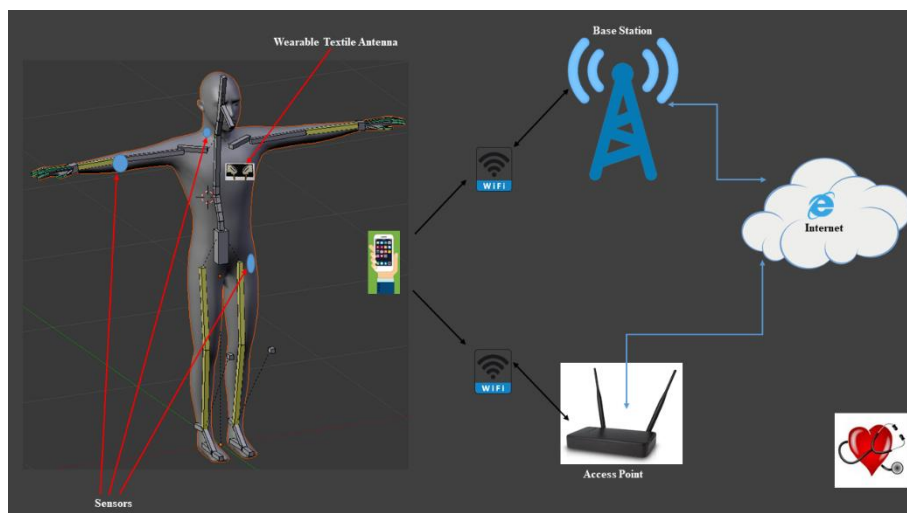


Fig. 7.1. Illustration of textile antenna for IoT

The textile fabrics have been used for many wearable applications because of their low profile, lightweight, robust nature, conformal, economical cost, and ease of integration with clothes and apparel [168], [169], [170]. However, the fabrication of

antennas using these materials is very critical. A textile antenna should radiate effectively and efficiently under all types of body movements. There are numerous methods for achieving high performance in wearable devices. The overall performance of these devices can be enhanced by employing MIMO antennas. The signals radiated by the antenna system are susceptible to multipath fading and interferences. MIMO technology helps in handling these issues in a significant manner. MIMO systems can provide higher data rates and reliability without demanding more bandwidth or transmitted power [75], [171].

MIMO antennas with circular polarization are more popular in modern wireless communication systems [172]. In multipath and reflective scenarios, circularly polarized MIMO antennas outperform linearly polarized MIMO systems [173]. They provide large spectral efficiency, as they do not encounter polarization mismatch between the transceivers. Furthermore, they are resistant to signal attenuation and are less sensitive to antenna physical orientation. However, according to the available literature, a very few circularly polarized fully-textile MIMO antennas have been designed by the researchers. A dual-polarized MIMO antenna with electromagnetic bandgap (EBG) and meandered serpentine resonator was presented for ultra wide band (UWB) applications in [173]. A two-port MIMO antenna having wide axial ratio bandwidth was proposed in [174]. In [72], a dual-polarized textile antenna was presented for wideband MIMO applications. In [69], the wideband MIMO antenna used a neutralization line as a decoupling structure. In [71], a compact MIMO antenna was proposed for “*ultra-wide-band (UWB)*” wearable applications. A small size wideband MIMO antenna was designed using textile fabrics for wearable applications in [70]. In [64], a foldable electro-textile antenna array was developed for mobile router MIMO applications. In [175], a fully-textile wideband antenna was proposed for ISM/wearable MIMO applications. The MIMO antennas presented in [173], [174] were circularly polarized, but designed for non-wearable applications. All other antennas, except for the one shown in [72], were linearly polarized. However, the antenna in [72] showed a narrow axial ratio bandwidth of 80 MHz.

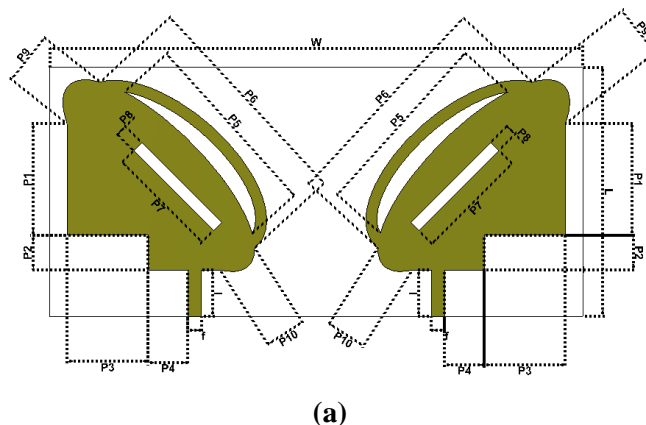
The fully-textile MIMO antenna presented in this paper is suitable for IoT and wearable (ISM, WLAN, and WBAN networks) applications. It covers the frequency spectra of 2.18-3.29 GHz and 3.92-6.90 GHz and exhibits significant port isolation in

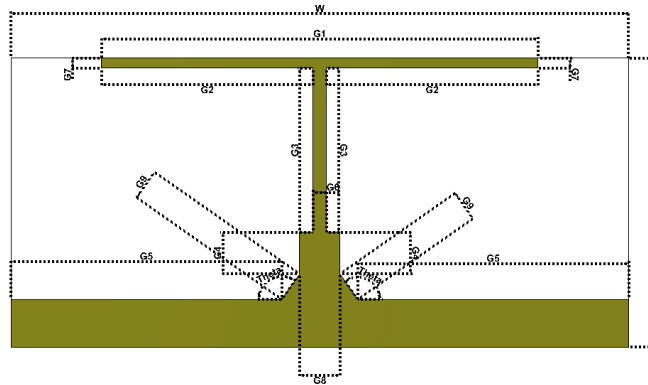
the resonating frequency bands. The antenna's on-body and off-body performance are thoroughly investigated in order to validate the design. The proposed fully-textile MIMO antenna can be easily fabricated and integrated with various RF components, such as transceiving systems or rectenna, because of its lightweight, low-profile and conformal design.

7.2 ANTENNA TOPOLOGY

7.2.1 Antenna Design

The designed and fabricated prototypes of the dual-band fully-textile two-element MIMO wearable antenna are depicted in Figs. 7.2 and 7.3, respectively. The MIMO antenna is made on a non-conducting Felt fabric substrate having dielectric constant (ϵ_r), loss tangent ($\tan \delta$) and thickness of 1.34, 0.02 and 1.0 mm respectively. The characterization of the non-conducting textile fabric was done using an Agilent E4991A RF impedance and material analyzer. The radiating elements (patch and ground plane) are made of Sheildit Superconductive (thickness=0.17 mm), which is a polyester-based Cu/Ni-plated thermally adhesive textile material. The thermally adhesive materials are suitable for fabricating textile antennas as they can easily be appended to the other textile substrate material simply by using a dry-iron [128]. The presented MIMO antenna is fabricated manually using cutting tools. The antenna elements are fed using 50 Ω microstrip feed lines. The antenna is simulated using the “*CST Microwave Studio software*®.” Table 7.1 gives the optimized dimensions of the proposed MIMO wearable antenna. The proposed antenna covers a total volume of $43 \times 92 \times 1 \text{ mm}^3$.





(b)

Fig. 7.2. Proposed fully-textile dual-band MIMO antenna: (a) top view, (b) bottom view.



(a)

(b)

Fig. 7.3. Prototype of the fully-textile MIMO antenna: (a) top view, (b) bottom view.

Table 7.1. Dimensions of the Fully-Textile Two-element MIMO Antenna

Parameter	Value (mm)	Parameter	Value (mm)
L	43.00	P_{10}	7.06
W	92.00	G_1	65.00
l	8.00	G_2	31.5
f	2.30	G_3	24.40
P_1	19.25	G_4	6.21
P_2	6.00	G_5	40.35
P_3	14.00	G_6	2.00
P_4	6.85	G_7	1.50
P_5	32.90	G_8	6.00
P_6	39.10	G_9	4.63
P_7	19.50	G_{10}	7.10
P_8	2.00	θ	125°
P_9	9.20		

7.2.2 Antenna Evolution

The step-wise development of the fully-textile 1×2 element MIMO antenna is depicted in Fig. 7.4. The S-parameters (S_{11} and S_{21}) and the axial ratio (AR) of the designing evolution are illustrated in Figs. 7.5, 7.6, and 7.7, respectively. In step-1, two monopoles, a combination of small- and large-sized rectangular patches, are considered to cover the middle (2.45 GHz) and upper (5.80 GHz) industrial, scientific and medical (ISM) bands. On the backside of the substrate, a partial ground plane (of the size of $92.0 \text{ mm} \times 7.10 \text{ mm}$) is used to achieve a wider resonance bandwidth. The antenna (ANT~1) has a broad impedance matching band ranging from 1.83 to 6.58 GHz but lacks isolation between the radiating elements. For such small antennas, the ground plane also serves as a radiator. The surface current causes coupling between the antenna elements in the ground plane and near-field. The spacing between the radiating antenna elements can be increased to lessen this coupling, but this result in an overall increased sizing of the MIMO antenna. In step-2, the gap between the large-sized rectangular-shaped patches is increased by moving them towards the outer side of the antenna (ANT~2). In addition, the patches of ANT~2 are cut diagonally to obtain circular polarization. This creates more space between the radiating elements, resulting in improved isolation. ANT~2 offers an impedance matching from 4.23 to 6.44 GHz and more than 15 dB isolation from 2.00 to 3.23 GHz. In step-3 (ANT~3), two elliptical-shaped patches are integrated on the monopole radiators to improve polarization at port#1/port#2. The ANT~3 shows good circular polarization (axial ratio ≤ 3 dB) around 4.91 GHz and 6.15 GHz, and an increase in resonating bandwidth (2.22 to 7.46 GHz). In step-4 (ANT~4), a rectangular-shaped slit is created in each radiating element for improving the axial ratio. The ANT~4 offers circular polarization around 2.24 GHz and 4.83 GHz. The impedance matching bandwidth and isolation are nearly identical to the ANT~3. In the next step (ANT~5), an elliptical-shaped ring is etched from the radiating element to control the frequency of circular polarization. Also, To improve inter-element isolation at higher frequencies, a vertical stub is added to the ground plane. The ANT~5 has an impedance matching in 1.69-2.80 GHz and 3.46-6.24 GHz frequency bands, and circular polarization at 2.99 GHz, 3.68 GHz, and 4.77 GHz. It is evident that there is a direct relationship between axial ratio and isolation, with higher isolation contributing to a

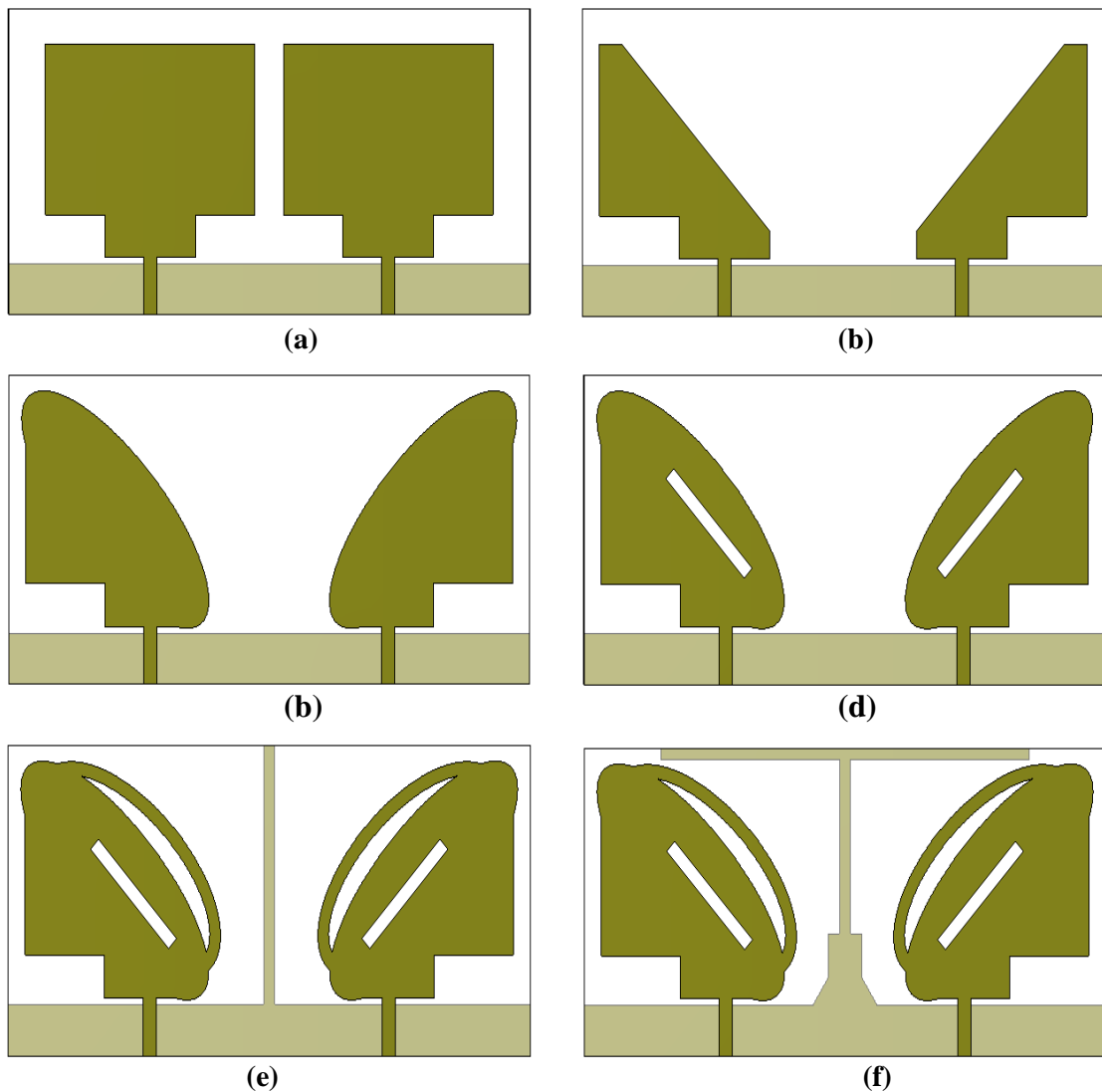


Fig. 7.4. Step-wise development of the fully-textile two-element MIMO antenna: (a) ANT~1, (b) ANT~2, (c) ANT~3, (d) ANT~4, (e) ANT~5, (f) ANT~6.

better axial ratio. If there is no coupling between the ports, the direction of the electric fields is not impacted, resulting in improved circular polarization. In step-6, horizontal and triangular-shaped stubs are introduced in the ground plane (ANT~6) to improve circular polarization at 5.80 GHz. Also, a rectangular-shaped stub is added to the ground plane to enhance the isolation between the radiating elements in the resonating bands. The proposed fully-textile dual-band, dual-sense MIMO antenna (ANT~6) resonates at 2.18-3.29 GHz and 3.92-6.90 GHz, covering ISM and WLAN bands. It offers isolation greater than 15 dB in the frequency bands of 1.94-2.99 GHz and 3.77-7.00 GHz. Circular polarization is achieved in the 4.92-5.94 GHz frequency band

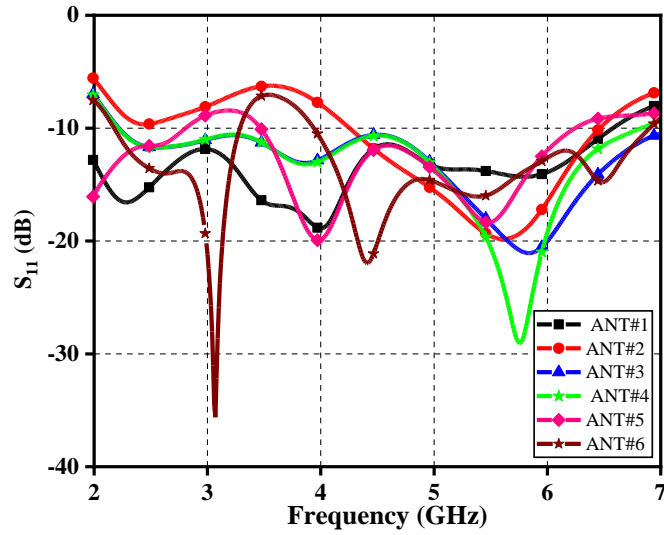


Fig. 7.5. Simulated S_{11} of the design steps.

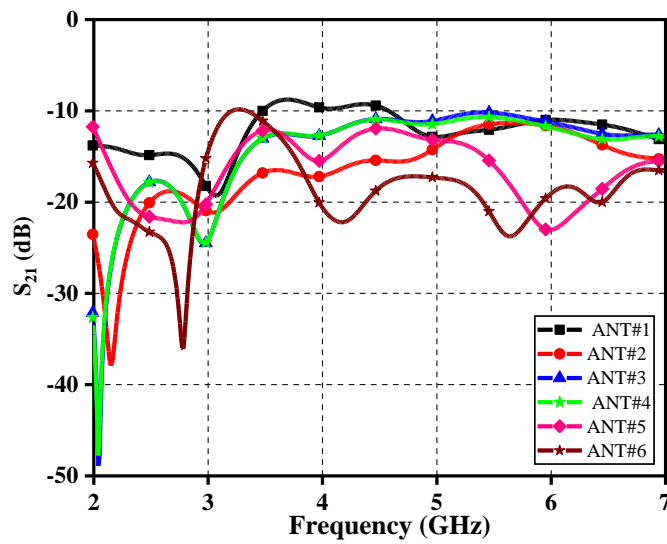


Fig. 7.6. Simulated S_{21} of the design steps.

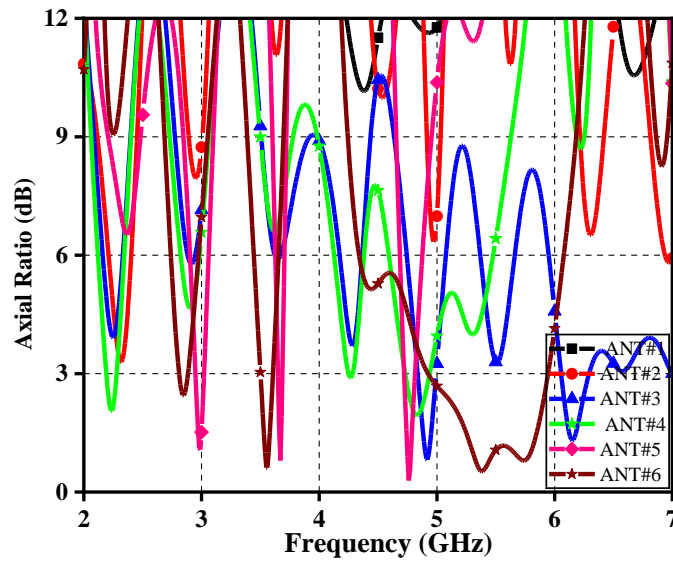


Fig. 7.7. Simulated axial ratio of the design steps.

7.2.3 Polarization Diversity

The ability of an antenna to offer both left-hand and right-hand circular polarizations (LHCP and RHCP) is known as polarization diversity. Antenna design techniques play an important role in achieving circular polarization. One of the best approaches for achieving polarization diversity in a MIMO antenna is to make a mirrored image of the antenna element. So, if the first radiating element exhibits LHCP, the second element shows RHCP, or vice versa.

Fig. 7.8 depicts the surface current distribution of the proposed fully-textile MIMO antenna at different phases ($\omega t = 0$ deg, $\omega t = 90$ deg, $\omega t = 180$ deg, and $\omega t = 270$ deg). In radiating element-1, E_1 and E_2 represent the mutually perpendicular current vectors, and E_3 is their vector sum. At the phase angle $\omega t = 0$ deg, as shown in Fig. 7.8(a), the surface current density increases on the upper left region of the patch (E_1) and the upper edge of the L-shaped strip (E_2), and the vector sum (E_3) of the two vectors is traveling in the upper direction towards right side.

At the phase $\omega t = 90$ deg, as shown in Fig. 7.8(b), the vector sum (E_3) is traveling in the lower direction towards right side of the left patch, which demonstrates that the clockwise rotation of the current vectors with time. At $\omega t = 180$ deg and $\omega t = 270$ deg, the vector sum (E_3) rotates in the same manner (clockwise direction), as shown in Figs. 7.8(c) and (d), respectively. Therefore, the antenna element-1 of the proposed

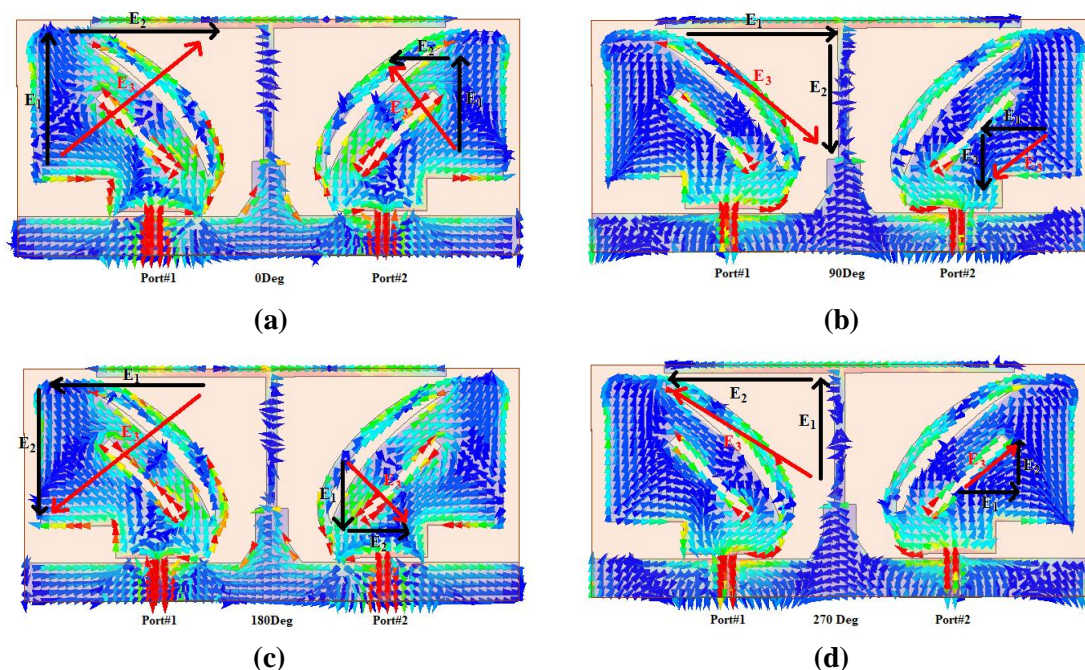


Fig. 7.8. Surface current distribution at 5.8 GHz when port#1 and port#2 are excited.

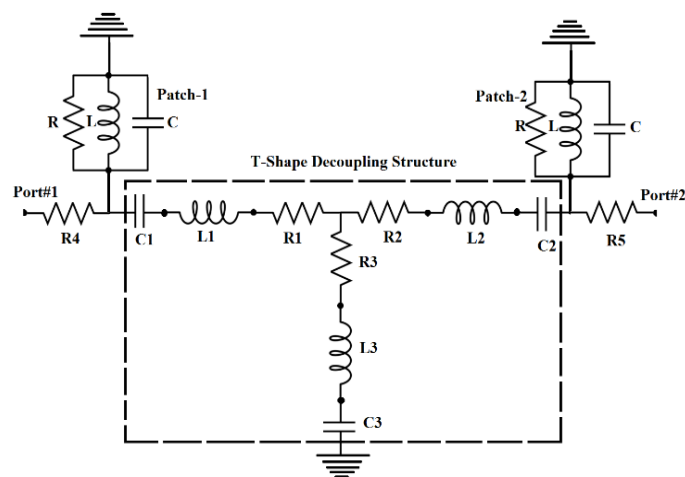
fully-textile MIMO antenna exhibits LHCP operation.

In the antenna element-2, at $\omega t = 0$ deg, the surface current densities E_1 and E_2 are increasing in such a way that the vector sum (E_3) is traveling in the upper direction towards left side, as shown in Fig. 7.8(a). At $\omega t = 90$ deg, the surface current densities E_1 and E_2 are resulting in vector sum (E_3) traveling in the lower direction towards left side of the right patch, as shown in Fig. 7.8(b). Similarly, at $\omega t = 180$ deg and $\omega t = 270$ deg, the vector sum (E_3) rotates in the anti-clockwise direction as shown in Figs. 7.8(c) and (d), respectively. Therefore, the antenna element-2 of the proposed fully-textile MIMO antenna exhibits RHCP operation.

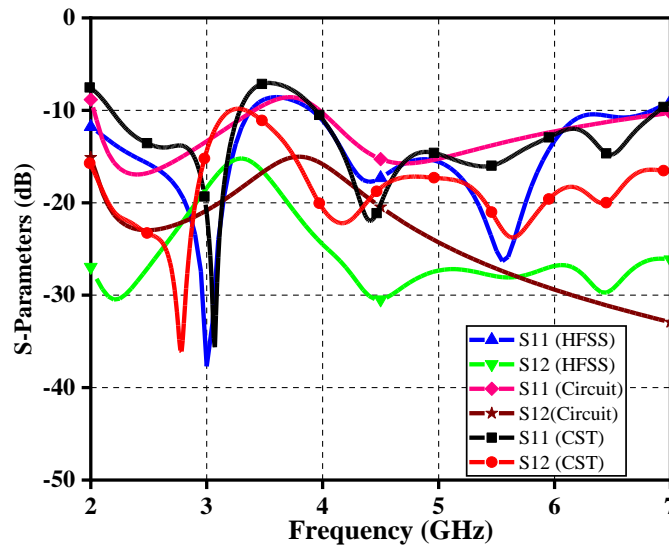
7.2.4 Circuit Model

In order to have a better understanding of the designed MIMO antenna, a circuit equivalent of the proposed antenna is drawn in Fig. 7.9(a). The radiating patches (patch-1 and patch-2) are represented by parallel resonating circuits, and the T-shaped decoupling structure is connected in series with them. One side of the radiating patch is connected to the 50Ω ports (ports#1 and port#2) and the other side with the ground. The upper two ends of the T-shaped decoupling structure connect to the corresponding patches, while the lower end connects to the ground.

The optimized lumped resistance, inductance, and capacitance values of the circuit are as follows: $R=31.05 \Omega$, $L=6.11 \text{ nH}$, $C=0.65 \text{ pF}$, $R_1=8.41 \Omega$, $L_1=4.3 \text{ nH}$, $C_1=0.393 \text{ pF}$, $R_2=1.0 \Omega$, $L_2=5.36 \Omega$, $C_2=0.35 \text{ pF}$, $R_3=1.0 \Omega$, $L_3=13.78 \text{ nH}$, $C_3=0.851 \text{ pF}$, $R_4=7.9 \Omega$, and $R_5=34.5 \Omega$. Fig. 7.9(b) depicts a comparison of S-parameters of EM simulators and circuit models. The behavior of the circuit model and the EM simulator is very similar, validating the equivalent circuit of the proposed antenna.



(a)



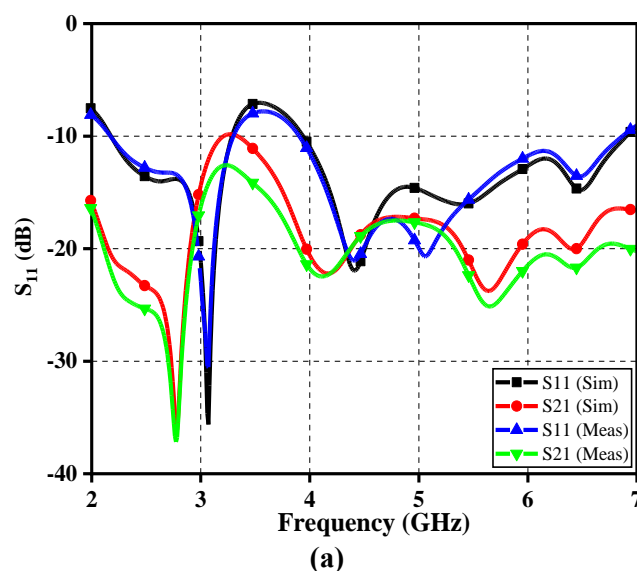
(b)

Fig. 7.9. (a) Equivalent circuit of the MIMO antenna, (b) $|S_{11}|$ and $|S_{12}|$ comparison of the EM and circuit models.

7.3 ANTENNA PERFORMANCES IN FREE SPACE

7.3.1 Return Loss, Isolation, Axial Ratio, and Gain

The proposed fully-textile MIMO antenna prototype was fabricated, and measurements were done with an RF vector network analyzer (VNA). The S-parameters (simulated and experimental S_{11} and S_{22}) of the proposed fully-textile MIMO antenna are depicted in Fig. 7.10(a). The resonating bands, bandwidths, and percentage bandwidths of the proposed antenna are 2.18-3.29 GHz (1.11 GHz, 40.58 %) and 3.92-6.90 GHz (2.98 GHz, 55.08 %). The simulated coupling between (S_{21}) port#1 and port#2 are “-23 dB” and “-22 dB” at “2.45 GHz” and “5.8 GHz”, respectively. The axial ratio (simulated and experimental) and gain responses of the proposed MIMO antenna are depicted in Fig. 7.10(b). The circular polarization is obtained at the 5.80 GHz frequency band. The peak gains of “3.77 dBi” and “6.16 dBi” are achieved at “2.45 GHz” and “5.8 GHz” respectively. The proposed fully-textile MIMO antenna's experimental features match the simulated findings well. A slight deviation between these results occurs because of the fabrication and measurement tolerance.



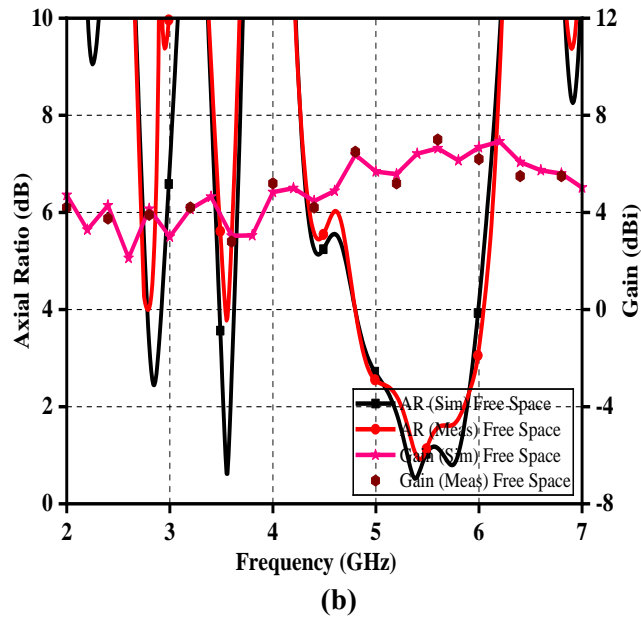


Fig. 7.10. Simulated and experimental results of the proposed antenna: (a) S-parameters (S_{11} and S_{22}), (b) gain and axial ratio.

7.3.2 Diversity Performance

Factors including the envelope correlation coefficient (ECC), diversity gain (DG), multiplexing efficiency (ME), and total active reflection coefficient (TARC) impact the diversity performance of MIMO systems [176].

The ECC can be used to measure the diversity performance of a MIMO antenna. In MIMO antenna systems, ECC measures the correlation between the n th element and the m th element. The S-parameters present reasonable results for antennas with very high radiation efficiency. The radiation efficiency of the printed antenna, however, is not very high due to its lossy nature. The far-field radiation patterns are preferred over s-parameters for calculating ECC as they are not dependent on antenna radiation efficiency [149], [177]. ECC can be evaluated using equation (7.1). The ECC of the designed fully-textile MIMO antenna is less than 0.12, as depicted in Fig. 7.11.

$$ECC_{nm}$$

$$= \frac{\left| \int_0^{2\pi} \int_0^\pi [XPR \cdot E_{\theta n} E_{\theta m}^* P_\theta + E_{\phi n} E_{\phi m}^* P_\phi] d\Omega \right|^2}{\int_0^{2\pi} \int_0^\pi [XPR \cdot E_{\theta n} E_{\theta n}^* P_\theta + E_{\phi n} E_{\phi n}^* P_\phi] d\Omega \times \int_0^{2\pi} \int_0^\pi [XPR \cdot E_{\theta m} E_{\theta m}^* P_\theta + E_{\phi m} E_{\phi m}^* P_\phi] d\Omega} \quad (7.1)$$

Another essential parameter of the MIMO systems is the DG, which can be evaluated using equation (7.2) [178].

$$DG = 10\sqrt{1 - ECC^2} \quad (7.2)$$

Fig. 7.11 shows the DG of the proposed fully-textile MIMO antenna, and it is observed that the antenna offers DG >9.90 dB in free space.

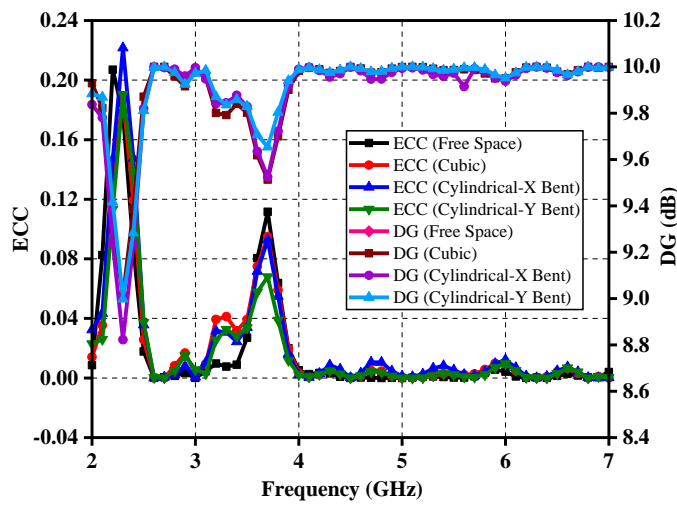


Fig. 7.11. ECC and DG of the proposed antenna.

ME is another important parameter to characterize the spectral efficiency of MIMO antennas. It can be evaluated using equation (7.3) [151].

$$\check{\eta}_{mux} = \sqrt{\eta_1 \eta_2 (1 - |r|^2)} \quad (7.3)$$

The ME of the fully-textile MIMO antenna is shown in Fig. 7.12 for both on-body and off-body conditions. The ME of the proposed fully-textile MIMO antenna varies between ± 2.0 .

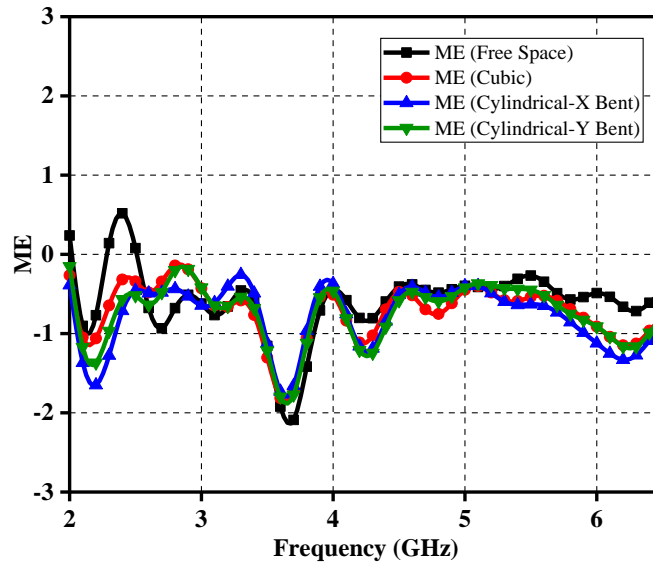


Fig. 7.12. ME of the fully-textile two-element MIMO antenna.

When multiport wireless systems work simultaneously, the antenna performance may be adversely affected. This effect can be calculated using equation (7.4) [179].

$$TARC = \frac{\sqrt{(S_{11}+S_{22})^2+(S_{21}+S_{12})^2}}{\sqrt{2}} \quad (7.4)$$

Fig. 7.13 shows the experimental and simulated curves of TARC. The TARC values are less than 10 dB throughout the resonating bandwidth.

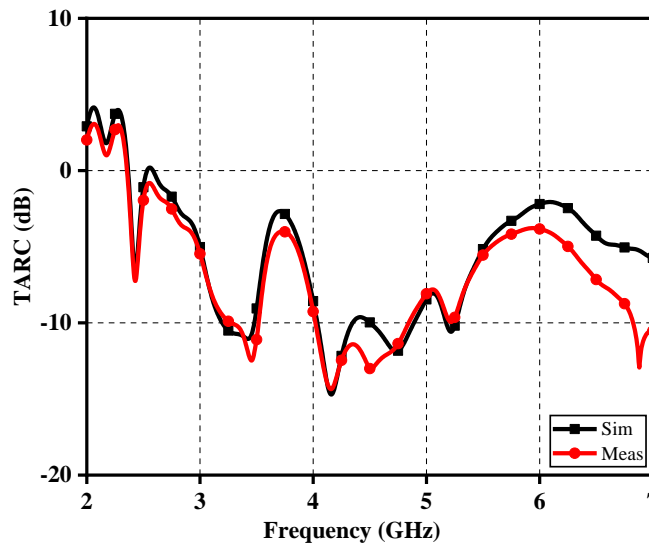


Fig. 7.13. TARC of the fully-textile two-element MIMO antenna.

7.3.3. Surface Current Distribution

The investigation of the surface current distribution was performed to understand the inter-element coupling. Figs. 7.14(a) and (b) compares the distribution of the surface current, with and without decoupling elements, of the fully-textile MIMO antenna at “2.45 GHz” and “5.8 GHz”, respectively. It's worth noting that the amount of surface current flowing from port-1/2 to port-2/1 in the proposed fully-textile MIMO antenna with decoupling structures is quite small. The structures inserted between the radiating elements induce a high isolation between them by decreasing the mutual coupling.

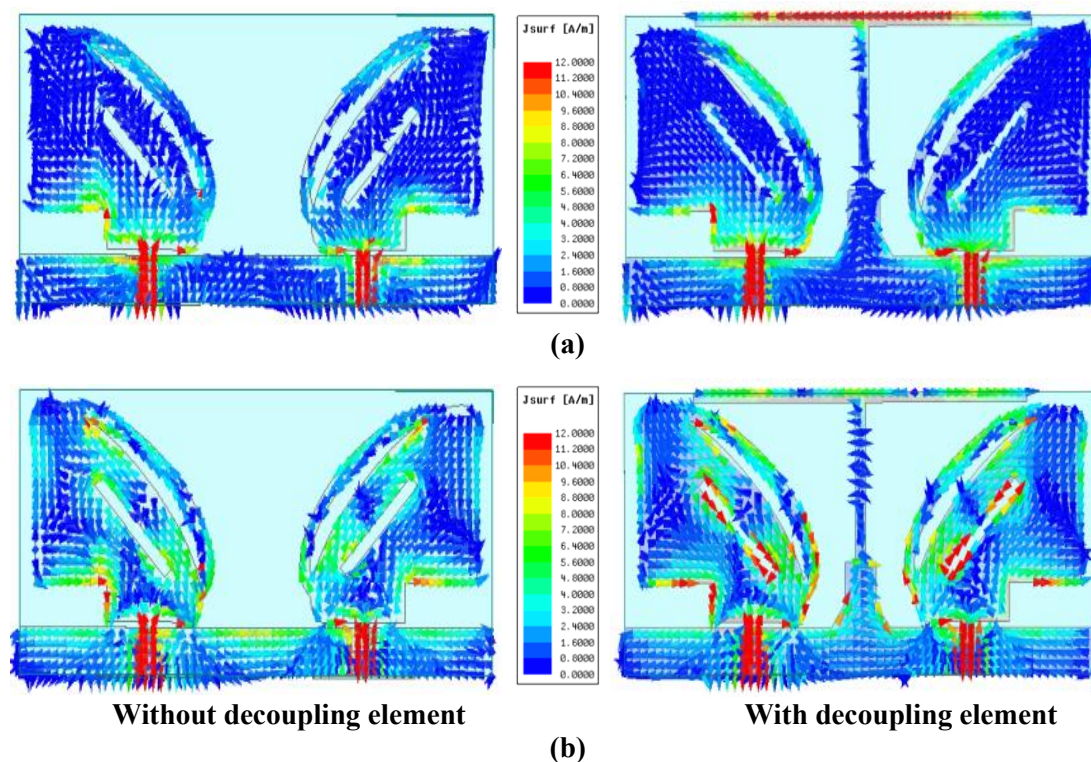


Fig. 7.14. Surface current distribution of the fully-textile MIMO antenna: (a) 2.45 GHz, (b) 5.8 GHz.

7.3.4 Radiation Pattern

Figs. 7.15 and 7.16 illustrate the far-field 3-D radiation patterns of the proposed fully-textile MIMO antenna at “2.45 GHz” and “5.8 GHz”, when either of the ports is excited and when both the ports are excited at the same instant of time. It is clearly seen that the proposed fully-textile MIMO antenna provides improved isolation as well as good polarization and pattern diversity.

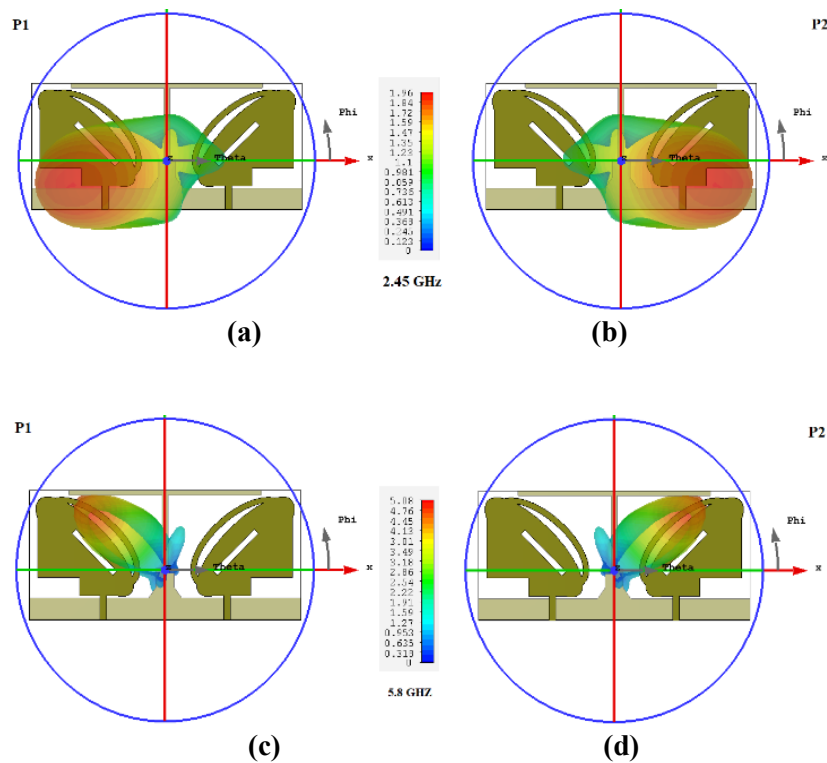


Fig. 7.15. Radiation patterns of the proposed antenna: (a) 2.45 GHz/Port#1, (b) 2.45 GHz/Port#2, (c) 5.8 GHz/Port#1, (d) 5.8 GHz/Port#2.

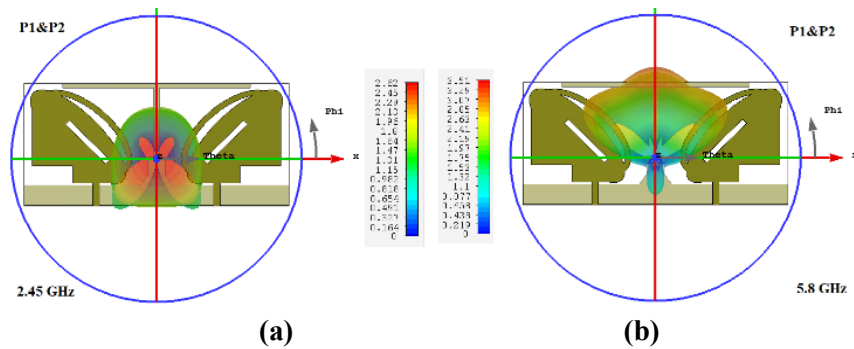


Fig. 7.16. Radiation patterns of the proposed antenna when port#1 and port#2 are excited simultaneously: (a) 2.45 GHz, (b) 5.8 GHz.

7.4 ANTENNA PERFORMANCES ON HUMAN BODY

Moreover, the proposed fully-textile MIMO antenna is characterized for various on-body scenarios. Fig. 7.17 depicts the human tissue models (phantoms) chosen to mimic the human chest/back and arm. A three-layered structure is used to mimic the tissue model for the human chest/back, while a four-layered structure is used to mimic the tissue model for the human arm. The dimensions of the two human phantoms are

furnished in Table 7.2. The size of the phantom for the cubic model is kept as $150 \times 150 \times 70 \text{ mm}^3$. The length of the arm phantom/model is kept as 300 mm [116]. The realistic model parameters for the dielectric properties of various tissue layers were acquired from the CST library of materials. A distance of 10 mm was used between the proposed fully-textile MIMO antenna and the skin to imitate the clothing layers [18]. The performance of cylindrical tissue models is investigated on the x -axis and y -axis. For the cylindrical models (human arm phantom), the fully-textile MIMO antenna was bent along the E/H-plane with a radius of 50 mm.

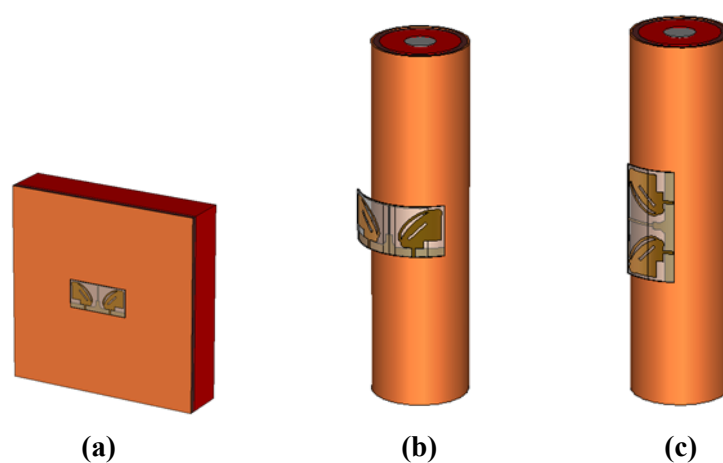


Fig. 7.17. Human tissue models/phantoms: (a) cubic phantom, (b) cylindrical phantom/ x -direction, (c) cylindrical phantom/ y -direction.

Table 7.2. Dimensions of the Tissue Models

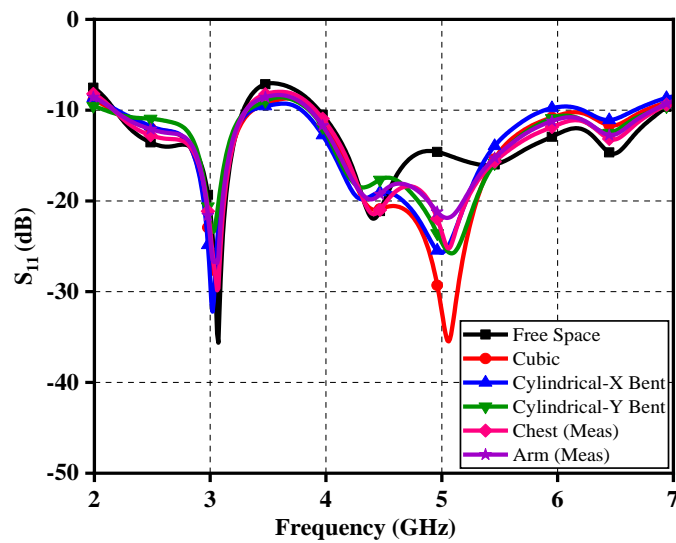
	Bone	Skin	Fat	Muscle
Cubic Model (Chest/Back)	---	3 mm	7 mm	60 mm
Cylindrical Model (Arm)	13 mm	2 mm	5 mm	20 mm

7.4.1 Return Loss (S_{11}), Isolation (S_{21}), Axial Ratio, Gain, and Radiation Efficiency

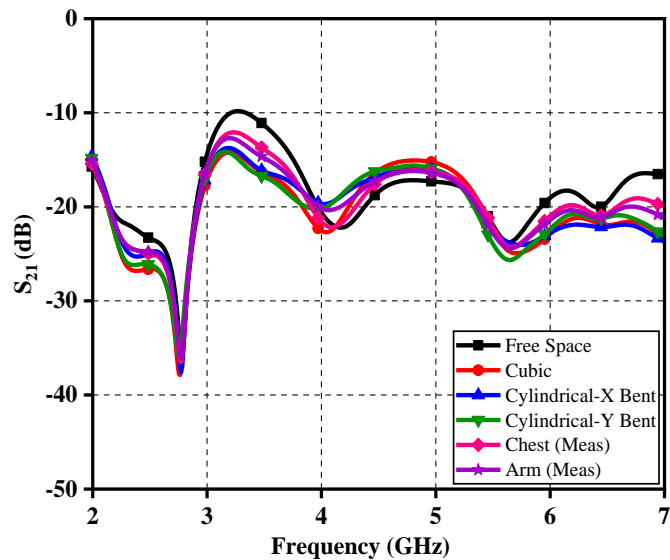
The S-parameters of the MIMO antenna for on-body and off-body conditions (along the x - and y -axis for cylindrical model) are depicted in Figs. 7.18(a) and (b), respectively. When the antenna is in close proximity to the cubic phantom, there is a significant change.

The simulated axial ratio for various tissue models is shown in Fig. 7.19. At the

5.80 GHz frequency, the circular polarization is maintained in all cases. The gain and radiation efficiency of the proposed fully-textile MIMO antenna are examined for various tissue models, as depicted in Figs. 7.20 (a) and (b), respectively. The gain of the MIMO antenna is varying from 2 to 7 dBi in the operating band for different tissue models. It is evident that the simulated radiation efficiency is more than 90 % for all the cases.



(a)



(b)

Fig. 7.18. Simulated S-parameters of the proposed antenna for different phantoms: (a) S_{11} , (b) S_{21} .

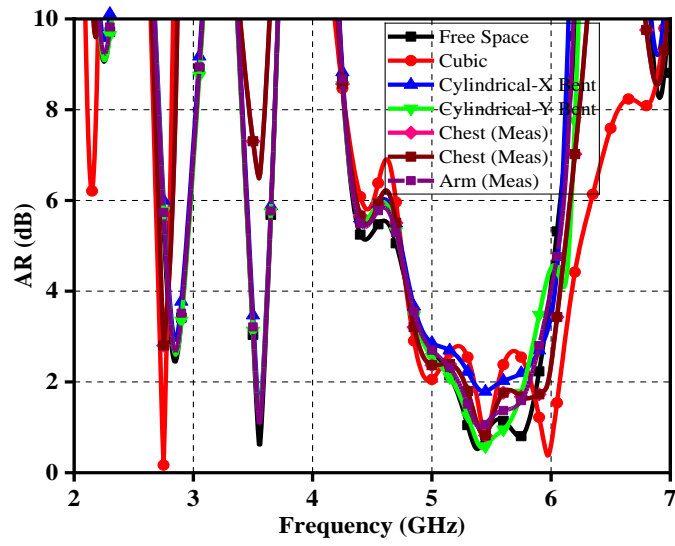
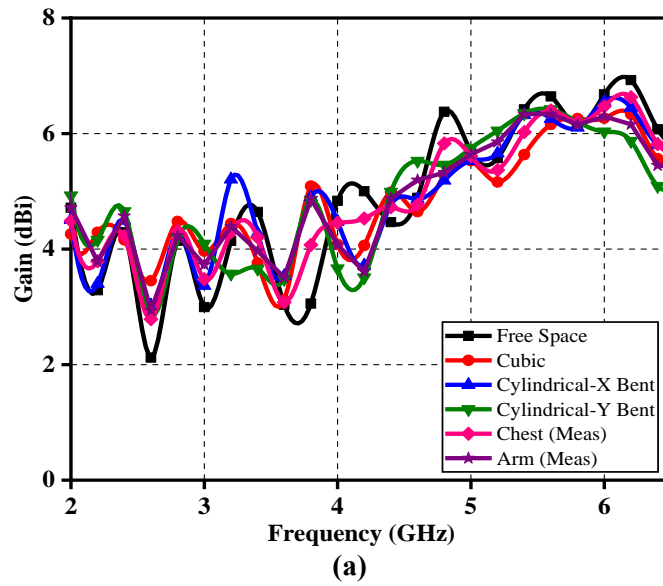
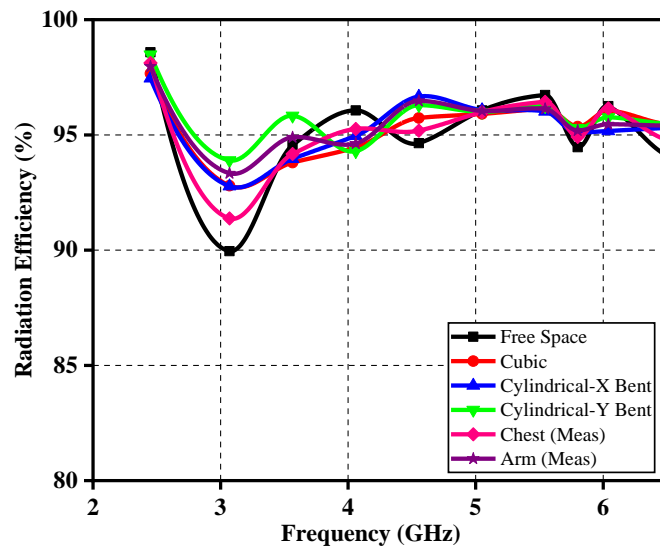


Fig. 7.19. Axial ratio (simulated) of the proposed antenna for various phantoms.





(b)

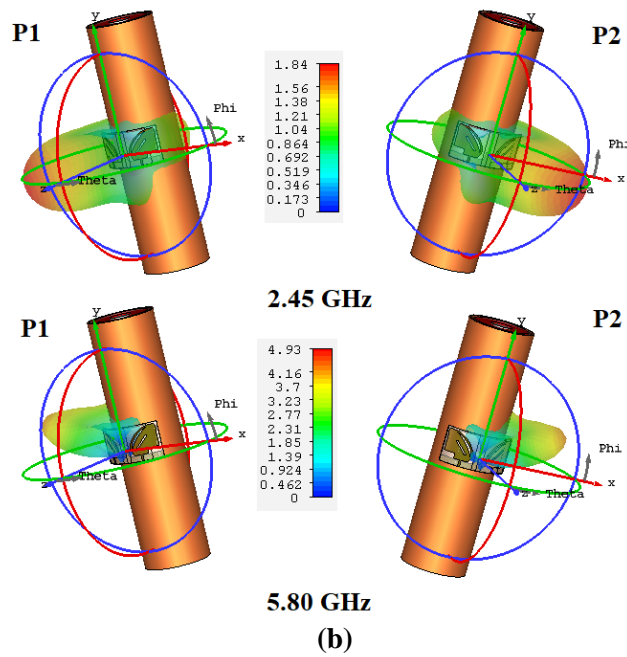
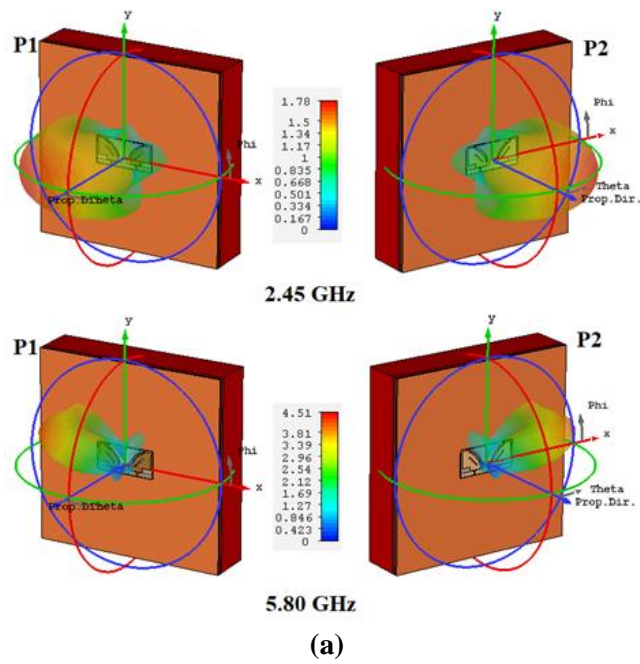
Fig. 7.20. Simulated results of the proposed antenna for different phantoms: (a) gain, (b) radiation efficiency.

7.4.2 Diversity Performance

For various human phantoms, the diversity performance of the suggested MIMO antenna is examined. The “*ECC (envelope correlation coefficient)*” and “*DG (diversity gain)*” of the proposed antenna for “*on-body*” and “*off-body*” conditions are shown in Fig. 7.11. The ME of the fully-textile MIMO antenna is also examined for both conditions and found to be between ± 2 for the entire resonating band, as illustrated in Fig. 7.12. The diversity performance of the MIMO antenna is found to be within the optimum desired range when loaded with different human phantoms.

7.4.3 Radiation Pattern

The 3-D radiation patterns for on-body conditions are examined at 2.45 GHz and 5.80 GHz, as depicted in Fig 7.21. The pattern diversity is maintained in all cases (cubic model, bent *x*-model, and bent *y*-model), as a result, there is good isolation between the radiating antenna elements.



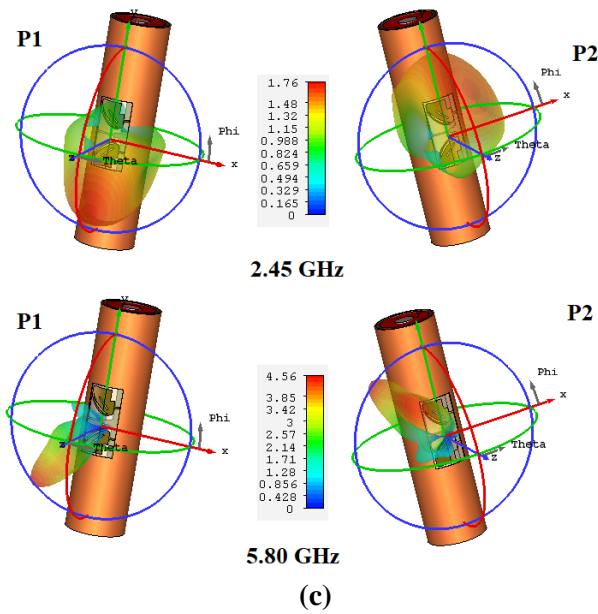
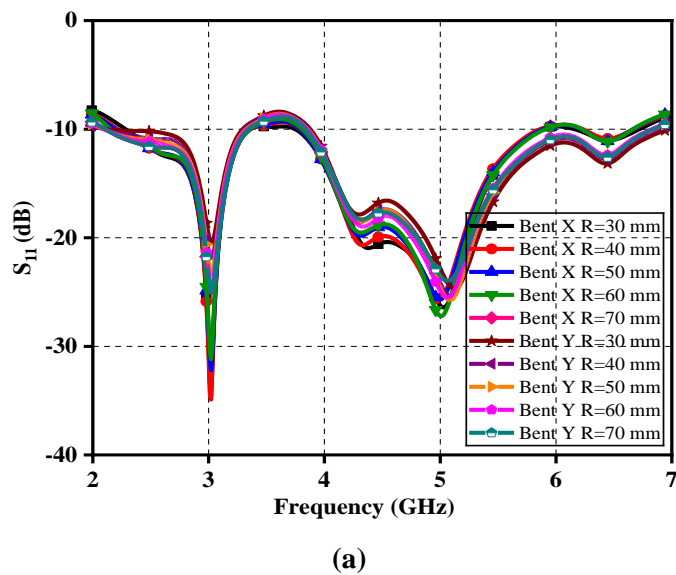


Fig. 7.21. 3-D radiation patterns of the proposed antenna: (a) cubic model, (b) bent x-model, (c) bent y-model.

7.4.4 Bending Analysis

The bending analysis of the MIMO antenna was performed at differing radii under the influence of cylindrical phantoms. The S-parameters (S_{11} , S_{21}) and the axial ratio of the proposed antenna for different bending radii are depicted in Figs. 7.22(a), (b), and (c), respectively. A distance of 10 mm was kept between the proposed antenna and the phantoms for all cases. A little change is observed in the characteristics of the antenna. But, the proposed MIMO antenna is found to be working well within the required resonating bands at all instances.



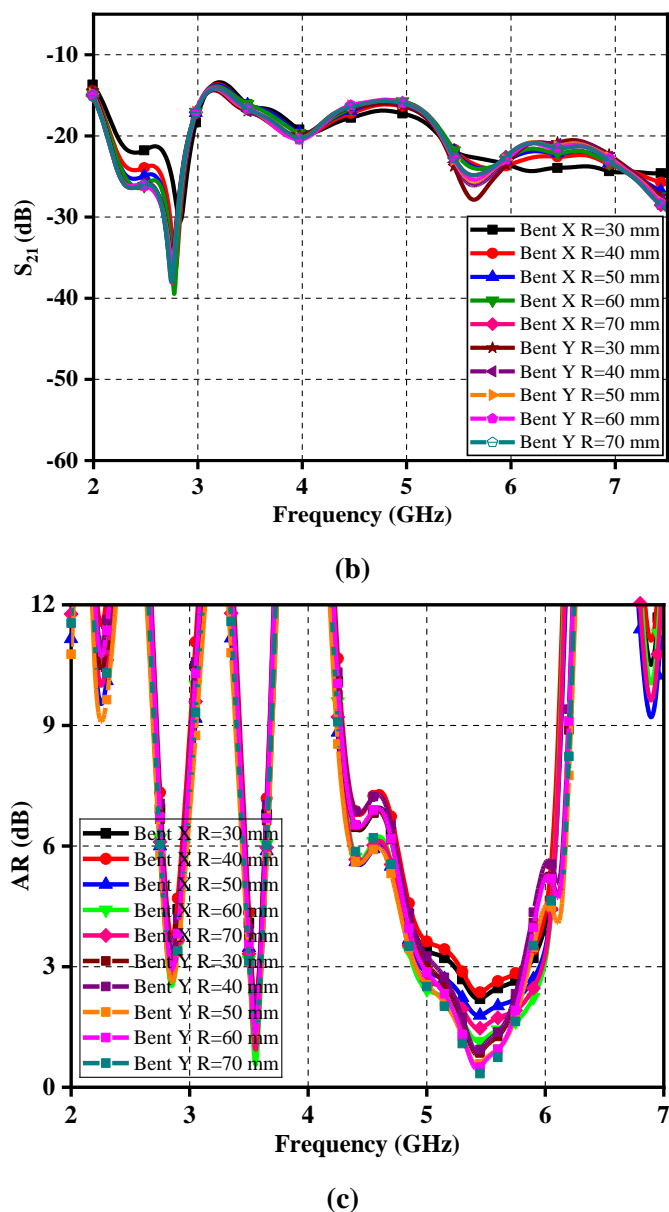


Fig. 7.22. Bending analysis of the proposed fully-textile MIMO antenna for various phantoms: (a) S_{11} , (b) S_{21} , (c) axial ratio.

7.4.5 Specific Absorption Ratio (SAR)

The SAR analysis of the proposed MIMO antenna is done using the CST Microwave Studio® for human phantom (cubic phantom) in accordance with the safety guidelines given by Federal Communications Commission (FCC). Fig. 7.23 depicts the maximum simulated power levels falling within an acceptable SAR range for both “United States (US)” and “International Commission on Non-Ionizing Radiation Protection (ICNIRP) standards.”

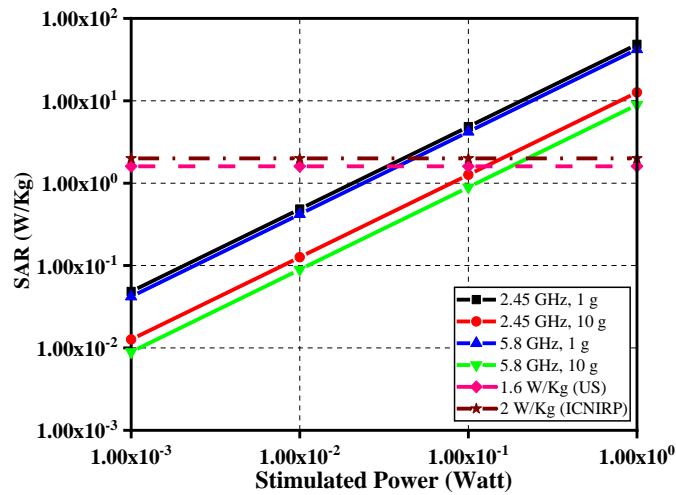


Fig. 7.23. Simulated results for maximum SAR.

The performance comparison of the proposed work with the recent state-of-art textile and non-textile wearable MIMO antennas is given in Table 7.3. Linearly polarized antennas make up the majority of the antennas described in the literature, except the one presented in [72], however, it showed a narrow axial ratio bandwidth. The proposed antenna, however, is designed with a significantly higher axial ratio bandwidth. The proposed dual-band dual-sense fully-textile MIMO antenna can be easily designed and integrated with RF circuitry (such as transceiving components or rectennas) due to its simple geometry, light-weight, low-profile and conformal nature.

Table 7.3. Comparison of the Proposed Work with other Reported MIMO Antenna

Ref.	Area (mm×mm)	Substrate (ϵ_r)	Impedance Band (GHz)	Impedance Bandwidth (GHz)	Axial Ratio Band (GHz)	Polarization	Application
[173]	29.0×58.0	FR4 (4.4)	3.10-10.60	7.50	6.00-10.60	Linear, Elliptical	Non-Wearable
[174]	94.0×94.0	FR4 (4.4)	1.10-1.70	0.60	1.07-1.73	Circular	Non-Wearable
[72]	110.0×97.0	Jeans (1.77)	1.50-3.80, 4.20-6.20	2.30, 2.00	2.20-2.48, ---	Circular, Linear	Wearable
[69]	30.0×50.0	Jeans (1.6)	3.14-9.73	6.59	---	Linear	Wearable
[71]	35.0×55.0	Jeans (1.6)	2.74-12.33	9.59	---	Linear	Wearable
[70]	40.0×70.0	Jeans (1.6)	2.40-8.00	5.60	---	Linear	Wearable
[64]	168.0×96.0	Felt (1.14)	1.40-5.00	3.60	---	Linear	Wearable
Prop.	43.0×92.0	Felt (1.34)	2.18-3.29, 3.92-6.90	1.11, 2.98	---, 4.92-5.94	Linear, circular	Wearable

7.5 CONCLUSION

The work was focused on the development of a textile-based, dual-band, dual-sense MIMO antenna for IoT and wearable applications. The presented MIMO antenna is completely textile, and its performances were studied for both on-body and off-body conditions. A rectangular-shaped stub, two triangular-shaped stubs, and a T-shaped stub (loaded on the backside of the substrate) were used decoupling structure. The simulated and experimental results are validated. The SAR analysis of the proposed fully-textile MIMO antenna was also studied for cubic and cylindrical phantoms (mimicking human chest/back and arm), and it was found to be working within the acceptable limits of SAR (1.6 W/Kg , as specified by FCC).

“It is the fundamental duty of all citizens of India to develop the scientific temper, humanism and the spirit of inquiry and reform.”

Constitution of India, Article 51A (h)

8

CONCLUSION AND FUTURE SCOPE

The key focus of this thesis is the investigation, designing, analysis and development of wearable non-textile and textile patch antennas for Body Area Network (BAN). This chapter concludes the so far reported works in the dissertation. A brief description of the need, adopted methodology and summary of the proposed work are also given. It also discusses the limitations and future scope of this work.

8.1 CONCLUSION

This thesis presents the work on the design and development of wearable antennas for “*body area networks (BAN)*.” The designing, simulation, analysis, fabrication and testing of five wearable antennas have been done in this work. In the initial phase, the antennas are designed and simulated for the study of various important antenna parameters such as s-parameters, bandwidth, gain, surface current distribution, radiation pattern, etc. After that, the parametric analysis is performed for optimization of the designed antenna to achieve the best possible desired result. Subsequently, the bending and specific absorption ratio (SAR) analysis were performed to check the suitability of designed antennas for wearable applications. In the final phase, the designed antennas are fabricated and tested to validate the simulated results.

In chapter 3, a dual-band patch antenna is proposed for 902-928 MHz and 2400-2500 MHz ISM bands. This antenna is designed for non-textile, flexible materials for wearable applications. It uses a microstrip line feed monopole antenna for the excitation of the antenna. The concept of slotting is utilized for achieving the dual resonance. The antenna was deliberately designed for covering lower and middle ISM bands to reduce the possibility of health hazards that arises due to EM wave exposure.

Although, the ISM bands are not allowed to be used for any RF purposes excluding telecommunication but they tend to face interference from the sources like Microwave ovens and RF Heating. To avoid this, the authors have proposed a wideband, non-textile, and flexible antenna for wireless telemetry services (WMTS) bands in chapter 4. The Federal Communications Commission (FCC) has established the WMTS exclusively for wireless medical telemetry. It provides interference-free medical telemetry from other radio frequency (RF) sources. The proposed antenna covers two WMTS bands namely 1395-1400 MHz and 1427-1432 MHz bands. It is a coplanar waveguide (CPW) fed antenna, which uses the concept of a meander-lined structure for achieving the wide bandwidth by covering the lower frequency. The proposed antenna overcomes the disadvantages posed by narrowband wearable antennas.

The antennas proposed in chapter 3 and chapter 4 are designed on non-textile and flexible substrates. For wearable applications, these antennas must be placed on the human body, which causes discomfort to the wearer. This can be overcome by using fully-textile antennas that can be integrated into clothes without creating any discomfort to the user. Hence, in chapter 5, a fully textile, ultra-miniaturized antenna is proposed for 2.45/5.8 GHz ISM bands. Many textile materials were considered for characterization to explore the design possibilities. The proposed antenna uses a simple C-shaped monopole structure excited by a microstrip feed line along with a partial ground plane. It is a low-cost antenna that can be easily integrated into clothes for wearable applications.

All the aforementioned antennas use single monopole structures and fall under the category of “*single-input-single-output (SISO)*” systems. The “*multiple-input-multiple-output (MIMO)*” systems have various advantages over SISO systems. The MIMO systems use many antennas for transmission and reception simultaneously. They are used to achieve high data rate, reduced bit-error-rate, low fading effect and high spectral efficiency. Besides, there were very few fully-textile MIMO antennas in the available literature for wearable applications. Thus, a fully-textile, two-element wide-band MIMO antenna is presented in chapter 6. The antenna uses two monopole structures excited by microstrip feed lines. It uses a T-shaped stub and three rectangular

rings for achieving the isolation between the radiating elements. The antenna has a high fractional bandwidth and can be ISM and WLAN bands for wearable applications.

The circularly polarized antennas are preferred over the linearly polarized antennas due to their ability to reject multipath interference. Their structures are generally complex and can be used in an enclosed environment. On the other hand, the linearly polarized antennas have a simple structure and can be used for long-distance communication. The dual-band antennas having dual-polarization can be used to cover both aspects. Thus, a dual-band, dual-sense, fully-textile MIMO antenna is proposed in chapter 7. This antenna covers 2.18-3.29 GHz and 3.92-6.90 GHz frequency bands with circular polarization in the frequency range of 4.92-5.94 GHz. The antenna uses a rectangular-shaped stub, a T-shaped stub and two triangular-shaped stubs for ensuring the isolation of greater than 15 dB between the radiating elements. The antenna can be used in wearable electronics due to its easy integration into clothes and could be a good candidate for a wireless body area network (WBAN).

The bending and SAR analysis performed for various human tissue models (phantoms) of all the proposed antennas show that they can be used for wearable applications in the body area network. The main characteristics of all the five proposed antennas are shown in Table 8.1.

Table 8.1. Summary of Proposed Antennas

Antenna Design	Antenna Size (mm ³)	Antenna Type	Dielectric Material (ϵ_r)	Conductive Material	($S_{11} \leq -10$) Band (GHz)	BW (MHz)	Application Band
ANT 1	50×70×0.8	Monopole	FR-4 (4.4)	Copper	0.902–0.928, 2.400–2.500	23, 80	ISM
ANT 2	52×48×0.8	Monopole	FR-4 (4.4)	Copper	1.395-1.400, 1.427-1.432	620	WMTS
ANT 3	20×30×1	Monopole	Felt (1.34)	ShieldIt Super	2.27–2.62, 4.67–6.33	350, 1660	ISM
ANT 4	37×76×1	Two Element MIMO	Felt (1.34)	ShieldIt Super	2.00–6.23	4230	ISM
ANT 5	43×92×1	Two Element MIMO	Felt (1.34)	ShieldIt Super	2.18-3.29, 3.92-6.90	1110, 2980	ISM, WLAN

8.2 IMPACT OF PROPOSED WORK

In this thesis, the proposed antennas have reasonable off-body and on-body performance characteristics for wearable applications. Out of five proposed antennas, the two antennas can be placed on the human body while three antennas can be easily integrated into clothes without creating any discomfort to the wearer. In addition, all the proposed antenna designs involve the basic concepts of microstrip patch antennas (MPAs) having simple constructions and easy fabrication techniques. Hence, the proposed designs are promising candidates for different wireless communication bands in the body area network (BAN).

8.3 LIMITATIONS OF PROPOSED WORK

Every research faces some limitations and the goal of the researchers is to overcome those limitations. The work presented in the thesis comprising of five designs also faced some limitations as follows:

- Fabrication of the antenna designs, especially fully-textile antennas, was done using manual methods, which resulted in a slight mismatching between the simulated and measured results.
- Realization of the accurate size of antenna designs was also difficult using manual cutting tools. The accurate designs can be realized by making use of laser cutting tools.

8.4 FUTURE SCOPE

This thesis investigates the wearable antennas for the “*wireless body area networks (WBANs)*.” It proposes the five antenna designs for wearable applications. There is a wide scope for further research in this field, which can be pursued in the future. Some of the important suggestions that can be taken up for further study are as follows:

- The robustness of the fully-textile antennas can be tested by doing measurements before and after washing and dry ironing.
- The concept of multilayer dielectric substrate of same and/or different textile materials can be explored further for enhancing the performance of the antenna.

- The wideband, circularly polarized, fully-textile MIMO antenna can also be designed and developed.
- The antennas for ultra wide band (UWB) can also be designed and developed using textile materials.
- More than two-element fully-textile MIMO antennas can also be developed.
- The concept of metamaterials can be used in fully-textile antennas for enhancing the performance of the antenna and reducing SAR levels.
- The energy harvesting techniques can also be used in fully-textile antennas for generating power from radio frequency (RF) energy available in free space.

REFERENCES

- [1] C. A. Balanis, *Antenna Theory Analysis and Design*. John Wiley & Sons, INC., 2016.
- [2] T. Mai, “What is an antenna? | NASA,” 2017. https://www.nasa.gov/directorates/heo/scan/communications/outreach/funfacts/txt_antenna.html.
- [3] “Antenna (radio) - Wikipedia.” [https://en.wikipedia.org/wiki/Antenna_\(radio\)](https://en.wikipedia.org/wiki/Antenna_(radio)).
- [4] D. M. Pozar, “Microstrip Antennas,” in *Proceedings of the IEEE*, 1992, vol. 80, no. 1, pp. 79–91, doi: 10.1109/5.119568.
- [5] E. Lier and K. R. Jakobsen, “Rectangular Microstrip Patch Antennas with Infinite and Finite Ground Plane Dimensions,” *IEEE Trans. Antennas Propag.*, vol. 31, no. 6, pp. 978–984, 1983, doi: 10.1109/TAP.1983.1143164.
- [6] J. Huang, “The Finite Ground Plane Effect on the Microstrip Antenna Radiation Patterns,” *IEEE Trans. Antennas Propag.*, vol. 31, no. 4, pp. 649–653, 1983, doi: 10.1109/TAP.1983.1143108.
- [7] J. T. Aberle and F. Zavosh, “Analysis of probe-fed circular microstrip patches backed by circular cavities,” *Electromagnetics*, vol. 14, no. 2, pp. 239–258, 1994, doi: 10.1080/02726349408908382.
- [8] H. F. Pues and A. R. Van De Capelle, “An Impedance-Matching Technique for Increasing the Bandwidth of Microstrip Antennas,” *IEEE Trans. Antennas Propag.*, vol. 37, no. 11, pp. 1345–1354, 1989, doi: 10.1109/8.43553.
- [9] R. E. Munson, “Conformal Microstrip Antennas and Microstrip Phased Arrays,” *IEEE Trans. Antennas Propag.*, vol. 22, no. 1, pp. 74–78, 1974, doi: 10.1109/TAP.1974.1140723.
- [10] D. M. Pozar and D. H. Schaubert, *Microstrip Antennas-The Analysis and Design of Microstrip Antennas and Arrays*. Wiley-IEEE Press, 1995.
- [11] Y. T. Lo and S. W. Lee, *Antenna Handbook-Theory, Applications and Design*. Springer US, 1988.
- [12] S. Bisht, S. Saini, V. Prakash, and B. Nautiyal, “Study The Various Feeding Techniques of Microstrip Antenna Using Design and Simulation Using CST Microwave Studio,” *Int. J. Emerg. Technol. Adv. Eng.*, vol. 4, no. 9, pp. 318–324, 2014.

- [13] K. R. Carver and J. W. Mink, "Microstrip Antenna Technology," *IEEE Trans. Antennas Propag.*, vol. 29, no. 1, pp. 2–22, 1981, doi: 10.1109/TAP.1981.1142523.
- [14] M. Rizwan, Y. Rahmat-Samii, and L. Ukkonen, "Circularly polarized textile antenna for 2.45 GHz," *2015 IEEE MTT-S Int. Microw. Work. Ser. RF Wirel. Technol. Biomed. Healthc. Appl. IMWS-BIO 2015 - Proc.*, pp. 21–22, 2015, doi: 10.1109/IMWS-BIO.2015.7303755.
- [15] R. P. Dwivedi and U. K. Kommuri, "Compact high gain UWB antenna using fractal geometry and UWB-AMC," *Microw. Opt. Technol. Lett.*, vol. 61, no. 3, pp. 787–793, 2019, doi: 10.1002/mop.31602.
- [16] N. Nasimuddin, X. Qing, and Z. N. Chen, "A wideband circularly polarized stacked slotted microstrip patch antenna," *IEEE Antennas Propag. Mag.*, vol. 55, no. 6, pp. 84–99, 2013, doi: 10.1109/MAP.2013.6781708.
- [17] M. Joler and M. Boljkovac, "A Sleeve-Badge Circularly Polarized Textile Antenna," *IEEE Trans. Antennas Propag.*, vol. 66, no. 3, pp. 1576–1579, 2018, doi: 10.1109/TAP.2018.2794420.
- [18] R. B. V. B. Simorangkir, Y. Yang, L. Matekovits, and K. P. Esselle, "Dual-Band Dual-Mode Textile Antenna on PDMS Substrate for Body-Centric Communications," *IEEE Antennas Wirel. Propag. Lett.*, vol. 16, pp. 677–680, 2017, doi: 10.1109/LAWP.2016.2598729.
- [19] D. M. Pozar and B. Kaufman, "Increasing the bandwidth of a microstrip antenna by proximity coupling," *Electron. Lett.*, vol. 23, no. 8, pp. 368–369, 1987, doi: 10.1049/el:19870270.
- [20] S. J. Chen, D. C. Ranasinghe, and C. Fumeaux, "A Robust Snap-On Button Solution for Reconfigurable Wearable Textile Antennas," *IEEE Trans. Antennas Propag.*, vol. 66, no. 9, pp. 4541–4551, 2018, doi: 10.1109/TAP.2018.2851288.
- [21] D. M. Pozar and S. M. Duffy, "A dual-band circularly polarized aperture-coupled stacked microstrip antenna for global positioning satellite," *IEEE Trans. Antennas Propag.*, vol. 45, no. 11, pp. 1618–1625, 1997, doi: 10.1109/8.650073.
- [22] W. C. Liu and P. C. Kao, "CPW-fed triangular monopole antenna for ultra-wideband operation," *Microw. Opt. Technol. Lett.*, vol. 47, no. 6, pp. 580–582, 2005, doi: 10.1002/mop.21235.

-
- [23] S. A. Kumar and T. Shanmuganatham, "Implantable CPW fed dual folded dipole antenna for biomedical applications," in *2012 3rd International Conference on Computing, Communication and Networking Technologies, ICCCNT 2012*, 2012, no. July, pp. 1–5, doi: 10.1109/ICCCNT.2012.6395948.
- [24] S. A. Patil and P. C. Dhanawade, "Microstrip Antenna and their Applications," 2017. <https://www.electronicsforu.com/technology-trends/microstrip-antenna-applications>.
- [25] I. Singh and V. S. Tripathi, "Micro strip Patch Antenna and its Applications : a Survey," *Int. J. Comput. Appl. Technol.*, vol. 2, no. 5, pp. 1595–1599, 2011.
- [26] "US5345599A - Increasing capacity in wireless broadcast systems using distributed transmission/directional reception (DTDR) - Google Patents." <https://patents.google.com/patent/US5345599A/en> (accessed Nov. 27, 2021).
- [27] S. Monisha and U. Surendar, "Survey on Wearable Antenna Design For ISM Band Applications," *IOSR J. Electron. Commun. Eng.*, vol. 4, pp. 49–54, 2017.
- [28] A. Chandravanshi, A. Rai, and G. Chaitanya, "Wearable antenna: A critical review," in *2016 11th International Conference on Industrial and Information Systems (ICIIS)*, 2016, pp. 486–491, doi: 10.1109/ICIINFS.2016.8262989.
- [29] M. Sharma and C. G. Parini, "A miniature wideband antenna for wearable systems," in *2013 Loughborough Antennas & Propagation Conference (LAPC)*, 2013, pp. 619–623, doi: 10.1109/LAPC.2013.6711975.
- [30] Y. J. Chi and F. C. Chen, "On-Body Adhesive-Bandage-Like Antenna for Wireless Medical Telemetry Service," *IEEE Trans. Antennas Propag.*, vol. 62, no. 5, pp. 2472–2480, May 2014, doi: 10.1109/TAP.2014.2308918.
- [31] J. Zhang, S. Yan, and G. A. E. Vandenbosch, "A Miniature Feeding Network for Aperture-Coupled Wearable Antennas," *IEEE Trans. Antennas Propag.*, vol. 65, no. 5, pp. 2650–2654, May 2017, doi: 10.1109/TAP.2017.2677262.
- [32] M. Kadry, M. E. Atrash, and M. A. Abdalla, "Design of an Ultra-thin Compact Flexible Dual-Band Antenna for Wearable Applications," in *2018 IEEE Antennas and Propagation Society International Symposium and USNC/URSI National Radio Science Meeting, APSURSI 2018 - Proceedings*, 2018, vol. 1, pp. 1949–1950, doi: 10.1109/APUSNCURSINRSM.2018.8609247.
- [33] Z. Hamouda, J. L. Wojkiewicz, A. A. Pud, L. Kone, S. Bergheul, and T. Lasri,

- “Magnetodielectric Nanocomposite Polymer-Based Dual-Band Flexible Antenna for Wearable Applications,” *IEEE Trans. Antennas Propag.*, vol. 66, no. 7, pp. 3271–3277, 2018, doi: 10.1109/TAP.2018.2826573.
- [34] M. A. Ullah, M. T. Islam, T. Alam, and F. Bin Ashraf, “Paper-based flexible antenna for wearable telemedicine applications at 2.4 GHz ISM band,” *Sensors (Switzerland)*, vol. 18, no. 12, p. 4214, 2018, doi: 10.3390/s18124214.
- [35] M. Haerinia and S. Noghianian, “A printed wearable dual-band antenna for wireless power transfer,” *Sensors (Switzerland)*, vol. 19, no. 7, p. 1732, 2019, doi: 10.3390/s19071732.
- [36] A. Nazeri, A. Abdolali, and M. Mehdi, “An Extremely Safe Low-SAR Antenna with Study of Its Electromagnetic Biological Effects on Human Head,” *Wirel. Pers. Commun.*, vol. 109, no. 2, pp. 1449–1462, 2019, doi: 10.1007/s11277-019-06621-6.
- [37] A. Smida, A. Iqbal, A. J. Alazemi, M. I. Waly, R. Ghayoula, and S. Kim, “Wideband Wearable antenna for Biomedical Telemetry applications,” *IEEE Access*, vol. 8, pp. 15687–15694, 2020, doi: 10.1109/ACCESS.2020.2967413.
- [38] P. Salonen and L. Sydanheimo, “DEVELOPMENT OF AN S-BAND FLEXIBLE ANTENNA FOR SMART CLOTHING,” in *IEEE Antennas and Propagation Society International Symposium (IEEE Cat. No.02CH37313)*, 2002, 2002, pp. 6–9, doi: 10.1109/APS.2002.1018143.
- [39] P. Salonen and H. Hurme, “A novel fabric WLAN antenna for wearable applications,” in *IEEE Antennas and Propagation Society, AP-S International Symposium (Digest)*, 2003, vol. 2, pp. 700–703, doi: 10.1109/aps.2003.1219332.
- [40] P. Salonen, Y. Rahmat-Samii, M. Schaffrath, and M. Kivikoski, “Effect of textile materials on wearable antenna performance: A case study of GPS antennas,” in *IEEE Antennas and Propagation Society, AP-S International Symposium (Digest)*, 2004, vol. 1, pp. 459–462, doi: 10.1109/aps.2004.1329673.
- [41] P. Salonen, Y. Rahmat-Samii, and M. Kivikoski, “Wearable antennas in the vicinity of human body,” in *IEEE Antennas and Propagation Society, AP-S International Symposium (Digest)*, 2004, vol. 1, pp. 467–470, doi: 10.1109/aps.2004.1329675.
- [42] P. J. Dimbylow and O. P. Gandhi, “Finite-difference time-domain calculations

- of SAR in a realistic heterogeneous model of the head for plane-wave exposure from 600 MHz to 3 GHz,” *Phys. Med. Biol.*, vol. 36, no. 8, pp. 1075–1089, 1991, doi: 10.1088/0031-9155/36/8/004.
- [43] P. Salonen, Y. Rahmat-Samii, H. Hurme, and M. Kivikoski, “Dual-band wearable textile antenna,” in *IEEE Antennas and Propagation Society, AP-S International Symposium (Digest)*, 2004, vol. 1, pp. 463–466, doi: 10.1109/aps.2004.1329674.
- [44] P. Salonen, K. Jaehoon, and Y. Rahmat-Samii, “Dual-band E-shaped patch wearable textile antenna,” in *2005 IEEE Antennas and Propagation Society International Symposium*, 2005, vol. 1 A, pp. 466–469, doi: 10.1109/APS.2005.1551354.
- [45] M. Klemm and G. Troester, “Textile UWB Antennas for Wireless Body Area Networks,” *IEEE Trans. Antennas Propag.*, vol. 54, no. 11, pp. 3192–3197, 2006, doi: 10.1109/TAP.2006.883978.
- [46] S. Sankaralingam and B. Gupta, “Development of Textile Antennas for Body Wearable Applications and Investigations on Their Performance Under Bent Conditions,” *Prog. Electromagn. Res. B*, vol. 22, pp. 53–71, 2010, doi: 10.2528/PIERB10032705.
- [47] S. Agneessens and H. Rogier, “Compact half diamond dual-band textile HMSIW on-body antenna,” *IEEE Trans. Antennas Propag.*, vol. 62, no. 5, pp. 2374–2381, 2014, doi: 10.1109/TAP.2014.2308526.
- [48] S. Agneessens, S. Lemey, T. Vervust, and H. Rogier, “Wearable, Small, and Robust: The Circular Quarter-Mode Textile Antenna,” *IEEE Antennas Wirel. Propag. Lett.*, vol. 14, pp. 1482–1485, 2015, doi: 10.1109/LAWP.2015.2389630.
- [49] J. Tak and J. Choi, “An all-textile louis vuitton logo antenna,” *IEEE Antennas Wirel. Propag. Lett.*, vol. 14, pp. 1211–1214, 2015, doi: 10.1109/LAWP.2015.2398854.
- [50] M. E. Lajevardi and M. Kamyab, “Ultraminiaturized Metamaterial-Inspired SIW Textile Antenna for Off-Body Applications,” *IEEE Antennas Wirel. Propag. Lett.*, vol. 16, pp. 3155–3158, 2017, doi: 10.1109/LAWP.2017.2766201.
- [51] M. I. Ahmed, M. F. Ahmed, and A. A. Shaalan, “Investigation of electrical

- properties of fully wearable antenna for ISM applications,” in *MIKON 2018 - 22nd International Microwave and Radar Conference*, 2018, no. 4, pp. 155–158, doi: 10.23919/MIKON.2018.8405163.
- [52] A. Y. I. Ashyap *et al.*, “Inverted e-shaped wearable textile antenna for medical applications,” *IEEE Access*, vol. 6, pp. 35214–35222, 2018, doi: 10.1109/ACCESS.2018.2847280.
- [53] G. P. Gao, C. Yang, B. Hu, R. F. Zhang, and S. F. Wang, “A Wide-Bandwidth Wearable All-Textile PIFA with Dual Resonance Modes for 5 GHz WLAN Applications,” *IEEE Trans. Antennas Propag.*, vol. 67, no. 6, pp. 4206–4211, 2019, doi: 10.1109/TAP.2019.2905976.
- [54] M. Klemm, I. Locher, and G. Tröster, “A novel circularly polarized textile antenna for wearable applications,” in *34th European Microwave Conference, 2004*, 2004, pp. 137–140.
- [55] C. Hertleer, H. Rogier, L. Vallozzi, and L. Van Langenhove, “A textile antenna for off-body communication integrated into protective clothing for firefighters,” *IEEE Trans. Antennas Propag.*, vol. 57, no. 4, pp. 919–925, 2009, doi: 10.1109/TAP.2009.2014574.
- [56] E. Kaivanto, J. Lilja, M. Berg, E. Salonen, and P. Salonen, “Circularly polarized textile antenna for personal satellite communication,” in *Antennas and Propagation (EuCAP), 2010 Proceedings of the Fourth European Conference on*, 2010, pp. 1–4.
- [57] E. K. Kaivanto, M. Berg, E. Salonen, and P. De Maagt, “Wearable circularly polarized antenna for personal satellite communication and navigation,” *IEEE Trans. Antennas Propag.*, vol. 59, no. 12, pp. 4490–4496, 2011, doi: 10.1109/TAP.2011.2165513.
- [58] M. Rizwan, L. Sydänheimo, and L. Ukkonen, “Impact of bending on the performance of circularly polarized wearable antenna,” in *Progress in Electromagnetics Research Symposium*, 2015, pp. 732–737.
- [59] U. Mussa, M. K. A. Rahim, and M. A. Hamid, “Circular polarized textile antenna at 2.4 GHz,” in *ISAP 2016 - International Symposium on Antennas and Propagation*, 2017, pp. 964–965.
- [60] E. A. Mohammad, H. A. Rahim, P. J. Soh, M. F. Jamlos, M. Abdulmalek, and

- Y. S. Lee, "Dual-band circularly polarized textile antenna with split-ring slot for off-body 4G LTE and WLAN applications," *Appl. Phys. A*, vol. 124, no. 8, pp. 1–10, 2018, doi: 10.1007/s00339-018-1991-9.
- [61] L. Zhou, S. Fang, and X. Jia, "Dual-band and dual-polarised circular patch textile antenna for on-/off-body WBAN applications," *IET Microwaves, Antennas Propag.*, vol. 14, no. 7, pp. 643–648, 2020, doi: 10.1049/iet-map.2019.1073.
- [62] A. Yadav, V. K. Singh, P. Yadav, A. K. Beliya, A. K. Bhoi, and P. Barsocchi, "Design of Circularly Polarized Triple-Band Wearable Textile Antenna with Safe Low SAR for Human Health," *Electronics*, vol. 9, no. 9, p. 1366, 2020, doi: 10.3390/electronics9091366.
- [63] E. Stavrou, H. Shakhtour, J. Pamp, and D. Heberling, "2-Port antenna on fleece substrate for on-body MIMO applications," in *Proceedings of 6th European Conference on Antennas and Propagation, EuCAP 2012*, 2012, pp. 3317–3321, doi: 10.1109/EuCAP.2012.6206256.
- [64] S. Choi and S. Lim, "Foldable thin electro-textile antenna array for 4×4 multiple-input multiple-output mobile router applications," *J. Electromagn. Waves Appl.*, vol. 29, no. 3, pp. 375–385, 2015, doi: 10.1080/09205071.2014.997839.
- [65] S. Yan, P. J. Soh, and G. A. E. Vandenbosch, "Dual-Band Textile MIMO Antenna Based on Substrate-Integrated Waveguide (SIW) Technology," *IEEE Trans. Antennas Propag.*, vol. 63, no. 11, pp. 4640–4647, 2015, doi: 10.1109/TAP.2015.2477094.
- [66] A. Shafqat, F. A. Tahir, and M. Umar Khan, "Textile based dual band MIMO quad-mode substrate integrated waveguide antenna for WiFi application," in *Progress in Electromagnetics Research Symposium*, 2017, pp. 1767–1770, doi: 10.1109/PIERS-FALL.2017.8293423.
- [67] I. Y. I. A. Shaweesh and Z. F. M. Himat, "Textile Multiple-Input Multiple-Output (MIMO) antennas at the millimeter-wave band (mmW)," in *4th IEEE International Conference on Engineering Technologies and Applied Sciences, ICETAS 2017*, 2018, vol. 2018-Janua, pp. 1–4, doi: 10.1109/ICETAS.2017.8277893.
- [68] H. Li, S. Sun, B. Wang, and F. Wu, "Design of Compact Single-Layer Textile

- MIMO Antenna for Wearable Applications,” *IEEE Trans. Antennas Propag.*, vol. 66, no. 6, pp. 3136–3141, 2018, doi: 10.1109/TAP.2018.2811844.
- [69] A. K. Biswas and U. Chakraborty, “Investigation on decoupling of wide band wearable multiple-input multiple-output antenna elements using microstrip neutralization line,” *Int. J. RF Microw. Comput. Eng.*, vol. 29, no. 7, pp. 1–11, 2019, doi: 10.1002/mmce.21723.
- [70] A. K. Biswas and U. Chakraborty, “A compact wide band textile MIMO antenna with very low mutual coupling for wearable applications,” *Int. J. RF Microw. Comput. Eng.*, vol. 29, no. 8, pp. 1–11, 2019, doi: 10.1002/mmce.21769.
- [71] A. K. Biswas and U. Chakraborty, “Compact wearable MIMO antenna with improved port isolation for ultra-wideband applications,” *IET Microwaves, Antennas Propag.*, vol. 13, no. 4, pp. 498–504, 2019, doi: 10.1049/iet-map.2018.5599.
- [72] S. Roy, S. Ghosh, S. S. Pattanayak, and U. Chakarborty, “Dual-polarized textile-based two/four element MIMO antenna with improved isolation for dual wideband application,” *Int. J. RF Microw. Comput. Eng.*, vol. 30, no. 9, p. e22292, 2020, doi: 10.1002/mmce.22292.
- [73] T. Ashtankar, N. K. Choudhari, and T. U. Pathan, “Design and Analysis of a Compact MIMO Textile Antenna with Improved Mutual Coupling for WBAN Applications,” vol. 15, no. 2, pp. 8–13, 2020, doi: 10.9790/1676-1502020813.
- [74] A. K. Biswas and U. Chakraborty, “Textile Multiple Input Multiple Output Antenna for X-Band and Ku-Band Uplink-downlink Applications,” in *2020 National Conference on Emerging Trends on Sustainable Technology and Engineering Applications, NCETSTEA 2020*, 2020, pp. 22–25, doi: 10.1109/NCETSTEA48365.2020.9119936.
- [75] S. Roy and U. Chakraborty, “Mutual Coupling Reduction in a Multi-band MIMO Antenna Using Meta-Inspired Decoupling Network,” *Wirel. Pers. Commun.*, vol. 114, pp. 3231–3246, 2020, doi: 10.1007/s11277-020-07526-5.
- [76] S. Rao et al., “Miniature implantable and wearable on-body antennas: towards the new era of wireless body-centric systems [antenna applications corner],” *IEEE Antennas and Propagation Magazine*, vol. 56, no. 1, pp. 271–291, 2014.
- [77] N. H. M. Rais, P. J. Soh, F. Malek, S. Ahmad, N. B. M. Hashim, and P. S. Hall,

- “A review of wearable antenna,” in *Loughborough Antennas and Propagation Conference, LAPC 2009 - Conference Proceedings*, 2009, pp. 225–228, doi: 10.1109/LAPC.2009.5352373.
- [78] R. Negra, I. Jemili, and A. Belghith, “Wireless Body Area Networks: Applications and Technologies,” in *Procedia Computer Science*, 2016, vol. 83, pp. 1274–1281, doi: 10.1016/j.procs.2016.04.266.
- [79] C. Mendes and C. Peixeiro, “A dual-mode single-band wearable microstrip antenna for body area networks,” *IEEE Antennas Wirel. Propag. Lett.*, vol. 16, pp. 3055–3058, 2017, doi: 10.1109/LAWP.2017.2760142.
- [80] Q. H. Abbasi, M. U. Rehman, X. Yang, A. Alomainy, K. Qaraqe, and E. Serpedin, “Ultrawideband band-notched flexible antenna for wearable applications,” *IEEE Antennas Wirel. Propag. Lett.*, vol. 12, pp. 1606–1609, 2013, doi: 10.1109/LAWP.2013.2294214.
- [81] Z. Wang, L. Z. Lee, D. Psychoudakis, and J. L. Volakis, “Embroidered multiband body-worn antenna for GSM/PCS/WLAN communications,” *IEEE Trans. Antennas Propag.*, vol. 62, no. 6, pp. 3321–3329, 2014, doi: 10.1109/TAP.2014.2314311.
- [82] S. Yan, V. Volskiy, and G. A. E. Vandenbosch, “Compact Dual-Band Textile PIFA for 433-MHz/2.4-GHz ISM Bands,” *IEEE Antennas Wirel. Propag. Lett.*, vol. 16, pp. 2436–2439, 2017, doi: 10.1109/LAWP.2017.2723419.
- [83] “Specific Absorption Rate (SAR) for Cellular Telephones | Federal Communications Commission.” <https://www.fcc.gov/general/specific-absorption-rate-sar-cellular-telephones> (accessed Apr. 02, 2019).
- [84] S. Moscato *et al.*, “Infill-Dependent 3-D-Printed Material Based on NinjaFlex Filament for Antenna Applications,” *IEEE Antennas Wirel. Propag. Lett.*, vol. 15, pp. 1506–1509, 2016, doi: 10.1109/LAWP.2016.2516101.
- [85] X. Lin and B. C. Seet, “Battery-Free Smart Sock for Abnormal Relative Plantar Pressure Monitoring,” *IEEE Trans. Biomed. Circuits Syst.*, vol. 11, no. 2, pp. 464–473, 2017, doi: 10.1109/TBCAS.2016.2615603.
- [86] H. Bahramiabarghouei, E. Porter, A. Santorelli, B. Gosselin, M. Popović, and L. A. Rusch, “Flexible 16 antenna array for microwave breast cancer detection,” *IEEE Trans. Biomed. Eng.*, vol. 62, no. 10, pp. 2516–2525, 2015, doi:

- 10.1109/TBME.2015.2434956.
- [87] S. Purohit and F. Raval, "A Review on Wearable – Textile Patch Antenna," *Int. J. Sci. Eng. Res.*, vol. 4, no. 12, pp. 696–702, 2013.
- [88] L. J. Xu, Y. X. Guo, and W. Wu, "Miniaturized circularly polarized loop antenna for biomedical applications," *IEEE Trans. Antennas Propag.*, vol. 63, no. 3, pp. 922–930, 2015, doi: 10.1109/TAP.2014.2387420.
- [89] M. L. Scarpello, I. Kazani, C. Hertleer, H. Rogier, and D. Vande Ginste, "Stability and efficiency of screen-printed wearable and washable antennas," *IEEE Antennas Wirel. Propag. Lett.*, vol. 11, pp. 838–841, 2012, doi: 10.1109/LAWP.2012.2207941.
- [90] P. M. Potey and K. Tuckley, "Design of wearable textile antenna for low back radiation," *J. Electromagn. Waves Appl.*, vol. 34, no. 2, pp. 235–245, 2020, doi: 10.1080/09205071.2019.1699170.
- [91] S. Yan, P. J. Soh, and G. A. E. Vandebosch, "Wearable Dual-Band Magneto-Electric Dipole Antenna for WBAN/WLAN Applications," *IEEE Trans. Antennas Propag.*, vol. 63, no. 9, pp. 4165–4169, 2015, doi: 10.1109/TAP.2015.2443863.
- [92] "CST Studio Suite–3D EM analysis software–SIMULIA by Dassault Systèmes®." <https://www.cst.com/products/csts2>.
- [93] M. Virili, H. Rogier, F. Alimenti, P. Mezzanotte, and L. Roselli, "Wearable textile antenna magnetically coupled to flexible active electronic circuits," *IEEE Antennas Wirel. Propag. Lett.*, vol. 13, pp. 209–212, 2014, doi: 10.1109/LAWP.2014.2301277.
- [94] H. M. R. Nurul, P. J. Soh, M. F. A. Malek, and G. A. E. Vandebosch, "Dual-band suspended-plate wearable textile antenna," *IEEE Antennas Wirel. Propag. Lett.*, vol. 12, pp. 583–586, 2013, doi: 10.1109/LAWP.2013.2259211.
- [95] J. C. Lin, "A new IEEE standard for safety levels with respect to human exposure to radio-frequency radiation," *IEEE Antennas Propag. Mag.*, vol. 48, no. 1, pp. 157–159, 2006, doi: 10.1109/MAP.2006.1645601.
- [96] K. N. Paracha, S. K. Abdul Rahim, P. J. Soh, and M. Khalily, "Wearable Antennas: A Review of Materials, Structures, and Innovative Features for Autonomous Communication and Sensing," *IEEE Access*, vol. 7, pp. 56694–

- 56712, 2019, doi: 10.1109/ACCESS.2019.2909146.
- [97] L. Corchia, G. Monti, E. De Benedetto, and L. Tarricone, “Wearable Antennas for Remote Health Care Monitoring Systems,” *Int. J. Antennas Propag.*, vol. 2017, pp. 1–11, 2017, doi: 10.1155/2017/3012341.
- [98] M. R. Yuce and C. K. Ho, “Implementation of body area networks based on MICS/WMTS medical bands for healthcare systems,” pp. 3417–3421, 2009, doi: 10.1109/iembs.2008.4649940.
- [99] “Wireless Medical Telemetry Service (WMTS) | Federal Communications Commission.” <https://www.fcc.gov/wireless/bureau-divisions/mobility-division/wireless-medical-telemetry-service-wmts> (accessed Jul. 03, 2019).
- [100] D. H. Werner and Z. H. Jiang, *Electromagnetics of body area networks: antennas, propagation, and RF systems*. John Wiley & Sons, 2016.
- [101] D. Vijayshanth, Mohana, and H. V. R. Aradhya, “Design and analysis of compact printed circuit antenna for wireless medical telemetry service,” *RTEICT 2017 - 2nd IEEE Int. Conf. Recent Trends Electron. Inf. Commun. Technol. Proc.*, pp. 1139–1142, 2018, doi: 10.1109/RTEICT.2017.8256776.
- [102] Z. Xia and H. Li, “Miniaturized Dual-Band Implantable Antenna,” *2018 Int. Conf. Microw. Millim. Wave Technol. ICMMT 2018 - Proc.*, pp. 1–3, 2018, doi: 10.1109/ICMMT.2018.8563491.
- [103] P. Soontornpipit and P. Satitvipawee, “Design and Development of a Dual-Band PIFA Antenna for Wireless Biotelemetry Applications,” in *iEECON 2018 - 6th International Electrical Engineering Congress*, 2018, pp. 1–4, doi: 10.1109/IEECON.2018.8712165.
- [104] S. Hossain, N. N. Jui, M. F. Hossain, and K. M. Morshed, “A simple triple-band antenna for implantable biomedical application,” in *5th IEEE Region 10 Humanitarian Technology Conference 2017, R10-HTC 2017*, 2018, pp. 564–568, doi: 10.1109/R10-HTC.2017.8289023.
- [105] O. Body and C. Unit, “Triple-band Electrically Coupled Loop Antenna (ECLA) for Biomedical implantation purposes,” in *35th National Radio Science Conference 2018*, 2018, pp. 475–480.
- [106] H. Sajjad, W. T. Sethi, S. Khan, and L. Jan, “Compact dual-band implantable antenna for E-health monitoring,” *2017 Int. Symp. Wirel. Syst. Networks, ISWSN*

- 2017, pp. 1–4, 2018, doi: 10.1109/ISWSN.2017.8250020.
- [107] T. Watanabe and H. Iwasaki, “Wearable finger multiband antenna for BAN use,” *Proc. 6th Eur. Conf. Antennas Propagation, EuCAP 2012*, pp. 3106–3109, 2012, doi: 10.1109/EuCAP.2012.6205860.
- [108] S. Ahdi Rezaeieh, A. Abbosh, and M. A. Antoniadis, “Compact cpw-fed planar monopole antenna with wide circular polarization bandwidth,” *IEEE Antennas Wirel. Propag. Lett.*, vol. 12, pp. 1295–1298, 2013, doi: 10.1109/LAWP.2013.2284003.
- [109] IEEE SCC39, “IEEE Standard for Safety Levels with Respect to Human Exposure to Radio Frequency Electromagnetic Fields, 3 kHz to 300 GHz,” 2005.
- [110] M. El Atrash, M. A. Abdalla, and H. M. Elhennawy, “A Wearable Dual-Band Low Profile High Gain Low SAR Antenna AMC-Backed for WBAN Applications,” *IEEE Trans. Antennas Propag.*, vol. 67, no. 10, pp. 6378–6388, 2019, doi: 10.1109/TAP.2019.2923058.
- [111] L. Corchia, G. Monti, and L. Tarricone, “Wearable Antennas: Nontextile Versus Fully Textile Solutions,” *IEEE Antennas Propag. Mag.*, vol. 61, no. 2, pp. 71–83, 2019, doi: 10.1109/MAP.2019.2895665.
- [112] Y. J. Chi and F. C. Chen, “On-body adhesive-bandage-like antenna for wireless medical telemetry service,” *IEEE Trans. Antennas Propag.*, vol. 62, no. 5, pp. 2472–2480, May 2014, doi: 10.1109/TAP.2014.2308918.
- [113] S. Ahmed, S. T. Qureshi, L. Sydanheimo, L. Ukkonen, and T. Bjorninen, “Comparison of Wearable E-Textile Split Ring Resonator and Slotted Patch RFID Reader Antennas Embedded in Work Gloves,” *IEEE J. Radio Freq. Identif.*, vol. 3, no. 4, pp. 259–264, 2019, doi: 10.1109/jrfid.2019.2926194.
- [114] A. Alemaryeen and S. Noghianian, “On-Body Low-Profile Textile Antenna with Artificial Magnetic Conductor,” *IEEE Trans. Antennas Propag.*, vol. 67, no. 6, pp. 3649–3656, 2019, doi: 10.1109/TAP.2019.2902632.
- [115] M. Mantash, A. C. Tarot, S. Collardey, and K. Mahdjoubi, “Design methodology for wearable antenna on artificial magnetic conductor using stretch conductive fabric,” *Electron. Lett.*, vol. 52, no. 2, pp. 95–96, 2016, doi: 10.1049/el.2015.3135.
- [116] S. Yan and G. A. E. Vandenbosch, “Radiation Pattern-Reconfigurable Wearable

- Antenna Based on Metamaterial Structure,” *IEEE Antennas Wirel. Propag. Lett.*, vol. 15, pp. 1715–1718, 2016, doi: 10.1109/LAWP.2016.2528299.
- [117] S. J. Chen, T. Kaufmann, D. C. Ranasinghe, and C. Fumeaux, “A Modular Textile Antenna Design Using Snap-on Buttons for Wearable Applications,” *IEEE Trans. Antennas Propag.*, vol. 64, no. 3, pp. 894–903, 2016, doi: 10.1109/TAP.2016.2517673.
- [118] Y. Jiang *et al.*, “e-Textile embroidered wearable near-field communication RFID antennas,” *IET Microwaves, Antennas Propag.*, vol. 13, no. 1, pp. 99–104, 2019, doi: 10.1049/iet-map.2018.5435.
- [119] “Elvy Silver: Cordura 500D Nylon Fabric, Short-time Waterproof Material, Abrasion-Resistant Fabric, Strong and Thick PU Coating Nylon: Amazon.in: Home Improvement.” https://www.amazon.in/Elvy-Silver-Short-time-Waterproof-Abrasion-Resistant/dp/B07F4G7TZY/ref=sr_1_1?keywords=cordura+500d&qid=1568533466&sr=8-1.
- [120] I. Agbor, D. K. Biswas, and I. Mahbub, “A comprehensive analysis of various electro-textile materials for wearable antenna applications,” in *Proceedings of the 2018 Texas Symposium on Wireless and Microwave Circuits and Systems, WMCS 2018*, 2018, pp. 1–4, doi: 10.1109/WMCaS.2018.8400628.
- [121] J. Lilja and P. Salonen, “Textile material characterization for softwear antennas,” in *Proceedings-IEEE Military Communications Conference MILCOM*, 2009, pp. 1–7, doi: 10.1109/MILCOM.2009.5380112.
- [122] R. Zajíček, L. Oppl, and J. Vrba, “Broadband measurement of complex permittivity using reflection method and coaxial probes,” *Radioengineering*, vol. 17, no. 1, pp. 14–19, 2008.
- [123] Y. Ouyang and W. J. Chappell, “High Frequency Properties of Electro-Textiles for Wearable Antenna Applications,” *IEEE Trans. Antennas Propag.*, vol. 56, no. 2, pp. 381–389, 2008.
- [124] S. Yan, P. J. Soh, and G. A. E. Vandenbosch, “made to be worn,” *Electron. Lett.*, vol. 50, no. 6, p. 420, Mar. 2014, doi: 10.1049/el.2014.0714.
- [125] K. Masrakin *et al.*, “Assessment of Worn Textile Antennas’ Exposure on the Physiological Parameters and Well-Being of Adults,” *IEEE Access*, vol. 7, pp.

- 98946–98958, 2019, doi: 10.1109/access.2019.2928343.
- [126] L. Corchia *et al.*, “Radio-frequency Identification Based on Textile, Wearable, Chipless Tags for IoT Applications,” in *2019 II Workshop on Metrology for Industry 4.0 and IoT (MetroInd4.0&IoT)*, 2019, pp. 1–5, doi: 10.1109/METROI4.2019.8792919.
- [127] Y. Jiang, T. Leng, Y. Fang, L. Xu, K. Pan, and Z. Hu, “A Novel e-textile Integrated Wideband Monopole Antenna for Body-worn Energy Harvesting Systems,” in *2019 IEEE MTT-S International Microwave Symposium (IMS)*, 2019, pp. 1057–1059.
- [128] LessEMF, “Electromagnetic Field Shielding Fabrics with a Natural Look and Feel.” <https://www.lessemf.com/fabric4.html>.
- [129] “Solvers | CST MICROWAVE STUDIO.” <https://www.cst.com/products/cstmws/solvers>.
- [130] M. A. R. Osman, M. K. A. Rahim, M. Azfar, N. A. Samsuri, F. Zubir, and K. Kamardin, “Design, Implementation and Performance of Ultra-Wideband Textile Antenna,” *Prog. Electromagn. Res. B*, vol. 27, no. December 2010, pp. 307–325, 2011.
- [131] J. Kapoor, “Miniaturization of Microstrip Patch Antenna Obtained by Patch Meandering and Shorting Pin Loading Technique,” 2012, vol. 2, no. 1, pp. 128–131, doi: 10.3850/978-981-07-1403-1_376.
- [132] P. S. Hall *et al.*, “Antennas and propagation for on-body communication systems,” *IEEE Antennas Propag. Mag.*, vol. 49, no. 3, pp. 41–58, 2007, doi: 10.1109/MAP.2007.4293935.
- [133] P. Nepa and G. Manara, “Design and characterization of wearable antennas,” in *Proceedings of the 2013 International Conference on Electromagnetics in Advanced Applications, ICEAA 2013*, 2013, pp. 1168–1171, doi: 10.1109/ICEAA.2013.6632428.
- [134] P. Salonen, M. Keskilammi, and Y. Rahmat-Samii, “Textile antennas: Effect of antenna bending on radiation pattern and efficiency,” *2008 IEEE Int. Symp. Antennas Propag. Usn. Natl. Radio Sci. Meet. APSURSI*, no. 2, pp. 4–7, 2008, doi: 10.1109/APS.2008.4619343.
- [135] D. Ferreira, P. Pires, R. Rodrigues, and R. F. S. Caldeirinha, “Wearable textile

- antennas: Examining the effect of bending on their performance,” *IEEE Antennas Propag. Mag.*, vol. 59, no. 3, pp. 54–59, 2017, doi: 10.1109/MAP.2017.2686093.
- [136] P. Salonen and Y. Rahmat-Samii, “Textile antennas: Effects of antenna bending on input matching and impedance bandwidth,” *IEEE Aerosp. Electron. Syst. Mag.*, vol. 22, no. 12, pp. 18–22, 2007, doi: 10.1109/MAES.2007.4408597.
- [137] H. Li, S. Sun, B. Wang, and F. Wu, “Design of Compact Single-Layer Textile MIMO Antenna for Wearable Applications,” *IEEE Trans. Antennas Propag.*, vol. 66, no. 6, pp. 3136–3141, 2018, doi: 10.1109/TAP.2018.2811844.
- [138] T. I. Yuk, Y. Sun, and S. W. Cheung, “Design of a textile ultra-wideband antenna with stable performance for body-centric wireless communications,” *IET Microwaves, Antennas Propag.*, vol. 8, no. 15, pp. 1363–1375, 2014, doi: 10.1049/iet-map.2013.0658.
- [139] A. Toktas, “G-shaped band-notched ultra-wideband MIMO antenna system for mobile terminals,” *IET Microwaves, Antennas Propag.*, vol. 11, no. 5, pp. 718–725, 2017, doi: 10.1049/iet-map.2016.0820.
- [140] S. Tripathi, A. Mohan, and S. Yadav, “A Compact Koch Fractal UWB MIMO Antenna with WLAN Band-Rejection,” *IEEE Antennas Wirel. Propag. Lett.*, vol. 14, pp. 1565–1568, 2015, doi: 10.1109/LAWP.2015.2412659.
- [141] J. D. Park, M. Rahman, and H. N. Chen, “Isolation Enhancement of Wide-Band MIMO Array Antennas Utilizing Resistive Loading,” *IEEE Access*, vol. 7, pp. 81020–81026, 2019, doi: 10.1109/ACCESS.2019.2923330.
- [142] H. Wang, L. Liu, Z. Zhang, Y. Li, and Z. Feng, “A Wideband Compact WLAN/WiMAX MIMO Antenna Based on Dipole With V-shaped Ground Branch,” *IEEE Trans. Antennas Propag.*, vol. 63, no. 5, pp. 2290–2295, 2015, doi: 10.1109/TAP.2015.2405091.
- [143] Y. Li, C. Y. D. Sim, Y. Luo, and G. Yang, “12-Port 5G Massive MIMO Antenna Array in Sub-6GHz Mobile Handset for LTE Bands 42/43/46 Applications,” *IEEE Access*, vol. 6, pp. 344–354, 2017, doi: 10.1109/ACCESS.2017.2763161.
- [144] A. K. Gautam, S. Yadav, and K. Rambabu, “Design of ultra-compact UWB antenna with band-notched characteristics for MIMO applications,” *IET Microwaves, Antennas Propag.*, vol. 12, no. 12, pp. 1895–1900, 2018, doi:

- 10.1049/iet-map.2018.0012.
- [145] R. Chandel, A. K. Gautam, and K. Rambabu, "Tapered Fed Compact UWB MIMO-Diversity Antenna with Dual Band-Notched Characteristics," *IEEE Trans. Antennas Propag.*, vol. 66, no. 4, pp. 1677–1684, 2018, doi: 10.1109/TAP.2018.2803134.
- [146] Y. Liu, X. Yang, Y. Jia, and Y. J. Guo, "A Low Correlation and Mutual Coupling MIMO Antenna," *IEEE Access*, vol. 7, pp. 127384–127392, 2019, doi: 10.1109/access.2019.2939270.
- [147] M. Li, L. Jiang, and K. L. Yeung, "Novel and Efficient Parasitic Decoupling Network for Closely Coupled Antennas," *IEEE Trans. Antennas Propag.*, vol. 67, no. 6, pp. 3574–3585, 2019, doi: 10.1109/TAP.2019.2902656.
- [148] M. Li, L. Jiang, and K. L. Yeung, "A Novel Wideband Decoupling Network for Two Antennas Based on the Wilkinson Power Divider," *IEEE Trans. Antennas Propag.*, vol. 68, no. 7, pp. 5082–5094, 2020, doi: 10.1109/tap.2020.2981679.
- [149] R. G. Vaughan and J. B. Andersen, "Antenna diversity in mobile communications," *IEEE Trans. Veh. Technol.*, vol. 36, no. 4, pp. 149–172, 1987, doi: 10.1109/T-VT.1987.24115.
- [150] G. Das, A. Sharma, and R. K. Gangwar, "Dielectric resonator based circularly polarized MIMO antenna with polarization diversity," *Microw. Opt. Technol. Lett.*, vol. 60, no. 3, pp. 685–693, 2018, doi: 10.1002/mop.31033.
- [151] R. Tian, B. K. Lau, and Z. Ying, "Multiplexing efficiency of MIMO antennas in arbitrary propagation scenarios," *IEEE Antennas Wirel. Propag. Lett.*, vol. 10, pp. 373–377, 2011, doi: 10.1109/EuCAP.2012.6205897.
- [152] S. Yan, V. Volski, and G. A. E. vandenbosch, "Compact Dual-band Textile PIFA for 433 MHz / 2.4 GHz ISM bands," *IEEE Antennas Wirel. Propag. Lett.*, vol. 16, pp. 1–1, 2017, doi: 10.1109/LAWP.2017.2723419.
- [153] B. Sanz-Izquierdo and J. C. Batchelor, "Button antennas for wearable applications," *IET Semin. Dig.*, vol. 2007, no. 11803, pp. 97–104, 2007, doi: 10.1049/ic:20070554.
- [154] A. Priya, A. Kumar, and B. Chauhan, "A Review of Textile and Cloth Fabric Wearable Antennas," *Int. J. Comput. Appl.*, vol. 116, no. 17, pp. 975–8887, 2015, Accessed: Dec. 05, 2017. [Online]. Available:

- <http://research.ijcaonline.org/volume116/number17/pxc3902741.pdf>.
- [155] J. Lilja, P. Salonen, T. Kaija, and P. De Maagt, "Design and manufacturing of robust textile antennas for harsh environments," *IEEE Trans. Antennas Propag.*, vol. 60, no. 9, pp. 4130–4140, 2012, doi: 10.1109/TAP.2012.2207035.
- [156] H. Xiaomu, S. Yan, and G. A. E. Vandenbosch, "Wearable Button Antenna for Dual-Band WLAN Applications with Combined on and off-Body Radiation Patterns," *IEEE Trans. Antennas Propag.*, vol. 65, no. 3, pp. 1384–1387, 2017, doi: 10.1109/TAP.2017.2653768.
- [157] S. Yan and G. A. E. Vandenbosch, "Design of Wideband Button Antenna Based on Characteristic Mode Theory," *IEEE Trans. Biomed. Circuits Syst.*, vol. 12, no. 6, pp. 1383–1391, 2018, doi: 10.1109/TBCAS.2018.2857466.
- [158] D. Vital, S. Bhardwaj, and J. L. Volakis, "A 2 . 45 GHz RF Power Harvesting System Using Textile-Based Single- Diode Rectennas," in *2019 IEEE MTT-S International Microwave Symposium (IMS)*, 2019, pp. 1313–1315.
- [159] P. J. Soh *et al.*, "A smart wearable textile array system for biomedical telemetry applications," *IEEE Trans. Microw. Theory Tech.*, vol. 61, no. 5, pp. 2253–2261, 2013, doi: 10.1109/TMTT.2013.2247051.
- [160] I. Saied, S. Chandran, and T. Arslan, "Integrated Flexible Hybrid Silicone-Textile Dual-Resonant Sensors and Switching Circuit for Wearable Neurodegeneration Monitoring Systems," *IEEE Trans. Biomed. Circuits Syst.*, vol. 13, no. 6, pp. 1304–1312, 2019, doi: 10.1109/TBCAS.2019.2951500.
- [161] T. Haagenon, S. Noghianian, P. De León, and Y. H. Chang, "Textile Antennas for Spacesuit Applications: Design, simulation, manufacturing, and testing of textile patch antennas for spacesuit applications," *IEEE Antennas Propag. Mag.*, vol. 57, no. 4, pp. 64–73, 2015, doi: 10.1109/MAP.2015.2453890.
- [162] L. Alonso-Gonzalez, S. Ver-Hoeye, C. Vazquez-Antuna, M. Fernandez-Garcia, and F. Las-Heras Andres, "Multifunctional Fully Textile-Integrated RFID Tag to Revolutionize the Internet of Things in Clothing [Wireless Corner]," *IEEE Antennas Propag. Mag.*, vol. 61, no. 3, pp. 104–110, 2019, doi: 10.1109/MAP.2019.2907910.
- [163] H. I. Azeez, H. C. Yang, and W. S. Chen, "Wearable triband E-shaped dipole antenna with low SAR for IoT applications," *Electron.*, vol. 8, no. 6, pp. 1–13,


- 2019, doi: 10.3390/electronics8060665.
- [164] I. Kruglyak, “20 Examples of wearables and IoT disrupting healthcare,” *Avenga*, 2020. <https://www.avenga.com/magazine/wearables-iot-healthcare/> (accessed Sep. 26, 2021).
- [165] H. Kalantarian, B. Motamed, N. Alshurafa, and M. Sarrafzadeh, “A wearable sensor system for medication adherence prediction,” *Artif. Intell. Med.*, vol. 69, pp. 43–52, 2016, doi: 10.1016/j.artmed.2016.03.004.
- [166] S. Hiremath, G. Yang, and K. Mankodiya, “Wearable Internet of Things: Concept, Architectural Components and Promises for Person-Centered Healthcare,” pp. 304–307, 2014, doi: 10.4108/icst.mobihealth.2014.257440.
- [167] ConsumerLab, “ConsumerLab report on Wearable Technology and IoT – Ericsson - Ericsson,” www.ericsson.com, 2021. <https://www.ericsson.com/en/reports-and-papers/consumerlab/reports/wearable-technology-and-the-internet-of-things>.
- [168] A. Sabban, *Wearable Systems and Antennas Technologies for 5G, IOT and Medical Systems*. CRC Press, 2021.
- [169] C. Loss, R. Gonçalves, C. Lopes, P. Pinho, and R. Salvado, “Smart coat with a fully-embedded textile antenna for IoT applications,” *Sensors (Switzerland)*, vol. 16, no. 6, 2016, doi: 10.3390/s16060938.
- [170] M. Stoppa and A. Chiolerio, “Wearable electronics and smart textiles: A critical review,” *Sensors (Switzerland)*, vol. 14, no. 7, pp. 11957–11992, 2014, doi: 10.3390/s140711957.
- [171] U. Ullah, I. Ben Mabrouk, S. Koziel, and M. Al-Hasan, “Implementation of Spatial/Polarization Diversity for Improved-Performance Circularly Polarized Multiple-Input-Multiple-Output Ultra-Wideband Antenna,” *IEEE Access*, vol. 8, pp. 64112–64119, 2020, doi: 10.1109/ACCESS.2020.2984697.
- [172] S. Saxena, B. K. Kanaujia, S. Dwari, S. Kumar, and R. Tiwari, “A Compact Dual-Polarized MIMO Antenna with Distinct Diversity Performance for UWB Applications,” *IEEE Antennas Wirel. Propag. Lett.*, vol. 16, pp. 3096–3099, 2017, doi: 10.1109/LAWP.2017.2762426.
- [173] G. Irene and A. Rajesh, “Dual polarized UWB MIMO antenna with elliptical polarization for access point with very high isolation using EBG and MSR,”

-
- Prog. Electromagn. Res. C*, vol. 99, pp. 87–98, 2020, doi: 10.2528/pierc19111706.
- [174] Y. Yao, X. Wang, X. Chen, J. Yu, and S. Liu, “Novel diversity/MIMO PIFA antenna with broadband circular polarization for multimode satellite navigation,” *IEEE Antennas Wirel. Propag. Lett.*, vol. 11, pp. 65–68, 2012, doi: 10.1109/LAWP.2012.2183335.
- [175] H. Singh, B. K. Kanaujia, A. Kumar, K. Srivastava, and S. Kumar, “Wideband textile multiple-input-multiple-output antenna for industrial, scientific and medical (ISM)/wearable applications,” *Int. J. RF Microw. Comput. Eng.*, vol. 30, no. 12, pp. 1–14, 2020, doi: 10.1002/mmce.22451.
- [176] D. S. Shiu, G. J. Foschini, M. J. Gans, and J. M. Kahn, “Fading correlation and its effect on the capacity of multielement antenna systems,” *IEEE Trans. Commun.*, vol. 47, no. 11, p. 1767, 1999.
- [177] M. S. Sharawi, A. T. Hassan, and M. U. Khan, “Correlation coefficient calculations for MIMO antenna systems: A comparative study,” *Int. J. Microw. Wirel. Technol.*, vol. 9, no. 10, pp. 1991–2004, 2017, doi: 10.1017/S1759078717000903.
- [178] A. Iqbal, A. Smida, A. J. Alazemi, M. I. Waly, N. K. Mallat, and S. Kim, “Wideband circularly polarized MIMO antenna for high data wearable biotelemetric devices,” *IEEE Access*, vol. 8, pp. 17935–17944, 2020, doi: 10.1109/ACCESS.2020.2967397.
- [179] S. I. Jafri, R. Saleem, M. F. Shafique, and A. K. Brown, “Compact reconfigurable multiple-input-multiple-output antenna for ultra wideband applications,” *IET Microwaves, Antennas Propag.*, vol. 10, no. 4, pp. 413–419, 2016, doi: 10.1049/iet-map.2015.0181.

Publications



A Planar Dual-Band Antenna for ISM/Wearable Applications

Hari Singh^{1,2} · Kunal Srivastava¹ · Sachin Kumar³  · Binod Kumar Kanaujia¹

Accepted: 23 December 2020 / Published online: 3 January 2021
© The Author(s), under exclusive licence to Springer Science+Business Media, LLC part of Springer Nature 2021

Abstract

In this paper, a small size, planar, dual-band antenna is proposed for ISM band applications. The antenna consists of a ground plane, a rectangular patch, and a microstrip feed line of 50Ω . The antenna patch is loaded with several slots to obtain dual resonances in the range of 902–928 MHz and 2400–2480 MHz, covering the lower and higher ISM band frequencies, respectively. The simulated and measured results are presented to validate the proposed antenna design. The specific absorption rate results show that the proposed antenna operates within the approved standard limits and can be used as a flexible antenna.

Keywords Antenna · Bending · ISM · Planar · Wearable

1 Introduction

Due to the increasing demand for wearable electronics systems, the wireless body area networks (BANs) and biotelemetry devices have gained considerable attention, recently. With the rapid growth of wearable technology in health monitoring, telecommunication, search/rescue operation, and various other civil and military applications, the designing of wearable antennas has garnered significant attention from researchers and engineers [1]. In support of body communication systems, IEEE 802.15 standardization group was established to standardize on-body, off-body, or in-body communication applications. Body-centric communication (BCC) takes its place firmly within the sphere of the personal area network (PAN) and BANs [2]. Recent advances in wireless technology led to the advent of BANs, which is an active research area as it has great potential for improvement in the above-mentioned applications, particularly in the healthcare sector [3]. Wireless BANs contain numerous heterogeneous biological sensors placed on different parts of the body or implanted under the skin. In BCC, several communication nodes are placed in close

✉ Sachin Kumar
gupta.sachin0708@gmail.com

¹ School of Computational and Integrative Sciences, Jawaharlal Nehru University, New Delhi 110067, India


² Department of Electronics, Sri Venkateswara College, University of Delhi, New Delhi 110021, India

³ School of Electronics Engineering, Kyungpook National University, Daegu 41566, Republic of Korea

Wireless Personal Communications
<https://doi.org/10.1007/s11277-021-09246-w>



A Compact Wideband Flexible Antenna for Wireless Medical Telemetry Services

Hari Singh^{1,2} · Binod Kumar Kanaujia¹ · Sachin Kumar³  · Kunal Srivastava¹

Accepted: 19 October 2021

© The Author(s), under exclusive licence to Springer Science+Business Media, LLC, part of Springer Nature 2021

Abstract

In this paper, a planar small size coplanar waveguide (CPW)-fed wideband antenna is presented for wearable applications. The antenna operates for 1395–1400 MHz and 1427–1432 MHz wireless medical telemetry service (WMTS) bands. The center frequencies of the two bands are 1397.5 MHz and 1429.5 MHz. The antenna occupies a volume of 48 mm × 52 mm × 0.8 mm. The simulated and measured reflection coefficients, radiation patterns and gain are calculated and found to be in good agreement, validating the proposed antenna design. The simulation results for SAR and bending are also presented to demonstrate that the proposed antenna operates within the approved limits and can be fabricated on a flexible substrate.

Keywords Antenna · Health monitoring · Wearable technology · Wideband · Wireless telemetry applications

1 Introduction

Wearable antennas are gaining popularity these days due to their attractive features, functionality and applications. Planar, conformal, flexible, lightweight, low cost and portable antennas are preferred for wireless communication and sensing applications. These

✉ Sachin Kumar
sachinkr@srmist.edu.in

Hari Singh
harisingh061985@gmail.com

Binod Kumar Kanaujia
bkkanaujia@ieee.org


Kunal Srivastava
kunal.1211@gmail.com

¹ School of Computational and Integrative Sciences, Jawaharlal Nehru University, New Delhi 110067, India

² Department of Electronics, Sri Venkateswara College, University of Delhi, New Delhi 110021, India

³ Department of Electronics and Communication Engineering, SRM Institute of Science and Technology, Chennai 603203, India

Published online: 06 November 2021

 Springer



International Journal of Electronics



ISSN: (Print) (Online) Journal homepage: <https://www.tandfonline.com/loi/tetn20>

Dual-resonance ultra-miniaturised textile antenna for ISM/wearable applications

Hari Singh, Binod Kumar Kanaujia, Ashwani Kumar, Kunal Srivastava & Sachin Kumar

To cite this article: Hari Singh, Binod Kumar Kanaujia, Ashwani Kumar, Kunal Srivastava & Sachin Kumar (2021): Dual-resonance ultra-miniaturised textile antenna for ISM/wearable applications, International Journal of Electronics, DOI: [10.1080/00207217.2021.2001870](https://doi.org/10.1080/00207217.2021.2001870)

To link to this article: <https://doi.org/10.1080/00207217.2021.2001870>



Published online: 26 Nov 2021.



Submit your article to this journal [↗](#)



Article views: 45



View related articles [↗](#)



View Crossmark data [↗](#)

Full Terms & Conditions of access and use can be found at
<https://www.tandfonline.com/action/journalInformation?journalCode=tetn20>

Received: 18 April 2020 | Revised: 28 July 2020 | Accepted: 3 September 2020
 DOI: 10.1002/mmce.22451



RESEARCH ARTICLE

INTERNATIONAL JOURNAL OF
 RF AND MICROWAVE
 COMPUTER-AIDED ENGINEERING WILEY

Wideband textile multiple-input-multiple-output antenna for industrial, scientific and medical (ISM)/wearable applications

Hari Singh^{1,2} | Binod K. Kanaujia¹ | Ashwani Kumar³ |
 Kunal Srivastava¹ | Sachin Kumar⁴

¹School of Computational and Integrative Sciences, Jawaharlal Nehru University, New Delhi, India

²Department of Electronics, Sri Venkateswara College, University of Delhi, New Delhi, India

³School of Engineering, Jawaharlal Nehru University, New Delhi, India

⁴School of Electronics Engineering, Kyungpook National University, Daegu, South Korea

Correspondence

Sachin Kumar, School of Electronics Engineering, Kyungpook National University, Daegu 41566, South Korea.
 Email: gupta.sachin0708@gmail.com

Abstract

A compact, wideband, two-element textile multiple-input-multiple-output (MIMO) antenna is presented for industrial, scientific and medical (ISM)/wearable applications. The proposed structure is composed of the Felt material substrate, and the ground plane and radiating patch are formed using Shieldit™ Super conductive material. The designed MIMO antenna offers a wide impedance matching bandwidth ($S_{11} \leq -10$ dB) of 2.00–6.23 GHz, a very low mutual coupling of ($S_{21, \max}$) -29.26 dB, low envelope correlation coefficient <0.01 , high diversity gain ~ 9.95 dB, and realized gain of more than 2.88 dBi, over the entire band. The prototype of the proposed antenna geometry is fabricated, and it has a size of 76×37 mm². The proposed antenna could be a good candidate for wearable electronic devices due to its compact size, all textile layers, easy integration, robustness, and reasonable on-body performance.

KEYWORDS

ISM band, multiple-input-multiple-output (MIMO), textile antenna, wearable, wideband

1 | INTRODUCTION

Recently, several studies have been done on wearable antenna design, as body-centric wireless communication systems are drawing substantial attention due to their broad applications in many areas.^{1,2} These wide ranges of applications include navigation, soldier communications, remote identification, security systems, wearable computer technology, entertainment, fashion, environmental/biophysical parameters, monitoring for rescue workers, and healthcare. The main component for all the aforementioned applications is a wearable antenna that transfers the data wirelessly from on-body sensors to a centralized database/computing unit. The textile

materials have been potential candidates for designing wearable antennas due to their comfort, robustness, and camouflaged integration with apparel. Moreover, the design and fabrication of a textile wearable antenna is a critical part of the performance of wearable links. These antennas need to radiate effectively and efficiently under different physical constraints such as stretching, crumpling, bending, and body movements.³⁻⁷

With the rapid advancement of wireless communication technology, the high-performance modern communication systems with very high data rate and low cost are becoming imperative. The technological growth in wireless communication requires an increased data transfer rate, which can be achieved by increasing the

